AN EXPERIMENTAL INVESTIGATION OF THE COUNTERCURRENT FLOW LIMITATION

A Thesis

by

MATTHEW A. SOLMOS

Submitted to the Office of Graduate Studies of
Texas A&M University
in partial fulfillment of the requirements for the degree of

Master of Science

May 2008

Major Subject: Nuclear Engineering

AN EXPERIMENTAL INVESTIGATION OF THE COUNTERCURRENT FLOW LIMITATION

A Thesis

by

MATTHEW A. SOLMOS

Submitted to the Office of Graduate Studies of
Texas A&M University
in partial fulfillment of the requirements for the degree of

Master of Science

Approved by:

Chair of Committee,	Karen Vierow
Committee Members,	Frederick Best
	Debjyoti Banerjee
Head of Department,	Raymond J. Juzaitis

May 2008

Major Subject: Nuclear Engineering

ABSTRACT

An Experimental Investigation of the Countercurrent Flow Limitation.(May 2008)

Matthew A. Solmos, B.S., Purdue University

Chair of Advisory Committee: Dr. Karen Vierow

A new correlation for the prediction of the Countercurrent Flow Limitation (CCFL) in a large diameter tube with a falling water film is proposed. Different from previous correlations, it predicts the onset of flooding by considering the relative velocities of the working fluids and the film thickness of the liquid layer. This provides a more complete accounting of the physical forces contributing to CCFL. This work has been undertaken in order to provide a better estimate of CCFL for reactor safety codes such as MELCOR, MAAP, and SCDAP/RELAP.

Experiments were conducted to determine the CCFL for a 3-inch inner diameter smooth tube with an annular liquid film and air injection from the bottom. The size of the test section and the range of working fluid flow rates were based on a scaling analysis of the surge line of a Pressurized Water Reactor pressurizer. An experimental facility was designed and constructed based on this analysis in order to collect data on the CCFL phenomenon.

In order to capture some of the physical phenomena at the onset of flooding visual pictures were taken at high speed. These pictures provided a new understanding of the process of transition to flooding. The facility also produced a new set of flooding data. This can also lead to a more comprehensive mechanistic model.

This thesis is dedicated to the memory of my father.

ACKNOWLEDGMENTS

The author would like to acknowledge the knowledge, assistance, and patience of the chair of his committee, Karen Vierow. Gratitude would be understating the point. The author also extends his gratitude to the members of his committee, Professor Frederick Best and Professor Debjyoti Banerjee, for their suggestions and time. The author would like to thank the entire Laboratory for Nuclear Heat Transfer Systems, staff, and students for their help and support. I could have accomplished nothing without the help and humor of all those involved. The author would also like to acknowledge the help of Aaron Totemeier and Kevin Hogan for their help in organizing the LaTeX template with which this thesis was constructed, and Doctor Isaac Choutapalli for his help with the experimental facility and the visualization techniques. The author would like to express his appreciation to his mother for her support and encouragement. Finally, the most sincere appreciation and thanks to the author's wife for her patience, support, and help throughout this entire process.

NOMENCLATURE

CCFL	Countercurrent Flow Limitation
DAQ	Data Acquisition System
PWR	Pressurized Water Reactor
A	Area [m^2]
C_d	Drag Coeffecient
C_{exp}	Experimental Constant
C_k	Constant for Kutateladze Correlation
C_0	Drift Flux Constant
D	Test Section Diameter [m]
D_h	Hydraulic Diameter [m]
D^*	Dimensionless Diameter
E_i	Error
g	Gravitational Acceleration [m/s^2]
h	Height [m]
j	Volumetric Flux [m/s]
j_f	Liquid Volumetric Flux [m/s]
j_g	Gas Volumetric Flux [m/s]
j_f^*	Liquid Wallis Number
j_g^*	Gaseous Wallis Number
j_{gf}	Drift Flux [m/s]
m	Correction Constant for Correlations
$\dot{m}$	Mass Flow Rate [kg/s]
p	pressure [kPa]
Q	Volumetric Flow Rate [m^3/s]

$\langle U_f \rangle$	Mean liquid layer velocity [m/s]
U_g	Critical Entrainment Gas Velocity [m/s]
u_g	Gas Core Velocity [m/s]
u_{gj}	Drift Velocity [m/s]
v_f	Liquid Phase Velocity [m/s]
v_g	Gas Phase Velocity [m/s]
Bo	Bond Number
Ku	Kutetaladze Number
Fr	Froude Number
Oh	Ohensorge Number
Re	Reynolds Number
Re_f	Liquid Reynolds Number
We	Weber Number
We_c	Critical Weber Number
α	Void Fraction
δ	Film Thickness [m]
δ^*	Dimensionless Film Thickness
μ	Dynamic Viscosity [Pa s]
ν	Kinematic Viscosity [m^2/s]
ρ	Density [kg/m^3]
ρ_f	Liquid Density [kg/m^3]
ρ_g	Gas Density [kg/m^3]
σ	Surface Tension [N/m]
Δ	Change

TABLE OF CONTENTS

Page

Page

LIST OF TABLES

LIST OF FIGURES

FIGURE Page

FIGURE Page

1. INTRODUCTION

In the case of two-phase flow, there exist several important and as of yet still unclarified phenomena. These phenomena affect many aspects of engineering design from calculations of pressure drops to the analysis of heat transfer characteristics. One such phenomena is known as the counter current flow limitation, or CCFL, and its appearances are many, its effects, legion. CCFL affects a great variety of systems both within the nuclear industry and beyond. This thesis documents a research study into the basic physical mechanisms and associated effects of CCFL in a large-diameter round duct under adiabatic conditions. An experimental program will be presented that reveals new insights into the occurence of flooding. From the experimental database, an empirical correlation was obtained for incorporation into reactor safety codes. Thus, it is necessary to give a brief discription of CCFL and its importance to the nuclear industry.

1.1 Relevance

The study of CCFL is of great importance to designers of both physical equipment and thermal hydraulic analysis computer codes. Phenomenon based models will allow the designers to provide the nuclear power industry with the tools to better protect both equipment and the public from harm. Reactor safety codes such as MELCOR, MAAP, and SCDAP/RELAP5, when modeling a design basis accident will call a number of correlations to the problem for reactor safety analysis. One such situation involves the flow regime and heat transfer characteristics of the surge line on a Pressurized Water Reactor pressurizer. The large diameter pipe that constitutes the surge line contains changes in inclination between the pressurizer and the hot leg.

This thesis follows the style of The International Journal of Heat and Mass Transfer.

Previous analyses of the flow characteristics in this section of the system have yielded contradictory and inconclusive results [1] [2]. To better understand the phenomena associated with this accident scenario, the research presented here was undertaken to gain more insight into the physics of the situation and to supply a more appropriate correlation than currently available. The correlation presented here is suitable for use in all large diameter counter current flow limitation problems and care has been taken to ensure the quality of both the data taken and the derivation of the correlation.

The surge line of a PWR is a connection between the hot leg of the primary system and a large, pressurized container [3]. The pressurizer serves the purpose of maintaining the pressure in the PWR system by acting as a pressure control mechanism. Since water is essentially incompressible, the pressurizer either heats water making steam to maintain system pressure (and thus increase the volume of water in the system) or condenses steam to accommodate water expansion [4]. In the case of a hypothetical station black out severe accident, where a steam generator pressure relief valve is stuck in the open position, the surge line would be subjected to high pressures. This could result in an increase in system pressure and ultimately a creep-rupture failure in the steam generator tubes or other primary side components. It is desirable to calculate accurately the distribution of temperature along these tubes for a better understanding of the creep-rupture failure mode. This mode is affected by CCFL in the pressurizer surge line. This situation was studied by Liao [5] who came to the conclusion that MELCOR's CCFL models were inadequate in defining the flooding limit for the pressurizer surge line. This is but one example of how CCFL is of the utmost importance to the safety analysis engineer, and the safety codes they use.

1.2 Countercurrent Flow Limitation

Countercurrent flow is defined as the two-phase flow regime in which the working fluids of a system flow with velocities of opposite signs; that is, fluids flowing in opposite directions. A simplified example of such a flow would be the downward flow

of milk leaving a bottle with the upwards flow of air replacing the subsequent void. As the liquid leaves the bottle, the remaining volume must be replaced by some fluid, in this case air. Thus, there exists a countercurrent flow situation in which milk is flowing with the aid of gravity into a pint glass and air is flowing in the opposite direction due to a pressure difference. Furthermore, if the milk is poured too quickly, a violent and chaotic situation arises: flooding. If the rate at which the liquid leaves the vessel is great enough that the associated air flowing into the vessel inhibits the flow of both, CCFL is said to have been achieved. While this is but a simple example, the physics are essentially the same as in a Pressurized Water Reactor surge line during an accident scenario. This example illustrates that there must be a point at which the velocities of two fluids differ in such a way that normal, steady flow is interrupted.

It is also necessary to introduce the term "flooding". In much of the literature, the term flooding is synonymous with CCFL. While CCFL and flooding both refer to essentially the same phenomenon, CCFL is defined as the point at which the relative velocities of two fluids results in a change in the direction of a portion of the liquid phase. The key word in the definition is point; that is, an instant when the phenomenon occurs which is different than the continuous nature of "flooding". Flooding is the situation associated with the system when at least a measurable portion of the liquid phase is flowing in the direction of the gaseous phase. Put another way, CCFL can be described as the onset of flooding, but not as the phenomenon of flooding itself. This thesis deals with CCFL, the onset of flooding, and not the characteristics of a system during the flooding stage.

Since there exists such a large range of experimental studies devoted to CCFL, it is difficult to determine which aspects need to be examined in detail. This thesis focuses on large diameter ducts of a circular cross section. Large diameter tubes closely model the surge lines of PWR pressurizers as opposed to small diameter tubes. The distinction between the sizes reiterates the complex nature of CCFL. The conditions for which the experiments are run are also well defined which add to the reliability of the data collected. The large diameter test section is unique in that it models a specific

component while it also generates a general set of flooding data. This investigation is also a preliminary step in a large scheme. The next step is to experimentally examine the same phenomenon under similar conditions using water and steam as the working fluids.

1.3 Objective and Scope of Thesis

The objectives of this thesis are given below.

1. To design and conduct experiments regarding CCFL in a large diameter, round duct using air and water as the working fluids under adiabatic conditions.
2. To better clarify the phenomena related to the onset of flooding.
3. To correlate the data and develope a correlation that may be used in reactor safety analysis to predict CCFL.

In order to further the field of two-phase fluid dynamics as it relates to the nuclear power generation industry, this research will investigate the phenomenon known as the countercurrent flow limitation. A better understanding of CCFL will lead to more accurate and more reliable reactor safety codes. While a great many experimental studies have been conducted on the topic of CCFL, this investigation will shed light on unexplained aspects associated with the phenomenon. Over 25 independent experimental investigations into CCFL have been conducted [6], each of which has its merits as well as its limitations. This investigation has been undertaken to reduce discrepancies and errors and to provide accurate and precise data. Finally, the ultimate goal of this thesis is to provide a new correlation that can be used to predict CCFL in large diameter round ducts.

This thesis is presented in seven sections.

- Section 1 is the introduction to the thesis in which a brief description of the project, it objectives, organization, and layout are given.

- Section 2 consists of a literature survey of available papers and texts on the CCFL phenomenon as they relate to the experiments conducted. This survey contains information needed to explain the techniques, methods, and rationale behind the design of the experiments. Furthermore, the survey also provides the methods for analysis of the new data to obtain the aforementioned correlation.

- Section 3 presents a scaling analysis that was performed in order to properly define the necessary parameters and properties which are believed to affect CCFL. Also provided is a detailed explanation as to how the final test matrix was determined.

- Section 4 provides a detailed explanation and description of the experimental facility with an emphasis on the design process and equipment used for the experiments conducted. This Section will also address the decisions made with respect to instrumentation and data collection. Many of the choices made regarding equipment design have an effect on the flooding point, so the rationale for each is given.

- In Section 5, a detailed operating procedure is given to provide the reader with a more succinct understanding of the data and where it comes from. Emphasis is placed on the start up procedures due to the fact that the apparatus must be placed in a consistent starting position before each test is conducted.

- The results of the experiments run are provided in Section 6 with analysis and discussion. The many characterization tests, or shake down tests, that were conducted to ensure the best possible data collection are explored first. Sample test runs are compared next which provide the reader with an understanding of the remainder of the experimental runs. The final correlation is presented in its final state along with justifications.

- Section 7 provides any conclusions that have been drawn from the experiments and the associated analyses. These conclusions will be explored based on how they will impact the field.

- Appendices are provided which contain the data collected, technical drawings and schematics of the facility, and full representations of analyses conducted.

2. LITERATURE SURVEY

There is a wealth of information in the journals and texts regarding the phenomenon of the countercurrent flow limitation (CCFL). The literature can be broken down into two categories: theoretical treatments and experimental investigation. Since this thesis is reporting on the efforts taken to experimentally investigate CCFL, the majority of the review focused on the experimental papers available. Presented here is a review of the literature discussing CCFL, its theory, experiments examining it, and correlations for predicting CCFL.

The organization of the literature review is as follows. A historical overview of the experiments and correlations resulting from them is given. This includes the derivation of several of the correlations and a discussion of the experimental procedures used to develop them. Next are disclosed the various mechanisms proposed to describe flooding and CCFL. This will include classifying the mechanisms into three groups. After this, a section will be included on the theory of CCFL experiment designs which should add to the understanding of the design choices made while designing the experiment used for this research. Also in this section is a discussion on the role of tube diameter, which will play a very large role in the discussions to follow. Finally, a review of phenomenon related to the final correlation will be given. This section will provide all adequate information needed to derive the final CCFL correlation presented in this thesis.

2.1 Historical Background

The study of flooding and CCFL resulted in numerous correlations for predicting CCFL and experimental investigations. The pioneering work of Wallis and Kutateladze served as a foundation for all subsequent work concerning the development of

correlations. The foundations of this work were developed for flooding in packed beds [7]. These findings include the early work of Sherwood in correctly identifying the effect that velocity plays on the phenomenon [8]. One of the most important findings of these early studies is the inverse dependence of the onset of flooding on the relative velocity of the working fluids. This effect can be seen from one of Wallis' early investigations in figure 2.1.

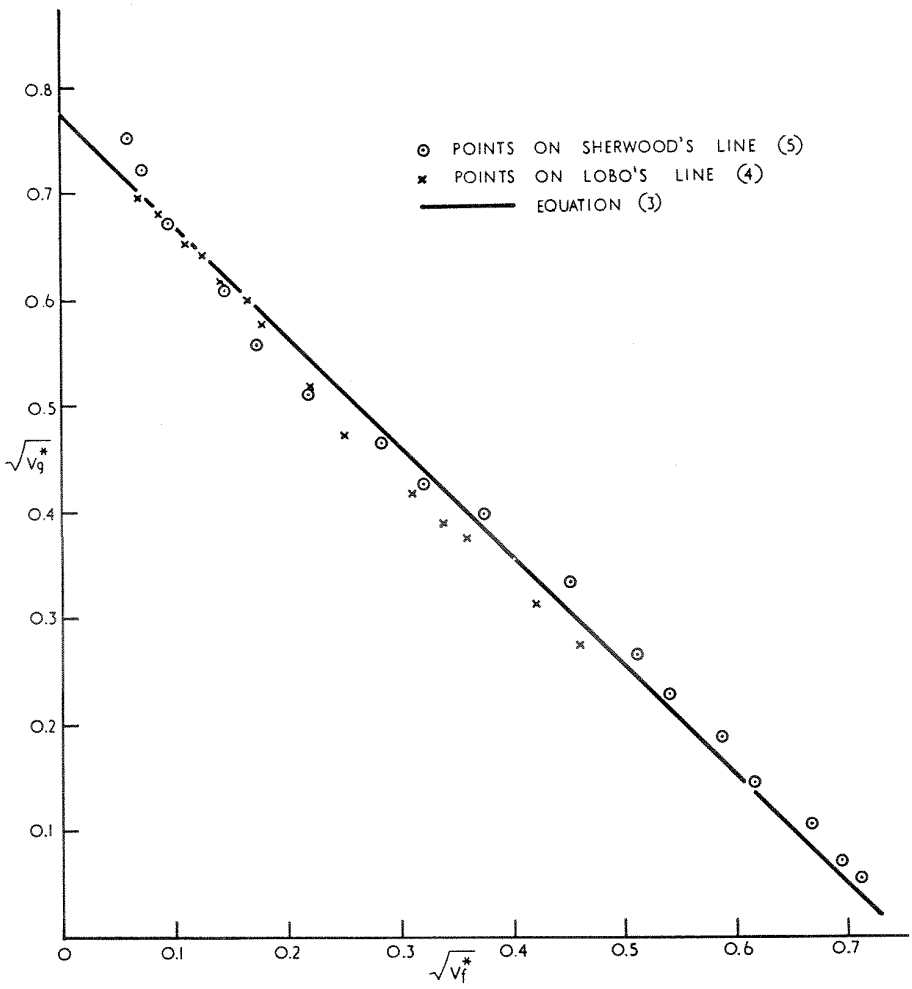

Figure 2.1. Relationship between liquid flow rate and air flow rate at CCFL [7].

As the liquid phase superficial velocity increases, the gaseous phase superficial velocity required to induce CCFL decreases. This trend appears in all of the flood-

ing data and should be considered a first principle upon which all other statements are built. The most widely accepted data and analysis comes from the aforementioned pioneering work of Wallis in the sixties. Wallis however does not fully define the phenomena when he derives the first accepted correlation and it is restricted to small diameter tubes [7]. In this study, he also defines what will become the hallmark for dimensionless studies on CCFL, the Wallis parameter, which is essentially a dimensionless velocity.

$$j_f^* = j_f \sqrt{\frac{\rho_f}{gD\left(\rho_f - \rho_g\right)}} \tag{2.1}$$

and

$$j_g^* = j_g \sqrt{\frac{\rho_g}{gD\left(\rho_f - \rho_g\right)}} \tag{2.2}$$

With this velocity, Wallis proceeds to formulate the Wallis-type flooding correlation. In it he concludes that the sum of the square root of these two dimensionless velocities is equal to a constant [7].

$$\left[j_g^*\right]^{1/2} + m\left[j_f^*\right]^{1/2} = C \tag{2.3}$$

Clift [9] in his experimental study claims that the Wallis parameter is a suitable correlation to predict flooding but concedes that his results work well due to the similarity in experimental apparati. This form of a flooding correlation only considers the diameter and the gravity term in addition to the volumetric fluxes. These are the three determining factors that Wallis is suggesting affect flooding. However, this is explained by the fact that he considered only small diameter pipes when conducting his experiments. It will be shown later that there is indeed a difference in "large" and "small" diameter pipes when flooding is considered [10], [11]. For the present, though, the small diameter constraint instituted by Wallis is taken care of by the second major flooding correlation, the Kutelatadze correlation [12] [13].

The so-called Kutelatadze correlation was first put forth by Pushkina and Sorokin [14] in their experimental work involving water, glycerin and ethyl alcohol. They define the Kutateladze criteria thus.

$$K_g \equiv \frac{\rho_g^{1/2} j_g}{\left[g\sigma\left(\rho_f - \rho_g\right)\right]^{1/4}} = 3.2 \tag{2.4}$$

The result of these criteria is that it assumes that the liquid flow rate is inconsequential to the flooding phenomenon. This is due mainly to the fact that the model created was one involving vapor generation from boiling [12], and that the driving force of both flows was vapor generation. That is, the liquid phase was not moving under any forces other than buoyancy. Another unique part of this correlation is its neglect of a diameter dependence. Pushkina contends that because none of his data appeared to depend on the diameters he tested, there should be no diameter dependence on the flooding point [14]. The stated cause for this neglect is that the occurence of flooding is found to be more dependent on the formation of "crests" on the liquid phases and furthermore that these crests have no dependence on the tube diameter. The final statement from this investigation is that the amount and profile shape of the momentum of the vapor phase must be the contributing factor which leads to CCFL.

However, the Kutateladze correlations as it is used today was defined neither by Kutateladze himself nor Pushkina et al. but by Tien in 1977 [13]. Using a Wallis type correlation as an analogous entity, Tien defined the criteria for flooding to be:

$$\sqrt{Ku_g} + \sqrt{Ku_f} = c_k \tag{2.5}$$

Where Tien uses the original formulation for Ku_g but adds the term:

$$Ku_f = \frac{\rho_f^{1/2} j_f}{\left[g\sigma\left(\rho_f - \rho_g\right)\right]^{1/4}} \tag{2.6}$$

Tien further states that the constant value, c_k, is equal to $\sqrt{3.2}$, similar to the original Kutateladze criteria. Another interesting point brought up by Tien is the

dependence of CCFL on the Bond number, Bo. The Bond number is a dimensionless diameter defined by:

$$Bo = \frac{\rho g D^2}{\sigma} \tag{2.7}$$

Tien claims that such dimensionless diameters must be large, greater then 30, for most CCFL situations in order to assume that the curvature effect of the tube is insignificant. He bases this suggestions on the results of Pushkina and Wallis [13]. A more in-depth look at the Bond number dependence is given below as it describes the effect that tube diameter has on CCFL and how to decide upon which correlation to use.

A more recent suggestion by Zapke is that the Kutateladze correlation is not sufficient to correlate data due to a lack of attention to the length of the tube [15]. While this study focuses mainly on rectangular ducts, its conclusions are reduced to general flow situations and thus should be considered here. Zapke defines two dimensionless numbers new to the realm of CCFL namely, the Froude and Ohnesorge numbers. The Froude number for this correlation is defined as the densimetric liquid Froude number, or:

$$Fr_{DL} = \frac{\rho_f V_f^2}{g D_h (\rho_f - \rho_g)} \tag{2.8}$$

Also defined is the liquid phase Ohnesorge number:

$$Oh_f = \sqrt{\frac{\mu_f^2}{\rho_f D_h \sigma}} \tag{2.9}$$

Zapke claims that the Froude number is representative of the ratio of the drag force exerted by the gas on the liquid phase and the weight of the liquid film [15]. This would imply that the drag force must exceed the body forces on the liquid phase for flooding to occur. The Ohnesorge number is used in this correlation to relate the liquid properties to the flooding gas velocity [16].

Since such a large number of experimental studies have been conducted with respect to flooding, there needs to be a standard manner of reporting the data [17]. Shown below in figure 2.2 is a standard plot of the data reported by Richter [18]. The use of the Wallis parameter as a plotting mechanism is seen throughout the experimental studies [17].

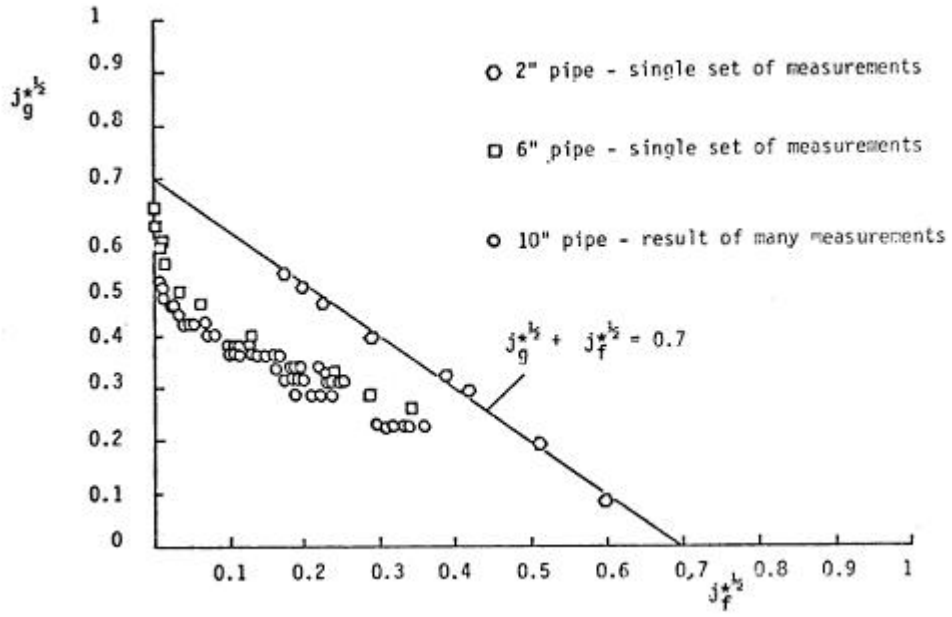

Figure 2.2. Richter's data for a variety of tube geometries. [18]

The spread in the flooding data is also of interest. McQuillan [6] has made the observation that the most of the correlations discovered only predict the data from which they were derived. Figure 2.3 illustrates this point by showing the results from 24 investigations and the large spread these points take.

2.2 Flooding Mechanisms

The mechanisms proposed to explain flooding and CCFL are discussed here. Throughout the literature theories have been proposed to explain under what conditions flooding will occur. It has been suggested that all of these theoretical mech-

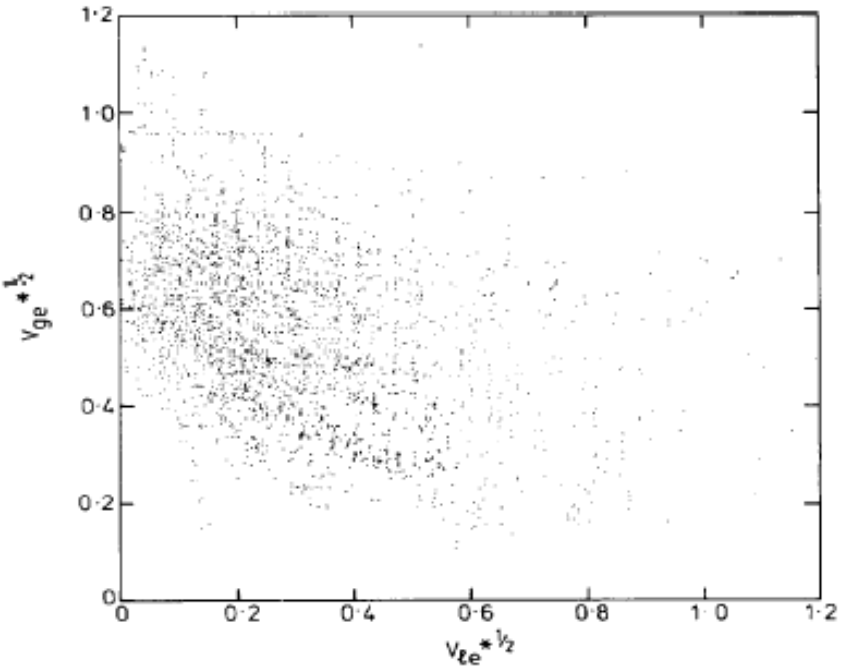

Figure 2.3. The large spread in the flooding data as reported by McQuillan [6]

anisms can be reduced to three broad categories [19] [20]. All other theories are considered to be variations on these three themes. As such, these mechanisms provide a comprehensive view of the factors which may or may not contribute to CCFL. The three major categories are:

1. Kinematic Waves
2. Upward Liquid Film Flow
3. Droplet Entrainment

2.2.1 Kinematic Waves

The kinematic wave mechanism comes directly from the drift flux model of two phase flow [20]. Wallis was the first to assign a drift flux solution to the flooding problem by examining the relative velocity of the phases to the drift flux. This model

stipulates that the shear forces at the interface are negligible when compared to the gravity forces acting on the liquid phase. Kinematic waves are formed only by density differences and thus depend only on the continuity equation by definition [20], and as such do not depend on the momentum equation. As a result, acceleration and frictional pressure losses are also neglected from the analysis. What is left is the drift flux relationship as Wallis defines it [21]. Ohkawa and Lahey have derived two terms that can be used to predict flooding [22].

$$\overline{j_g} = \left(C_o \overline{j} + \overline{U_{gj}}\right) \overline{\alpha} \tag{2.10}$$

Where $\overline{\alpha}$ is the average gas volume fraction. If the drift velocity, $\overline{U_{gj}}$, is only a function of physical properties and the average void fraction, we arrive at the following relationship for the drift flux:

$$\overline{j_{gf}} = \overline{\alpha} \left(\overline{u_g} - \overline{j}\right) \tag{2.11}$$

This final equation can be plotted and a graphical solution for $\overline{j_{gf}}$ can be found. Shown in figure 2.4, the drift flux, $\overline{j_{gf}}$, is dependent only on the void fraction if the velocities of the two fluid are known.

The lines numbered one through four correspond to different values for the volume flux as indicated on the axes [20]. The meanings of the lines are given below.

1. Represents concurrent flow, from the figure it is obvious that the values for $\overline{j_f}$ and $\overline{j_g}$ are such that they maintain the same sign and thus are moving in the same direction.

2. Represents countercurrent flow without flooding. Again, the magnitude and direction of the terminus points of the line should indicate the directions of the fluid flows.

3. Represents CCFL. Line 3 is tangent to the curve and as such it is the only solution that results in a singular value for the drift flux.

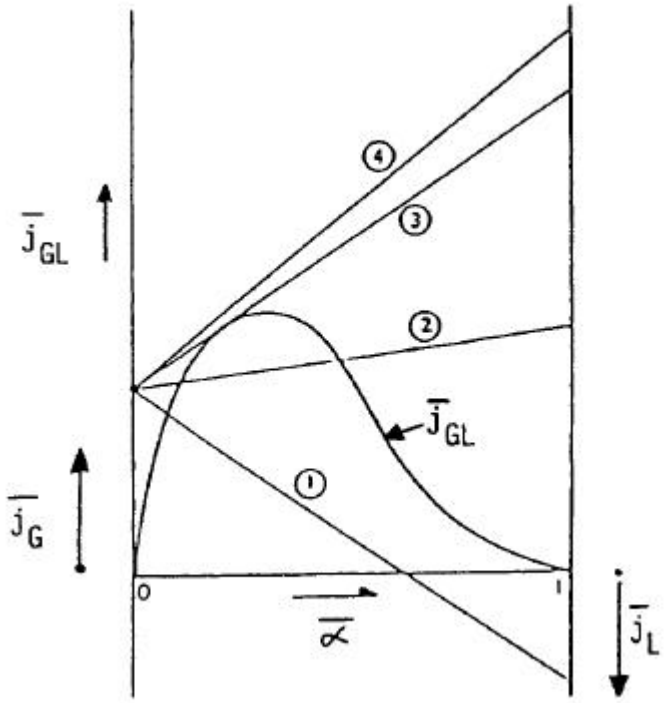

Figure 2.4. Graphical solution to the Drift Flux problem [20].

4. There is no intersection with the curve, physically impossible.

While this analysis does yield a very good approximation to the flooding problem, the curve shown above can only be constructed from experimentally gathered data. This is because there are three unknowns; j_f, j_g, and α. As such, a fully deterministic prediction of flooding is not possible [20] and this solution only provides a qualitative picture of CCFL.

The experiments and studies done to further the kinematic wave theory are numerous. Starting with Wallis in 1961 [7], and continuing through the decades, [23] [24] [25], there has been a host of agreements. However, as prevalent as kinematic waves are, over half of the experimental investigations have be conducted on small diameter pipes.

2.2.2 Upward Liquid Film Flow

The upward liquid film model makes use of dynamic waves as opposed to kinematic ones. Imura [23] states that a change in the wave amplitude on the surface of the fluid leads to bridging, which in turn leads to flooding. This theory is based on the belief that the process of flooding comes from the bridging of liquid across the cross section of the channel. This is also dependent, unlike the kinematic wave model, on the shear stresses acting on the interface between the gas and liquid phases [26]. Cetinbudaklar [27] makes the case that the shear forces on the liquid interface can only be considered if the wave propagation is moving in the same direction as the gas flow due to the magnitude of the velocity.

Chung admits that due to the rather complex nature of this analysis, the liquid film flow model lacks the acceptance of the Wallis and Kutetaladze correlations [26]. Taitel et al. [28] make the case that if the interfacial shear terms are known or can be calculated, then characteristics of the flooding process can be found. They add that any entrance effects can be attributed to their effect on the interfacial shear, and thus on CCFL. This analysis was followed by an experimental investigation of Dukler concerning liquid film movement in vertical pipes [29]. The claim is made that the upward shear on the liquid from the gaseous phase is sufficient to lift a liquid film upwards. The Reynolds number of the liquid film affects CCFL by contributing to a friction factor at the interface. Furthermore, this friction factor is related to the ratio of the film thickness and the tube diameter. Work by Barnea has suggested physical agreement with this theory [30].

2.2.3 Droplet Entrainment

The droplet entrainment model was first mentioned by Dukler with respect to the momentum transfer of entrained droplets of liquid in the gaseous flow. It has been suggested that the small drops that are seen to be ripped from the surface of the fluid just before flooding occurs may lead to CCFL [31]. The occurrence of flooding then

becomes linked to a gas velocity that is capable of suspending the largest stable drop of water. This analysis is performed by conducting a force balance between the drag forces on a drop of water and the gravity forces acting on it as well. Moalem [31] claims that this velocity can be found by means of the critical Weber number, We_c, and the drag coefficient of the drop, C_d.

$$U_g = \left(\frac{4We_c}{3C_d}\right)^{1/4} \left[\frac{\sigma g\left(\rho_f - \rho_g\right)}{\rho_g^2}\right]^{1/4} \quad (2.12)$$

Moalem further asserts that the results of such an analysis match the flooding correlation given by Sorokin et al [14] [31]. From these conclusions, the entrained droplet model does seem to offer a good approximation to the CCFL problem. However, there are conditions that need to be met for this to be true. First, the interfacial waves must be small in order to keep the air volume fraction high.

2.3 Geometric Dependencies

The majority of geometric considerations concerning CCFL deal with the entrance configuration and flow mechnism of the liquid phase. These so-called "entrance effects" will undoubtedly contribute to a great deal of the issues facing the CCFL experimenter. Wallis was the first to recognize that such effects will change the conditions inside the test section [7]. He discovered that flooding would occur more readily for a "smooth" entrance than for a "sharp" entrance. The smooth and sharp differentiation is with respect to the location where the liquid is entering the test section; that is, smooth indicates that the entrance ports were rounded flanges whereas sharp indicates a stepped flange entrance.

The geometry effect is further examined in detail by Chung [26] in which he concludes that the entrance and exit disturbances have an effect on the diameter dependence of the system. The result is that the constant values used in the Wallis correlation must be altered to allow for agreement. For the experiments he used, Chung suggests the Kutateladze constants m and C_k from equation 2.5 be adjusted

according to the geometry. However, Chung ultimately concludes that as the diameter of the test section increases the effect of entry conditions decreases. Finally, it has been suggested that much of the disagreement in the flooding data is a direct result of these separate entrance conditions [6].

The second important geometrical consideration is the actual test section diameter. The distinction between large and small diameter pipes with respect to CCFL was first made by Wallis. Wallis discovered that there does exist a dependence on diameter for the flooding point [7]. This is most clearly illustrated by the definition of the Wallis dimensionless velocity which contains the pipe diameter as the characteristic length. This dependence on geometry is not specific to the transition from countercurrent flow to cocurrent flow but between all flow regimes [32]. The Pushkina study [14] claims that there is no diameter dependence on the actual CCFL point other than the Bond number limit. Numerous experimental investigation and analytical studies were conducted with respect to the accuracy of each correlation under separate diameters [18] [23] [33] [6] [34]. It remains unclear as to what diameter should be used as a cutoff point between the two correlations. Richter [33] suggests the following cutoffs: for pipes with an inner diameter up $50.8mm$, the Wallis parameter should be used; for diameters greater than $152mm$, the Kutateladze should be used instead. It is obvious that based on this criterion there is a large gap of applicable diameters. Jayanti [35] claims the diameter dependence is limited to its effect on the two mechanisms for flooding; droplet entrainment and wave transport. The argument is that as the diameter of the pipe increases, the velocity of gas required to deliver liquid drops out of the test section is less than the gas velocity required to move a wave up the test section. There is no actual size given for this transition to take place. Vijayan [10] attempted to reconcile this discrepancy by conducting similar experiments on several different pipe diameters. The final result of the study was that in tube diameters above 67 mm only the Kutetaladze correlation should be used. Furthermore, Bankoff establishes that the diameter plays no part in the

magnitude of the gas velocity if the dimensionless diameter, D^*, also described as the square root of the Bond number, is above 30 [19].

$$D^* = D\left[\frac{g\left(\rho_f - \rho_g\right)}{\sigma}\right]^{1/2} \tag{2.13}$$

Based on this wealth of knowledge on the topic of tube diameter and its relationship to flooding, it is concluded that the large diameter supposition is valid based on the findings of the abovementioned articles and the lack of any known contradictory data.

2.4 Other Considerations

The are other aspects of CCFL which will play a role in the development of a correlation. Presented in this section is a review of these phenomena.

2.4.1 Annular Flow

From the above definition and examples of countercurrent flow, it stands to reason that the results of such a scenario depend on or result in a change in flow regime. The field of two phase flow depends heavily on the concept of two phase flow regimes. Of importance to this study is the annular regime. Such a flow regime is characterized by the liquid phase flowing down the walls of the duct in a thin film with a stagnant, cocurrent, or countercurrent gas core taking up the center [21]. This flow regime is of interest to the current investigation because of its occurence in the PWR Pressurizer surge line. It is desirable in an accident scenario to have the water in the pressurizer drain into the coolant loop. Under certain conditions the flow regime in the surge line would be annular in a vertical section with the working fluids being steam and water. Thus, in order to closely model the prototypical situation, an annular film flow is chosen.

2.4.2 Liquid Film Thickness

Dimensionless numbers can be used to identify parameters upon which a phenomenon depends. This is necessary for both scaling purposes and to properly generalize the situation. During the course of the research performed for this investigation, a dimensional analysis was conducted. Using the Buckingham Pi theorem, several dimensionless groups were defined as being descriptive of the CCFL scenario. There exists some contention as to the validity or choice of a representitive length scale. In most fluid dynamic systems where ducts or pipes are of primary interest, the hydraulic diameter is most frequently used [19]. Due to the nature of the phenomenon, the choice of length scale is not well defined. First, since the flow regime of study is annular flow in a large diameter pipe, the geometric description of the liquid phase of the flow is much more dependent on the film thickness than the diameter. That is, due to the symmetric nature of the flow regime, the film thickness is more characteristic of the flow than the fixed diameter. Second, due to the fact that the diameter of the present study's test section is above the "large diameter" cutoff [10], the flow system itself can be assumed to closely model a flat plate as opposed to a round duct. It is intuitively obvious from this assumption that the diameter is being ignored and as such it would not be sound to use it as a characteristic length. Finally, the film thickness itself is closely related to the void fraction [21]. In fact, void fraction is tightly coupled to the film thickness in that it can be used to describe the surface of the liquid-vapor interface.

All the correlations found to date rely on first defining a dimensionless film thickness parameter and then backing out a reasonable film thickness from this value [36] [3] [19]. In order to accomplish this, a Reynolds number must be assigned. The Reynolds number used in the following correlations is not a descriptive number for the system or for the flooding phenomenon. A liquid Reynolds number of the form [3]:

$$Re_f = \frac{4Q_p}{D \cdot \mu_f} \tag{2.14}$$

Where Q_p is the liquid volume flow rate per unit perimeter. This definition of a Reynolds number assumes that the entirety of the flow is in the liquid phase.

For vertical falling film thickness, Belkin et al. [36] was the first to formulate the dimensionless film thickness under laminar flow conditions. This model was further expanded to turbulent regimes by the work of Wallis [21]. However, under most of these uses was the assumption that the correlation was only valid for flows of liquid down a vertical surface without gas flow. It would, therefore, be inappropriate to use such a correlation to reduce the data set acquired from the current set of experiments in which there is a countercurrent gas flow. There have been studies into whether or not such a correlation is applicable to systems in which there is an appreciable gas flow. Guedes de Carvalho has stated that such a correlation can be used in the case of countercurrent gas flow on a falling film up to the point of flooding [37]. While he makes the point that the phenomenon itself will affect the film thickness, it does not pose a great enough modifying effect so as to render the correlation unusable.

The film thickness can be calculated by using the following relationships. By beginning with calculating the liquid film Reynolds number, Re_f, the dimensionless film thickness, δ^*, can be found from the Belkin correlations [36]:

$$\delta^* = 0.304 Re_f^{7/12} \tag{2.15}$$

This characteristic film thickness is then used to find the actual film thickness which will be used as the characteristic length for the system. This relationship was first derived by Nusselt [36] as the definition of such a dimensionless film thickness:

$$\delta = \delta^* \left[\frac{\nu_f^2}{g\left(1 - \frac{\rho_g}{\rho_f}\right)} \right]^{1/3} \tag{2.16}$$

This film thickness is the characteristic length used both in further dimensionless groups and in the calculations of the actual phase velocities of the fluids. These

velocities are the bases upon which the correlating factors have been defined. They are arrived at because of the fact that the void fraction in the test section can now be defined from the film thickness by a simple geometric analysis and the definition of the void fraction, α.

$$\alpha \equiv \frac{A_{gas}}{A_{total}} = \left(1 - 2\frac{\delta}{D}\right) \tag{2.17}$$

This definition of alpha is dependent only on the known diameter of the test section and the film thickness above defined. Thus, the velocities of the fluids, as found from the volumetric fluxes, are known and as such used to describe the system. If fact, these velocities are instrumental in the definition of the correlation here presented. These velocities are found by the following relationships [21].

$$v_f = \frac{j_f}{1 - \alpha} \tag{2.18}$$

$$v_g = \frac{j_g}{\alpha} \tag{2.19}$$

2.4.3 The Froude and Ohnesorge Numbers

The final segment of the correlation deals with two dimensionless parameters that were found from a similarity study conducted on the CCFL experiment. A detailed description of this analysis can be found in the self-titled section along with a discussion of the dimensional dependence of other parameters. The result of this dimensional analysis was the discovery that the gravity, surface tension, viscous, and inertia forces can all be related to the CCFL phenomenon. Namely, the Froude number, Fr, and the Ohnesorge number, Oh, are both dimensionally linked to the CCFL experiment. The relationships of these numbers to CCFL have been seen before. Zapke and Kroger [15] have made the case that the Froude number is merely an alteration to the Kutateladze number by pointing out that if the length scale used

in the Froude number is altered to include a gravity term the Kutateladze factor is obtained.

Mouza also makes the claim that both the Froude number and the Ohnesorge number are important factors in CCFL [25]. He suggests that the Froude number successfully captures the interactions of the physical properties of the system and the liquid layer thickness. His definition of Fr for vertical flows takes the form of

$$Fr = \frac{\langle U_f \rangle^2}{D_h g} \tag{2.20}$$

Where $\langle U_f \rangle$ is the mean liquid layer velocity given by:

$$\langle U_f \rangle = \frac{Q_f}{A_f} \tag{2.21}$$

This is similar to Zapke's definition from equation 2.8 but lacks the densimetric term. Mouza only used density to calculate his values for liquid flow rates and does not use them in his correlating terms. He claims that due to the forces acting on the interface, the viscosity and surface tension are much more important than density. This is a result of Mouza assuming that the surface and line forces, i.e. the interface, are responsible for CCFL.

3. SCALING ANALYSIS AND TEST MATRIX

Presented in this section is the scaling analysis to identify the primary dimensional dependencies of the phenomenon and the parameters of interest for both the experiment and the final analysis as they relate to the prototype. A dimensional analysis was done according to the Buckingham Pi theorem as explained in [38]. This approach determines the dependence of physical parameters on each other so that a functional relationship between such parameters may be found. Also known as a scaling analysis, this technique will highlight the characteristics of the system which should lead to CCFL. Also included in this section is a brief description of the test matrix used to conduct the experiments. This will include an explanation of the entire global set of values for which the test was run.

3.1 Scaling Analysis

The purpose of this analysis is to determine which parameters need to be scaled to the proper dimensions and magnitudes to best represent the prototype PWR pressurizer surge line. The first step is to address which parameters are important to the CCFL phenomenon and compare them to the available properties and hardware characteristics in the lab, this is shown in Table 3.1.

Tube diameter is a primary factor in determining the scale of the experiment. As stated previously in the literature survey, there are two main groups of tube diameters, large and small. Since the prototype PWR pressurizer surge line diameter is 10 inches, this falls well within the bounds of the large tube diameter classification. The cutoff as suggested by Vijayan [10] based on his experiments is 67 mm, or approximately 2.6 inches. Furthermore, Vijayan's conclusions are that any diameter above this threshold will reach CCFL under similar conditions. That is, above 67 mm, tube diameter no

Table 3.1
Parameters of importance during a scaling analysis of the CCFL phenomenon

Parameter	Effect	Reference
Density Ratio	Disturbance and Instability Effects, Very Important	Zapke [39]
Tube Diameter	Many Aspects, Very Important	Vijyan [10], Jayanti [35]
Tube Length	Location of CCFL	Jeong [40]
Surface Tension	Slight Stabilizing Effect on CCFL	Deendarlianto [41]
Liquid Viscosity	Interface Instability	Chung [26]
Gas Viscosity	None	Zapke [39]
Gas Re	Independent of CCFL	Zapke [39]
Liquid Re	Film Thickness	Carvalho [42]

longer affects the flooding point. Therefore, any tube diameter over 2.6 inches will act similarly to any other tube with a diameter over 2.6 inches. To keep the tube diameter to a value for which the existing facilities can accomodate flow rates of the fluids to induce flooding, the scale of the experiment, geometrically speaking, is set to a three inch inner diameter.

According to Zapke, the gas phase Reynolds number is independent of the CCFL phenomenon. Thus, it is not a good indicator nor should it be used to scale the experiment and its working fluid parameters. The implication is that if the gas phase Reynolds number is insignicant, so is the gas velocity. This result would neglect the affect that the viscous forces have on the Reynolds number. The real meaning behind Zapke's conclusion is that the gas Reynolds number should not be used for correlating flooding data. The liquid phase Reynolds number would require velocities which are well outside the bounds of a laboratory. This is shown by looking at the prescribed

prototype conditions as mentioned by Liao [5]. The Re value for the prototype is approximately 218,000. This number is based on a liquid volume flux, j_f, of 0.1 m/s and liquid water and steam at 160 bar and 630 K. If this Re was to be matched by an experiment with a 3 in diameter tube, the resulting j_g would be 21 m/s. While this seems reasonable, the corresponding air velocity in a one and a half inch approach tube would be greater than 100 m/s.

A better scaling parameter would be the liquid Froude number. This number appears in a dimensional analysis for the phenomenon and can be considred to be a descriptive and characteristic number. For the prototype, the Froude number for the liquid phase is found to be 4×10^{-4}. At the same Froude number, an air and water facility would have to have a value for j_f of 0.055 m/s. This would require an inlet water volumetric flow rate of 4.2 GPM which is well within the bounds of the present experimental limits.

Since the working fluids of the prototype and the experiment are dissimilar, the density ratio parameter is not likely to be closely scaled. For water and air, the ratio $\frac{\rho_g}{\rho_f}$ is essentially zero, indicating that the density ratio is particularly skewed. For the prototype situation, the same ratio is approximately equal to 0.154, suggesting that this will affect the final gas velocity to induce flooding. The ratio of densities is also an important property to consider according to Zapke [39], where he states that the densities of the fluids are proportional to the gas velocity needed to induce flooding. This proportionality is shown in equation 3.1.

$$j_g \propto \frac{D^{0.55} g^{0.5} \rho_f^{0.55} \sigma 0.05}{\rho_g^{0.5} \mu_f^{0.1}} \tag{3.1}$$

It should be noted that this result was derived by assuming that $(\rho_f - \rho_g) \approx \rho_f$ and solving a modified Wallis correlation for j_g. Since for the prototype condition there is only 15% disagreement between the phase densities, this assumption, while not perfect, is at least allowable. The density ratio scaling will be partially addressed in the steam-water tests on a separate facility.

3.2 Dimensional Analysis

In order to properly assess the parameters that govern CCFL, a scaling analysis must be completed to determine which physical properties of the system are linked are independent. This is accomplished by first conducting a Buckingham Pi Theorem analysis on the system. The parameters of importance were chosen to be the densities of the working fluids, their viscosities, their relative velocity, surface tension, film thickness, diameter, and gravity:

$$f(\rho_f, \rho_g, \mu_f, \mu_g, v_r, \sigma, \delta, D, g) \tag{3.2}$$

For the purposes of the analysis, mass (m), time (t), and length (L) were chosen as the primary dimensions. From this, it is obvious that there must be 9-3, or 6, dimensionless groups. After completing the Pi theorem analysis, the groups shown in Table 3.2 appear:

Table 3.2
The dimensionless groups arrived at from the Buckingham Pi Theorem

Pi Group	Parameters
Π_1	$\frac{\rho_g}{\rho_f}$
Π_2	$\frac{\mu_f}{v_r \rho_f D}$
Π_3	$\frac{\mu_g}{v_r \rho_f D}$
Π_4	$\frac{\sigma}{v_r^2 \rho_f D}$
Π_5	$\frac{Dg}{v_r^2}$
Π_6	$\frac{\delta}{D}$

The Π_5 group is essentially the Froude number. As stated above in the literature survey, the Froude number relates the kinematic forces in the flow to the gravity force. This indicates that this relationship is of importance to the CCFL phenomenon. In

order to include the film thickness in the Froude number, the Pi groups can be rearranged in the following manner:

$$Fr = \frac{v_r^2}{g\delta} = \frac{1}{\Pi_5 \Pi_6} \tag{3.3}$$

Another interesting result of this analysis is Π_6, which is the ratio of the film thickness to the test section diameter. This number characterizes the system in a way which takes tube diameter into account. Based on this analysis, all of the parameters upon which CCFL depends are well defined.

In addition to these groups, there are several other dimensionless numbers that are widely used in the study of CCFL, shown below in Table 3.3. Most of these have been covered in the literature survey; however, they deserve to be revisited.

Table 3.3
Additional dimensionless numbers used in the analysis of CCFL

Dimensionless Number	Symbol	Definition
Ohnesorge Number	Oh	$\frac{\mu_f}{\sqrt{\rho_f \sigma \delta}}$
Bond Number	Bo	$\frac{j_f \mu_f}{\rho_f D^3}$
Wallis Parameter	j^*	$j_g^* = j\sqrt{\frac{\rho}{gD\left(\rho_f - \rho_g\right)}}$
Kuteteladze Parameter	Ku	$Ku \equiv \frac{\rho^{1/2} j}{\left[g\sigma\left(\rho_f - \rho_g\right)\right]^{1/4}}$

The Ohnesorge number relates the viscous forces to the surface tension forces. This ratio will play an important role in correlating the data taken and provides another means of accounting for the forces involved. Furthermore, the Ohnesorge can be found from the Pi groups by the following relationship:

$$Oh = \left[\frac{\Pi_2^2}{\Pi_4 \Pi_6}\right]^{1/2} \tag{3.4}$$

Also, the Bond number has been referred to as a dimensionless diameter [13]. As such, this parameter is also a good characterization of the system and usually is used

as a term for validating the use of the Kutelatadze correlation. In addition to these, there are, of course, the Kutetaladze and Wallis numbers which have been used for the prediction of flooding in many studies and examples.

3.3 Test Matrix

The largest restriction on the test matrix with the CCFL rig is the physical limits to the flow rates achievable. That is, there was a limited range of both liquid and air flow rates that could be used for the experiments. The liquid flow rate is bound on both sides by the supply of water coming from the water main in the laboaratory and the available air flow rates achievable by the blower. The upper limit of water flow rates was found to be approximately 7.2 GPM as delivered from the water main. Attempts were made to increase this flow rate by means of a AMT1900 pump. However, the physical restrictions of the flow loop itself, i.e. pressure drops across the system, were too great for this pump to overcome. As a result, the pump had no effect on boosting the possible flowrates of the liquid phases. On the lower bound of liquid flow rates, the obvious answer is that there were no physical limits as the flow rate of water, controlled by the rotometer pair, could be reduced to zero and thus any value in between this and the max value. The air flow rate, then, becomes the limiting factor in the lower water flow rate scenario.

The air flow rate limits of the test matrix are now defined in order to more completely characterize the system and define the working test matrix. Again, as previously stated above, there exists no lower limit to the air flow rate by physical logic. However, due to the method of flow control mentioned in the facility description section above, the bypass control valve restricted flow in such a way that the minimum controllable air velocity was found to be $24.4 m/s$ centerline maximum velocity in the air approach line. This value corresponds to a volume flow rate, Q_g, of approximately $2.14 \times 10^{-2}\ m^3/s$. The maximum flow rate of the air is determined again as with the water flow rate case by the physical pressure drops in the system that the air

phase experiences. These are due to the geometric factors in the design as built and cannot be altered. The final configuration of the system results in a maximum air flow rate of approximately 39.0 m/s, or $3.41 \times 10^{-2}\ m^3/s$. With this information it now becomes possible to define the test matrix for the experiment by which the most efficient and concise method of collecting the necessary data can be arrived at. By using a Kutelatdze type correlation to approximate the flooding velocity of water given the maximum air flow rate attainable, the lowest water flow rate becomes 3.90 GPM. If it is assumed that air flooding flow rate will decrease as liquid flooding flow rate increases, this yields a range of liquid flow rates at which the blower can supply the requisite amount of air of 3.90 GPM to 7.20 GPM. The test matrix can be found in Table 3.4.

Table 3.4
Full fluid range test matrix

Working Fluid	Water	Air
Upper Limit	7.10 GPM	40.0 m/s
	6.70	
	6.30	
	5.90	
	5.50	
	5.10	
Region of	4.70	
Interest	4.30	
Lower Limit	3.90 GPM	32.4 m/s

The region of interest is the section of the test matrix that is closest to the scaled values. For this investigation, a j_f of $0.055 m/s$ was found to be the lowest obtainable liquid flowrate. This corresponds to a liquid flow rate of 4.2 GPM, which represents

the bottom portion of the test matrix. The remainder of the test matrix is devoted to acquiring a large enough range of data for the development of the correlation.

It should finally be noted that the increments taken for each liquid flow rate were determined by the accuracy of the liquid flow magnetic flow meter. Since the available incremental steps are at a minimum of 0.1 GPM, care was taken to evenly distribute test runs at small multiples of this value.

4. FACILITY DESCRIPTION

This section details all structural and physical components of the experiment and provides both an explanation of the facility and an outline of the rationale for each component. This section is divided into several sections. First, the physical support structure, referred to as the "frame" is described, followed by an explanation of the structure holding the test section, referred to as the "cage". The next section is concerned primarily with the test section and all of its attachments and physical attributes. This section will deal with all parts of the experimental facility that are made from optically clear acrylic. Finally, the third major section deals with the instrumentation and the data acquisition system. This section details all data gathering instruments and equipment including but not limited to electronic instruments (pressure cells, thermocouple, etc.) and manual equipment (rotometers). A final section explains how the data is reduced; the final LabVIEW data acquisition program and arrangement will be explained and the rationale provided, followed by a description of the integral experimental system.

4.1 The Frame

The "ground level" system upon which all other equipment is ultimately supported is the structural frame. This large structure provides both the physical grounding for the test section and instrumentation and also provides the rigidity needed for both stable operation and safety. This structure is a ten foot long by two foot wide by ten foot high steel box made from $1-5/8$ inch slotted steel channel. The frame is shown in figure 4.1.

The standard trade name for the construction material is "single channel slotted Unistrut (TM)". Standard fittings were used to connect all components and the

Figure 4.1. The frame used to support the test section and the necessary experimental equipment.

structure is anchored to the concrete floor of the lab using standard half inch concrete anchors on all six uprights.

4.1.1 Design Details

The slotted channels allow for the attachment of other structural and nonstructural components to the frame from two sides of the channel as opposed to only one

side of the channel where standard single channel strut was used. For most fittings and junctions, the standard side of the channel was used. The size of the major sections of the frame were decided by the design size of test section and cage and the fact that it was most convenient to use the standard ten-foot length. Ten-foot lengths for the uprights allow for the cage to rotate a full 90 degrees without being impeded either at the top or the bottom. Since drains, exhausts, and fluid inlets are needed at the top and the bottom of the cage, flexibility was of utmost importance. This dimensional decision allows for the cage to be in essentially the same orientation when situated at a horizontal configuration as in a vertical one. That is, the associated instrumentation and fluid connection systems migrate less as a result.

The cage is located at the "near" end of the frame. This convention is arbitrary and will be used for easy reference. Also located at the near end of the frame is the water delivery system, the details of which will be given in the instrumentation section. Finally, a torque induction system involving two springs is also located at the near end to secure the test section into position. Conversely, the far end of the frame is composed of the winch system and the air supply or blower system. A schematic of the test facility is shown in Figure 4.2.

4.1.2 The Frame Near End

The near end of the frame consists of the cage rotation bearings, water delivery system, and the torque supply system. The cage bearings are located on the upper cross beams approximately 18 inches from the end of the channels. The bearings are standard sealed one-inch bearing assemblies mounted to the cross beams with 3/8" bolts. Additionally, they are isolated from vibrations in the frame by means of vibration damping pads in order to minimize the effect of vibration on the test section. The size of a one-inch rotational rod was struck upon after estimating the greatest possible mass that the cage could theoretically exhibit. That is, if it is assumed that the test section and plenums are full of water, what is the maximum weight of the test

facility including aluminum cage, acrylic test section, and water. After performing a material mechanics analysis using this mass, it was found that a one-inch round steel shaft would support the cage with an acceptable factor of safety and would not deflect by an appreciable amount.

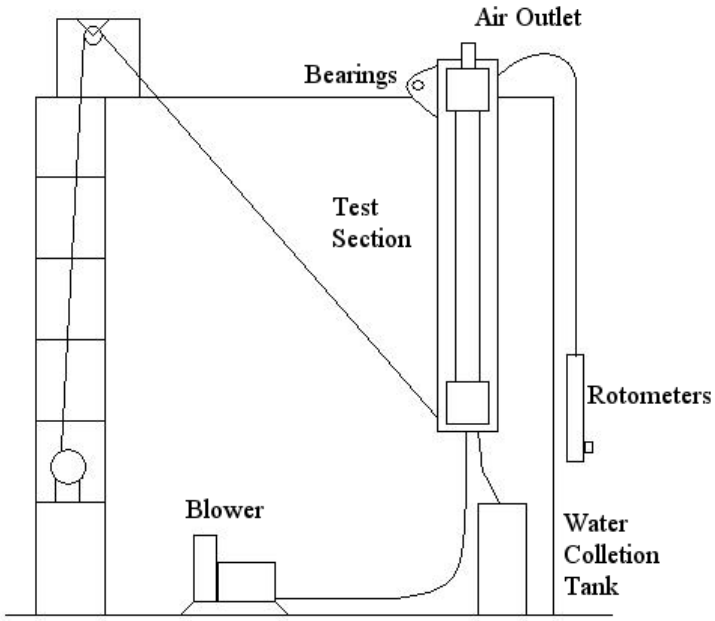

Figure 4.2. A schematic view of the experimental setup.

The water delivery system is also located at the near end of the frame. This system includes the magnetic flow meter, the two manual control rotometers, and all associated piping and tubing. The location of the water delivery system minimizes the distance to the upper plenum of the test section for all inclination angles. All water is supplied by the building water main and feeds directly into the magnetic flow meter by way of a nominal one-half inch pipe. From the flow meter, the water approaches the rotometers and is split in such a way that the flow meters receive an equal amount of water flow. Thus, the magnetic flow meter will provide all necessary flow data while the rotometers will allow for fine control. After the rotometers, one-inch standard pipe traverses the height of the frame and is then connected to flexible

hosing. The hosing allows for the water to enter the upper plenum without being affected by the inclination of the cage. If rigid plumbing where implemented, the cage would not be easily rotated.

Finally, the torque system is a correction system resulting from the physical nature of the test section cage. The cage is hung in such a way that its center of mass is not located directly under the bearing when the test section is fully vertical. When the cage is allowed to hang free, the test section rests at an inclination angle of approximately 10 degrees from vertical. Thus, it was necessary to design a system which would alter the inclination of the system when measurements less than 10 degrees are desired. Two long springs were attached to the cage at its lowest point, thus ensuring the greatest moment arm, and attached to the near end of the frame. Before their final terminus, the springs are routed upwards by way of spring pulleys in order to allow adjustments to the tension supplied. This is accomplished by adjusting the j-bolts connecting the end of the springs to the rigid frame. The springs supply enough torque to keep the cage at the desired angle for the experimental range, thus compensating for the discrepancy caused by the location of the center of mass.

4.1.3 The Frame Far End

The far end of the frame is primarily for the location of the winch. It also consists of the air supply, or blower system and instrumentation. The winch was outfitted with new, 3/16-inch aircraft cable specified mainly by the aforementioned maximum theoretical cage weight. The newly cabled winch provides 3 inches of linear cable movement per one full rotation of the control boss. This relates to approximately 0.5 degrees of inclination angle per one full rotation of the control boss. This fine control is extremely useful when considering the inclination angle affect on CCFL.

The winch is mounted on the frame in such a way that the control boss' plane of rotation is parallel with the ground. This was accomplished by means of a fabricated mounting system. The cable leaves the winch and travels vertically up the frame

freely until it encounters a hard mounted pulley attached to the upper portion of the far end of the frame. From the pulley, the cable travels back to the lower end of the cage and attaches there by means of a hook and eye configuration. Thus, the winch can control the inclination angle of the cage easily due to the large moment arm created by the location of the eye hook. Although the test facility was constructed with the capacity to run tests at $0 - 90^o$ inclination angles, inclined tests will be run as part of future test programs.

The far end of the frame is also home to the air supply system. The blower is located past the near end of the frame with the air supply pipe being attached directly to the uprights. This section of the blower system was designed to allow for the air leaving the blower to become fully developed before encountering the pitot tube air velocity meter. It is also necessary that this section of piping be rigid and stable to ensure fully developed flow of the air.

4.2 The Cage

The test section is situated inside a rigid aluminum structure referred to as the "cage". The cage was designed to give a structural rigidity to the test section and to allow for instrumentation to be attached near the test section, eliminating the need for long, error inducing approach tubes. This is of increasing importance when the test section is inclined. The decision to use the aluminum structural material, as opposed to more steel channel, was made based on several factors. The first factor was weight. In order to make the system safe, it was determined that the lighter a facility was, the less chance there was of encountering a design limit on hardware. That is, it was necessary to design a facility that would remain rigid during operation, but would not prove too heavy to move via the winch, or that would compromise the tensile strength of the aircraft cable. Aluminum structural material is half as massive as equivalent steel channel, but is comparatively strong.

Another reason for choosing the aluminum structural material has to do with the availability of "attachable sides". That is, all four sides of the aluminum strut are capable of receiving t-bolts, thus components (fittings, mounting hardware, etc.) can be attached to any open section of the material. This allowed for a more rigid design of the cage with respect to the attachment of the test section and a more convenient locating of instrumentation. This fact is highlighted in the instrumentation section regarding the pressure transducers below.

Yet another factor in choosing the aluminum material for the cage follows from the previous convenience; that being the ability to change out components while the cage is hung. Due to the nature of the t-slotted aluminum framing system, it is possible to change out parts of the acrylic test section assembly while the cage is attached to the frame. This also eliminates the time consuming procedure of taking the cage down and putting it back up.

Most of the reasons for the design choices about the cage come directly from the design of the test section. However, some of the test section design choices were in turn decided upon because of the cage design. The cage assembly rotates about a set of enclosed bearing units. These bearings also attach directly to the cage approximately 10 inches from the end of the cage. The bearing attaches directly below the second set of cross members. The members that the bearings attach to are the longest continuous pieces of aluminum and measure 86 inches in length. This length encompasses the entire length of the test section and associated plenums, flanges, and outlet components.

The cross members measure five inches in length and are used both for structural support of the cage, and as an attachment point for the test section flanges. Since the aluminum strut cross section is a 1.5 inch square, the cage, when fully assembled, exhibits a square cross section of 8 inches. The cage is assembled by means of commercially available fittings of both angled, 90 degree braces and flat mending plates. This means of construction allows for unparalleled rigidity which results in safety and structural reliability.

4.3 Acrylic Components

All parts of the experiment constructed with optically clear acrylic or those attaching to said acrylic are referred to as the test section. This distinction is necessary due to the fact that the actual "test section" is a 3-inch inner diameter, 72 inch long acrylic tube in which CCFL occurs. However, for ease of description, the convention in this section is to refer to all components directly attached or affected by this tube as the test section. It is necessary to briefly state all components which compose the test section and present a schematic view of the test section, shown in figure 4.3. Starting from the "top", i.e. those components located highest on the test section when it sits in a vertical position, there are: the air outlet assembly and flange, the upper plenum and flanges (which include all the water inlet ports and tubing), the test section tube (with associated flanges and pressure ports), the lower plenum and flanges, and the air inlet assembly (with associated fittings). The following subsections will detail the design of each listed component.

4.3.1 The Air Outlet

The uppermost component of the test section is the air outlet. This component provides the air (and entrained water) a method of leaving the test section. Furthermore, the air outlet is also responsible for inducing an annular flow within the test section by creating a constant 1/8-inch gap for the water entering the test section to flow through. The air outlet consists of two parts, the outlet body and a flange. A construction picture is provided in figure 4.4.

The outlet body is a cast acrylic tube of 1/4-inch thickness and 2.75 inch outer diameter. The end of the tube that lies inside of the test section has a 30 degree bevel on the inner surface. This bevel was added in order to reduce the flow resistance that the air would see as it leaves the test section. The first design of this part had a flat, 90 degree end which was observed to create unwanted turbulent vortices and disturb the incoming water to a large degree. With the implementation of this design, such

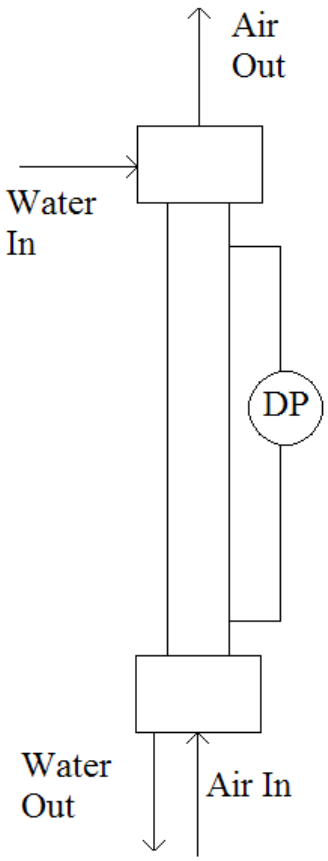

Figure 4.3. A schematic of the test section showing the relative locations of the fluid inlets and outlets.

vortices have not been observed. On the other end of the tube, a small relief has been machined in to allow for the future attachment of an outlet fitting. This differs from the original design which contained a reducer at this end of the tube. This reducer took the diameter of the tube from its 2.25 inch inner diameter to a 3/4 inch NPT female thread over approximately 3 inches. The resulting pressure drop across this reducer proved to be too great during initial shake down tests and required removal. It is at this point in the design process that the issue of pressure drops became important. The pressure drop across this reducer was large enough to affect the flow

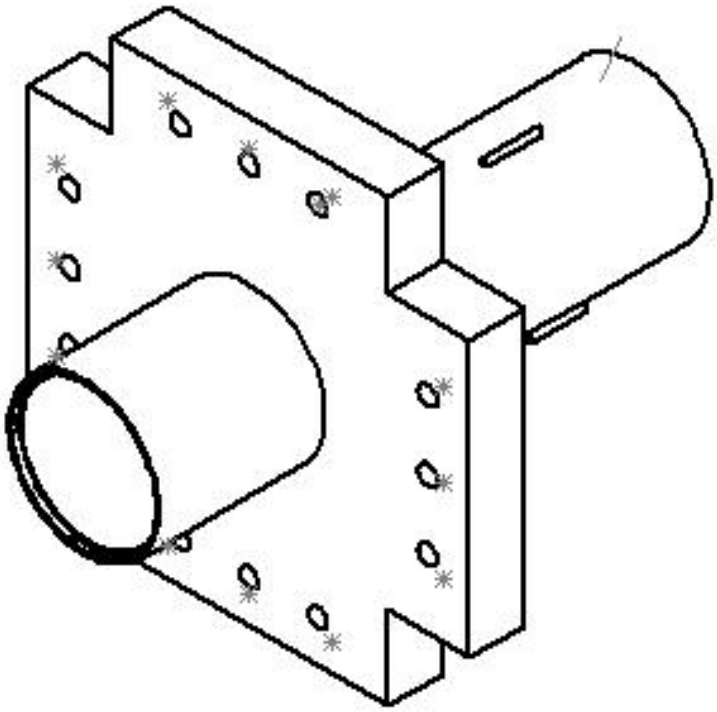

Figure 4.4. The air outlet assembly.

through the entire experimental facility. The drop caused the test section to become pressurized and reduced the air flow through the system to a point where flooding was no longer achievable.

Finally, a mounting flange is attached to the air outlet 8 inches from the beveled end of the tube by using acrylic solvent weld. This flange mounts to the upper plenum and the uppermost stringers of the cage.

For the experiments conducted for this thesis, the upper end of the air outlet was left open to the environment. This allows for the working fluids to exit the test section with a minimum of flow friction and acceleration pressure losses. The only friction seen by the fluids as they exit are wall friction and a slight reduction in flow diameter. This reduction in flow diameter, though, is small and does not contribute

greatly to any inherent pressure drop. As a result, this component should not induce a significant pressurization of the test section. Thus, the pressure inside the test section can be assumed to be at atmospheric. The second purpose of the air outlet is to aid in the formation of annular flow. Since the air outlet tube rests inside of the test section, the end of which is situated below the holes which allow water into the test section, an annular film is formed within the test section.

4.3.2 Upper Plenum

The upper plenum of the test section provides the means by which the water enters the test section. The plenum consists of three pieces, the plenum body and two flanges. The plenum body is a 5-inch inner diameter cast acrylic tube of 6-inch length. Into this tube, four 1-inch holes have been milled to allow for water to enter the plenum. Attached to the outside of these holes are threaded acrylic blocks into which hose fittings are inserted as shown in figure 4.5. These fittings accept hoses from the water supply system. At each end of the plenum a flange has been solvent welded which will attach to the air supply flange or the test section flange. Each of these plenum flanges has an o-ring grove that seats a 232-3 o-ring which seals the plenum from the outside environment.

As stated above, the upper plenum provides the water pre-injection system for the test section. That is, water enters the plenum via the one-inch holes, referred to as "injection ports", and comes to a relative fluid equilibrium, i.e. fixed gravity head and a fixed stagnation pressure. This results in the upper plenum acting as a stagnation chamber, allowing for the flow entering the test section holes to do so at relatively the same conditions. The plenum contains four injection ports; however, only two of them are actually used for the experimental runs considered in the runs analyzed in this thesis. These ports are situated on the top and bottom of the plenum were it to sit in a horizontal position. These two ports create an equal distribution of volumetric flow entering the upper plenum. In the first design, only one port was included and

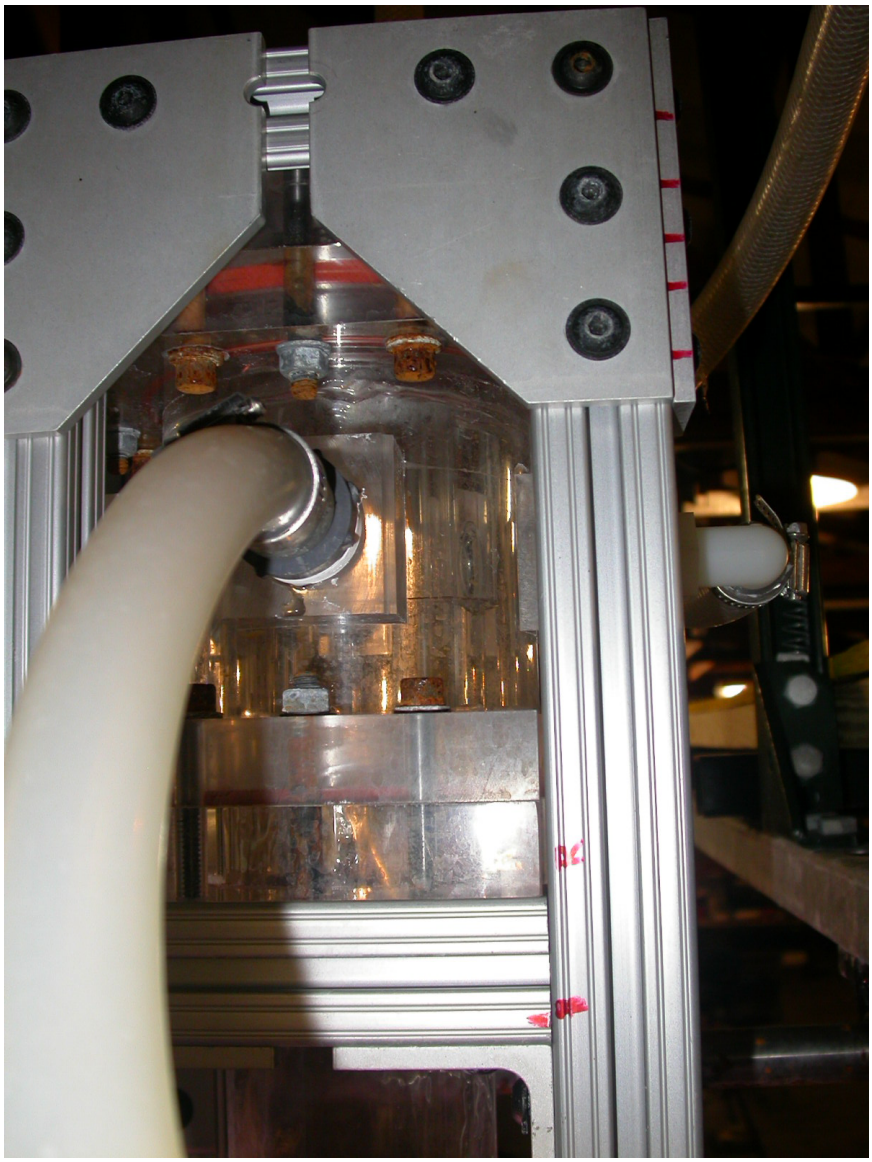

Figure 4.5. The upper plenum of the test section.

it was observed that the water level in the plenum at the port was markedly higher than on the opposite side. This discrepancy in water level would produce an unequal gravity head and disturb the annular flow created in the test section. The addition of a second port negated this unevenness and a uniform water level has been seen to result. The second two ports were added as options so future investigations would benefit from the added control over inlet water flow rate.

4.3.3 Test Section

The test section is the clear acrylic tube in which CCFL is observed to occur. The test section used for this experiment measures 72 inches in length and has a nominal inner diameter of 3 inches. The wall thickness of the test section is one quarter of an inch. Four pressure ports have been added, two on each side, to accommodate a differential pressure transducer and two absolute pressure transducers. On the upper end of the test section, inside of the upper plenum, the water enters the test section through a series of 12 evenly spaced 1/4-inch holes. These holes are placed at the same axial plane and are radially symmetric. The air outlet pipe extends into the test section and terminates approximately two inches below these water inlet holes. This has the effect of forming the annular flow regime within the test section. The lower end of the test section descends into the lower plenum and extends about 4 inches below the air inlet pipe.

The water inlet of the test section directs the flow into an annular regime, alleviating many of the entrance effect problems encountered by previous experiments [23]. This water inlet configuration also allows for the symmetric entry of water into the test section. By separating the flow into 12 distinct flow paths, the flow is evenly distributed around the test section. If, instead, the flow were allowed to enter the test section via slits cut into the tube, any flow disturbances induced by the water entering the upper plenum would be compounded and annular flow would not be maintained. The pressure ports are situated such that the differential pressure ports

are located 52 inches apart on the "bottom" side of the test section. The bottom side refers to the side of the tube that would be under the rest of the test section if the cage where held in a horizontal position. This is due to the fact that for increased inclination angles, the annular flow regime breaks down and a stratified flow regime takes over. For these situations it would still be necessary to record differential pressure data and since the pressure transducer water lines would drain in the absence of a liquid level, the ports needed to be placed on the bottom side of the test section. The absolute pressure measurements are of lesser importance to the experiments at hand. They are needed only to gain a basic picture of the pressure in the test section and, as such, having two is a redundancy. Thus, they are placed on the "top" of the test section to recorded data for the vertical tests. Finally, the bottom end of the test section must be addressed. The test section extends past the air inlet into the lower plenum. This configuration ensures that all of the air entering the test section will, at least initially, progress upwards into the test section after leaving the air inlet pipe. Previous designs of the test section/lower plenum/air inlet resulted in a noticeable amount of air leaving the air inlet and being redirected into the lower plenum and out the liquid drain. By locating the air inlet within the test section, this effect is minimized.

4.3.4 Lower Plenum

The lower plenum is dimensionally identical to the upper plenum, but it does not have water injection ports. This component of the facility is a 6-inch long, 5-inch inner diameter cylinder with a 1/4-inch wall thickness. The primary purpose of the lower plenum is as a transfer tank for the water leaving the bottom of the test section. As such, it has no penetrations. This provides a good viewing chamber for both the water leaving the test section and the exhaust portion of the air inlet. Many important observations can be made by viewing these conditions while the test is running.

4.3.5 Air Inlet

The air inlet is the only part of the experimental facility that is not constructed from acrylic and the component has undergone the most changes as far as design is concerned. The air inlet is a 3-foot length of standard schedule 40 PVC pipe attached to a fiberglass and plywood flange. This flange is identical to the acrylic flanges used throughout the facility with exception of 4 drains added to facilitate the removal of water from the lower plenum. Also, in order to stabilize the air inlet tube and to provide rigidity, a second "flange" was added that connects to the cage.

The air inlet pipe was designed so that the incoming air flow would be fully developed when it entered the test section. According to Fox [38], this requires an L/D ratio of at least 30. When the flow is fully developed, it will enter the test section at a known, fairly uniform air stream. Four 1/2-inch diameter holes were cut into the flange to expedite the water drainage from the lower plenum. To these holes are attached four hose connectors which run to the holding tank located below the test facility. The rigidity adding flange connects to the cage while allowing for the drain hoses to run through it. This both protects the drain hoses from disconnecting from the flange and adds rigidity to the pipe. Since the inlet pipe is 3 feet long, any force could feasibly knock it off center and redirect the flow of air into the test section.

4.3.6 Additional Equipment

To facilitate the purging of the absolute and differential pressure transducer lines, a pressure vessel was added to deliver water to the upper ports safely. The vessel consists of a 6-inch diameter stainless steel cylinder which is 24 inches tall. Shown in figure 4.6, the vessel has the following connections. The pressure vessel connects to the air compressor when the appropriate valve is opened. The vessel can then vent when the appropriate lines need to be purged. Water is added via the ball valve located at the top of the pressure vessel when the system is at atmospheric pressure. The pressure vessel is connected to the subsystem that is to be purged by

way of a compression fitting which may at will be switched from the absolute pressure transducer system to the differential pressure system when the purge system is not pressurized. Once the appropriate subsystem is chosen, the purging process may be started by pressurizing the vessel and the appropriate subsystem.

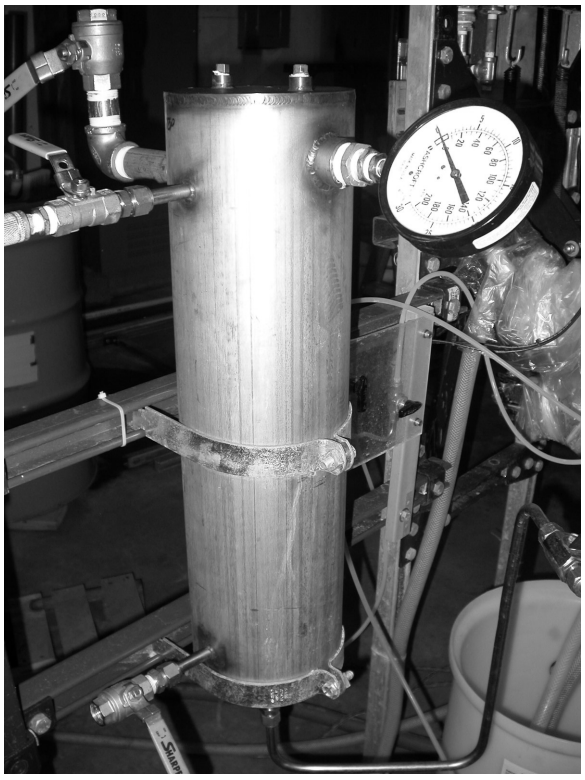

Figure 4.6. The pressure vessel that can deliver water to the upper pressure transducers, aiding in the purging process.

4.4 Instrumentation

There are two major groups of instrumentation; the actual physical instrumentation and the data acquisition system. The setup of these two systems greatly affects the quality of the data taken and impacts the data taking process.

4.4.1 Instruments and Equipment

The instruments used in this experiment were decided upon after taking inventory of the measurements that need to be recorded. Table 4.1 illustrates the quantities to measure and the type of measurement device to use.

Table 4.1
Experimental measurements and devices

Quantity	Measurement Device
Air Velocity	Pitot Tube
Water Velocity	Rotometers and Magnetic flowmeter
Pressure Gradient	Differential Pressure Transducer
Upper Location Absolute Pressure	Absolute Pressure Transducer
Lower Location Absolute Pressure	Absolute Pressure Transducer
Air and Water Temperature	T-type Thermocouples

The liquid flowrate is the only measurement of the system that uses two devices in series. This is due to the fact that one of these instruments, the rotometers, serves a dual purpose as both a flowmeter and as a control device. Figure 4.7 shows these rotometers as they are attached to the facility.

The error associated with the rotometers is additive across the two of them, and the error incurred by the two rotometers would be unacceptable. Thus, it was necessary to use another instrument to determine the liquid flow rate. A 1/2" Yamatake MGG-18D magnetic flow meter was placed before the rotometers in order to more accurately measure the liquid flow rate. The advantages of using the magnetic flowmeter are two fold. The accuracy of the flow meter is ± 0.01 GPM. This can be contrasted to the rotometer accuracy of ± 0.1 GPM. The magnetic flow meter also can be connected to the data acquisition system as it outputs a voltage signal proportional to the flowrate. The magnetic flow meter is factory calibrated and connected to a communications protocol to send the data signals to the data acquisition system.

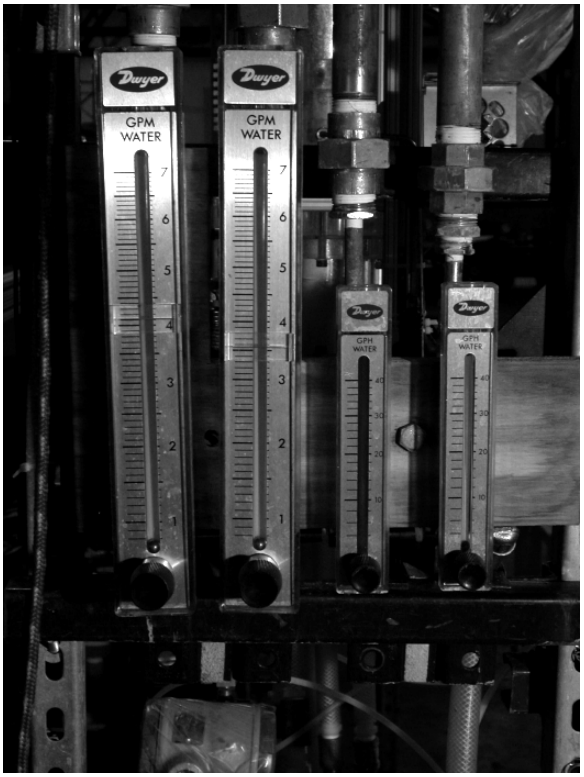

Figure 4.7. The rotometers used to control the liquid flow into the system.

The air velocity measurement is made with the use of a pitot static tube system. The basic theory behind a pitot static tube air speed measurement states that if the stagnation pressure and the static pressure are known, from the Bernoulli equation, the dynamic pressure of the flow can be calculated.

$$\frac{\rho v^2}{2} + \rho g h + p = constant \tag{4.1}$$

Where the fraction on the left hand side of the equation represents the dynamic pressure of the system. Also, the flow is assumed to be moving in streamlines so the change across them is zero, allowing for the $\rho g h$ term to be assumed zero. This allows for equation 4.1 to be simplified into:

$$\frac{\rho v^2}{2} + P = P_0 \tag{4.2}$$

Where P_0 is the "total pressure" of the system. With this in mind, a pitot static tube is inserted into an approach pipe leaving the blower at a distance sufficient for the flow to become fully developed. This probe contains both a pitot tube and a static pressure port which are then connected to a differential pressure transducer. The difference between their pressures is the dynamic pressure. The dynamic pressure is related to the velocity by the following relationship:

$$\Delta P_{dynamic} = \rho \frac{V^2}{2} \tag{4.3}$$

Thus a value is arrived at for the centerline velocity which can be related to the average velocity by a simple relationship. According to [38] the average velocity across the section of pipe is equal to two thirds of the maximum centerline velocity. Furthermore, the pressure transducer can also be directly connected to the data acquisition system and the measurements automatically displayed and recorded.

Both the upper and lower pressure ports on the test section are measured using absolute pressure transducers. These are Honeywell model STA940 pressure transducers. This means that they require a wetted connection to the port at which the pressure is to be measured. To accommodate this requirement, small lengths of 1/4"' tubing are connected to the transducers at the test section. The tubing must also be purged of air bubbles in order to guarantee the proper and accurate operation of the pressure transducers. A detailed procedure for purging the lines can be found below in the Operating Procedures section. The pressure transducers measure only the pressure seen at the transducer. That is, an associated gravity head is reported by the transducers according to the physical height of the water column described by the tube attaching it to the pressure port. For the upper absolute pressure transducer, this height is approximately 9 inches where, as for the lower port, the height is approximately 3 inches. This added pressure must be subtracted from the pressure reading in order to define the actual pressure in the test section at those two locations.

The differential pressure measurement in the system is also made by way of a pressure transducer, a Honeywell STD924. The pressure transducer is a differential

type and as such will measure the difference in pressure between the two pressure ports on the test section. However, the ports on the pressure transducer must also be wetted, as was the case with the absolute pressure transducers. Since the test section pressure ports are 52 inches apart, there will consequently be a 52 inches of water pressure reading on the transducer as a zero point. This is important in Section 6, Results, when looking at the data plots. When the differential pressure is being used for comparisons, the 52 inch zero point is removed. That is, when the actual differential pressure, or change in differential pressure is considered it becomes reduced. However, when a general trend or observation is examined, the raw reading from the differential pressure transducer is used and includes the 52 inch factor. This convention is used to properly compare raw signals from the DAQ instead of converting all of the signals when only a trend is being discussed. All three of the pressure transducers (the two absolute pressure transducers and the differential pressure transducer) are calibrated by means of the SMART protocol designed into them. A SMART communicator is used to check and reestablish the calibration periodically.

The final measurement needing to be made is the temperature of the working fluids in the system. These temperatures are necessary in order to properly define the state of the fluids. Properties such as density and viscosity, which are both used in the data reduction and in the construction of the final correlation. To take these measurements, two T-type thermocouples have been inserted into the incoming flows of both the air and the water. Both measurements take place along a length of pipe near the respective flow meters and in a section of the flow which is considered fully developed. Both thermocouples are connected directly to the data acquisition system so that continuous temperature data can be taken from the system and are calibrated by LabVIEW using its built in cold junction. The high speed camera used for visualization is an X-Stream XS-4 CMOS camera with a resolution of 512×512. It has a maximum capture rate of $5000 Hz$.

4.4.2 Data Acquisition System

The data acquisition system, or DAQ, utilized in this experiment consists of a Dell Precision Desktop connected to a National Instruments SCXI-1000 chassis. Within the SCXI-1000 chassis is a SCXI-1102b analog module connected to SCXI-1300 terminal block. Connected to the block are the data connections to the above described instruments. The physical specifications of the system as it is currently described allow for a data collection rate of well over 50 kHz. While this is well beyond the needs of the current experiment, such data acquisition power would greatly aid in any visual acquisition setups. The final data collection rate was set to be 10 Hz.

The data acquisition system accepted analog voltage signals between 0 and 5 V. A terminal box is responsible for converting the few instruments that produce current signals into voltages that the DAQ can read. The thermocouples create a 0 to 10 mV signal which is conditioned and amplified in the SCXI-1300 block. A LabVIEW program gathers the voltage signals and displays them on the monitors. The program also applies the calibration curves described above. A screen shot of the LabVIEW front panel is given in Figure 4.8.

4.4.3 Data Reduction

After the data has been taken, it needs to be reduced into a usable form that can be analyzed and understood. The raw signals that are gathered by the DAQ are internally converted to physical properties by the LabVIEW script. However, data in this form is not in an optimal state and need to be reduced to usable numbers. Once these data are in the proper form, they still need to be correlated and adjusted to better suit the problem at hand. Several MatLAB scripts were written that can read the data as it is reported by LabVIEW, perform all of the necessary mathematics, and output values that are both meaningful and useful.

The data is output from the DAQ in spreadsheet form and the data for each run takes up one data file. However, the most important data with respect to CCFL are

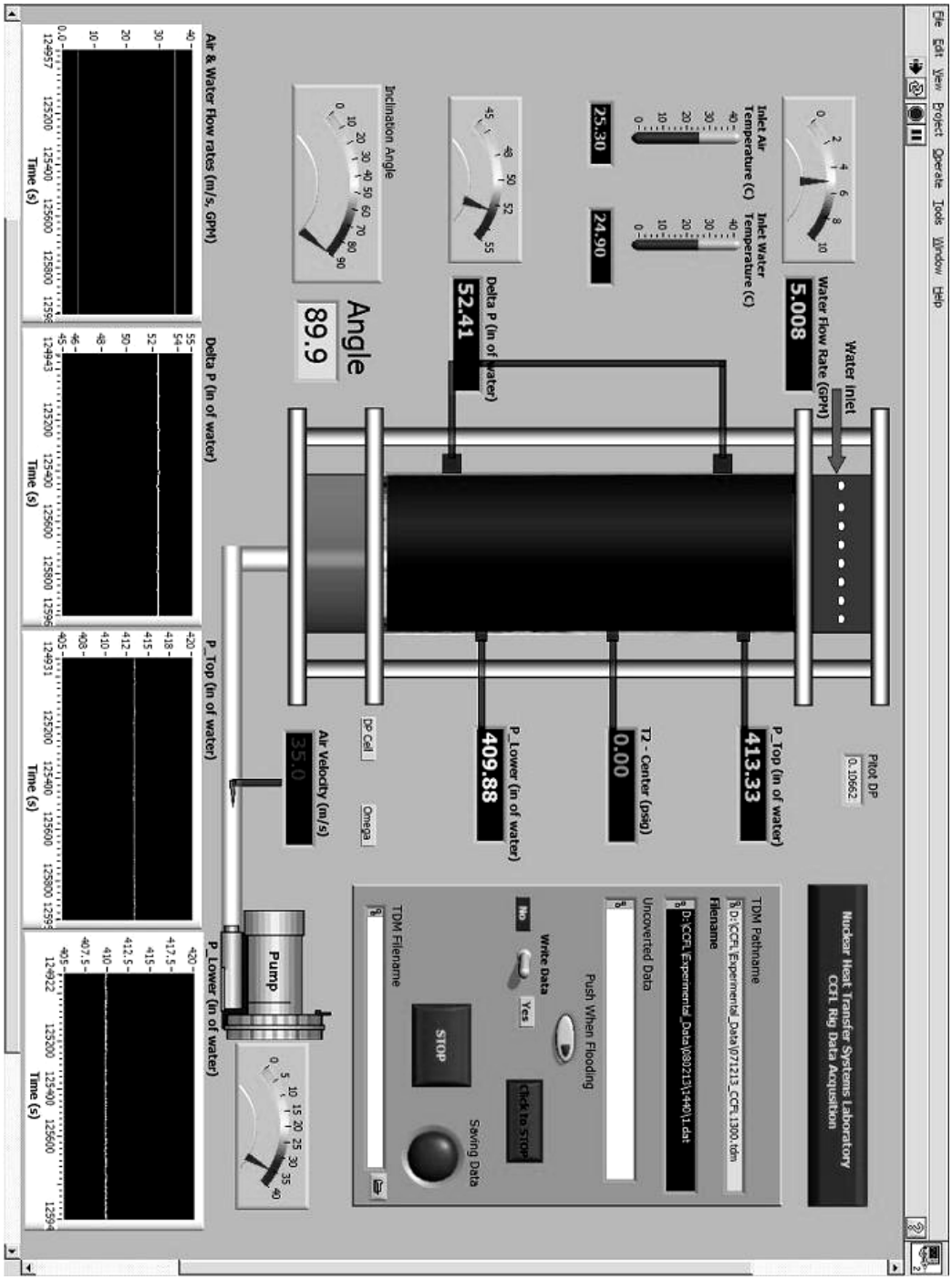

Figure 4.8. The front panel of the LabVIEW program used to collect data.

the steady flow rates and the differential pressure readings that occur at the flooding velocities. That is, the last steady and constant segment of data that is taken before

CCFL contains all of the information needed to perform the analysis. The LabVIEW program contains a trigger button on the front panel that allows for the experimenter to indicate when the system is being adjusted, i.e. when the air flow rate is being increased. This trigger fills the last column of the data spread sheet with either a one or a zero; a one for a transient system, a zero for a steady state system. The first task of the MatLAB script is to recognize when in the data file the system is being adjusted and when it is steady. By reading this column, the script parses the data into separate matrices and writes them to appropriate Excel spreadsheets. When the last reading in the spreadsheet is reached, the script then determines the point of CCFL from the last stretch of steady data. This is accomplished by reading the first 30 points in the spreadsheet and averages them. This average is then compared point by point in the spreadsheet until the characteristic pressure drop is encountered. The script marks this location and performs its averaging and error analysis on the entire final steady data set up to this point.

5. STANDARD OPERATING PROCEDURES

The standard operating procedures are presented here both as a guide to operating the experiment and as an in-depth explanation of how the experiment is designed. As with all experiments, care should be taken to fully understand the procedure and to follow all steps to their fullest and in the order presented. The SOP are broken up into three parts: Start Up, Experimental Run, and Shut Down. All component names are referenced to in the following figures.

5.1 Startup

The startup procedures should be conducted before all test runs unless it is deemed unnecessary by an initial check of the pressure reading instruments. The start up procedures are primarily used for two reasons. First, they allows for the experiment to be run safely by including a double check of all valve initial positions. These starting positions ensure that if any of the first experimental run steps are omitted no serious harm will come to the experimenters or to the equipment. Secondly, the startup procedures initialize the pressure instruments, i.e. the differential pressure transducer and the two absolute pressure transmitters. Since all three of these probes require wet connections to the test section, it is important that all pressure lines are purged of air. Also, since some of the pressure lines occasionally void during operation or rest, it is necessary to bring these readings to at least the same relative reading before each run. Doing so increases the accuracy of data taken.

5.1.1 Initial Steps

To ensure the safe use of this equipment (both to the experimenter and the facility) there are certain primary steps which must first be taken. A schematic of the test section valve positions is given in Figure 5.1 It is necessary to close all valves related to the test facility. These valves respectively isolate the lower plenum from the drain; isolate the test facility from the main water supply; and ensure full air velocity from the blower. The reasons for each valve's position upon starting the procedure are given below.

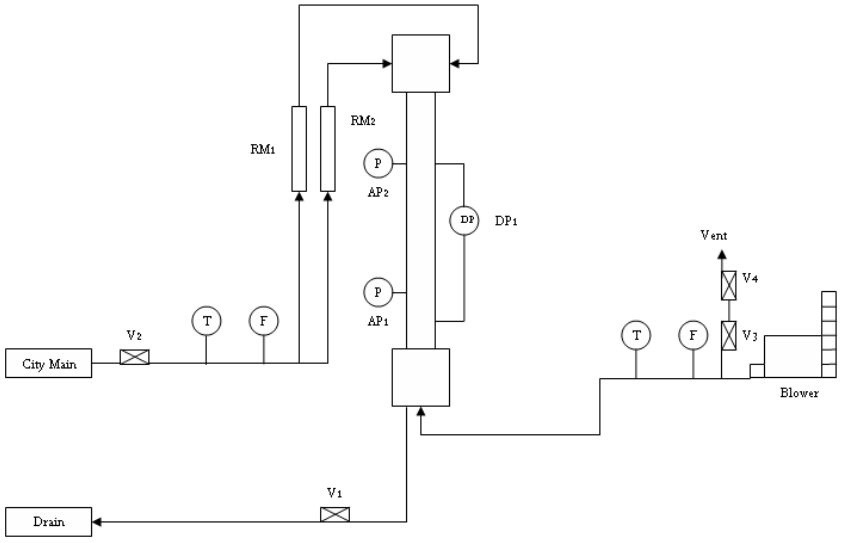

Figure 5.1. Schematic of the CCFL facility.

The valve on the liquid collection tank (V1) is set to the closed position during start up to isolate the facility from the drain. While this is not of extreme importance to the safety of the experiment, it does allow for a more thorough state of rest for the experiment. That is, when a pre-run walkaround is performed (see below) the closed drain line puts the system in a totally isolated state, in addition to the valve positions listed below. The valve connecting the water main to the experiment (V2) in a closed state isolates the facility from the main water supply. Closing this valve during the start up procedure ensures that if the rotometers are left open, no water

will enter the system accidentally. This is fairly important with respect to purging the pressure instrument lines as unwanted water flow in the test section could alter the initial measurements gathered thereby. The bypass valves located on the blower (V3 and V4) are redundant control mechanisms situated in series. Both act as a bypass control mechanism for the air supply subsystem. When open, these valves bypass a majority of the air flow to the atmosphere. When either one of them is closed, all air supplied by the blower is directed into the test section. See the Experimental Run section for more details on the function of these valves.

5.1.2 Purging the Pressure Lines

There are two subsystems for the collection of pressure data from the test section. The first consists of two absolute pressure transducers, isolated from each other and located at two separate axial locations on the test section. The first pressure port, used for the lower absolute pressure transducer, is located 9 inches above the bottom of the test section. The second pressure port, for the upper absolute pressure transducer, is located at the same radial location but is placed 59 inches from the bottom of the test section. While both transducers are connected via the purging subsystem, they are isolated from each other after the purge has been completed. The differential pressure transducer and its associated ports are located on the radially opposite side of the test section. The ports for this instrument are located at 6 inches from the bottom of the test section and again 59 inches from the bottom of the test section. Again, while the appropriate ports are connected by a purging subsystem, each is isolated from the other during operation and data taking. Schematics of each subsystem, absolute pressure transmitter side and differential pressure transducer side, are shown in figures 5.2 and 5.3 respectively. It should also be noted that while the absolute pressure transducer subsystem procedure is given first here, the differential pressure transducer system may be purged first.

5.1.3 Purging the Absolute Pressure Transducers

Refer to figure 5.2 regarding the names of the appropriate valves discussed below. The process is started by opening all valves in this subsystem. This will allow for the pressurized water to enter all lines of the subsystem and initially clear all air from the tubes. Once a sufficient amount of water is seen to be leaving the ports into the test section the valve nearest the lower absolute pressure transducer, PV2, is closed to isolate it from the purging system. As water continues to leave the pressure port for the upper absolute pressure transducer with increasing velocity, the isolation valve nearest it, PV4, is cycled several times to ensure all air has been removed and that the tubes are completely filled with water. Once it has been sufficiently determined that the upper absolute pressure transducer lines are free of air, the isolation valve is closed. The subsystem has now been purged. In order to judge the success of the purging, the data acquisition system is started to see what pressure each pressure transducer is measuring.

Since these modules are absolute pressure transducers, each will have a background reading of atmospheric pressure. Also, the preferred measurement for the transducers is in units of inches of water. If they were to be left open to the atmosphere, the base reading would be 406.7 inches of water. However, due to the nature of the test section cage and the tubes connecting the pressure transducers to the test section, an associated hydrostatic pressure is induced in the transducers. For the lower absolute pressure transducer, the transducer itself lies approximately 3 inches below the pressure tap. Thus, a reading of about 409 inches of water would indicate that the lines have been adequately purged. Similarly, the upper absolute pressure transducer lies approximately 9 inches below the upper pressure port resulting in an appropriate initial reading of 415 inches of water. Once the readings have been confirmed as those given above, the absolute pressure transducer system can be considered purged and functional.

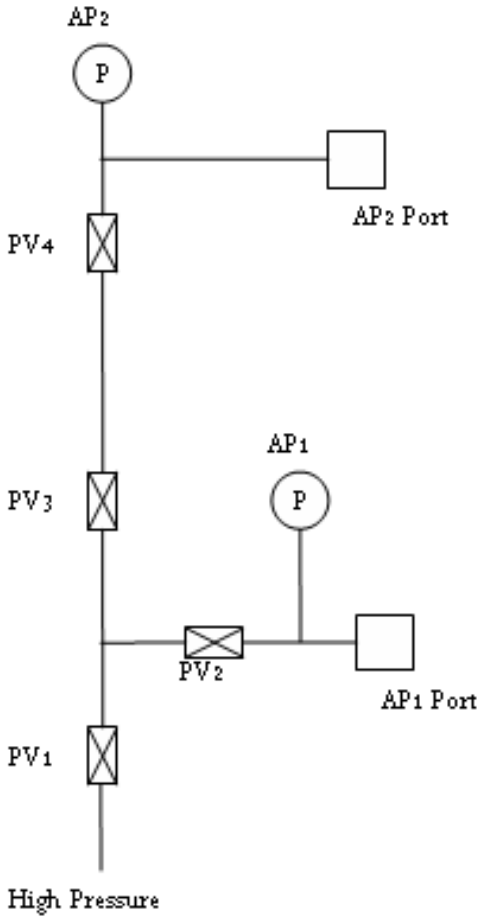

Figure 5.2. Absolute pressure transducer schematic. This figure illustrates all of the valves and lines mentioned in the purging the absolute pressure transducers section.

5.1.4 Purging the Differential Pressure Transducer

Refer to figure 5.3 regarding the names of the appropriate valves discussed below. This process is similar but notably different from the one described above for the absolute pressure transducer subsystem. The first step in purging the differential pressure transducer system is to make sure that the feed from the pressurized water source is properly connected. Once connected, all valves within the differential pres-

sure transducer subsystem are opened. Water should be seen to exit both the upper, high pressure port and the lower, low pressure port. Once a significant amount of water has passed through the two ports, the valve closest to the upper pressure port is closed to isolate it from the rest of the system. The bypass valve, DPV4, should then be cycled several times to eliminate any air bubbles trapped in the tubing network leading to the lower pressure port. Once it has been established that the DPL lines are free of air, the bypass valve is closed. The upper port isolation wave is opened and again water is allowed to flow through the upper port. Cycle the three way valve to ensure all air bubbles are purged.

Again, it is necessary to check whether or not the purge of the lines was successful. Similarly to the absolute pressure transducer side, a reference value needs to be reached in order to ensure that the data taken is sound and repeatable. This is again achieved by noting the pressure reading from the DPT on the DAQ screen. Since this transducer is of a differential type, the static pressure difference between the ports is of importance. The ports are located 52 inches apart from one another so it follows that the static reading without any flow should read approximately 52 inches of water. This is in relation to the fact that if both tubes from the DPT to the respective ports are full of water, the resulting pressure differential should be equal to the head of that water. If, however, the DPT outputs something other than 52 inches of water, the lines to the differential pressure transducer may also need to be purged. This is accomplished by the use of bleed valve located on the back of the differential pressure transducer system. The bleed valve is a three way valve connected to tubes leading from the bleed ports on the differential pressure transducer. In the nominal, aka closed, position, the valve knob should point away from both tubes. To bleed a port, simply turn the valve knob so that it point to the port that needs to be purged. To purge the DPT itself, merely point the knob to one port and then the other, making sure not to let too much water drain from the system. Once the DPT has been purged, repeat the previous procedure to re-purge the differential pressure transducer port system.

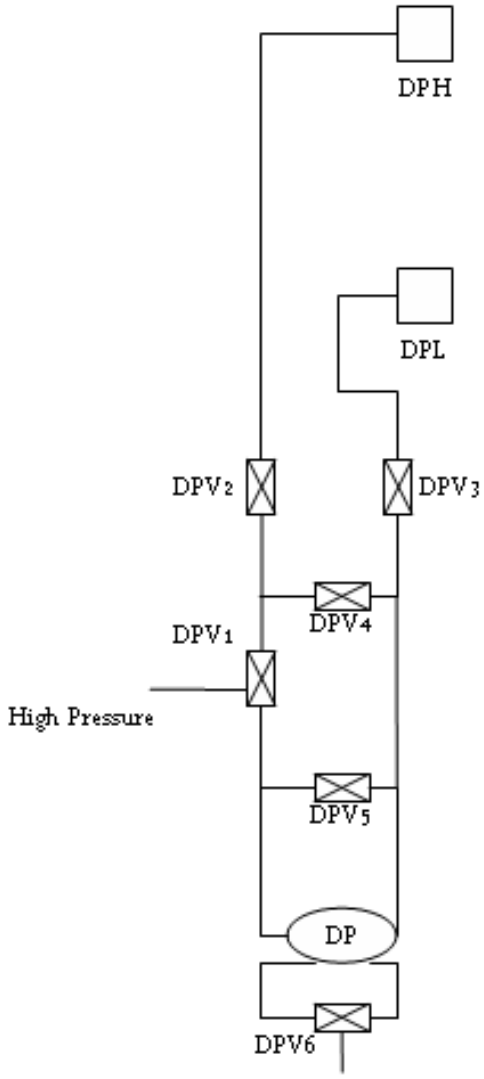

Figure 5.3. Differential pressure transducer schematic. All valves and lines associated with the differential pressure transducer lines are shown here.

5.1.5 Final Start Up Procedures

After the pressure instrumentation lines have been successfully purged, the final steps can be taken before running an experiment. These steps are needed to bring the facility to the proper running state with respect to the position of valves and the overall conditions. It should also be noted that the following steps are given in no

particular order. The importance of these operations is not their sequence but their completion. At this point, the drain valve (V1) from figure 5.1 must be opened to allow all fluid entering the system to exit it. If this step is omitted, water could back up in the lower plenum and enter the air inlet lines. This might result in damage to both the pitot tube air flow instrument and/or the blower itself. Opening the water collection tank valve will also drain any water in the catch basin accumulated from the purge, allowing for a more uniform starting state. Next, the blower bypass valves will be open to set the blower to a starting state. If these valves are set to closed, full air flow will be directed to the test section when the blower is turned on. This results in an incomplete test since the approach to CCFL will not be recorded. Also, any test has the tendency to alter the water level in the pressure instrument lines resulting in the need to re-purge them. When all of the preceding steps have been successfully completed in their entirety, the actual test may be run. The zero readings for the pressure transducers should be $52.0 in H_2O$ for the differential pressure transducer and $515.0 in H_2O$ and $509.0 in H_2O$ for the upper and lower absolute pressure transducers respectively. It should also be noted that all steps in this section should be completed before running the experiment so that nothing untoward befall the experimenters, the equipment, or the final data desired.

5.2 Test Procedures

The following section outlines the proper and standard methods for conducting an experimental run on the CCFL facility. The steps given here should be run in the order given and in their entirety. Any deviation could result in damage to the system, the data acquisition system, or injury to the experimenters. A test matrix for each individual test provides the primary operator with a physical means of recording data and taking notes. Since each test run consists of several approaches to CCFL, it is handy to have a rubrik for recording the data for each approach. The necessary data for each test are the date, time, and liquid flow rate.

The first step in the run is to open the main water valve. Since the rotometers should be closed at this point, incoming water should pressurize the lines up to the rotometers. The rotometers should slowly be opened and set to the desired flow rate. Both rotometers should read the same value to ensure that equal flow rates at the upper plenum be achieved. To do so, they will have to be adjusted until this state is achieved. It has been witnessed that it takes several seconds for the flow to fully develop in the system. That is, once the rotometers are opened, the flow rate measurement as returned by the magnetic flow meter slowly increases until it reaches a final state. Because of this phenomenon it is necessary to let the system stabilize before the next steps are taken. Once the system has come to steady state, a base line measurement is taken without any air flow in the test section. This is done by first naming the file in the DAQ screen (preferably as *0.dat), clicking "Record Data" button on the DAQ screen and letting the data record for approximately 10 seconds before clicking "Stop Recording". This measurement will act as a control to compare the flow rates with air later in the test.

The blower is now switched on with the bypass valves open to allow for minimum air flow in the system. Even though the bypass is open, there is still a measurable amount of air flow through the test section. The write data file is renamed and once the system comes to steady state, data is again recorded for approximately 10 seconds. It is now required to incrementally increase the air flow rate to properly record the entire approach to CCFL. Just before the system is perturbed, the trigger button on the DAQ screen is switched to "on" signifying that the system is in a transient state. To increase the air flow rate incrementally, the bypass valve must be closed slowly and with fine control. To facilitate this, a 10-turn gate valve is used on the bypass with the initial position set to full open. From the fully open position and at steady state, this gate valve is moved a maximum of one half (1/2) of a turn closed and the system is allowed to equilibrate making sure to record the air flow rate on the test worksheet, remembering to click the trigger button to set the trigger to off. Data is taken, making sure to change the file name, for approximately 10 seconds. This

process is then repeated until sustained flooding is observed, making sure to record the air flow rate at which CCFL occurs on the work sheet. After the final data are taken, the air bypass line is opened and the water allowed to flow without air. A final data point is taken. The blower is then shut off at this point.

If further tests are scheduled, the pressure instrument starting conditions are checked per the start up section. If the measurements are within the prescribed limits, the procedure can immediately be repeated for the next liquid flow rate. If, however, the measurements are outside the bounds set, the lines must be purged again before any tests are run. Also, if there are no more liquid flow rate tests scheduled for the current inclination angle, the procedure must start again at the beginning of the start up section, but the shut down procedure need not be performed.

5.3 Shut Down

This section details the steps taken to bring the facility to a "Final Shut Down State" from which the start procedure may be run for the next set of experiments. Since the only secondary equipment of safety concern is the blower, little work needs to be done to safely return the lab to a non-working state. Since the water main has been isolated during the final steps of the actual procedure and the blower has been switched to off, the system itself need only be safely isolated from these ports. The rotometers are closed completely to ensure that if the main is switched on, no water will enter the system. At this point it is desired to let the system "dry", that is let all of the accumulated moisture in the system settle to its lowest point. While this step is not at present necessary, for future work regarding visualization it will be necessary to dry the test section so that clear pictures can be obtained through the test section.

Now that the system has been fully closed, the levels in the pressure instruments should be checked via the DAQ system. Checking the levels gives a preliminary estimation as to how these ports react to the tests being run. Also, it will give the

experimenter an idea as to how involved the next purging will be, saving time in the long run. Once a check of the levels has been completed, a final walk around of the facility should be taken. All plumbing junctions should be checked for leaks and care should be taken to distinguish between water accumulated from leaks and water accumulated from the normal operation of the facility. All electronic connections and terminal blocks should be checked for both water and that the necessary connections are still good. The test section and all associated acrylic attachments (e.g. plenums and tubing) should be checked for cracks or other instances of structural stability. Finally, the cage and frame should be checked for any structural problems or loose fittings. Once a complete walk around of the facility has been completed, the experiment may be considered "Shut Down".

6. RESULTS

This section presents the data gathered using the CCFL facilities described above. It begins with a brief description of flooding as it is defined based on these experiments. Then, a description of the characterization tests performed on the facility is given. These test help to confirm the data taken. Next, a section covers the raw data taken with the experimental facility. A description of the error analysis methods used to judge the data is provided. The steps taken to correlate the data are presented. These involve the initial observations and trials used to create the final analysis. This error is then added to the data points in the form of error bars and presented. A final section provides the visual data taken for the experiments.

CCFL should also be fully defined as it relates to the gathered data. A full definition is found in Section 2. For these experiments, flooding is defined as the occurence of flow reversal in a countercurrent flow system which is accompanied by a characteristic pressure drop across the test section.

6.1 Characterization Tests

In order to have confidence in the data that the CCFL facility produces, it is necessary to characterize several of the attributes of the system. This includes testing for:

- Test Section Orientation
- Working Fluid Flow Rates
- Annular Liquid Film
- Air flow through inlet/air flow approach

- Air supply history
- Instrument shakedown tests
- Absolute Pressure transducers

For the current set of data and for the eventual derivation of a correlation, the test section must be in as close to a vertical position as possible. In order to check this orientation, three methods were used. The first required the use of a standard carpenter's level, also known as a torpedo. The torpedo was placed on the test section at two radial locations, one in the plane of inclined motion to check that the winch and counter torque springs are equal. The second radial location is 90 degrees from this position to ensure that the rotational bearings are properly aligned. This will give a rough estimate of the orientation and allow for the test section to be close to vertical to a first approximation. The next test allowed for a more accurate measure by using a plumb bob. By hanging the bob from the upper plenum and accurately measuring the distance of the test section from the line, a much more accurate confirmation that the test section is vertical can be achieved. This test was also conducted at two radial locations similar to the previous tests. The final test for vertical orientation involved the use of a laser level. This test was used only as a redundancy to the plumb test as there is no real way to improve upon it. Again, testing at two radial locations, the laser level was pointed at the edge of the test section. When the edge was found, it was checked against the level line.

Another test used to characterize the test section to double check the flow rates of the working fluids. The easiest way to check the liquid flow rate was to double check the measurement with the rotometer readings. For a range of liquid flow rates, the magnetic flow meter readings were compared to the rotometer readings. The more inaccurate instrument would be the rotometer with the $\pm 0.2 GPM$ increments. The test is used to make sure that there is no discrepancy between the flow meters. The pressure gradient across the test section will change as the liquid flow rate changes. As the liquid flow rate increases, the pressure gradient will decrease due to the increased

amount liquid in the test section. That is, as the the liquid flow increases, the film thickness of the liquid increases adding to the body forces on the water.

The air test double check was accomplished by testing to different kinds of pressure measurement devices. The first test used two independent absolute pressure transducers, one for the center static pressure and a second for the stagnation pressure, to measure the pressure difference. The difference between the readings was taken as the pressure differential. This differential, however, is inherently more erroneous than using a single differential pressure transducer. The two absolute pressure transducers return an error of approximately $\pm 0.7 m/s$, while the differential pressure transducer returns an error of $\pm 0.16 m/s$ for the maximum centerline velocity. As long as the two readings were comparable, the pitot tube can be considered to be an accurate measuring device.

Some observations about the facility while it is running should also be added. An important check on the state of annular flow that can be observed in the lower plenum while the water is running in the test section. The bottom of the test section is clearly visible through the lower plenum as is the water running from the test section into the lower plenum. At all pre-flooding liquid flow rates a clear annular sheet of fluid is seen running into the lower plenum. This indicates that the flow within the test section is annular in nature and assures the experimenter that an annular regime is in fact being observed. Furthermore, one can look down the air outlet pipe on top of the experiment for another form of visual inspection. Since the air outlet is a 2-1/2 inch tube, it is easy to see what is happening in the test section. Shown in figure 6.1 is a photograph of the inside of the test section as viewed in this manner.

As can be seen in the picture, the flow regime is obviously annular and there are very little disturbances on the film.

Another annular flow characteristic can be seen from visually observing the test facility. At the pressure ports located on the test section, there appears to be waking of the liquid film. A snapshot of this phenomenon is shown in figure 6.2.

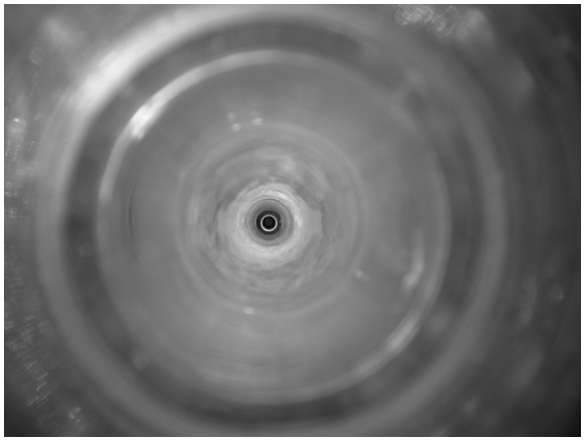

Figure 6.1. An image of the flow in the test section without air flow showing the annular nature of the flow regime.

In this figure, the wake is seen as the region between the two lines sprouting from the pressure port and extending down the test section while simultaneously spreading out. This wake is caused by the pressure port penetration into the test section. While no structures actually pass through to the inside of the test section, the hole milled into the test section itself was quite large, 1/4 inch, and does disturb the flow. This represents a design flaw. However, once there is air flow in the system, these wake lines visually disappear and it is believed that an effect they may have on destabilizing the flow is miniscule due to the fact that the flow is fully turbulent for all flow rates tested as defined by equation 2.14.

Early designs were plagued by an air supply problem. These included an air inlet section design which proved to cause too great of a pressure drop. This problem was compounded by the pressure drops of the approach lines to the test section. The original hard plumbing was replaced with $1 - 1/2in$ inner diameter flexible hosing which reduced the length of the approach and the friction seen by the incoming air. The friction being the standard tube wall friction for fluid flows.

Originally it was assumed that a large air compressor could supply the needed air flow rates using only pressure as a driving force. However, it soon became apparent that the compressor on hand could not deliver the needed flow rates for a long ex-

Figure 6.2. An image showing the appearance of wakes in the flow during a liquid only run of the facility.

periment time. The cause of this was insufficient knowledge of the duration and air requirements. That is, a compressor and tank are meant only to supply pressure and not necessarily air, at least not in great quantity. While the compressor could supply a pressure of upwards of 125 psig, it could not do so for more than a brief moment. Thus, it became impossible to generate enough air flow for a long enough time period to induce flooding in the experiment. The solution to this problem came in the form of a regenerative blower. Blowers have historically been used in flooding experiments

The instruments were also tested to ensure their accuracy. All pressure sensing equipment was calibrated, or their calibration checked, before being used on the facility. Also, the thermocouples were exposed to a wide range of temperatures to ensure that they were working correctly. Finally, as stated above, the liquid flow rate measurements were double checked against the control rotometer readings for a variety of flow rates.

It should also be noted that the length of the hose approaching the test section from the air blower was changed in order to expand the range of data taken. The longer hose was to be used if inclination angles were to be tested. However, this induced a large frictional pressure drop across the air inlet and thus reduced the available air velocity. The shorter hose reduced the frictional pressure drop and a higher maximum air velocity could be used. It was found that this had no effect on the trends or on the correlation results.

Finally, the absolute pressure transducers located on the test section are used to gather state data for the experiments. These two instruments provide valuable data that is later used by the data reduction scheme about the properties of the fluids being used. Using the thermocouples to measure the temperature, the physical properties of the fluids can be found.

6.2 Raw Data and Observations

For early tests using the same liquid flow rate, the increments by which air flow rate is first increased are large so that a general understanding of the CCFL point can be obtained. Once flooding is observed to occur, the resulting air flowrate is recorded and the air flow rate immediately reduced to a point at which flooding no longer occurs. This would complete one "run". The subsequent runs are conducted by starting the air flow rate, without altering the water flow rate, at a point much lower than the expected air flow rate to induce flooding, and then very slowly increasing the air flow rate. The system is then again allowed to reach an equilibrium and steady

state data are recorded. Thus, for each liquid flow rate, the final run will contain the minimum air flow rate at which CCFL will occur. For runs which contain many incremental air velocity increases, the data for each steady point can be plotted as a function of air velocity and pressure gradient across the test section. An example of this is shown in figure 6.3.

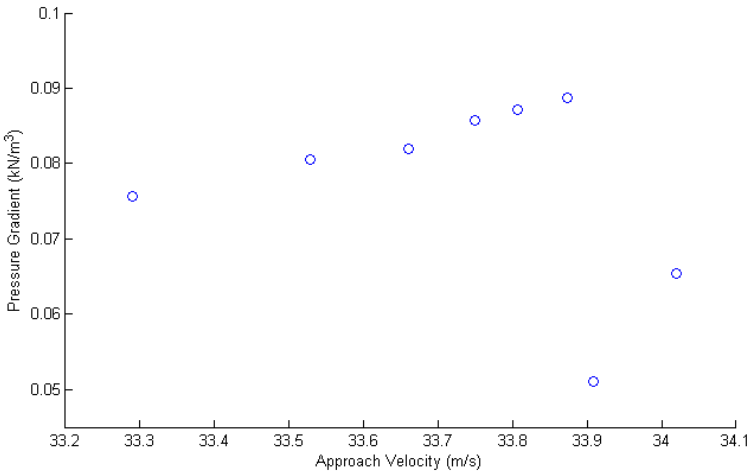

Figure 6.3. Slow run of data leading up to the flooding point by small incremental steps

This figure illustrates the slow run technique. The ordinate is described as the pressure drop seen by the liquid due to the air flow in the test section over the distance between the pressure ports. By taking many data readings at steady air flow rates, a more accurate picture of the run up to flooding can be seen. The final portion of each run contains the flooding point. That is, the average velocity of the final steady interval will be the flooding velocity for a given liquid flow rate. In figure 6.4, a typical final steady interval segment of a run is shown.

When the data from each run are examined, several key factors must be considered. As can be seen from the figure, the air velocity is a constant until the flooding point. At this point, the velocity drops significantly and begins to exhibit an oscillatory nature indicative of CCFL for this experimental facility. The important part of this data is the time before this point. That is, all data preceding the drop in

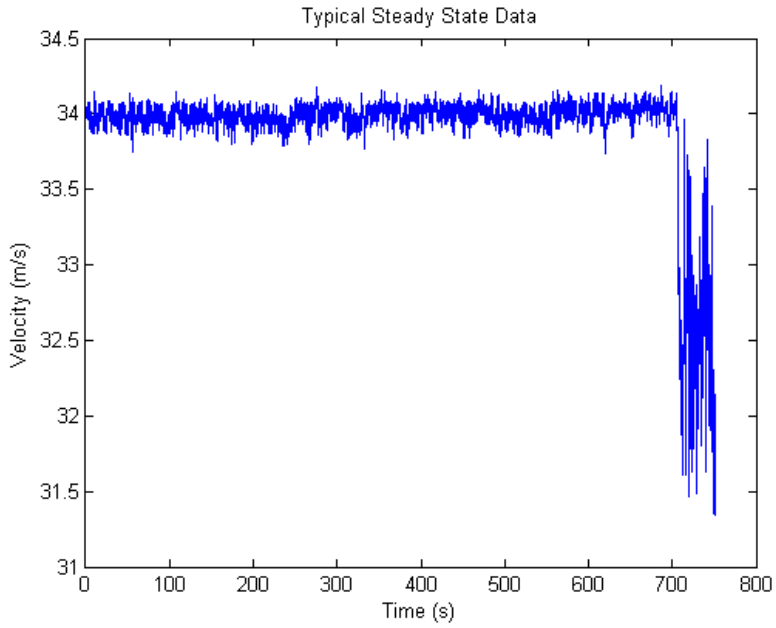

Figure 6.4. Typical data plot showing the centerline air velocity as a function of time for a steady state data run that achieves flooding.

air velocity should be averaged over the length of time preceding it. This average velocity, averaged over the time elapsing before the CCFL point, is the flooding air velocity.

The air flow rate at which flooding occurs is not always the point at which sustained flooding was seen to occur. An unstable flooding band was observed during several very slow approaches. It has been seen that when the flow rates of the system are very near to the flooding velocities, flooding may begin and progress for several flooding undulations, but then suddenly stop and return to a non-flooding state. This is shown in figure 6.5. While logic would dictate a priori that there are extremely high velocities which will always result in flooding and low air velocities which will always result in countercurrent flow, there appears to be a band of velocities in which flooding may or may not occur and remain stable. That is, from the experiments run, there are air velocities for any given liquid velocity which will result in periodic or unsustainable flooding in the system.

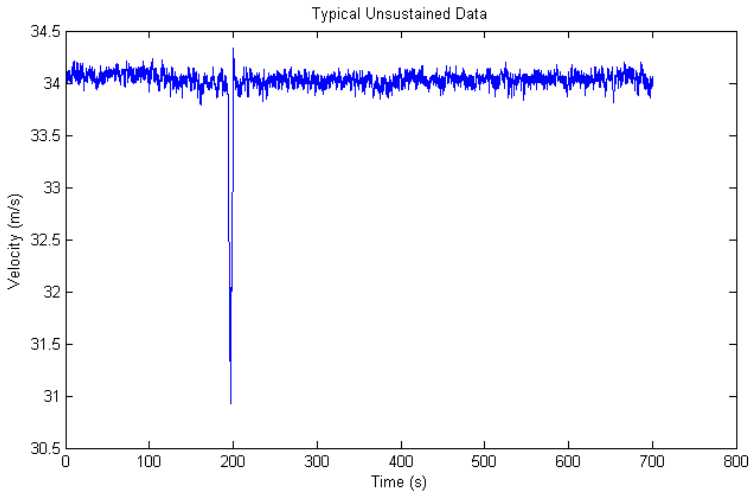

Figure 6.5. Sample data point in which flooding appears to occur but soon reverts back to a counter current flow

This leads to a discussion about the time given for each air velocity increment. It has been observed that even at air velocities over the CCFL point, it may take as long as 2 or 3 minutes for flooding to occur. Because of this, it is necessary to allow the system to run at steady state for at least 5 minutes per air velocity value before any conclusions can be drawn. Conversely, flooding may not occur at one velocity for over 15 minutes, but when nudged to a higher air velocity, flooding is almost instantaneous. The result is that each air velocity should be run for 10 minutes to account for the time needed to generate CCFL and that the proper air flow rate is found.

While the onset of flooding can easily be recognized by the chaotic and violent actions of the fluids in the test section, it would be preferable to have a concrete, easily identified, and recordable method for deciding when CCFL is reached. It has been pointed out in the literature survey that there is an associated differential pressure drop in an experimental test section on the onset of flooding [10]. If this pressure drop is seen to occur in the test section, it would be an acceptable indicator that CCFL has been reached.

Shown in Figure 6.6, such measurements have been made in the test section and as a result a reliable method for indicating CCFL has been reached. From the figure it is obvious that the pressure across the test section is essentially constant up to the point of flooding. When this point is reached, that is, when the conditions in the test section are right, a large drop in the pressure difference across the test section is seen along with the associated drop in air velocity. From the data it appears that this drop in pressure across the test section happens almost instantaneously, indicating that there is no delay in the change of air velocity.

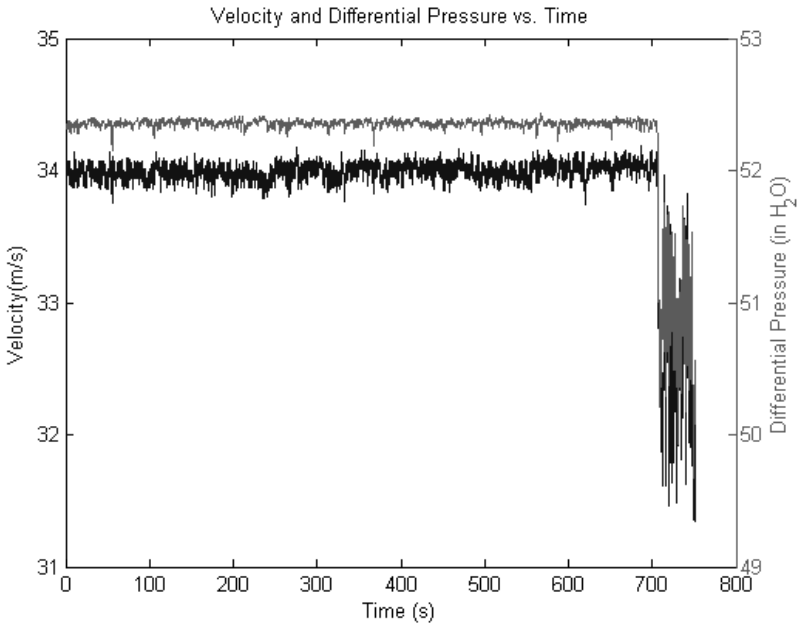

Figure 6.6. Simultaneous behavior of pressure drop across the test section and the gas velocity at the onset of flooding.

From visual observations at the point of flooding, several conclusions can be made. The first point is that CCFL results in the formation of a visible wave towards the bottom of the test section. This wave then proceeds up the length of the test section carrying a large portion of the liquid in the test section with it. Additional waves may or may not form while the initial wave is travelling upwards. The flooding wave is seen to begin above the lowest pressure port. Since this wave is above the pressure port,

any pressure that is necessary to push it upwards would be seen by it. The pressure reading is the low pressure side of the differential pressure transducer, accounting for the weight of the water head for the upper pressure port. Therefore, any increase in pressure at this location will result in a decrease of differential pressure, and thus return the observed drop in differential pressure.

6.2.1 Data Selection for Correlation

All of the acquired data are presented in the above section. However, there are necessary reasons for disregarding some of these data when considering the construction of a correlation for predicting the onset of flooding.As noted above, many tests exhibited intermittent flooding and a return to annular flow. For each liquid flow rate, it is necessary to find an approximate span of air flow rates that will induce flooding. This is analogous to using a rough estimate to later zero in on an exact solution. When conducting experiments, it is common practice to find the rough flooding point by using large incremental changes in air flow rate and recording data for shorter time intervals. This results in overshooting the actual flooding point, sometimes to a large degree. It is these points that need to be removed when formulating a correlation because they do not reflect the actual CCFL. It is this fact that necessitates the need to run several tests at one liquid flow rate, the first hunting run and several slow approaches to zero in on the actual air flow rate.

Another source of erroneous data points is the "unstable band". This refers to the data points where flooding is not seen to occur sustainably. As mentioned above, at some air flow rates just below the actual CCFL, flooding will start and then stop. This has the opposite effect than the one described previously; these values underestimate the air flow rate necessary to induce flooding. Once these points have been identified and removed, the process of discovering the correlation of parameters can begin.

6.3 Visual Images

Pictures of the CCFL phenomenon were obtained by means of the high speed camera. The basic results are shown in Figure 6.7. In this series of pictures, the onset of flooding is captured at a frame rate of $2000Hz$.

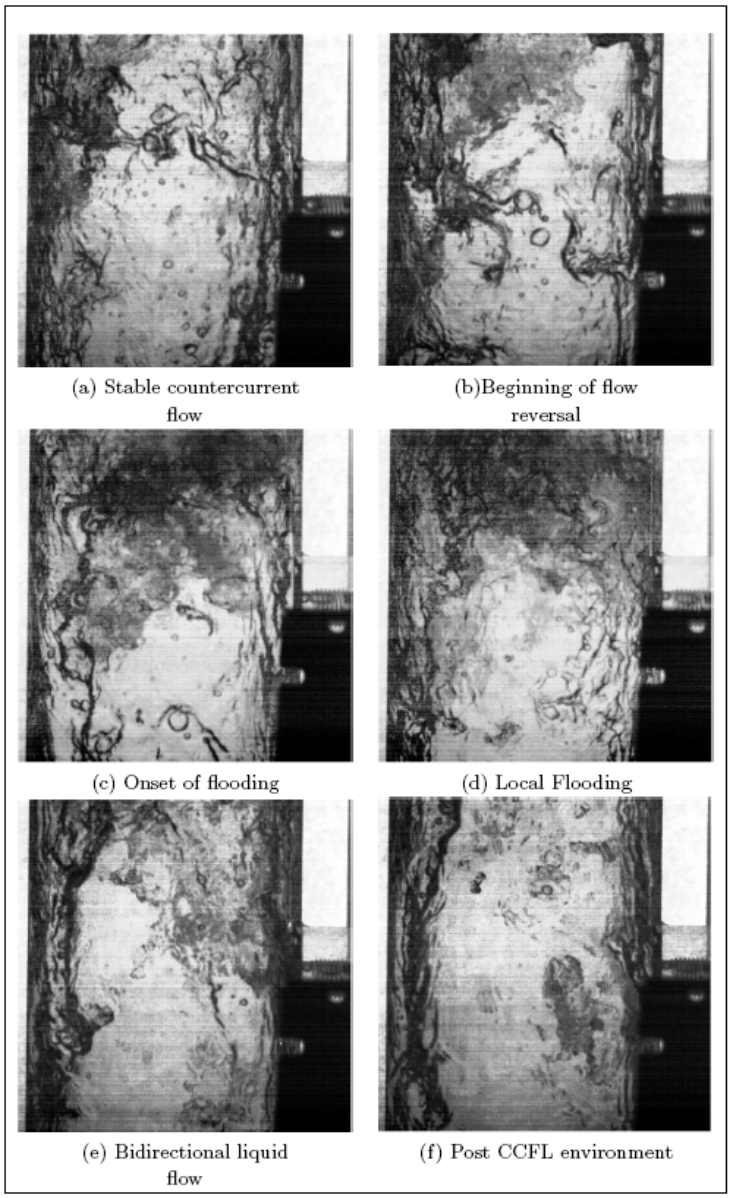

Figure 6.7. Series of pictures capturing the onset of flooding.

In these images the state of the fluids in the test section changes dramatically. In (a), the system is at steady countercurrent flow at the air velocity which will eventually induce flooding. In (b), the beginning of flow reversal is taking place. The chaotic nature of CCFL is starting to become visible near the top of the picture. Flooding has begun in (c) as evident by the violent mixing of the phases shown as the dark cloud. In (d) the local layer of liquid has started to move upwards. In (e) the liquid film is moving in two directions. Finally, (f) the liquid flow near the wall is still in the downwards direction while at the interface the liquid is progressing up. It should be noted that another wave similar to the one shown in (c) will form near this location and the process will repeat.

6.4 Error Analysis

Once the data can be satisfactorily reduced to a usable form, the process of assessing its accuracy begins. This was done to both double check the data against itself and to perform an error analysis on the data. Error in the tests comes from two sources, systematic error and random error. Systematic error is that error which is inherent in the experimental equipment. Random error is error incurred in the measurement by the experimental process.

6.4.1 Random Error

In order to verify that the system is exhibits acceptable repeatability, many tests runs were conducted at a set flow rate, 6.8 GPM. This test case was conducted 20 times in order to obtain a large enough sample of test data for a statistical analysis to be valid. Once this was achieved, a standard statistical analysis was done on the results [43]. Presented here are the results shown in figure 6.8.

It is obvious that a standard normal curve can represent the results for this one liquid flow rate. This lends credence to the data and ensures the repeatabilility of further tests. Furthermore, the standard deviation from this set was found to be

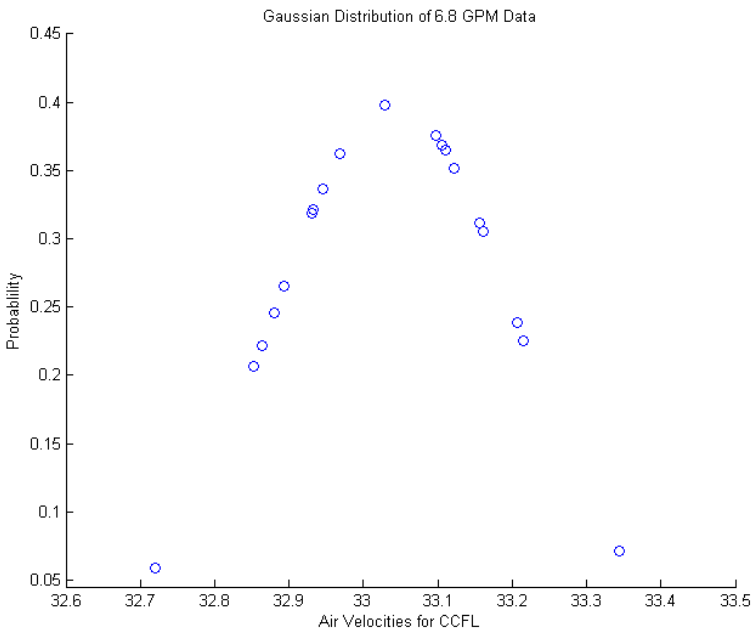

Figure 6.8. Statistical fit to the collected data at one liquid flow rate.

$0.16 m/s$ in air velocity. This corresponds to a difference from the mean value of less than 0.5%. It is assumed, based on the precision illustrated through this statistical analysis, that this error can be assigned to other air velocity values in the error propagation calculations.

6.4.2 Systematic Error and Propagation

There also exists error in the system in the form of the data taking instruments. This error must also be accounted for and reported. Each instrument has its own accuracy which is given in the manuals. This error must then propagate through all calculations using this value. There is also an error associated with the conversion of units and the geometric measurements of the facility. The standard rules for error propogation were used to report the error associated with each data point. This error was traced through every step of the calculations and is displayed as error bars on the following plots. The systematic error can be catagorized by several different

errors that must be combined. Given in table 6.1 are the sources of errors from the experiment.

Table 6.1
List of the systematic error found in the experiment

Error	Description of Error
$E_{instrument}$	Error inherent in the instrument as it reports to the DAQ
$E_{geometric}$	Error resulting from the measuring of geometric properties
$E_{conversion}$	Error resulting from converting units
$E_{calibration}$	Error resulting from the calibration of equipment

These sources of error are then combined using standard error propagation techniques [43]. This results in the combination of several different sources of error. For example, to calculate the error incurred by the calculation of the air volumetric flow rate, Q_g, several steps must be taken. First, the error from the instrument is found and calculated. This results in a differential pressure and error. This value must now be adjusted for random error. Next, a geometric error term must be added to account for the cross sectional area of the pipe which is used to calculate the volumetric flow rate. For each calculated parameter, the error was found using this technique.

6.5 The Full Data Set

The data points, in their entirety, are presented in graphical form below in figure 6.9 as a plot of the roots of j_f^* versus j_g^* in order to compare it with the published reports.The terms j_f^* and j_g^* are defined by [7] as:

$$j_f^* = j_f \sqrt{\frac{\rho_f}{gD\left(\rho_f - \rho_g\right)}} \tag{6.1}$$

$$j_g^* = j_g \sqrt{\frac{\rho_g}{gD\left(\rho_f - \rho_g\right)}} \tag{6.2}$$

From this figure there is an obvious downward trend. The downward trend confirms that as the liquid flow rate increases, the necessary air flow rate for CCFL decreases as is seen other experiments [6, 19]. Also, the relative scale of the $\sqrt{j^*}$ values is comparable to other sources, e.g. figure 6.10.

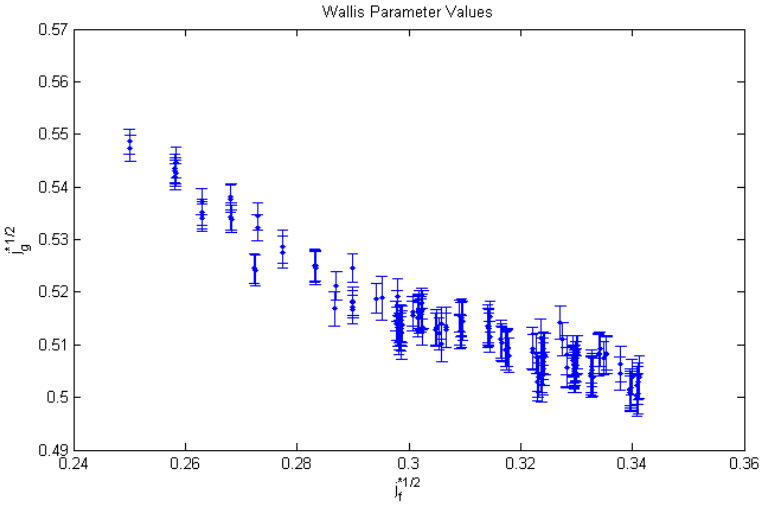

Figure 6.9. All of the collected data presented at CCFL as a function of the Wallis Parameter

6.6 Correlation Development

Even from a cursory glance at the data provided by the experiments, there does appear to be a strong trend in the data. This trend, however, must be more properly described before any sort of correlation can be created. The first step in forming a new correlation is to review the possible means of characterizing the flow conditions. This is primarily done by the use of dimensionless numbers and parameters. These numbers were described in the scaling analysis. The first number of note is the liquid Reynolds number, Re_f as defined in the literature [42].

$$Re_f = \frac{j_f D}{\nu_f} \tag{6.3}$$

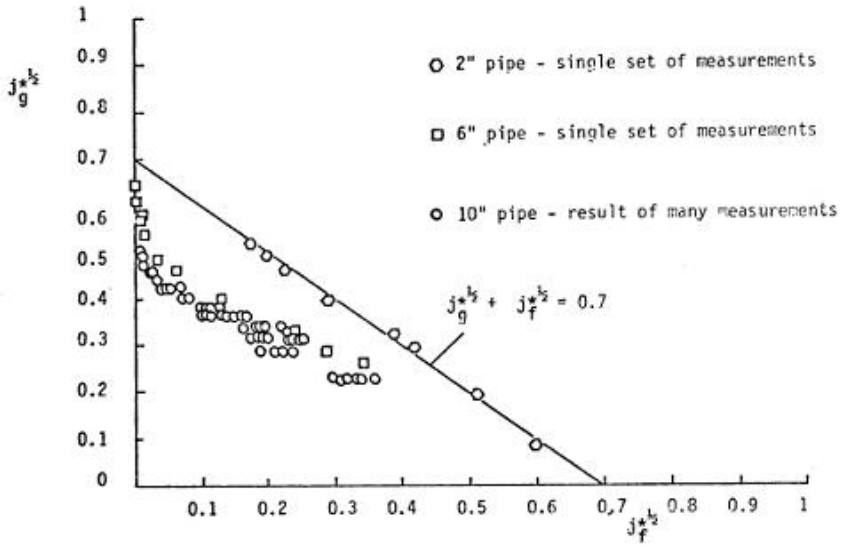

Figure 6.10. Richter's data for a variety of tube geometries. [18]

Where in this relationship, j_f is the volumetric flux defined by [21] as:

$$j_f = \frac{Q_f}{A} \tag{6.4}$$

Re_f characterizes the regime in the annular flow in such a way that a film thickness may eventually be found [37].

$$\delta = 0.135 \left(\frac{\nu^2}{g\left(1 - \frac{\rho_g}{\rho_f}\right)} \right)^{1/3} Re_f^{7/12} \tag{6.5}$$

This film thickness in turn can be used to find other important parameters in the fluid system such as the void fraction.

$$\alpha = \left(1 - 2\frac{\delta}{D}\right)^2 \tag{6.6}$$

More importantly, the film thickness becomes the characteristic length for the system. As such, the film thickness is used here in the calculation of the Ohnesorge number and implied in the calculation of the Froude number through the fluid velocities. The Ohnesorge number is defined in this manner by:

$$Oh_f = \frac{\mu_f}{\sqrt{\rho_f \sigma \delta}} \tag{6.7}$$

The relationship is a ratio of the viscous and the surface tension forces. Also, since the film thickness is a function of the film Reynolds number, it is also dependent on the liquid flow rate. Were this not the case, the Ohnesorge number would not change over the range of flow rates used in this system, which would erroneously suggest that the relationship between viscous and surface tension forces remains constant. It would be hard to believe that this is the case due to the fact that the viscous forces in the system will change based on flow rates while the surface tension is essentially constant given two fluids.

Another point to raise is that the Froude number presented here is based on the relative velocities of the fluids and not upon one or the other individually. This provides a more realistic look into the relationship between the fluids as opposed to each fluid's independent properties.

An important look into the interrelationship of these properties can be first glimpsed by examining how Oh changes across the test range. Looking at how the Oh reacts to different liquid flow rates reveals some of the fluid mechanics involved. In figure 6.11 it is clear that as the liquid flow rate increases, the Oh number decreases between the range of 3.0×10^{-3} and 3.8×10^{-3}.

The most relevant reasoning behind this behavior can be found by examining what the Oh number represents. Because Oh is the ratio of viscous forces to surface tension forces, by increasing the velocity of the liquid, the surface tension on the interface is decreased. It has also been suggested [16] that the Ohnesorge number is a good indicator of the effect that liquid viscosity has on CCFL. The effect of viscosity as a CCFL motivator is a continuation of the work of Cetinbudaklar [27] which supplants density differences as the most important parameter for flooding. However, since film thickness is also playing a part, the logic of the trend is revealed. Since the film thickness of the annular flow increases as the flow rate is increased, the surface tension forces on the liquid phase decreases due to a smaller interface.

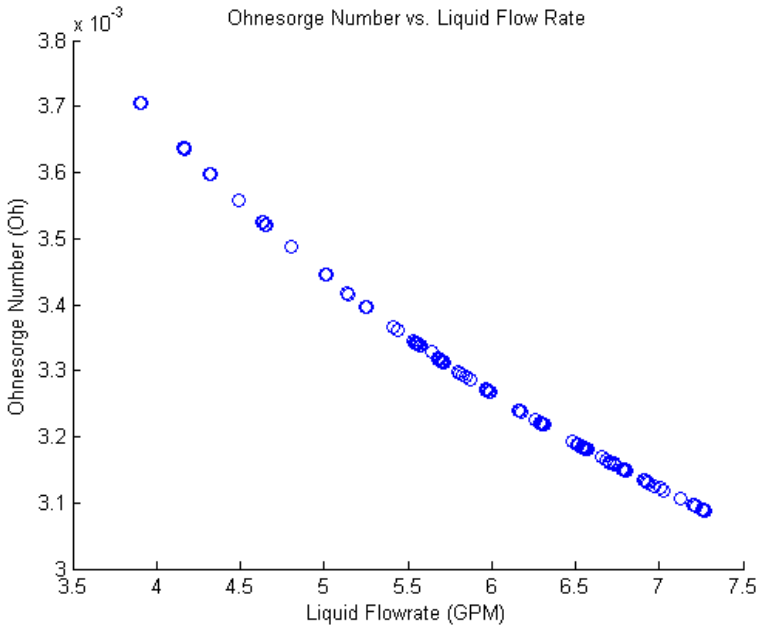

Figure 6.11. The Ohnesorge number as a function of the liquid flow rate and at variable air flow rates.

Likewise, it would be a good idea to examine how the Froude number changes as a function of the liquid and air velocities 3.3. These relationships are shown in figures 6.12 and 6.13 respectively.

It should be noted that these points represent the respective numbers only at the onset of flooding. These figures reveal two trends. The first, shown in figure 6.12, relates the modified Froude number to liquid flow rate entering the test section. As expected, when the liquid flow rate increases, the Froude number decreases. This is mainly due to the the Froude number dependence on film thickness which is itself dependent on the film Reynolds number. If the liquid flowrate increases, the magnitude of Re_f will also increase, increasing the film thickness. This is also expected when looking at the definition of the Froude number with respect to the liquid flow rate. It is expected that the inertial forces will play a more prominent role than the gravity forces when the area that these forces act over decreases. Also of note is the slight curvature to the trend shown in Figure 6.12. However, in figure 6.13, we see that

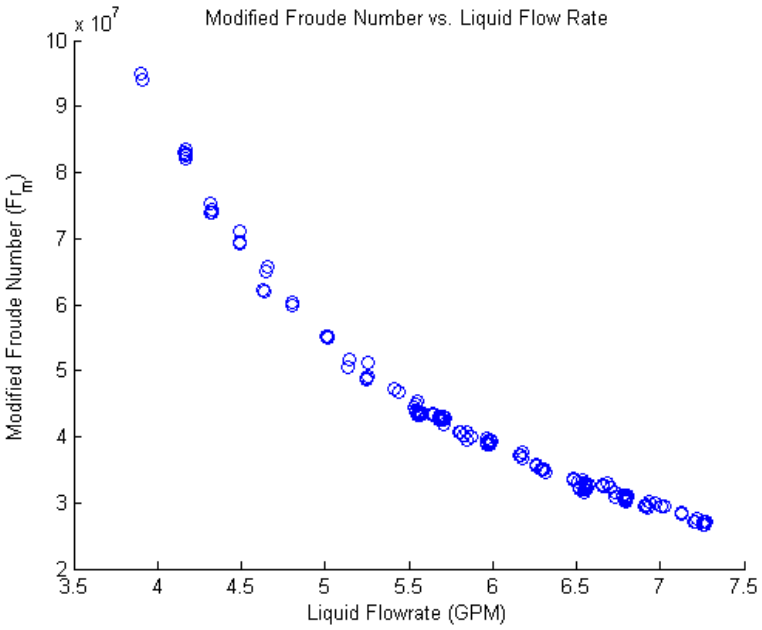

Figure 6.12. The Froude number as a function of liquid flow rate and at variable air flow rates.

the Froude number increases with increasing air velocity. In this formulation of the Froude number, the relative velocity of the fluids is used as the inertial term. Thus, since the air velocity is larger than the liquid velocity, and changes at a greater rate, the air velocity term is the dominant number in the calculation.

There is still a lot of spread in the data. In order to reduce this spread there must be a more correct method of correlating the data. By combining terms from the dimensional analysis, a well defined functional relationship can be found [38]. From this analysis, it is suggested here that the most logical choice would be the film thickness to diameter ratio. This is because the film thickness to diameter contains terms that are independent of the Froude number. As a result, the final modified Froude number is defined as:

$$Fr_m^* \equiv Fr \left(\frac{\delta}{D} \right)^{-2} \tag{6.8}$$

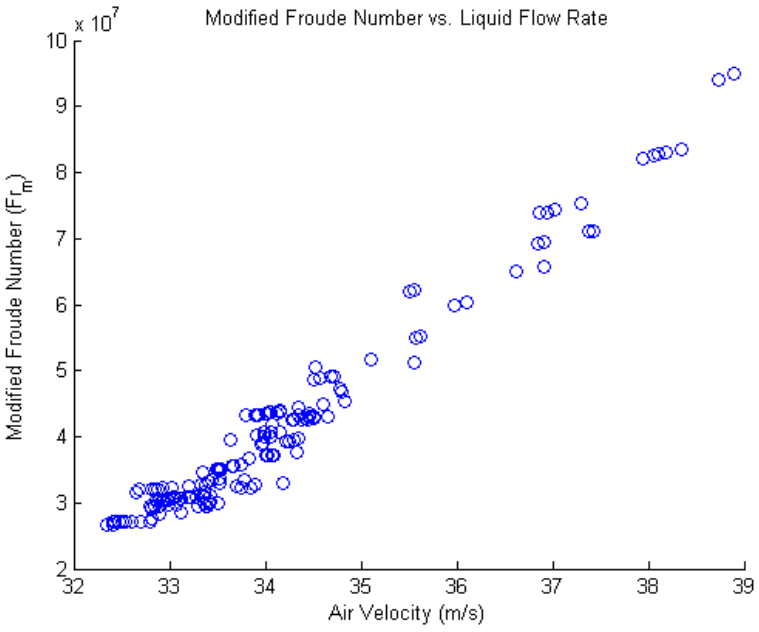

Figure 6.13. The Froude number as a function of the air velocity and a variable liquid flow rate.

Now that there is a good foundation for the two dimensionless numbers applicable to this system, their combined effects can be discussed and final correlation of the data can be made. Since both the Froude and Ohnesorge numbers have been shown to describe the flooding experiment, their combination should be able to provide insight into the phenomenon. By relating the Froude number to the Ohnesorge number, an obvious trend line appears. Shown in figure 6.14, all of the data falls neatly into a linear pattern.

It would be desirable to eliminate the curvature of this line. To this end, a linear regression model was used to find the value of an exponent which would yield an acceptably straight line. It was found that by taking the Froude number to the 0.1 power accomplishes just this and the result is as shown below in figure 6.15.

The additonal error bars were calculated to be approximately 3% of the final value. The two bands seen in the figure are the 5% error bands. That is, these lines are 95% and 105% of the value of the correlation line. The straight line represents

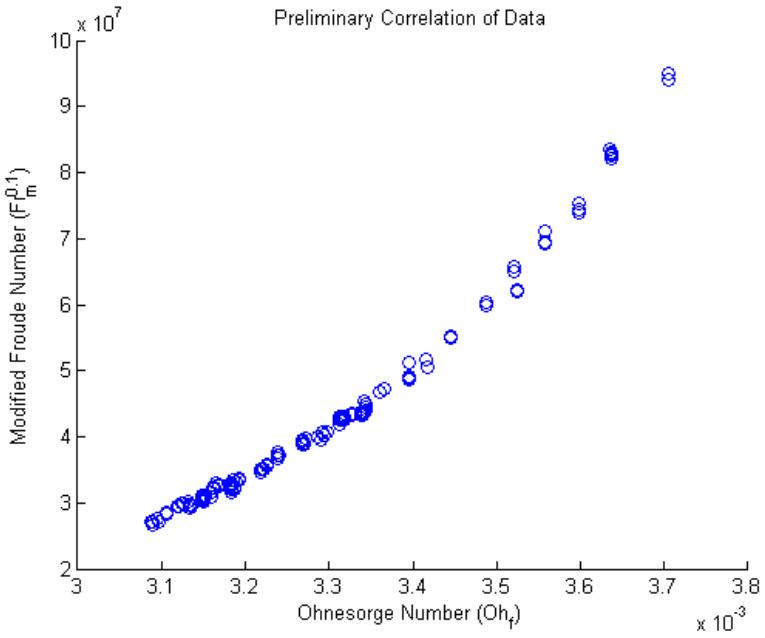

Figure 6.14. The data as correlated using the Froude number and the Ohnesorge number.

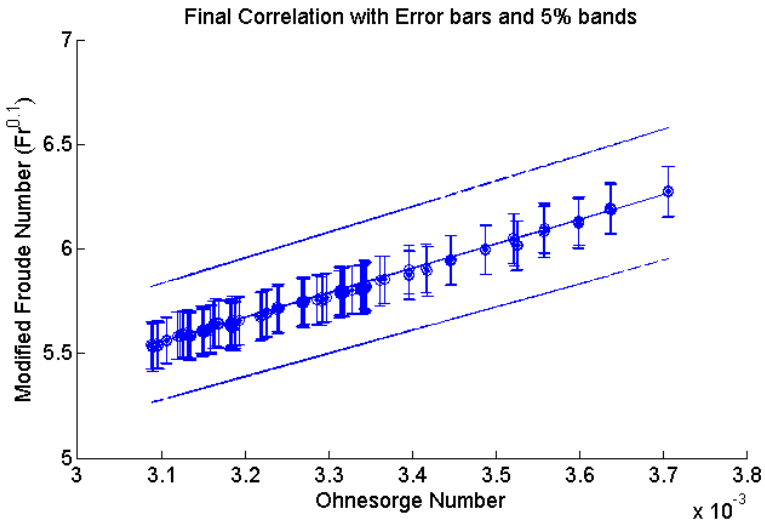

Figure 6.15. The corrected Froude number verses the Ohnesorge number.

the flooding point, or CCFL, for a two fluid system. The equation of this line can be written as:

$$Fr_m^{0.1} - 1.17 \times 10^3 Oh_f = 1.93 \tag{6.9}$$

Or as:

$$Fr_m^{0.1} - mOh_f = C_{exp} \tag{6.10}$$

This equation properly correlates the data taken in this investigation.

6.6.1 Prediction of Data by Existing Correlations

The data should, however, be compared to the other correlations of note. First, the relationship to the Wallis correlation is examined. Shown in figure 6.16 is the results of using the Wallis parameters to characterize the flow as well as the location of the correlation line. The line was generated from equation 2.3 using the data collected with the experimental setup for the liquid flow rates and predicts the associated air flow rate.

The figure shows that the Wallis correlation consistently under-predicts the velocities need to achieve CCFL. The poor agreement is not surprising given that the experimental apparatus is of a large diameter type where Wallis' parameter is used strictly for small diameter geometries.

The Kutateladze correlation is also of interest. Shown in figure 6.17, the line represents the prediction of the Kutateladze correlation given a range of liquid flow rates from the experiments.

In this figure, the correlation is much more accurate in predicting the flow rates. This is mostly because the Kutateladze correlation is diameter independent and should work for large diameters. However, with the exception of the few point lying directly on the line. The disagreement comes from the fact that the Kutateladze correlation neglects the affect of diameter entirely. Without accounting for diameter at all, the correlation neglects affect of film thickness on the flooding phenomenon.

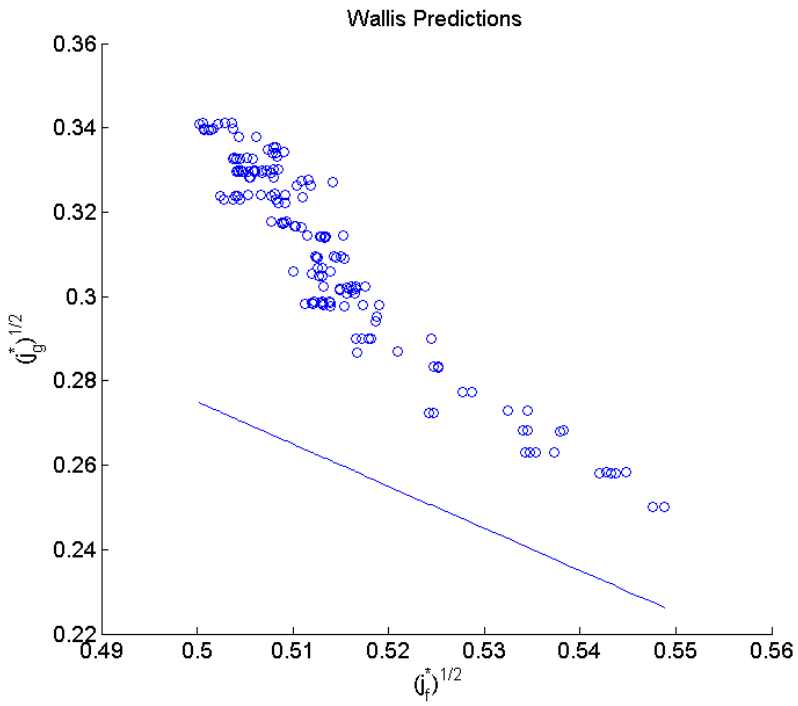

Figure 6.16. Collected data and the location of the Wallis correlation.

Since existing correlations are unable to predict the onset of flooding under the conditions of interest, a new correlation must be developed.

6.6.2 Correlation Validation with Previous Data

The new correlation should also be applied to previously published data in order to validate it. This was done with data culled from Lacy's investigation [44]. Shown in figure 6.18, the data is compared with the correlation line.

The overall comparison is good. The trend matches the data well and the slope of the results is in good agreement. The average difference between the correlation prediction and the actual data was found to be 7.9%. The difference is small over the lower range of the data, 6.0%, and increases as the Ohnesorge number increases to a maximum difference of 11.8%. The correlation is over-predicting the results from this experiment, as can be seen from the plot. One possible cause of disagreement is

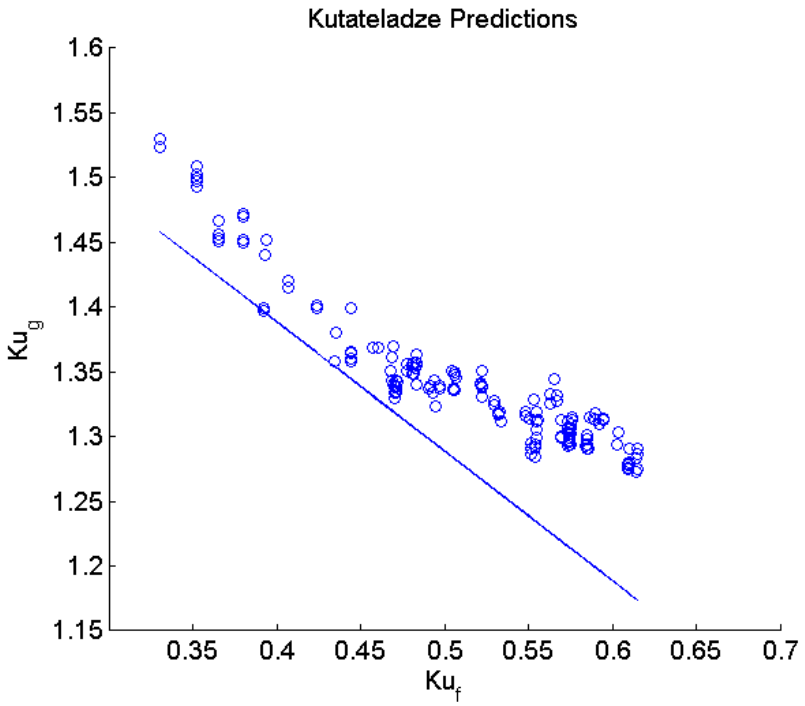

Figure 6.17. Collected data and the Kutateladze correlation.

in the estimation of the reported values, since no error was reported with the data it is impossible to know its accuracy. However an 11% error is reasonable in two-phase flows.

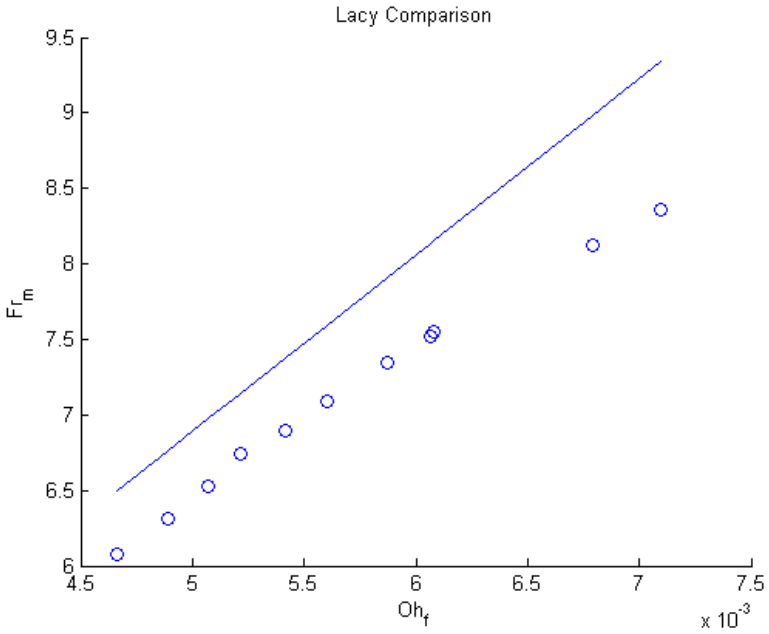

Figure 6.18. Comparison of the correlation derived here and the reported results of Lacy et al [44]

7. CONCLUSIONS AND FUTURE WORK

7.1 Conclusions

The phenomenon of countercurrent flow limitation was investigated experimentally in order to arrive at a useful correlation for the onset of flooding in large-diameter vertical tubes.

Intended to clarify the basic mechanisms begind the phenomenon of flooding, this investigation has also provided valuable knowledge for follow-up steam-air experiments that will model the PWR surge line. Furthermore, it can be used for further work on the phenomenon of CCFL and other two-phase fluid dynamics problems. The data collected can also be used for the determination of a mechanistic model of CCFL.

The experiments conducted produced a large set of data consisting of fluid velocities and pressure measurements. The experimental facility was designed and constructed to investigate a large range of fluid velocities. These data showed similar trends with those reported by other investigators with respect to the relationship between the fluid velocities. Also, the characteristic pressure drop change across the test section was observed to take place during the onset of flooding. These trends are described throughout the published literature and lend credibility to the collected data. The correlations of Wallis and Kutateladze were compared to the collected data and found to be deficient. The data also exhibits a low amount of error. Such a data set can be used by the scientific community to gain a better understanding of the CCFL phenomenon.

A correlation suitable for use in reactor safety codes was derived from the resulting data. The correlation is used by calculating the film thickness in the tube and thus the void fraction. Once the void fraction is determined, the fluid velocities can be

measured and their relative velocity calculated. This relative velocity is used to calculate a modified Froude number which is compared with a constant to determine if CCFL has been reached. This correlation was found to correctly predict the onset of flooding for large diameter tube for liquid flow rates as low as 3.9 GPM and as high as 7.2 GPM. The corresponding air flow rates for these liquid flow rates are given as superficial velocities ranging from 7.47 m/s to 6.45 m/s respectively.

7.2 Recommended Future Work

While this investigation provided new and important information to the field of two-phase fluid dynamics, there are some suggestions as to what should be attempted next.

- A more thorough and detailed measurement of the film layer would provide validation to its use as a characteristic length scale for CCFL determination. This would involve taking actual film thickness measurements and comparing them with the correlations used here.

- An investigation into the effect of inclination angles on the flooding phenomenon. Since the prototype surge line contains many different inclination angles on its approach to the pressurizer, it is important to take these angles into account. The experimental facility designed here is capable of examining different angles.

- To more closely model a real pressurizer, steam and water tests should be conducted in order to take into account the effect of mass transfer. This condensation effect is suspected to greatly affect the CCFL in closed geometries and should be examined.

- A more stable and powerful source of air should be found in order to examine the post flooding environment inside the test section. This would provide valuable data as to the nature of the post-CCFL regime.

- Looking at various test section diameters would improve the justification for the large diameter threshold. This would also add valuable observation of the diameter effect for large diameter tubes.

- A mechanistic model of the CCFL phenomenon should be developed using this data as a basis. Such a model would be valuable to the field of two-phase fluid dynamics.

REFERENCES

[1] Y. Liao and K. Vierow. Optimum channel inclination for gas venting under countercurrent flow limitations. in International Conference on Nuclear Engineering 14, number 14-89665, Miami, FL 2006.

[2] K Takeuchi, Young M.Y., and Gagon A.F. Flooding in the pressurizer surge line of ap600 plant and analyses of apex data. Nucl. Eng. Des., 192:(1999)45-58.

[3] N.E. Todreas and M.S. Kazimi. Nuclear Systems I: Thermal Hydraulic Fundementals, volume 2. Taylor & Francis, 1993.

[4] J.R. Lamarsh and A.J. Baratta. Introduction to Nuclear Engineering. Prentice Hall, 2001.

[5] Y. Liao and K. Vierow. Melcor analysis of steam generator tube creep rupture in station blackout severe accident. Nuclear Technology, 152(2005):302-313.

[6] K.W. McQuillan and P.B. Whalley. Comparison between ooding correlations and experimental flooding data for gas-liquid flow in vertical circular tubes. Chem. Eng. Sci., 40(1985):1425-40.

[7] G.B. Wallis. Flooding velocities for air and water in vertical tubes. Technical report, AEEW-R-123, United Kingdom Atomic Energy Authority. Reactor Group. Atomic Energy Establishment, Winfrith, Dorset, 1961.

[8] T.K. Sherwood, G.H. Shipley, and F.A.L. Holloway. Flooding velocities in packed columns. Industrial and Engineering Chemistry, 30(1938):765-769.

[9] R. Clift, C.L. Pritchard, and R.M. Nedderman. The effect of viscosity on the flooding conditions in wetted wall columns. Chem. Eng. Sci., 21(1966):87-95.

[10] M. Vijayan, S. Jayanti, and A.R. Balakrishnan. Effect of tube diameter on flooding. Int. J. Multiphase Flow, 27(2001):797-816.

[11] G.B. Wallis and J.T. Kuo. The behavior of gas-liquid interfaces in vertical tubes. Int. J. Multiphase Flow, 2(1976):521-536.

[12] S.S. Kutateladze. Elements of the hydrodynamics of gas-liquid systems. Fluid Mechanics Soviet Research, 1(4), 1972.

[13] D.L. Tien. A simple analytical model for counter-current flow limiting phenomena with vapor condensation. Letters in Heat and Mass Transfer, 4(1977):231-238.

[14] O.L. Pushkina and Y.L. Sorokin. Breakdown of liquid film motion in vetical tubes. Heat Transfer Sov. Res., 1(1969):56-64.

[15] A. Zapke and D.G. Kroger. Countercurrent gas-liquid flow in inclined and verti-

cal ducts II: The validity of the Froude-Ohnesorge number correlation for flooding. Int. J. Multiphase Flow, 26(2000):1457-1468.

[16] A. Zapke and D.G. Kroger. Countercurrent gas-liquid flow in inclined and vertical ducts II: Flow patterns, pressure drop characteristics and ooding. Int. J. Multiphase Flow, 26(2000):1439-1455.

[17] S.G. Bankoff and S.C. Lee. A critical review of the ooding literature. Technical report, NUREG/CR-3060, Dept. Chem. Eng., Northwestern U., Evanston, IL, 1983.

[18] H.J. Richter, G.B. Wallis, and M.S. Speers. Effect of scale on two-phase countercurrent flow flooding. Technical report, NUREG/CR-0312, Dartmouth Coll., Hanover, NH (USA). Thayer School of Engineering, 1979.

[19] S.G. Bankoff and S.C. Lee. A critical review of the flooding literature. Technical report, NUREG/CR-3060, Northwesting Univ., Evanston, IL, 1983.

[20] S. Levy. Two-Phase Flow in Complex Systems. Wiley-IEEE, 1999.

[21] G.B. Wallis. One Dimensional Two Phase Flow. McGraw-Hill, 1969.

[22] K. Ohkawa and R.T. Lahey. The analysis of CCFL using drift-flux models. Nucl. Eng. Des., 61(1980):245-255.

[23] H. Imura, H. Kusuda, and S. Funatsu. Flooding velocity in a countercurrent annular two-phase flow. Chem. Eng. Sci., 32(1977):79-87.

[24] G. Karimi and M. Kawaji. Flooding in vertical counter-current annular flow. Nucl. Eng. Des., 200(2000):95-105.

[25] A.A. Mouza, S.V. Paras, and A.J. Karabelas. Incipient ooding in inclined tubes of small diameter. Int. J. Multiphase Flow, 29(2003):1395-1412.

[26] S.K. Chung, L.P. Liu, and C.L. Tien. Flooding in two-phase counter current flows-II experimental investigation. Physicochem. Hydrodyn., 1(1980):209-220.

[27] A.G. Cetinbudaklar and G.J. Jameson. The mechanism of ooding in vertical countercurrent two-phase flow. Chemical Engineering Science, 24(1969):1669-1680.

[28] Y. Taitel, D. Barnea, and A.E. Dukler. A film model for the prediction of flooding and flow reversal for gas-liquid flow in vertical tubes. Int. J. Multiphase Flow, 8(1982):1-10.

[29] A.E. Dukler, L. Smith, and A. Chopra. Flooding and upward film flow in tubes I: Experimental studies. Int. J. Multiphase Flow, 10(1984):585-597.

[30] D. Barnea, B. Yoseph, and Y. Taitel. Flooding in inclined pipes-effect of entrance section. Can. J. Chem. Eng., 64(1986):177-184.

[31] D. Moalem Maron and A.E. Dukler. Flooding and upward film flow in vertical tubes II: Speculations on film flow mechanisms. Int. J. Multiphase Flow, 10(1984):599-621.

[32] Y. Taitel, D. Barnea, and A.E. Dukler. Modelling flow pattern transitions for steady upward gas-liquid flow in vertical tubes. AIChE Journal, 26(1980):345-354.

[33] H. Richter. Flooding in tubes and annuli. Int J. Multiphase Flow, 7(1981):647-658.

[34] A.H. Govan, G.F. Hewitt, H.J. Richter, and A. Scott. Flooding and churn flow in vertical pipes. International J. Multiphase Flow, 17(1991):27-44.

[35] S. Jayanti, A. Tokarz, and G.F. Hewitt. Theoretical investigation of the diameter effect on ooding in countercurrent flow. Int. J. Multiphase Flow, 22(1996):307-324.

[36] H.H. Belkin, A.A. MacLeod, C.C. Monrad, and R.R. Rothfus. Turbulent liquid flow down vertical walls. AIChE journal, 5(1959):245-248.

[37] J.R.F. Guedes de Carvalho, M.A.R. Talaia, and M.J.F. Ferreira. Flooding instability of high-density gas slugs rising in vertical tubes filled with water. Chem. Eng. Sci., 55(2000):3785-3802.

[38] R.W. Fox and A.T. McDonald. Introduction to Fluid Mechanics. John Wiley & Sons New York, 1985.

[39] A. Zapke and D.G. Kroger. The inuence of uid properties and inlet geometry on flooding in vertical and inclined tubes. Int. J. Multiphase Flow, 22(1996):461-472.

[40] J.H. Jeong and H.C. No. Experimental study of the effect of pipe length and pipe-end geometry on ooding. Int. J. Multiphase Flow, 22:(1996)499-514.

[41] A. Deendarlianto, A. Ousaka, A. Kariyasaki, T. Fukano, and M. Konishi. The effects of surface tension no the flow pattern and counter-current flow limitation (CCFL) in gas-liquid two-phase flow in an inclined pipe. Japanese Journal of Multiphase Flow, 18(2004)337-350.

[42] J.R.F. Guedes de Carvalho and M.A.R. Talaia. Interfacial shear stress as a criterion for flooding in counter current film flow along vertical surfaces. Chem. Eng. Sci., 53(1998):2041-2051.

[43] N. Tsoulfanidis. Measurement and Detection of Radiation. Taylor-Fancis, 1995.

[44] C.E. Lacy and A.E. Dukler. Flooding in vertical tubes I: Experimental studies of the entry region. Int. J. Multiphase Flow, 20(1994):219-233.

APPENDIX A

This appendix contains all of the raw data as it was collected with the DAQ. The units are given in the table heading and all runs are numbered chronological order starting with the earliest set. The air velocity is the centerline maximum velocity through the 1-1/2 SCH 80 PVC pipe. The liquid flow rate is the magnetic flow meter readings and the pressure readings are measured in inches of water.

Table A.1 Reduced collected data

Test. No	Air Velocity m/s	Liquid Flowrate GPM	Water Temperature ^oC	Differential Pressure inH_2O	Lower Pressure inH_2O	Upper Pressure inH_2O
1	34.34	5.97	15.23	55.02	407.72	412.46
2	34.50	5.71	15.09	54.76	407.73	412.33
3	34.28	5.68	14.97	54.65	407.60	412.29
4	34.79	5.44	14.96	55.09	406.69	410.59
5	34.18	6.68	14.33	54.91	406.58	410.44
6	33.76	6.70	14.37	54.75	406.69	410.66
7	32.90	7.13	14.25	54.78	406.54	410.21
8	33.13	7.13	14.42	54.92	406.63	410.28
9	34.08	6.16	14.07	54.85	406.79	410.25
10	34.07	6.16	14.18	54.86	406.89	410.55
11	34.78	5.41	13.85	54.99	406.98	410.48
12	34.05	5.88	12.53	52.24	412.52	416.92
13	33.65	5.84	12.63	52.27	412.41	416.74
14	34.16	5.84	12.77	52.33	412.49	416.74
15	33.98	5.88	12.87	52.11	412.59	416.81
16	33.68	6.26	13.10	52.38	412.17	416.56
17	33.66	6.26	13.13	52.37	412.15	416.61
18	33.67	6.26	13.17	52.40	412.06	416.45
19	33.75	6.26	13.19	52.37	411.94	416.45
20	33.83	6.17	13.35	52.41	411.84	416.25
21	34.33	6.18	13.34	52.39	411.75	416.23
22	34.01	6.17	13.34	52.32	411.64	416.19
23	34.03	6.17	13.35	52.42	411.58	416.05
24	34.10	6.17	13.35	52.42	411.43	415.85
25	34.21	5.99	12.81	52.29	410.52	415.13

Test. No	Air Velocity m/s	Liquid Flowrate GPM	Water Temperature ^oC	Differential Pressure inH_2O	Lower Pressure inH_2O	Upper Pressure inH_2O
26	34.24	5.98	12.76	52.29	410.69	415.32
27	34.30	5.98	12.68	52.37	410.55	415.13
28	33.95	5.98	12.67	52.33	410.52	415.13
29	33.98	5.97	12.63	52.24	410.62	414.89
30	33.96	5.97	12.64	52.38	410.49	414.93
31	34.46	5.68	12.67	52.38	410.51	414.84
32	34.39	5.70	12.66	52.28	410.63	415.28
33	34.42	5.69	12.64	52.40	410.65	415.18
34	34.29	5.69	12.63	52.38	410.61	415.28
35	34.51	5.69	12.64	52.39	410.56	415.23
36	33.53	6.48	12.59	52.34	410.56	414.89
37	33.44	6.48	12.56	52.29	410.49	415.25
38	32.80	7.27	13.15	52.78	408.33	413.21
39	32.61	7.26	13.59	53.39	408.38	413.36
40	32.41	7.27	14.15	53.86	408.43	413.42
41	32.35	7.25	14.66	53.66	408.41	413.35
42	32.71	7.26	15.66	53.92	408.56	413.39
43	32.81	7.22	15.93	53.86	408.39	413.28
44	32.51	7.20	16.08	53.68	408.37	413.29
45	32.48	7.20	16.53	53.90	408.36	413.24
46	32.42	7.20	16.78	53.78	408.46	413.17
47	32.41	7.21	16.78	53.77	408.44	413.13
48	32.54	7.21	17.16	53.91	408.34	412.99
49	33.07	6.91	17.40	53.93	408.20	412.98
50	33.00	6.92	17.46	53.93	408.13	412.85

Test. No	Air Velocity m/s	Liquid Flowrate GPM	Water Temperature ^oC	Differential Pressure inH_2O	Lower Pressure inH_2O	Upper Pressure inH_2O
51	32.85	6.91	17.52	53.75	408.09	412.84
52	32.89	6.91	17.67	53.98	408.01	412.85
53	32.80	6.91	17.74	53.69	407.98	412.75
54	32.82	6.92	17.81	53.74	407.93	412.73
55	33.54	6.30	12.73	52.33	408.25	412.89
56	33.52	6.30	12.70	52.48	408.24	413.06
57	33.34	6.31	12.69	52.46	408.18	412.98
58	33.49	6.29	12.65	52.54	408.31	413.17
59	33.50	6.29	12.64	52.54	408.42	413.32
60	33.38	7.03	12.74	52.51	408.56	413.32
61	33.29	7.00	12.74	52.34	408.66	413.29
62	33.40	7.03	12.76	52.44	408.66	413.39
63	34.06	5.55	16.60	52.38	412.17	416.77
64	33.80	5.55	16.58	52.40	412.20	417.05
65	33.91	5.56	16.35	52.44	412.21	416.86
66	34.04	5.56	16.31	52.37	412.16	416.97
67	34.58	5.25	16.44	52.45	412.17	416.83
68	35.56	5.25	16.42	52.37	412.25	416.80
69	34.51	5.25	16.44	52.30	412.17	416.89
70	34.68	5.25	16.41	52.39	412.03	416.82
71	34.72	5.25	16.40	52.39	412.07	416.77
72	33.52	6.56	16.67	52.34	412.00	416.66
73	33.34	6.55	16.71	52.39	411.89	416.77
74	33.38	6.57	16.57	52.39	411.70	416.59
75	33.36	6.73	16.30	52.37	411.58	416.34

Test. No	Air Velocity m/s	Liquid Flowrate GPM	Water Temperature ^oC	Differential Pressure inH_2O	Lower Pressure inH_2O	Upper Pressure inH_2O
76	33.04	6.73	16.17	52.39	411.58	416.54
77	33.05	6.73	16.05	52.39	411.51	416.50
78	34.83	5.55	16.59	52.33	412.30	416.94
79	34.60	5.54	16.60	52.42	412.38	417.18
80	34.34	5.53	16.71	52.39	412.27	417.21
81	34.15	5.54	16.70	52.37	412.20	417.08
82	34.16	5.56	16.67	52.38	412.20	417.16
83	34.12	5.57	16.81	52.44	412.34	417.06
84	34.03	5.57	16.81	52.45	412.34	417.08
85	33.93	5.57	16.77	52.39	412.46	417.12
86	33.90	5.57	16.73	52.45	412.44	417.10
87	34.01	5.57	16.61	52.46	412.23	416.97
88	34.83	5.55	16.59	52.33	412.30	416.94
89	34.60	5.54	16.60	52.42	412.38	417.18
90	34.34	5.53	16.71	52.39	412.27	417.21
91	34.15	5.54	16.70	52.37	412.20	417.08
92	34.16	5.56	16.67	52.38	412.20	417.16
93	33.20	6.56	14.49	52.38	411.83	416.53
94	32.85	6.55	14.49	52.40	411.85	416.56
95	33.03	6.56	14.46	52.34	411.72	416.44
96	32.81	6.52	14.46	52.32	411.62	416.56
97	32.65	6.55	14.48	52.35	411.55	416.46
98	32.88	6.55	14.48	52.38	411.99	416.52
99	35.10	5.15	14.50	52.34	411.84	416.58
100	34.52	5.13	14.52	52.43	411.72	416.55

Test. No	Air Velocity m/s	Liquid Flowrate GPM	Water Temperature ^oC	Differential Pressure inH_2O	Lower Pressure inH_2O	Upper Pressure inH_2O
101	33.43	6.81	14.17	52.24	412.15	416.91
102	33.37	6.80	14.22	52.35	412.02	416.64
103	32.88	6.80	14.24	52.37	411.92	416.75
104	33.28	6.80	14.25	52.36	412.26	416.76
105	33.21	6.79	14.29	52.33	412.00	416.64
106	33.11	6.80	14.33	52.29	411.84	416.74
107	32.93	6.79	14.36	52.31	411.73	416.64
108	33.78	6.54	11.71	52.38	406.78	411.41
109	32.92	6.52	11.80	52.35	406.67	411.52
110	32.69	6.52	13.04	52.34	406.65	411.42
111	33.41	6.51	13.56	52.40	406.55	411.25
112	33.90	5.83	10.03	52.39	406.01	410.81
113	34.05	5.81	10.65	52.47	406.39	411.23
114	33.99	5.80	10.69	52.36	406.42	411.30
115	33.34	6.78	12.82	52.29	409.43	414.20
116	33.22	6.78	12.80	52.18	409.55	414.22
117	33.10	6.79	12.48	52.37	409.28	414.09
118	32.86	6.78	12.45	52.38	409.23	414.12
119	33.12	6.78	12.27	52.35	409.24	413.98
120	32.94	6.78	12.21	52.28	409.00	413.78
121	32.97	6.79	12.06	52.37	408.72	413.64
122	33.03	6.78	11.87	52.39	408.57	413.45
123	32.89	6.79	11.87	52.36	408.55	413.49
124	33.11	6.79	11.67	52.36	408.71	413.38
125	35.51	4.64	24.92	52.59	408.29	413.00

Test. No	Air Velocity m/s	Liquid Flowrate GPM	Water Temperature ^oC	Differential Pressure inH_2O	Lower Pressure inH_2O	Upper Pressure inH_2O
126	35.56	4.63	24.92	52.69	408.36	412.95
127	38.90	3.90	24.91	52.77	408.82	413.37
128	38.73	3.91	24.91	52.77	408.87	413.46
129	37.95	4.16	24.91	52.79	408.93	413.52
130	38.05	4.17	24.91	52.68	409.12	413.57
131	38.18	4.16	24.91	52.78	409.04	413.70
132	38.11	4.16	24.91	52.77	409.05	413.76
133	38.35	4.17	24.91	52.78	409.11	413.70
134	36.91	4.49	24.91	52.35	409.82	414.02
135	37.43	4.49	24.91	52.68	409.59	414.12
136	36.85	4.49	24.91	52.62	409.62	414.22
137	37.37	4.49	24.91	52.73	409.71	414.40
138	36.62	4.65	24.91	52.15	410.63	414.74
139	36.92	4.66	24.91	52.75	409.97	414.80
140	35.63	5.01	24.90	52.36	409.90	413.43
141	35.57	5.01	24.90	52.42	409.76	413.03
142	35.62	5.01	24.89	52.43	409.76	412.82
143	36.10	4.81	24.89	52.43	409.93	412.54
144	35.98	4.81	24.89	52.45	409.93	412.49
145	37.02	4.32	24.89	52.46	409.56	412.08
146	36.87	4.32	24.89	52.46	409.56	412.17
147	36.94	4.32	24.89	52.48	409.77	412.16
148	37.29	4.32	24.89	52.46	409.91	412.21
149	34.46	5.65	24.90	52.39	409.52	412.07
150	34.35	5.65	24.90	52.40	409.55	412.03

Test. No	Air Velocity m/s	Liquid Flowrate GPM	Water Temperature ^oC	Differential Pressure inH_2O	Lower Pressure inH_2O	Upper Pressure inH_2O
151	37.02	4.32	24.89	52.46	409.56	412.08
152	36.87	4.32	24.89	52.46	409.56	412.17
153	36.94	4.32	24.89	52.48	409.77	412.16
154	37.29	4.32	24.89	52.46	409.91	412.21
155	34.07	5.71	11.34	52.41	409.61	409.17
156	34.65	5.71	11.07	52.39	409.63	409.15
157	34.45	5.71	11.02	52.39	409.56	409.34
158	34.38	5.70	10.69	52.40	409.22	408.86
159	33.51	6.97	10.56	52.32	409.12	408.56
160	33.36	6.97	10.53	52.33	409.00	408.86
161	33.41	6.97	10.35	52.34	408.74	408.49
162	33.43	6.93	10.22	52.33	408.89	408.36
163	33.89	6.65	11.56	52.33	409.89	409.26
164	33.85	6.71	11.54	52.24	409.91	409.44
165	33.70	6.65	11.43	52.37	409.69	409.37

APPENDIX B

This appendix presents the data in graphical form. These data are the steady state data that was used to correlate the data set. Each plot has a caption which gives its Test Number. This test number is the same as is listed in the Appendix A table.

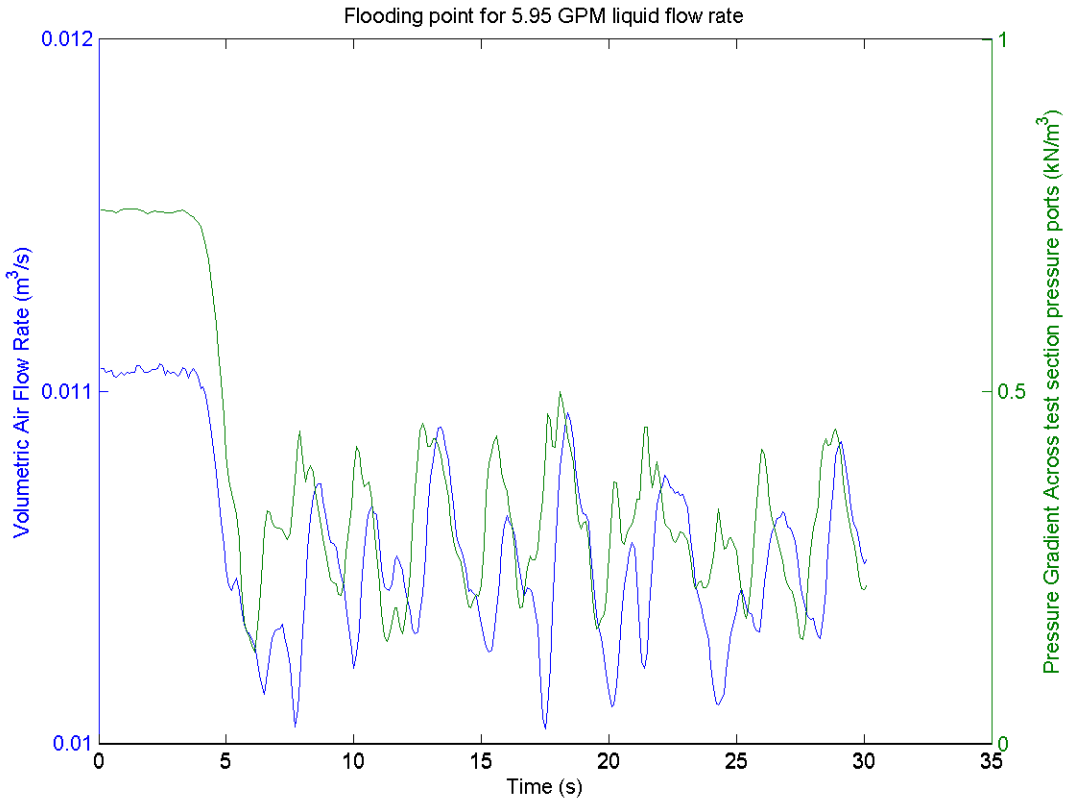
Flooding point for 5.95 GPM liquid flow rate
Volumetric Air Flow Rate (m3/s)
Pressure Gradient Across test section pressure ports (kN/m3)
Time (s)
0.012
0.011
0.01
1
0.5
0
0
5
10
15
20
25
30
35

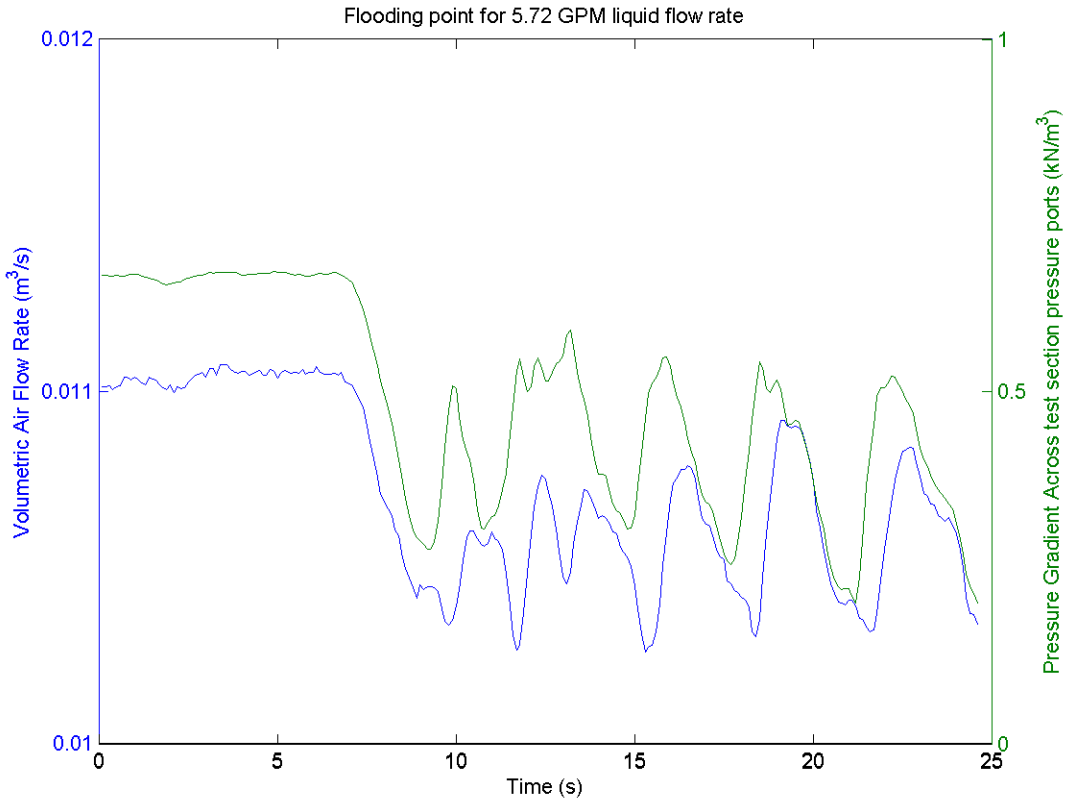
Flooding point for 5.72 GPM liquid flow rate
0.012
0.011
0.01
Volumetric Air Flow Rate (m3/s)
1
0.5
0
Pressure Gradient Across test section pressure ports (kN/m3)
0
5
10
15
20
25
Time (s)

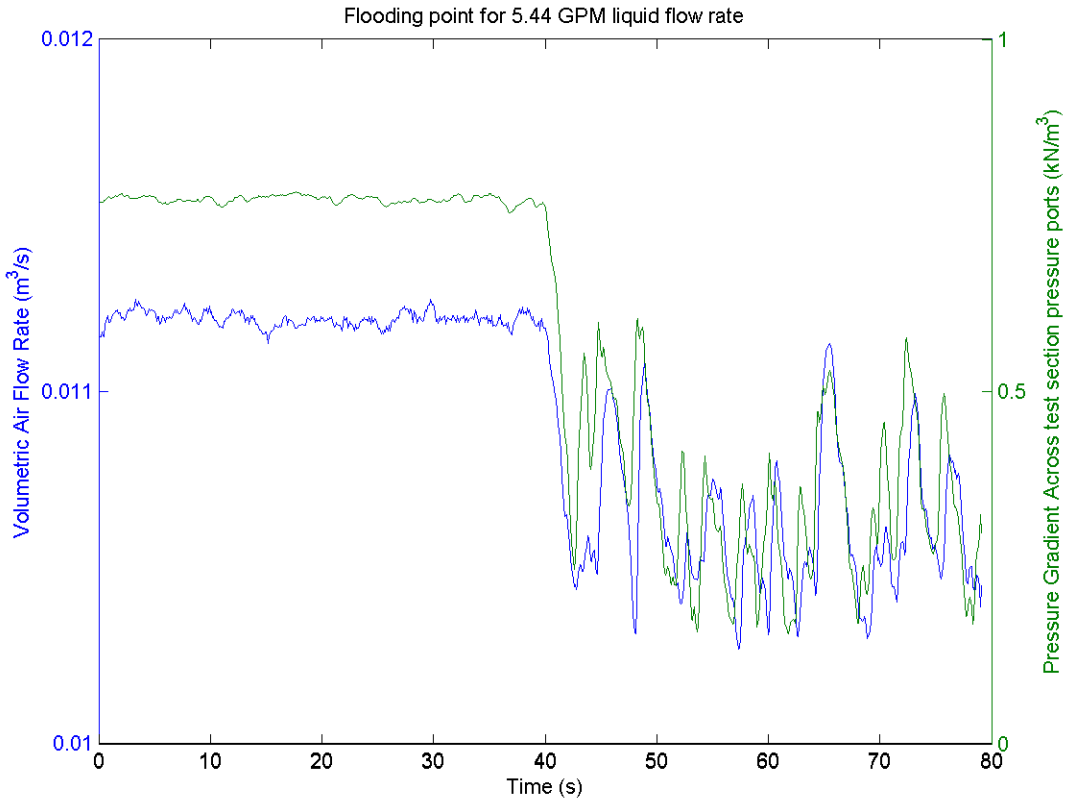
Flooding point for 5.44 GPM liquid flow rate
Volumetric Air Flow Rate (m3/s)
Pressure Gradient Across test section pressure ports (kN/m3)
Time (s)
0.012
0.011
0.01
1
0.5
0
0
10
20
30
40
50
60
70
80

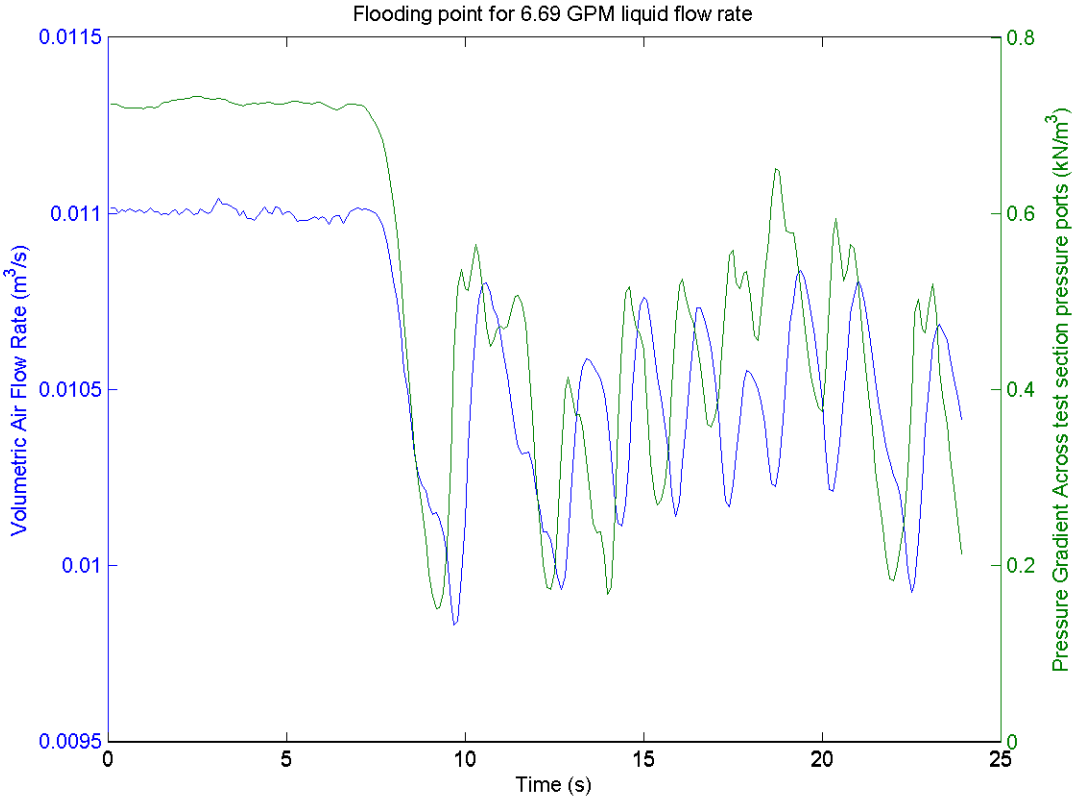
Flooding point for 6.69 GPM liquid flow rate
Volumetric Air Flow Rate (m3/s)
Pressure Gradient Across test section pressure ports (kN/m3)
Time (s)
0.0115
0.011
0.0105
0.01
0.0095
0.8
0.6
0.4
0.2
0
0
5
10
15
20
25

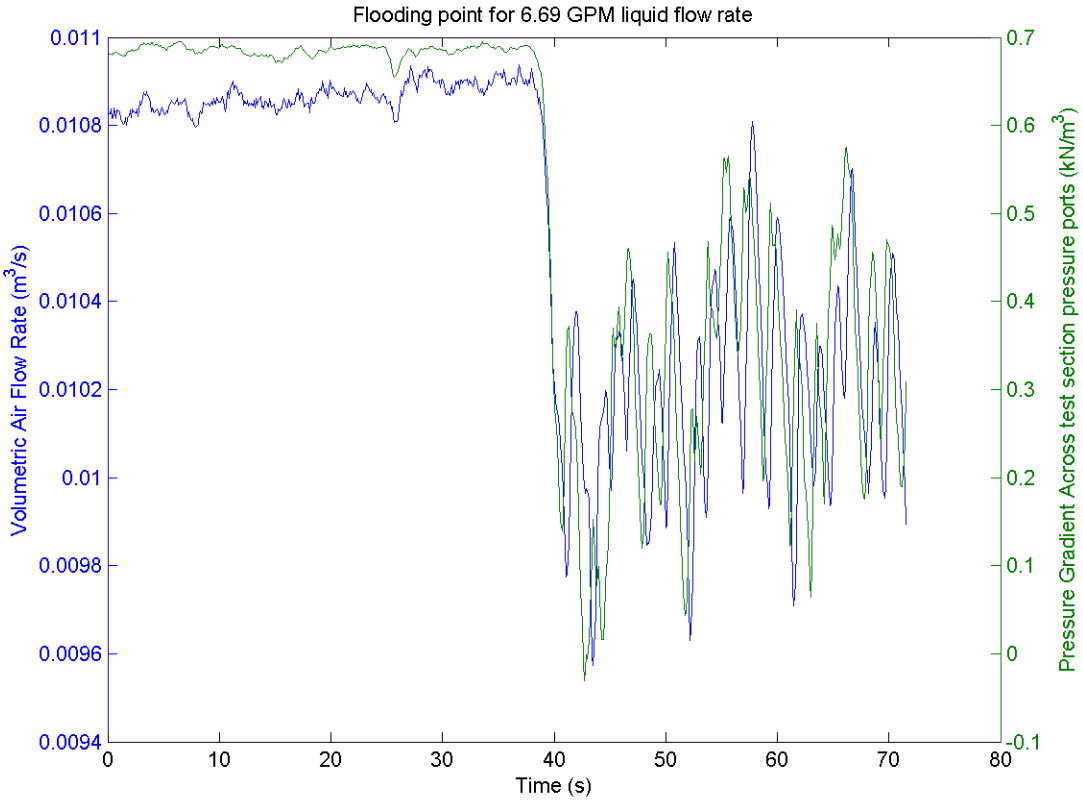
Flooding point for 6.69 GPM liquid flow rate
Volumetric Air Flow Rate (m3/s)
Pressure Gradient Across test section pressure ports (kN/m3)
Time (s)
0.011
0.0108
0.0106
0.0104
0.0102
0.01
0.0098
0.0096
0.0094
0.7
0.6
0.5
0.4
0.3
0.2
0.1
0
-0.1
0
10
20
30
40
50
60
70
80

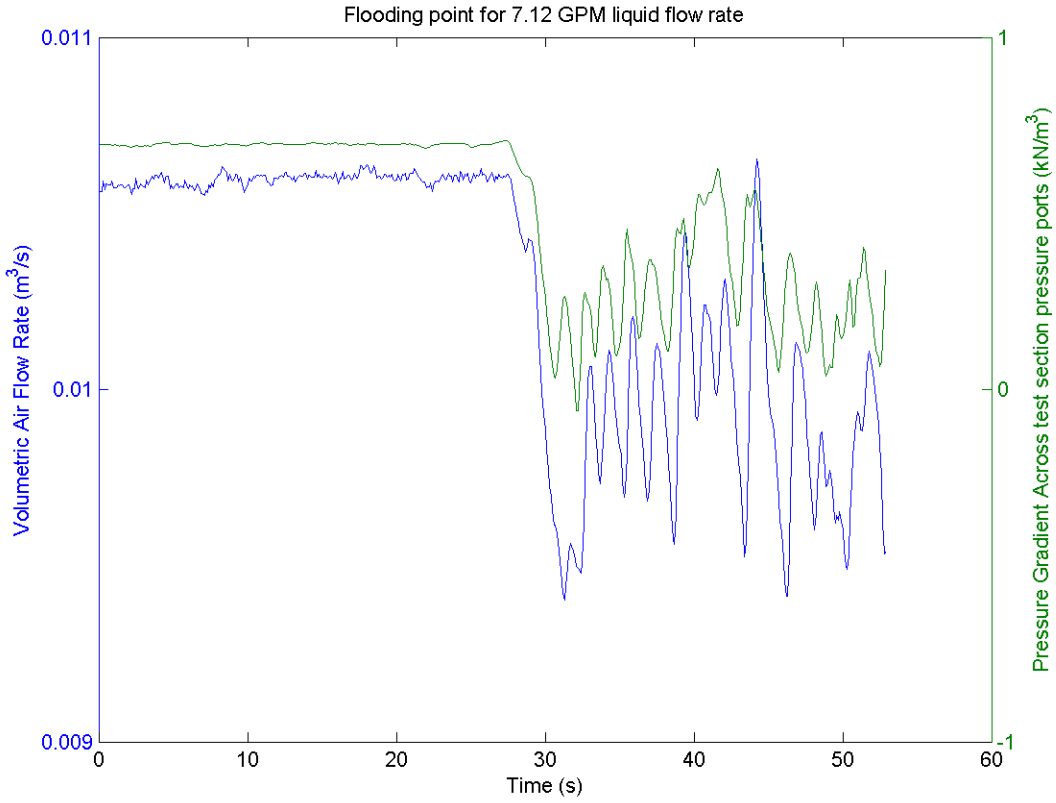
Flooding point for 7.12 GPM liquid flow rate
0.011
0.01
0.009
Volumetric Air Flow Rate (m3/s)
1
0
-1
Pressure Gradient Across test section pressure ports (kN/m3)
0
10
20
30
40
50
60
Time (s)

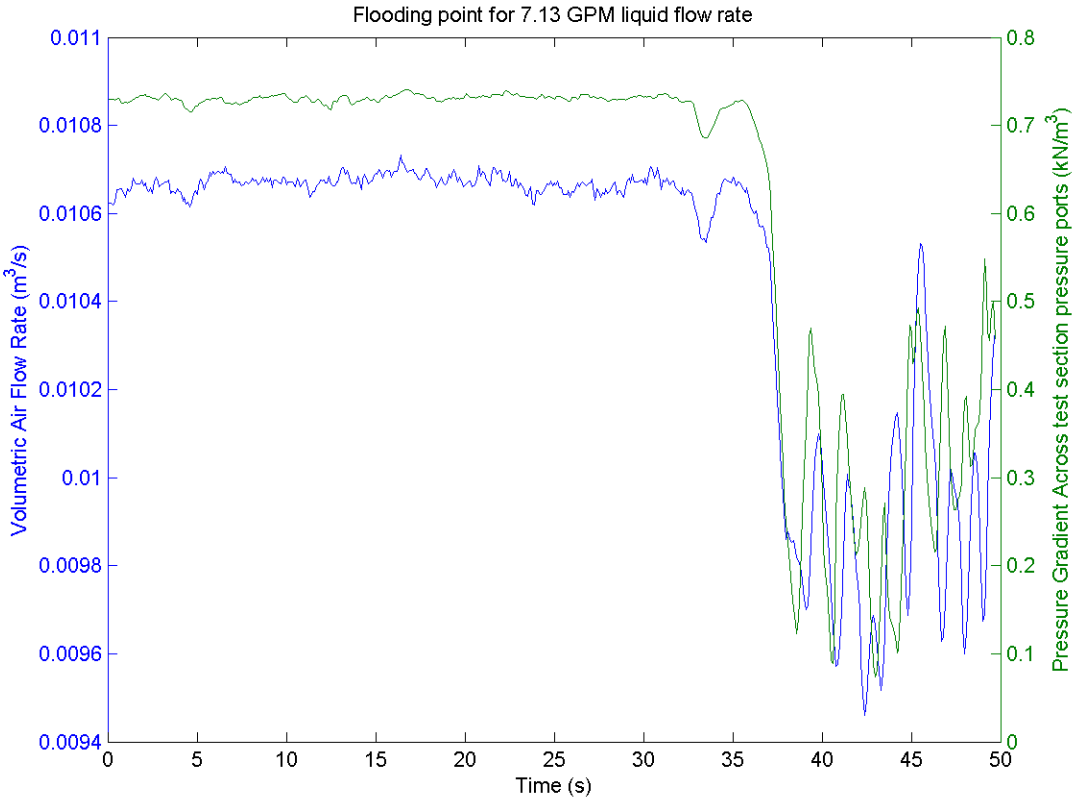
Flooding point for 7.13 GPM liquid flow rate
Volumetric Air Flow Rate (m3/s)
Pressure Gradient Across test section pressure ports (kN/m3)
Time (s)
0.011
0.0108
0.0106
0.0104
0.0102
0.01
0.0098
0.0096
0.0094
0.8
0.7
0.6
0.5
0.4
0.3
0.2
0.1
0
0
5
10
15
20
25
30
35
40
45
50

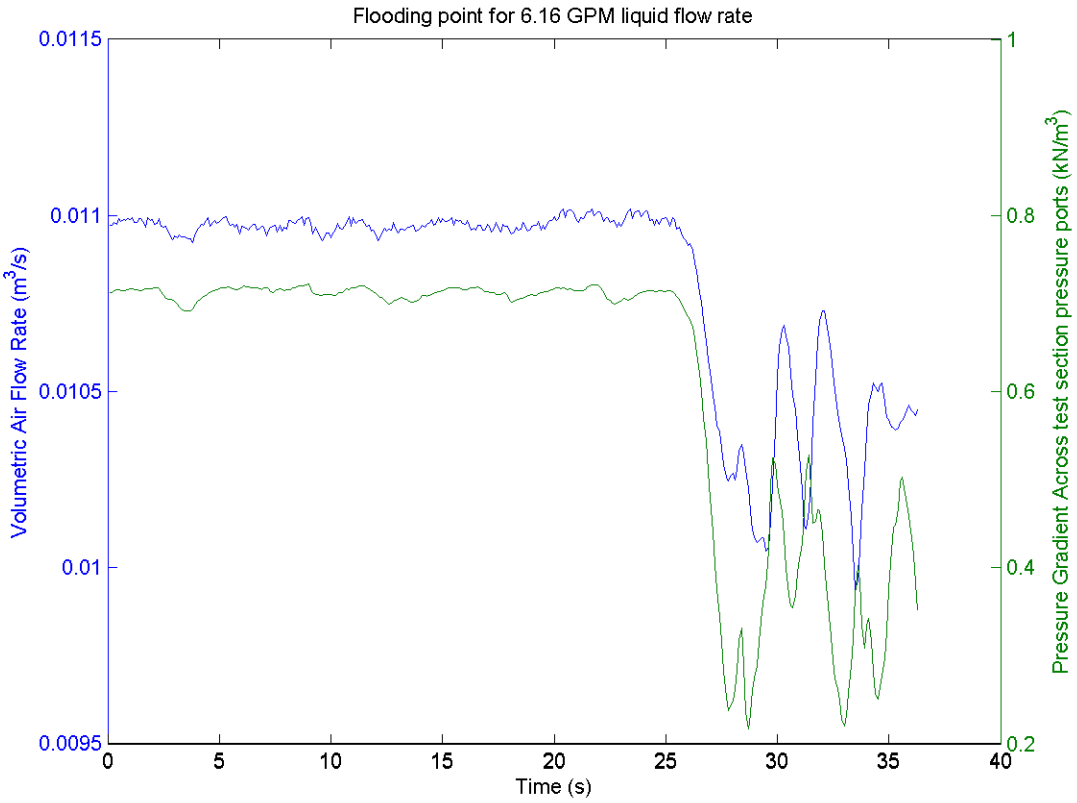
Flooding point for 6.16 GPM liquid flow rate
Volumetric Air Flow Rate (m3/s)
Pressure Gradient Across test section pressure ports (kN/m3)
Time (s)
0.0115
0.011
0.0105
0.01
0.0095
1
0.8
0.6
0.4
0.2
0
5
10
15
20
25
30
35
40

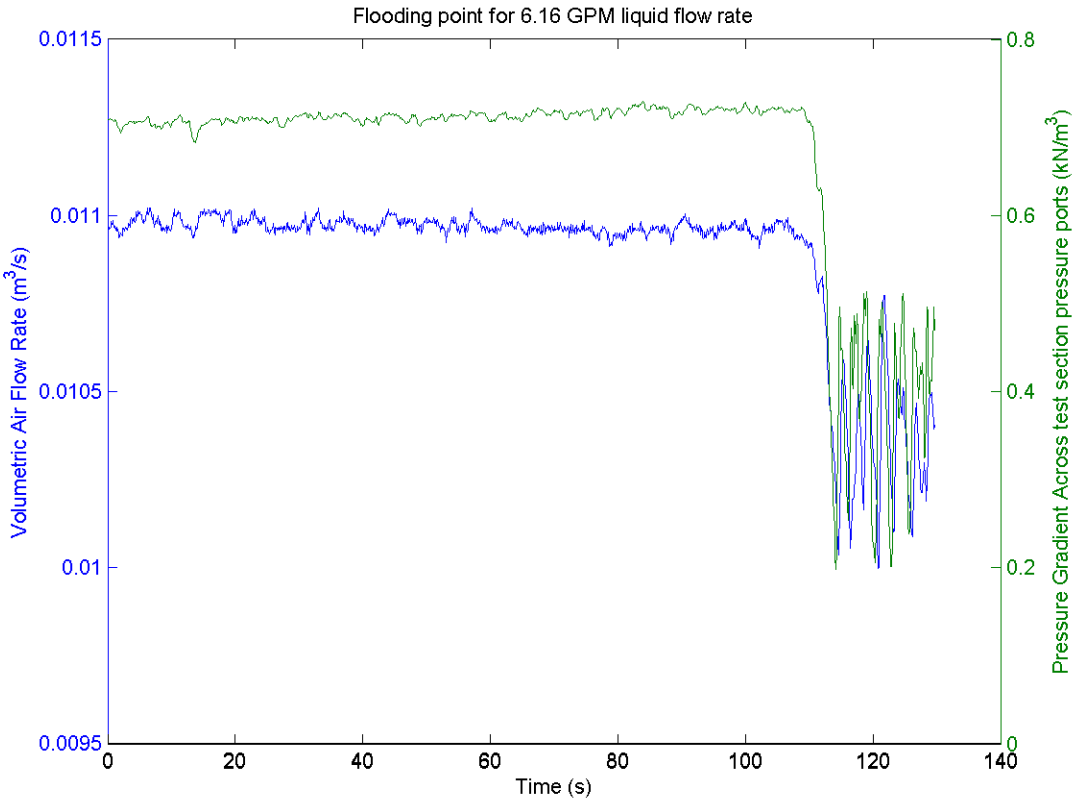
Flooding point for 6.16 GPM liquid flow rate
Volumetric Air Flow Rate (m3/s)
Pressure Gradient Across test section pressure ports (kN/m3)
Time (s)
0.0115
0.011
0.0105
0.01
0.0095
0.8
0.6
0.4
0.2
0
0
20
40
60
80
100
120
140

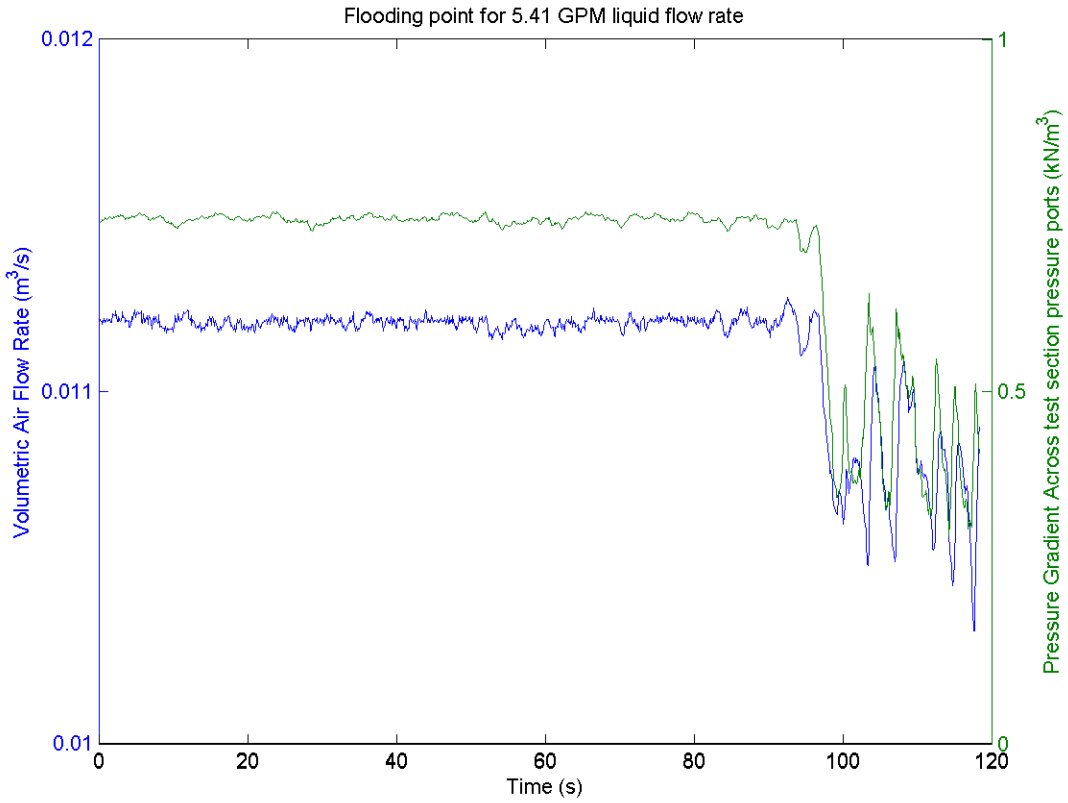
Flooding point for 5.41 GPM liquid flow rate
Volumetric Air Flow Rate (m3/s)
Pressure Gradient Across test section pressure ports (kN/m3)
Time (s)
0.012
0.011
0.01
1
0.5
0
0
20
40
60
80
100
120

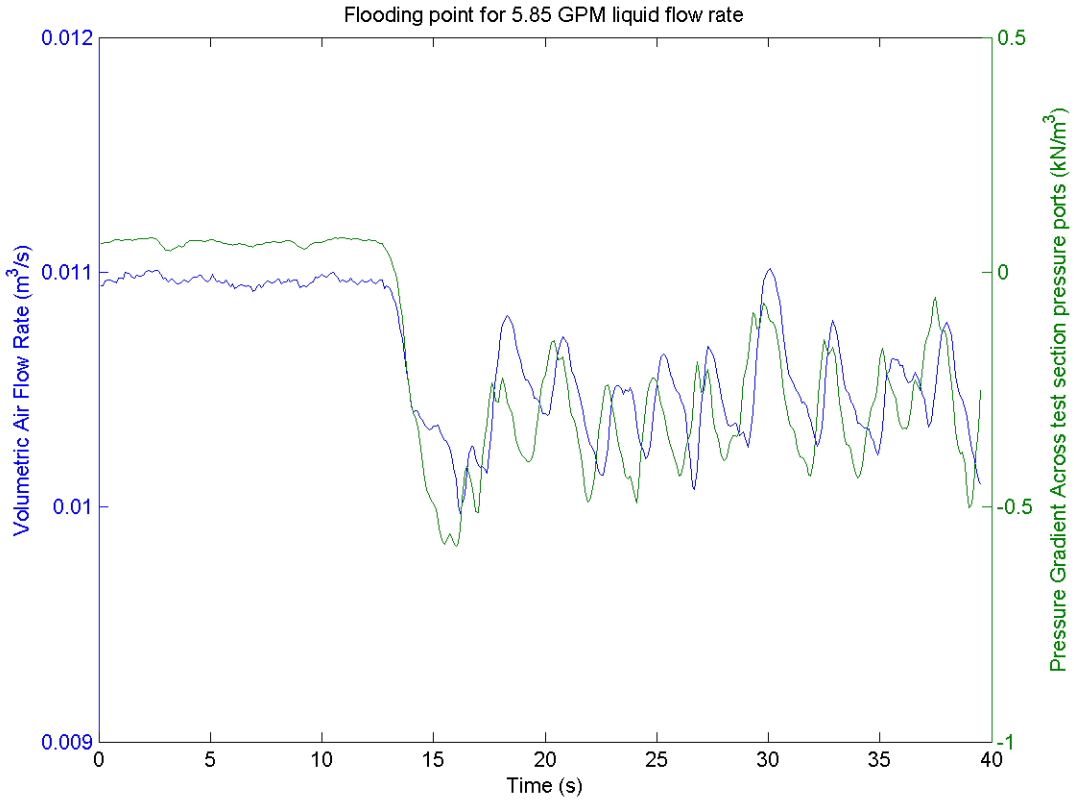
Flooding point for 5.85 GPM liquid flow rate
Volumetric Air Flow Rate (m3/s)
Pressure Gradient Across test section pressure ports (kN/m3)
Time (s)
0.012
0.011
0.01
0.009
0.5
0
-0.5
-1
0
5
10
15
20
25
30
35
40

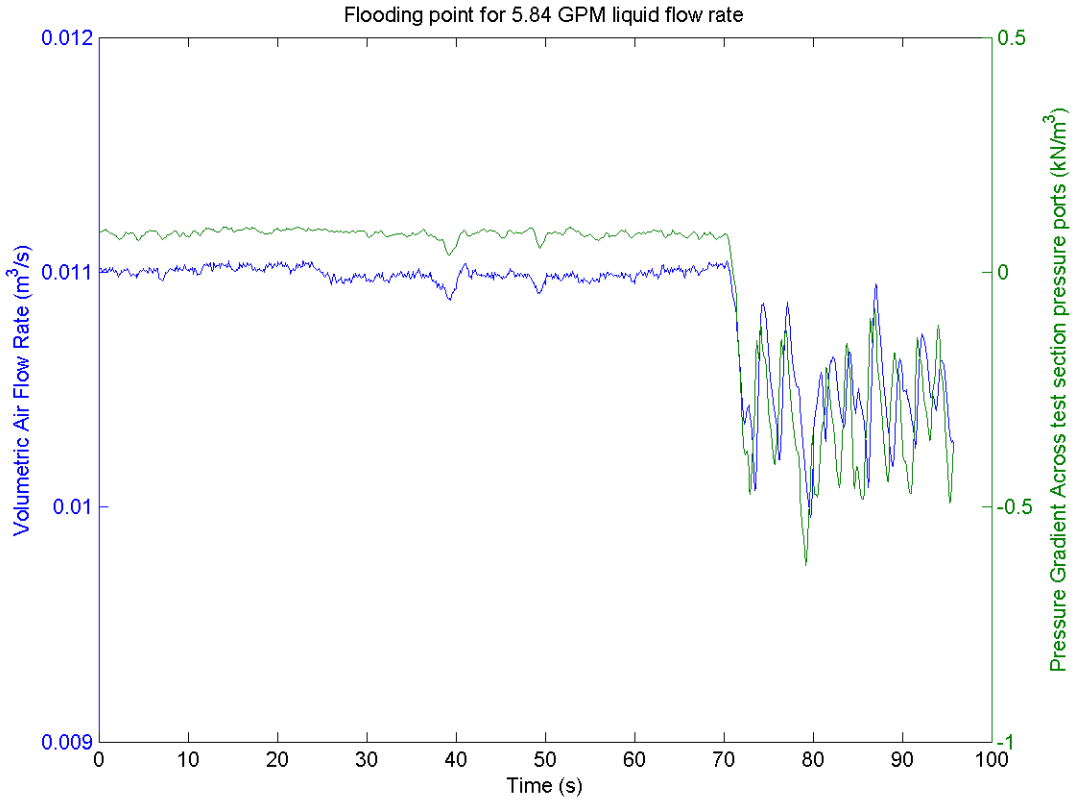
Flooding point for 5.84 GPM liquid flow rate
Volumetric Air Flow Rate (m3/s)
Pressure Gradient Across test section pressure ports (kN/m3)
Time (s)
0.012
0.011
0.01
0.009
0.5
0
-0.5
-1
0
10
20
30
40
50
60
70
80
90
100

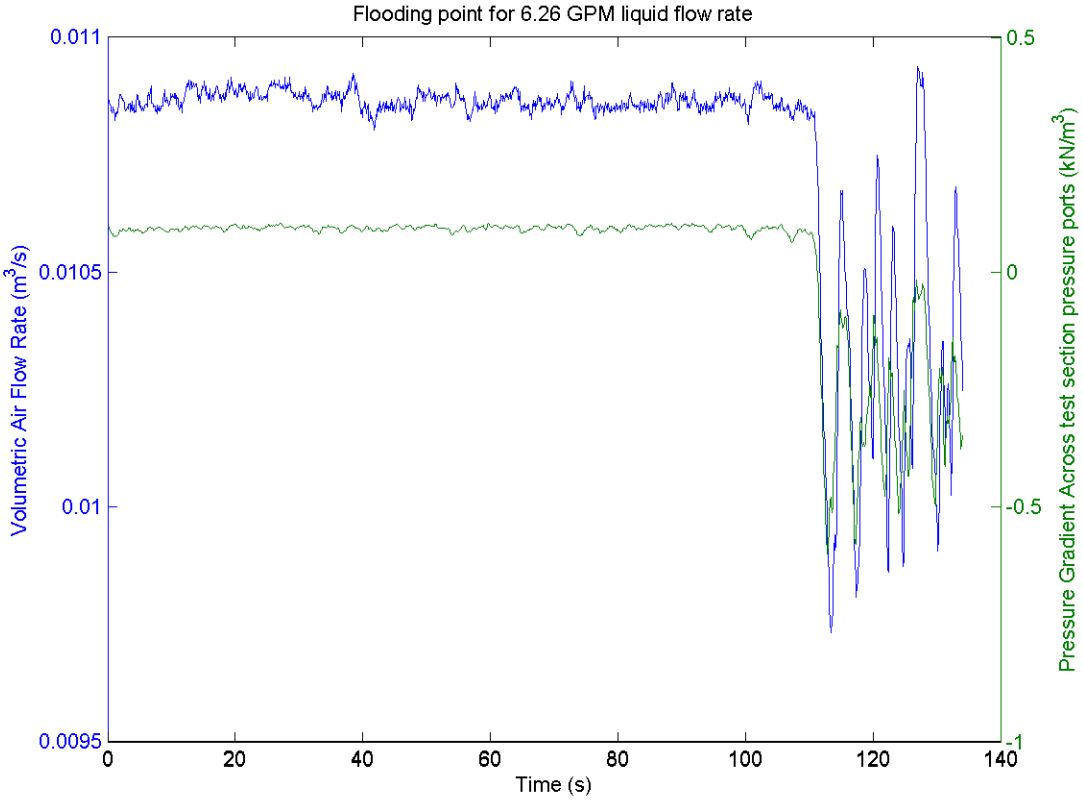
Flooding point for 6.26 GPM liquid flow rate
Volumetric Air Flow Rate (m3/s)
Pressure Gradient Across test section pressure ports (kN/m3)
Time (s)
0.011
0.0105
0.01
0.0095
0.5
0
-0.5
-1
0
20
40
60
80
100
120
140

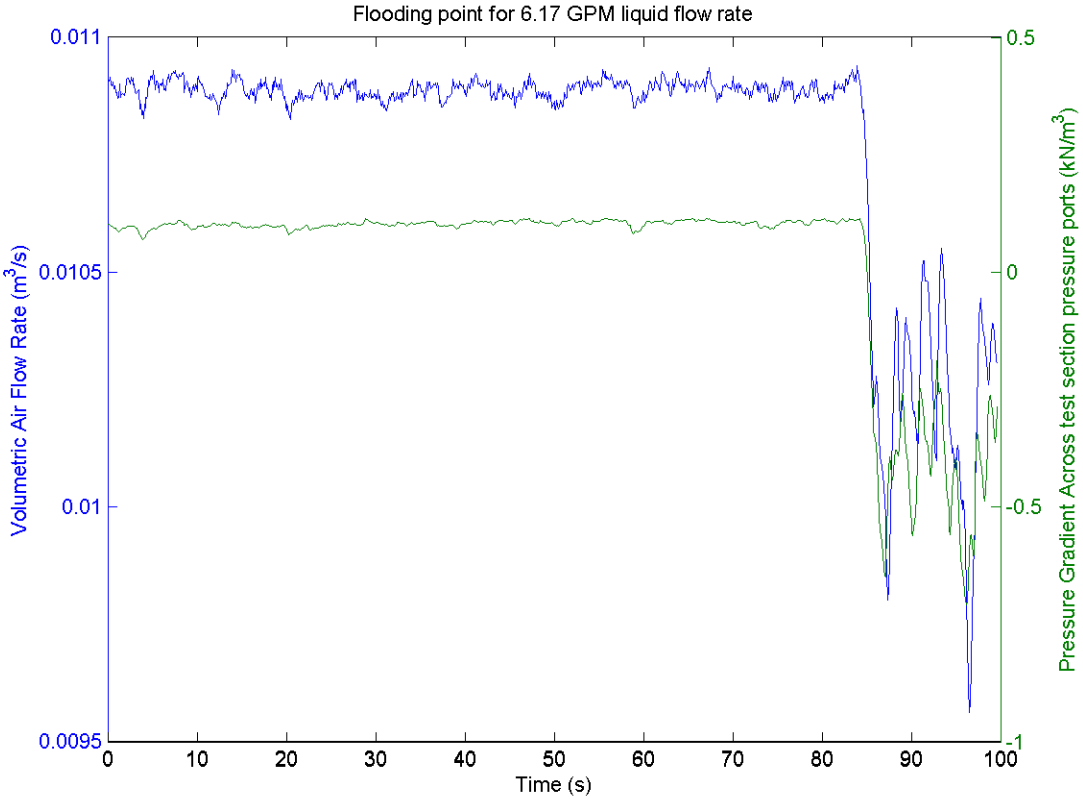
Flooding point for 6.17 GPM liquid flow rate
Volumetric Air Flow Rate (m3/s)
Pressure Gradient Across test section pressure ports (kN/m3)
Time (s)
0.011
0.0105
0.01
0.0095
0.5
0
-0.5
-1
0
10
20
30
40
50
60
70
80
90
100

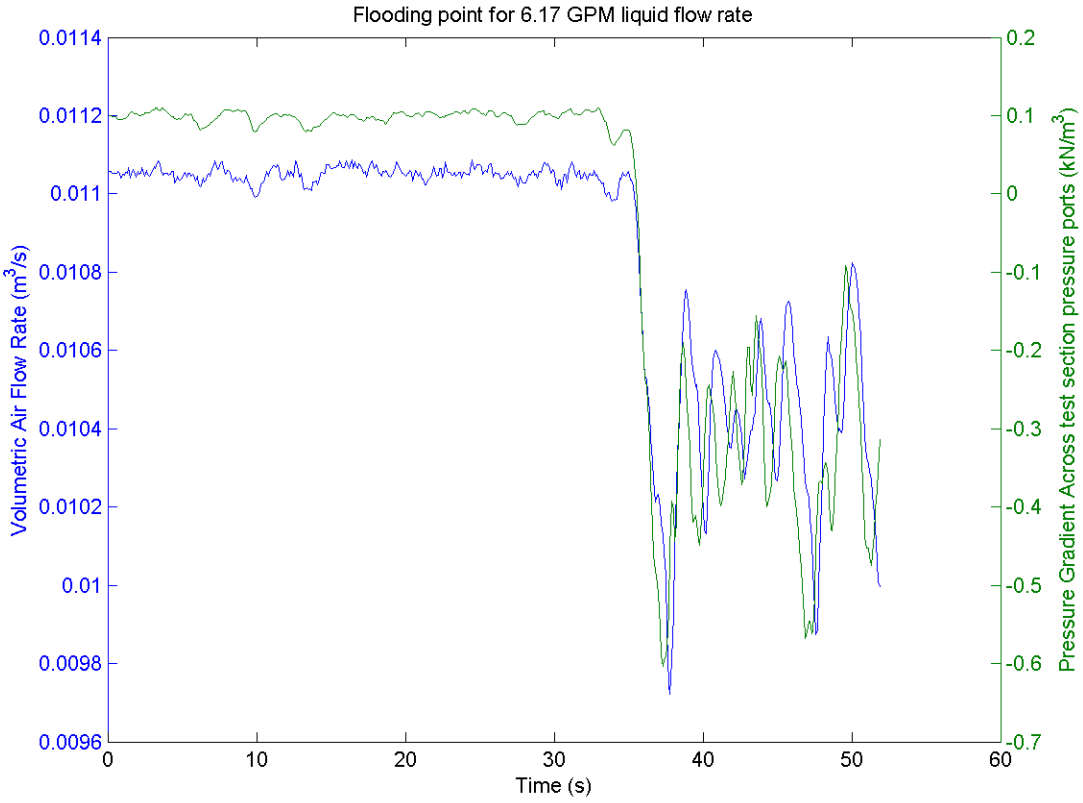
Flooding point for 6.17 GPM liquid flow rate
Volumetric Air Flow Rate (m3/s)
Pressure Gradient Across test section pressure ports (kN/m3)
Time (s)
0.0114
0.0112
0.011
0.0108
0.0106
0.0104
0.0102
0.01
0.0098
0.0096
0.2
0.1
0
-0.1
-0.2
-0.3
-0.4
-0.5
-0.6
-0.7
0
10
20
30
40
50
60

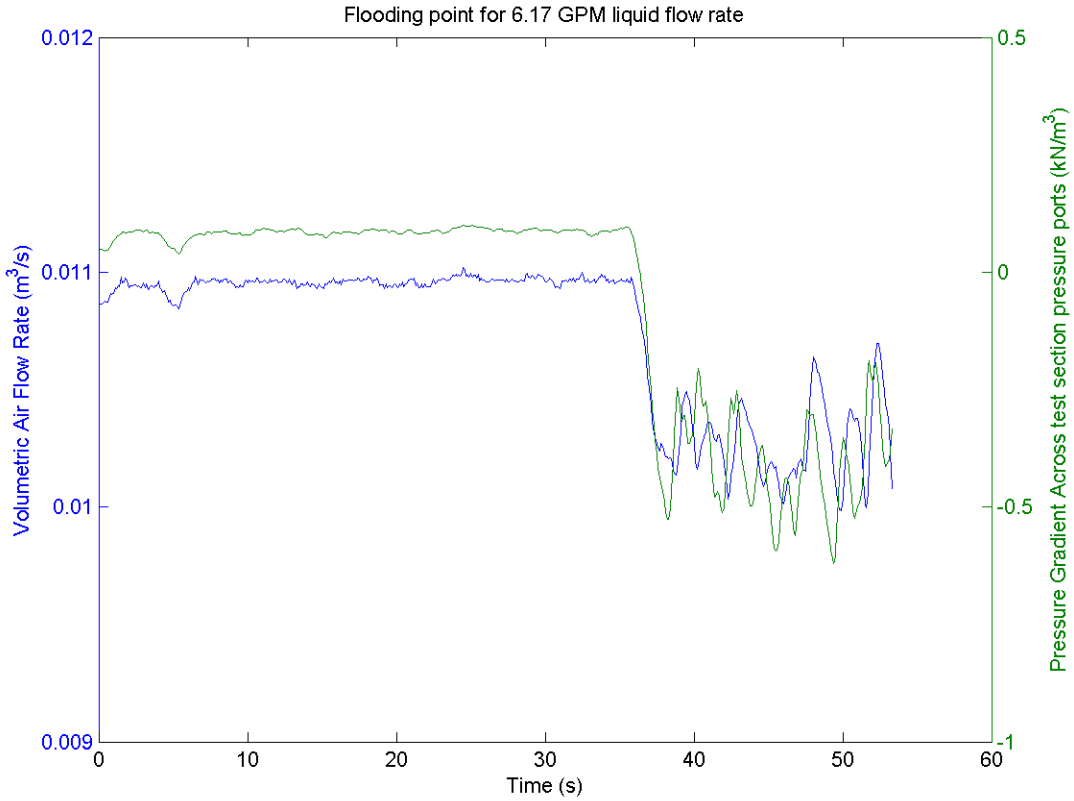
Flooding point for 6.17 GPM liquid flow rate
Volumetric Air Flow Rate (m3/s)
Pressure Gradient Across test section pressure ports (kN/m3)
Time (s)
0.012
0.011
0.01
0.009
0.5
0
-0.5
-1
0
10
20
30
40
50
60

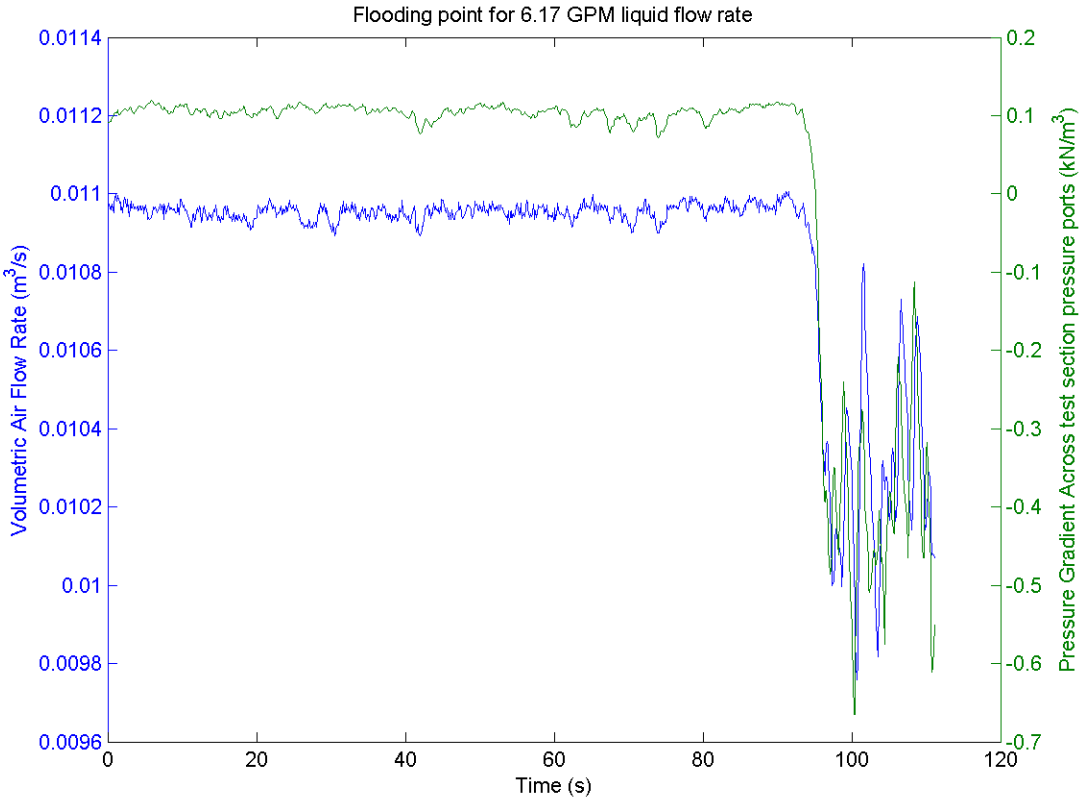
Flooding point for 6.17 GPM liquid flow rate
Volumetric Air Flow Rate (m3/s)
Pressure Gradient Across test section pressure ports (kN/m3)
Time (s)
0.0114
0.0112
0.011
0.0108
0.0106
0.0104
0.0102
0.01
0.0098
0.0096
0.2
0.1
0
-0.1
-0.2
-0.3
-0.4
-0.5
-0.6
-0.7
0
20
40
60
80
100
120

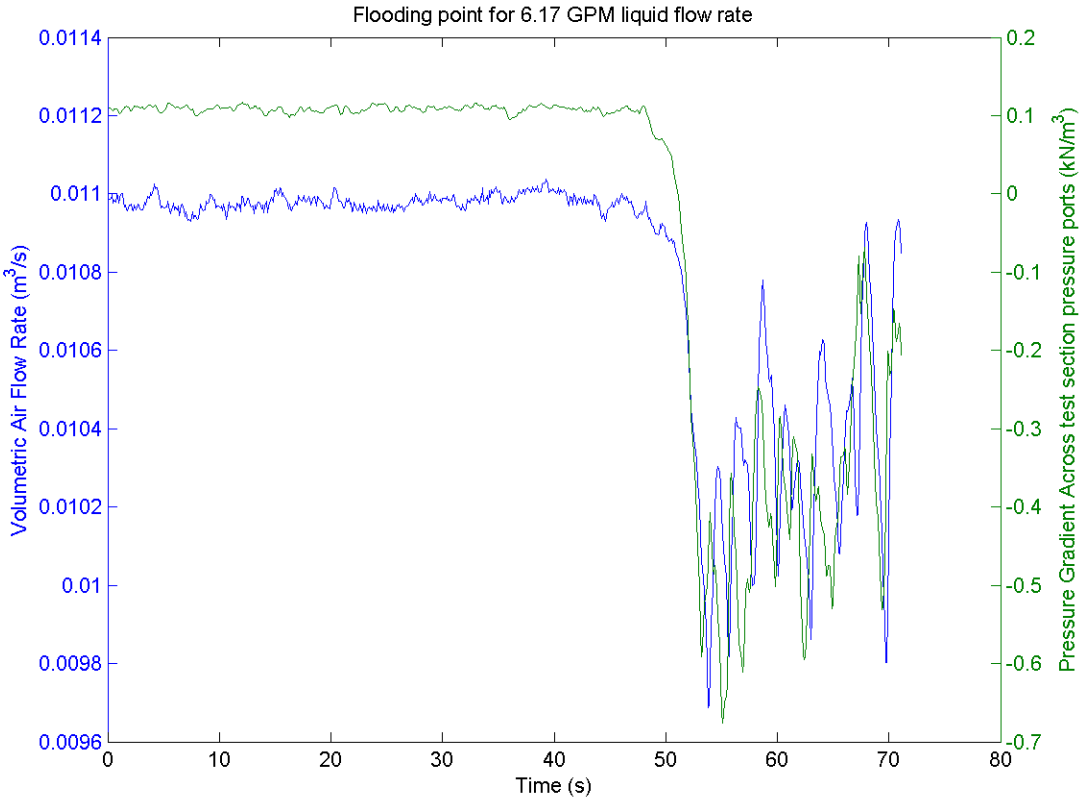
Flooding point for 6.17 GPM liquid flow rate
Volumetric Air Flow Rate (m3/s)
Pressure Gradient Across test section pressure ports (kN/m3)
Time (s)
0.0114
0.0112
0.011
0.0108
0.0106
0.0104
0.0102
0.01
0.0098
0.0096
0.2
0.1
0
-0.1
-0.2
-0.3
-0.4
-0.5
-0.6
-0.7
0
10
20
30
40
50
60
70
80

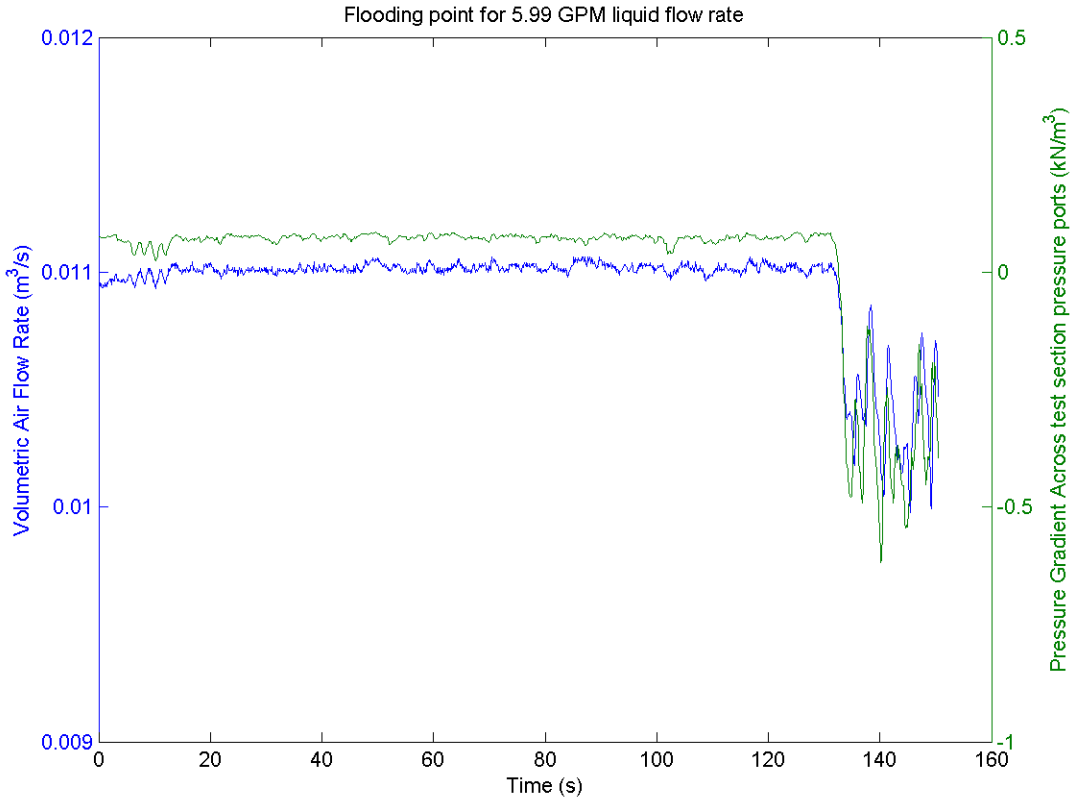
Flooding point for 5.99 GPM liquid flow rate
Volumetric Air Flow Rate (m3/s)
Pressure Gradient Across test section pressure ports (kN/m3)
Time (s)
0.012
0.011
0.01
0.009
0.5
0
-0.5
-1
0
20
40
60
80
100
120
140
160

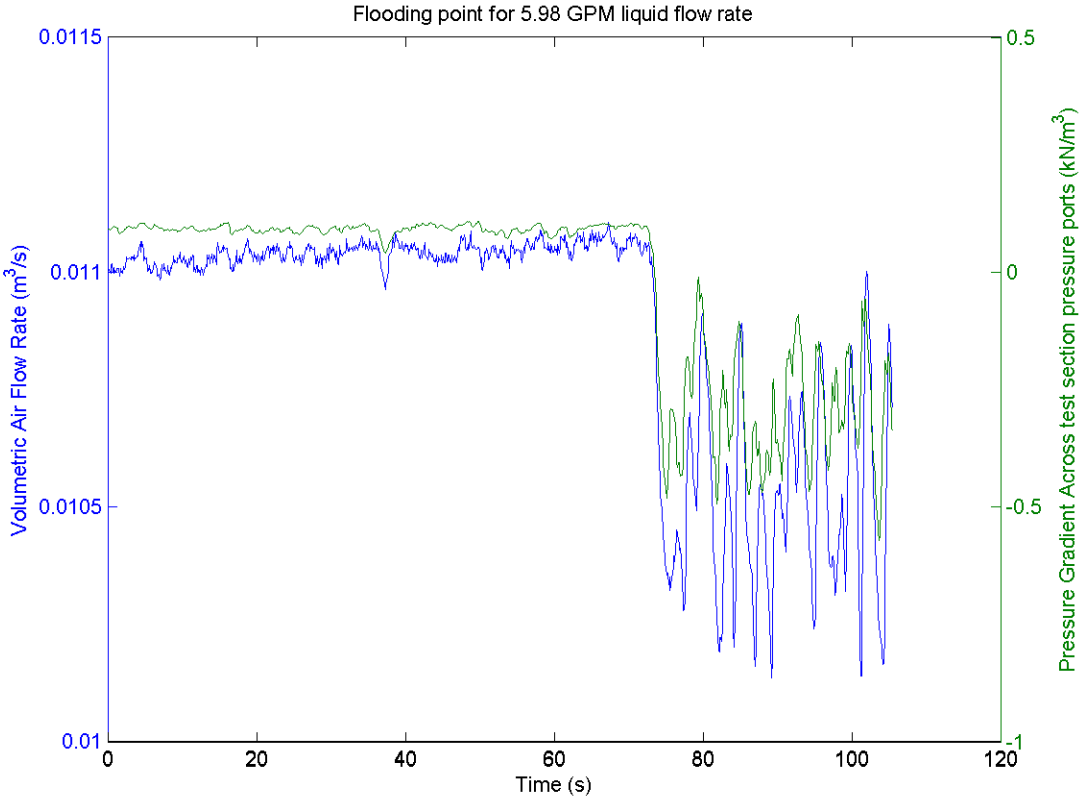
Flooding point for 5.98 GPM liquid flow rate
Volumetric Air Flow Rate (m3/s)
Pressure Gradient Across test section pressure ports (kN/m3)
Time (s)
0.0115
0.011
0.0105
0.01
0.5
0
-0.5
-1
0
20
40
60
80
100
120

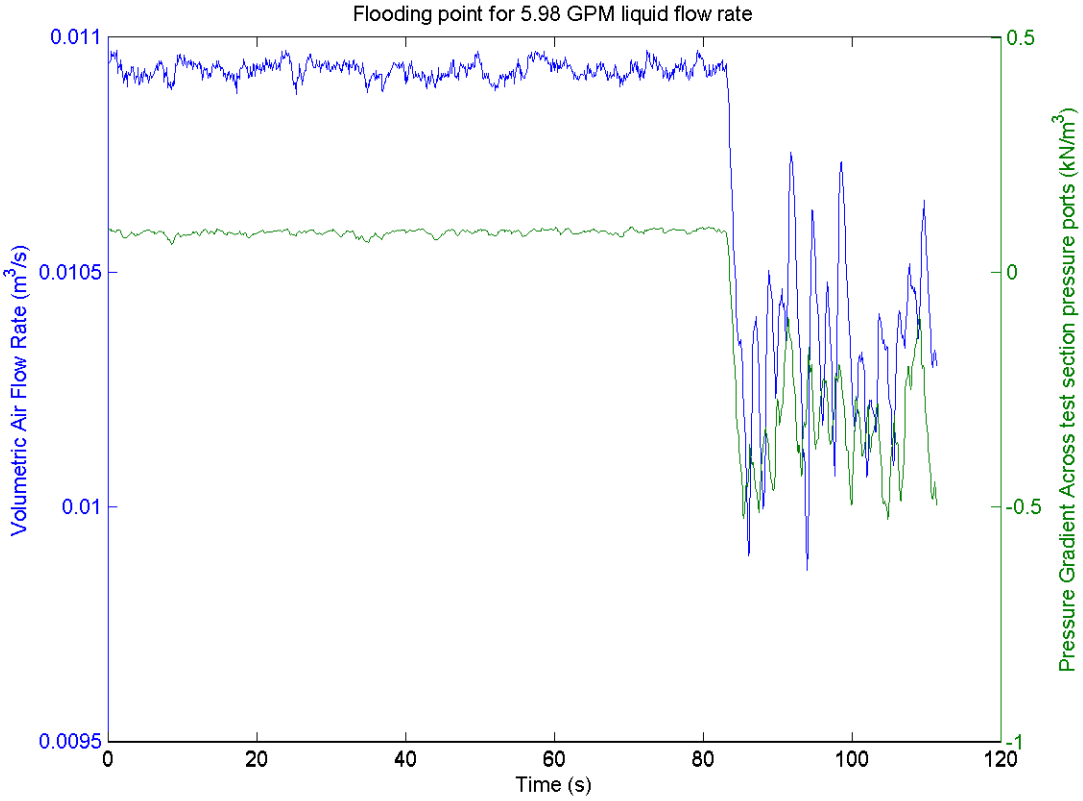
Flooding point for 5.98 GPM liquid flow rate
Volumetric Air Flow Rate (m3/s)
Pressure Gradient Across test section pressure ports (kN/m3)
Time (s)
0.011
0.0105
0.01
0.0095
0.5
0
-0.5
-1
0
20
40
60
80
100
120

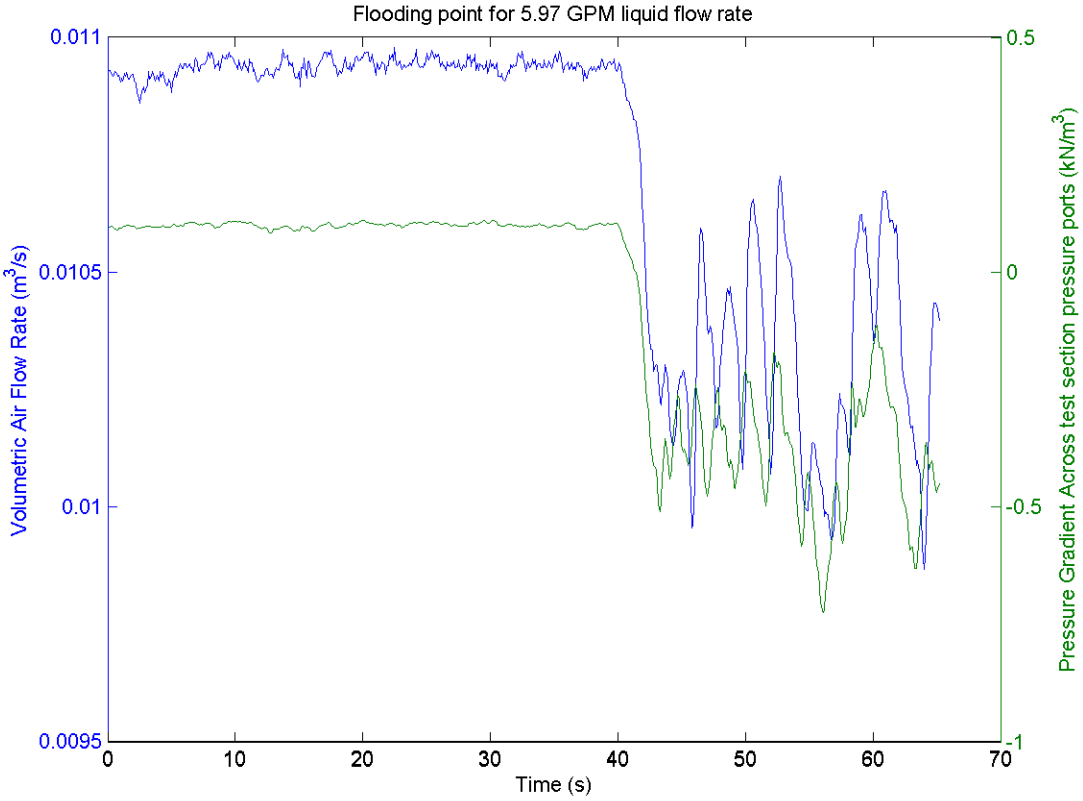
Flooding point for 5.97 GPM liquid flow rate
Volumetric Air Flow Rate (m3/s)
Pressure Gradient Across test section pressure ports (kN/m3)
Time (s)
0.011
0.0105
0.01
0.0095
0.5
0
-0.5
-1
0
10
20
30
40
50
60
70

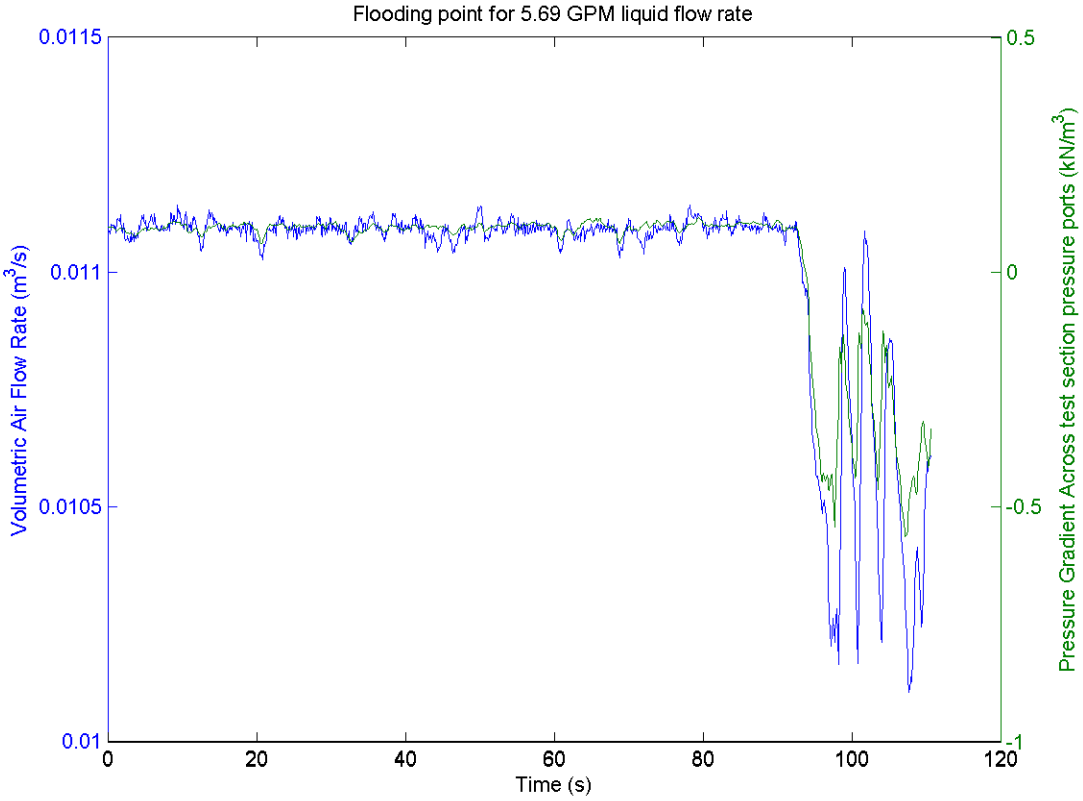
Flooding point for 5.69 GPM liquid flow rate
Volumetric Air Flow Rate (m3/s)
Pressure Gradient Across test section pressure ports (kN/m3)
Time (s)
0.0115
0.011
0.0105
0.01
0.5
0
-0.5
-1
0
20
40
60
80
100
120

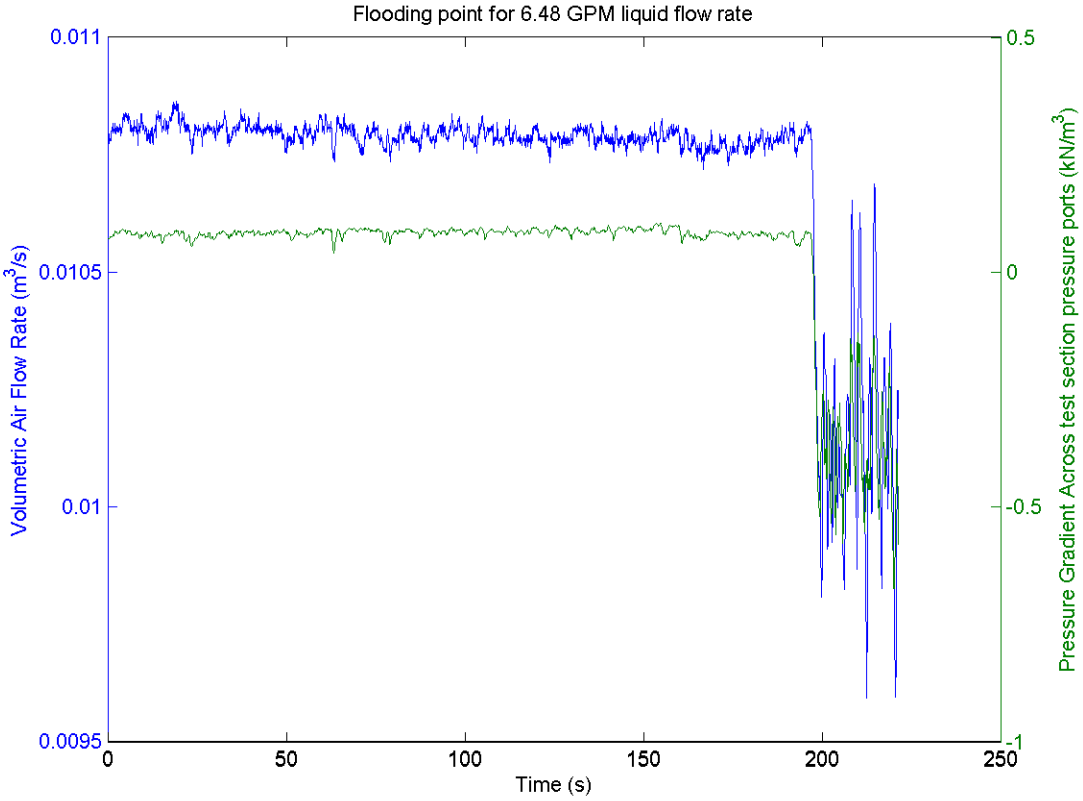
Flooding point for 6.48 GPM liquid flow rate
Volumetric Air Flow Rate (m3/s)
Pressure Gradient Across test section pressure ports (kN/m3)
Time (s)
0.011
0.0105
0.01
0.0095
0.5
0
-0.5
-1
0
50
100
150
200
250

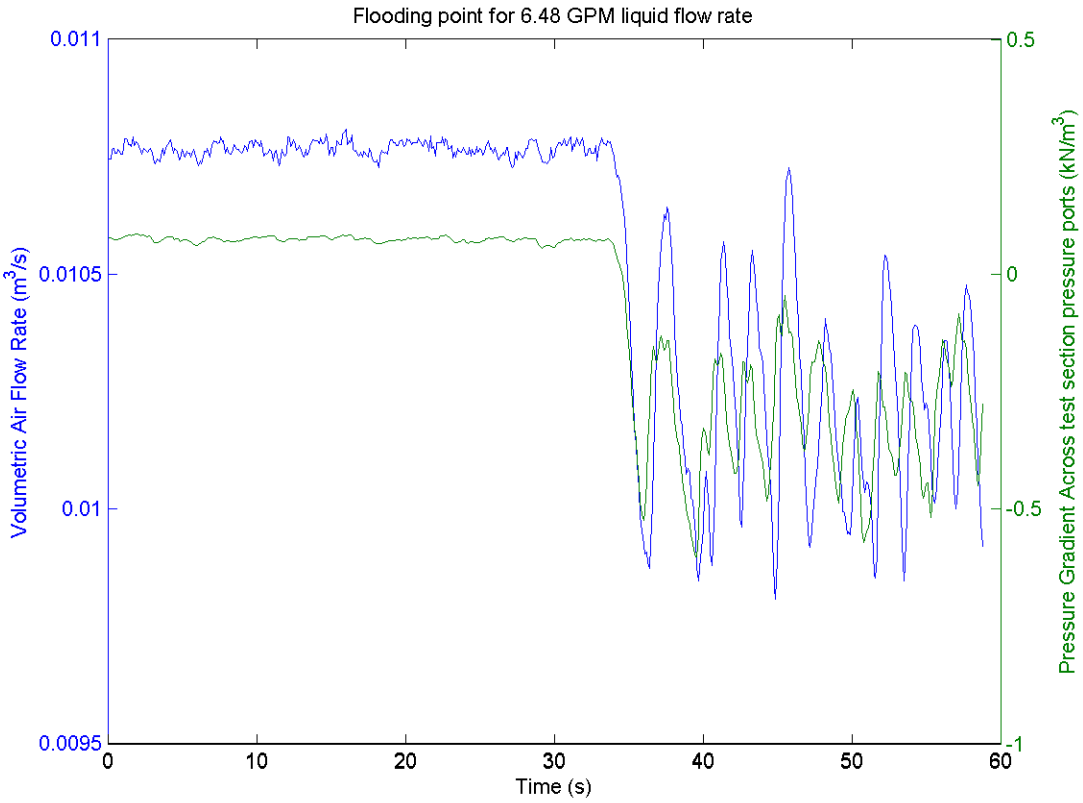
Flooding point for 6.48 GPM liquid flow rate
Volumetric Air Flow Rate (m3/s)
Pressure Gradient Across test section pressure ports (kN/m3)
Time (s)
0.011
0.0105
0.01
0.0095
0.5
0
-0.5
-1
0
10
20
30
40
50
60

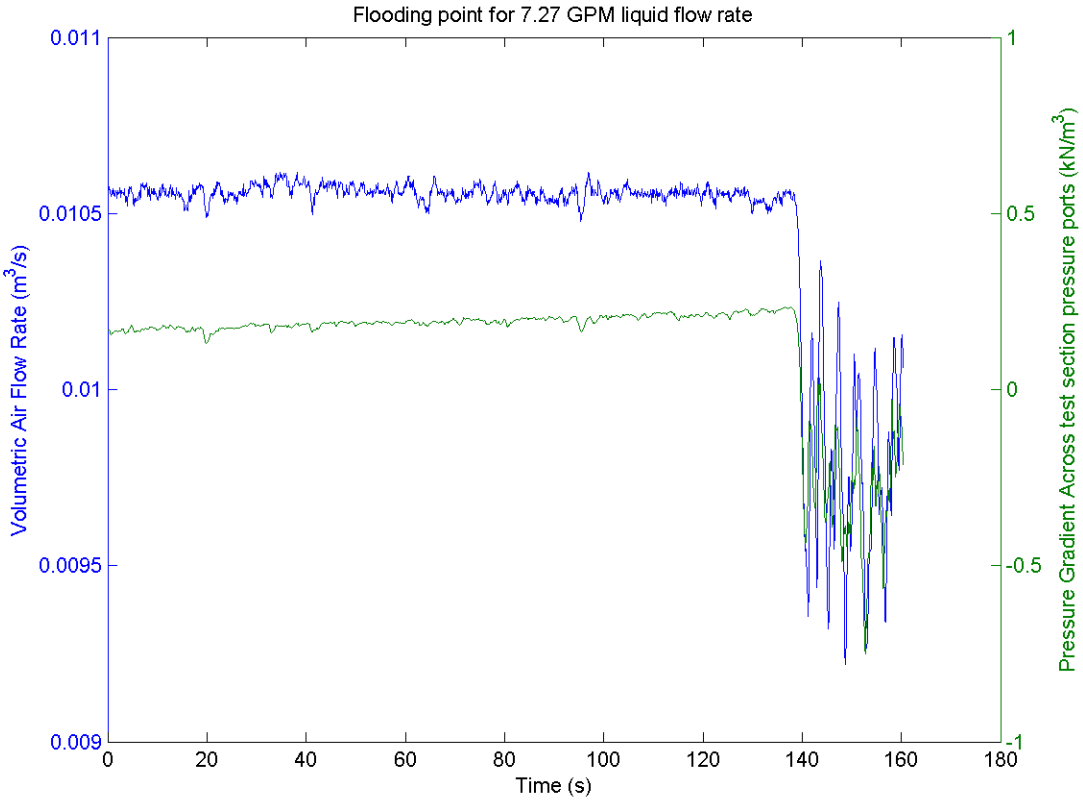
Flooding point for 7.27 GPM liquid flow rate
Volumetric Air Flow Rate (m3/s)
Pressure Gradient Across test section pressure ports (kN/m3)
Time (s)
0.011
0.0105
0.01
0.0095
0.009
1
0.5
0
-0.5
-1
0
20
40
60
80
100
120
140
160
180

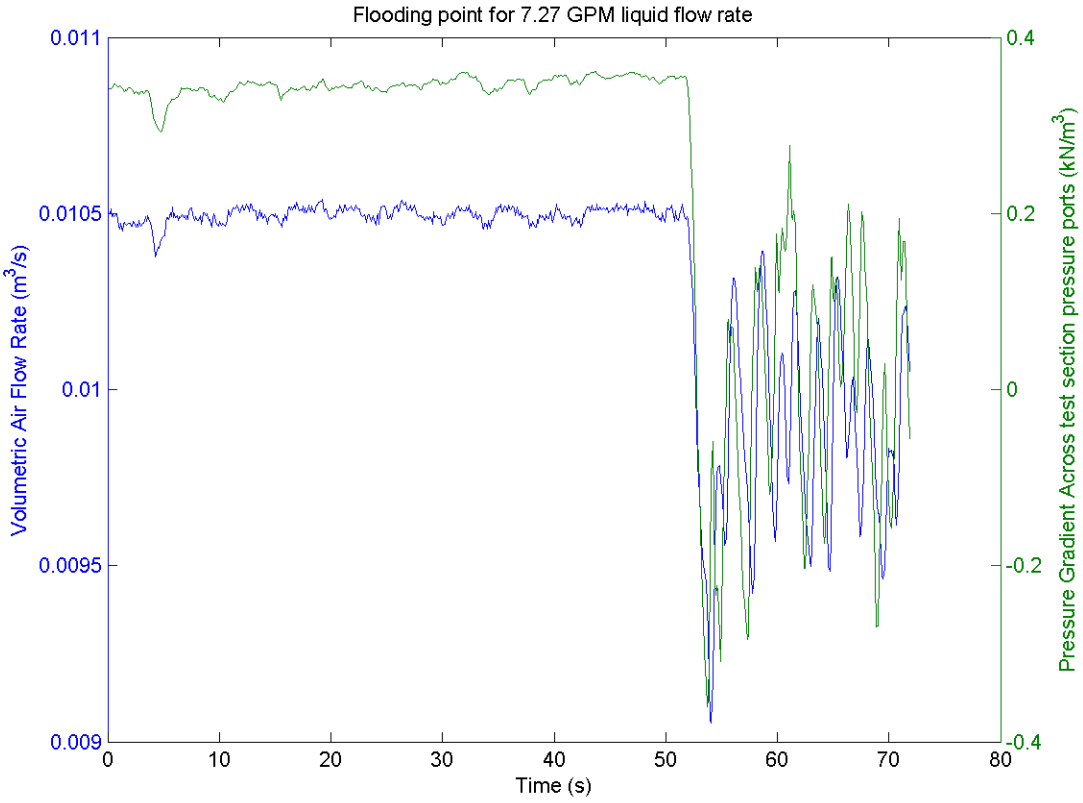
Flooding point for 7.27 GPM liquid flow rate
Volumetric Air Flow Rate (m3/s)
Pressure Gradient Across test section pressure ports (kN/m3)
Time (s)
0.011
0.0105
0.01
0.0095
0.009
0.4
0.2
0
-0.2
-0.4
0
10
20
30
40
50
60
70
80

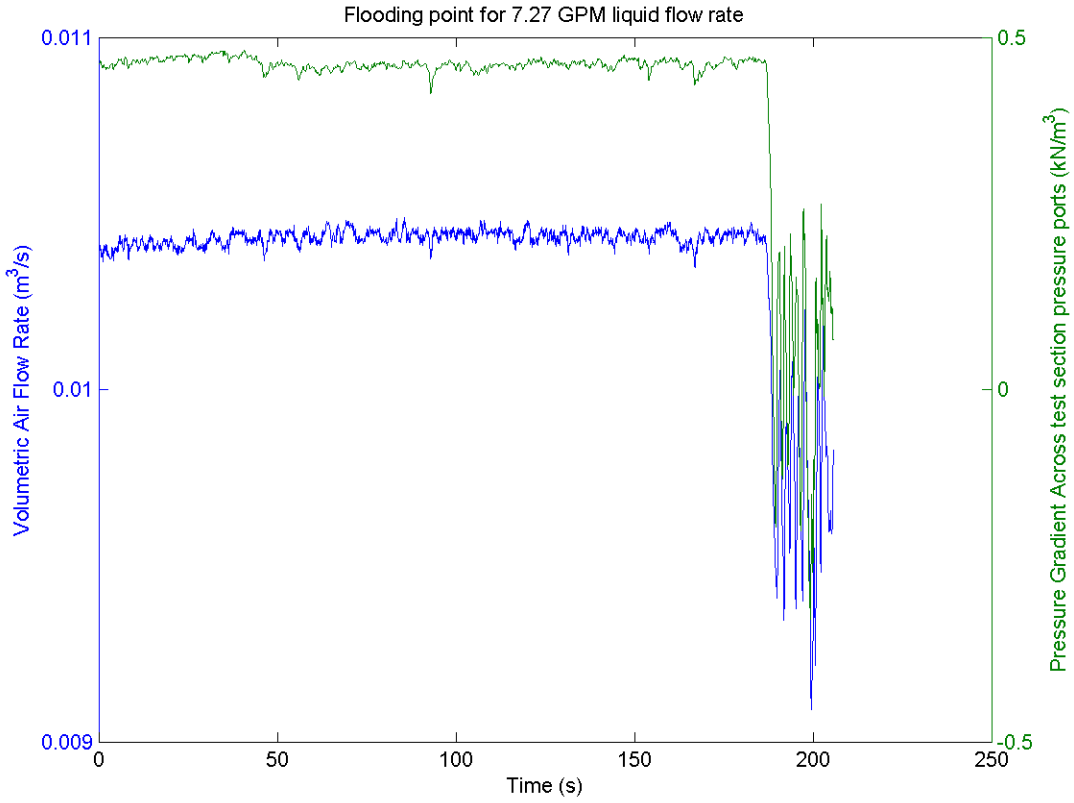
Flooding point for 7.27 GPM liquid flow rate
0.011
0.01
0.009
0.5
0
-0.5
0
50
100
150
200
250
Time (s)
Volumetric Air Flow Rate (m3/s)
Pressure Gradient Across test section pressure ports (kN/m3)

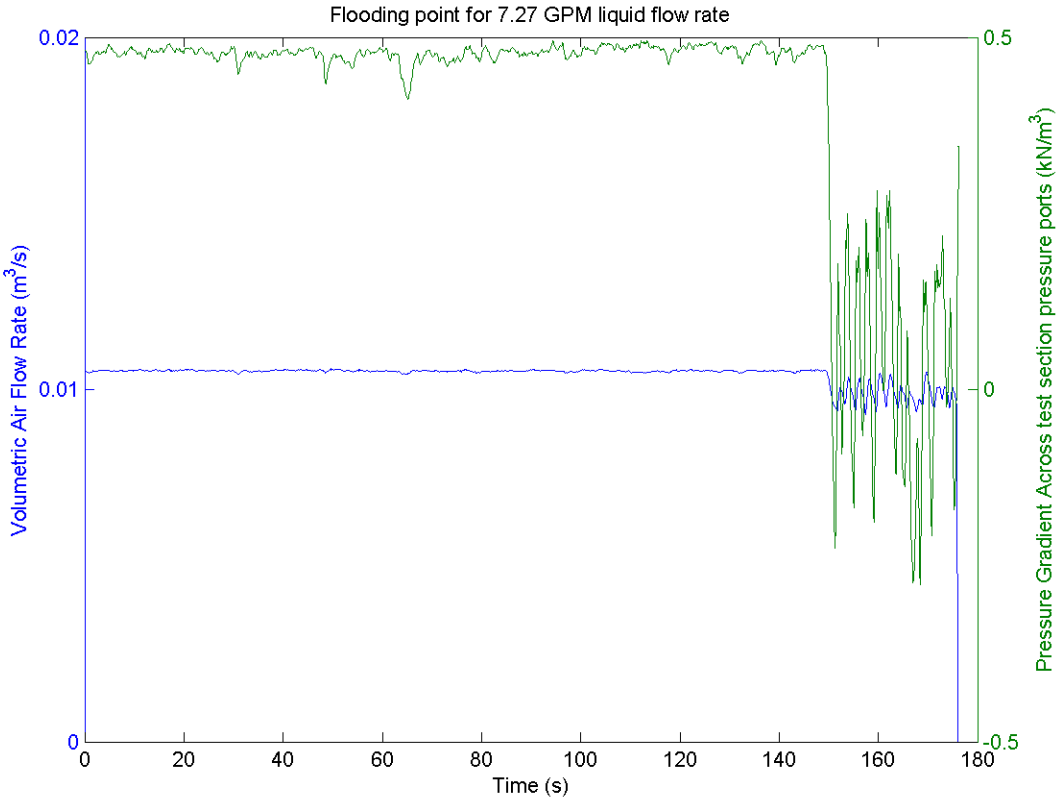
Flooding point for 7.27 GPM liquid flow rate
Volumetric Air Flow Rate (m3/s)
Pressure Gradient Across test section pressure ports (kN/m3)
Time (s)
0.02
0.01
0
0.5
0
-0.5
0
20
40
60
80
100
120
140
160
180

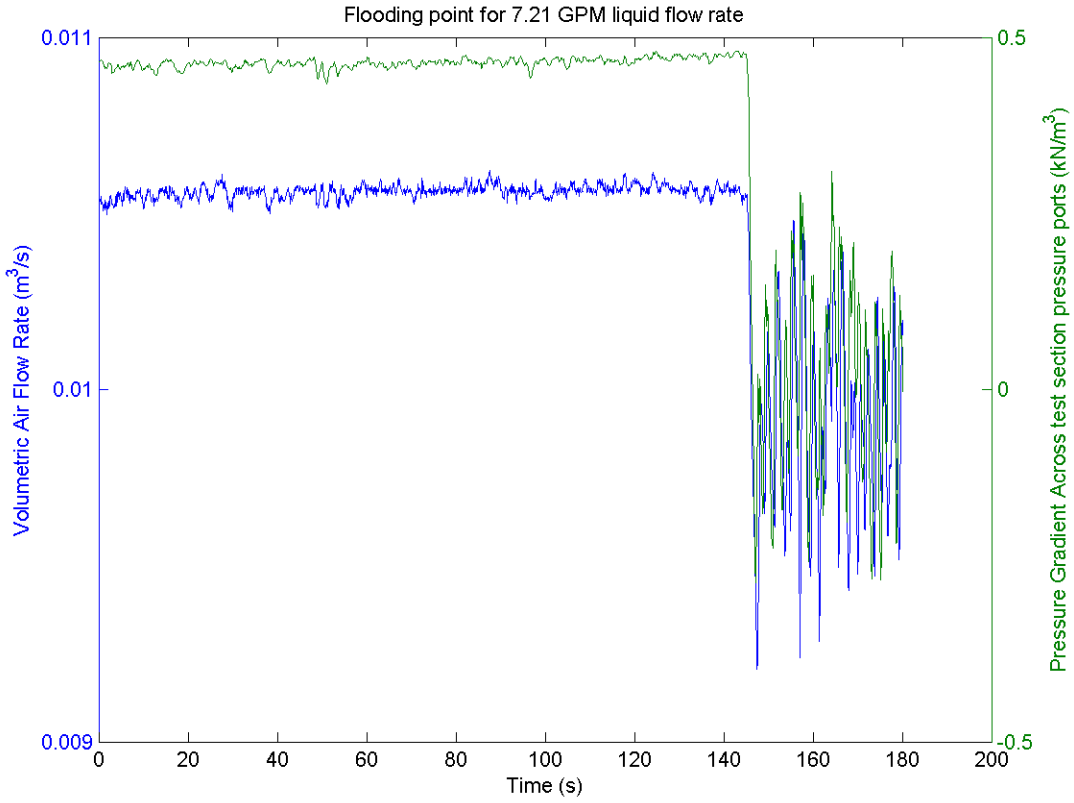
Flooding point for 7.21 GPM liquid flow rate
0.011
0.01
0.009
Volumetric Air Flow Rate (m3/s)
0.5
0
-0.5
Pressure Gradient Across test section pressure ports (kN/m3)
0
20
40
60
80
100
120
140
160
180
200
Time (s)

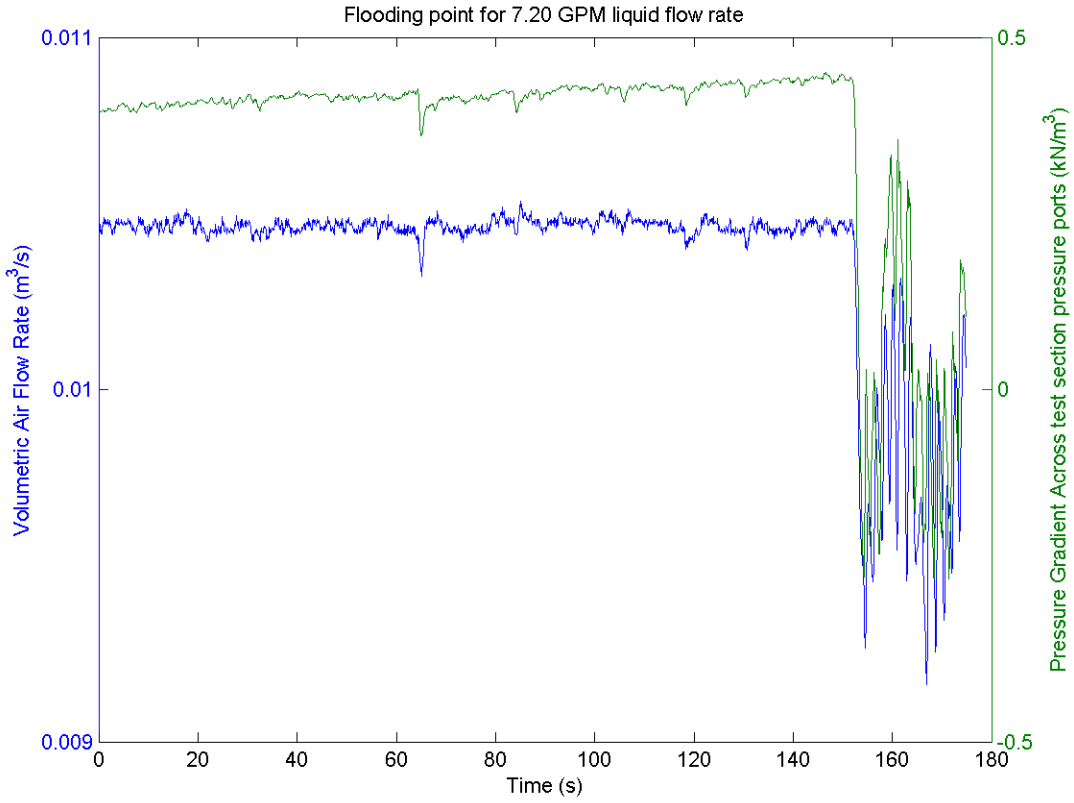
Flooding point for 7.20 GPM liquid flow rate
0.011
0.01
0.009
0.5
0
-0.5
0
20
40
60
80
100
120
140
160
180
Time (s)
Volumetric Air Flow Rate (m3/s)
Pressure Gradient Across test section pressure ports (kN/m3)

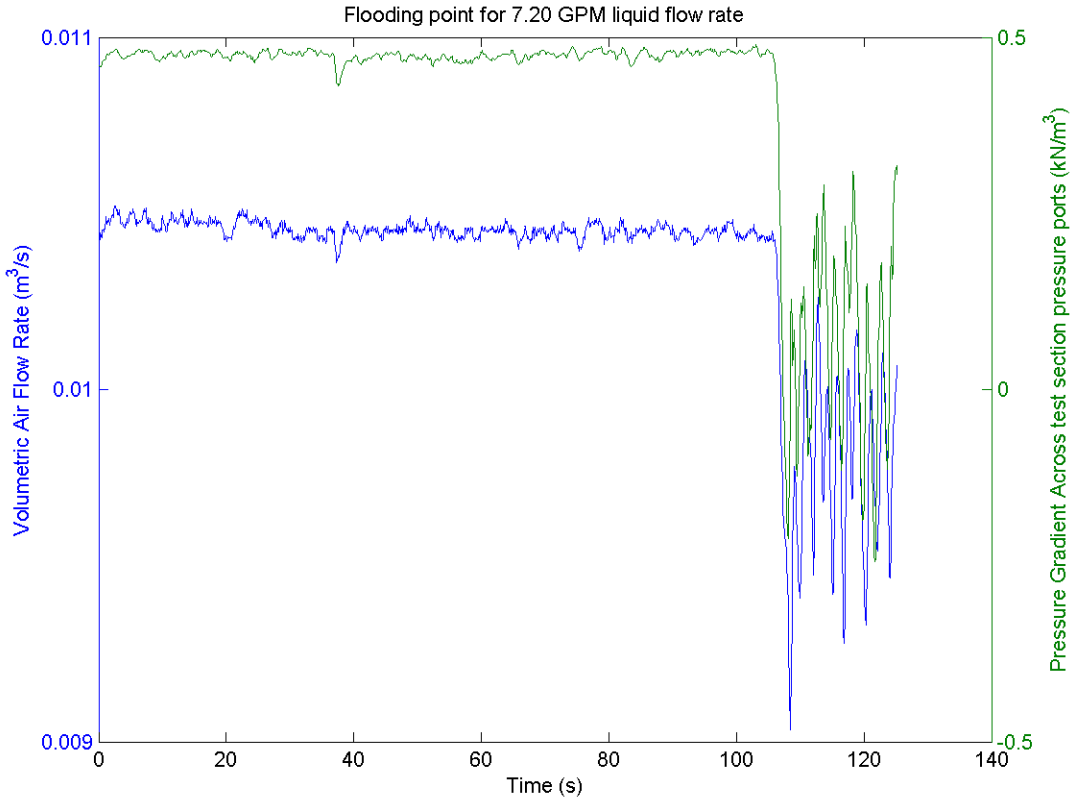
Flooding point for 7.20 GPM liquid flow rate
Volumetric Air Flow Rate (m3/s)
Pressure Gradient Across test section pressure ports (kN/m3)
Time (s)
0.011
0.01
0.009
0.5
0
-0.5
0
20
40
60
80
100
120
140

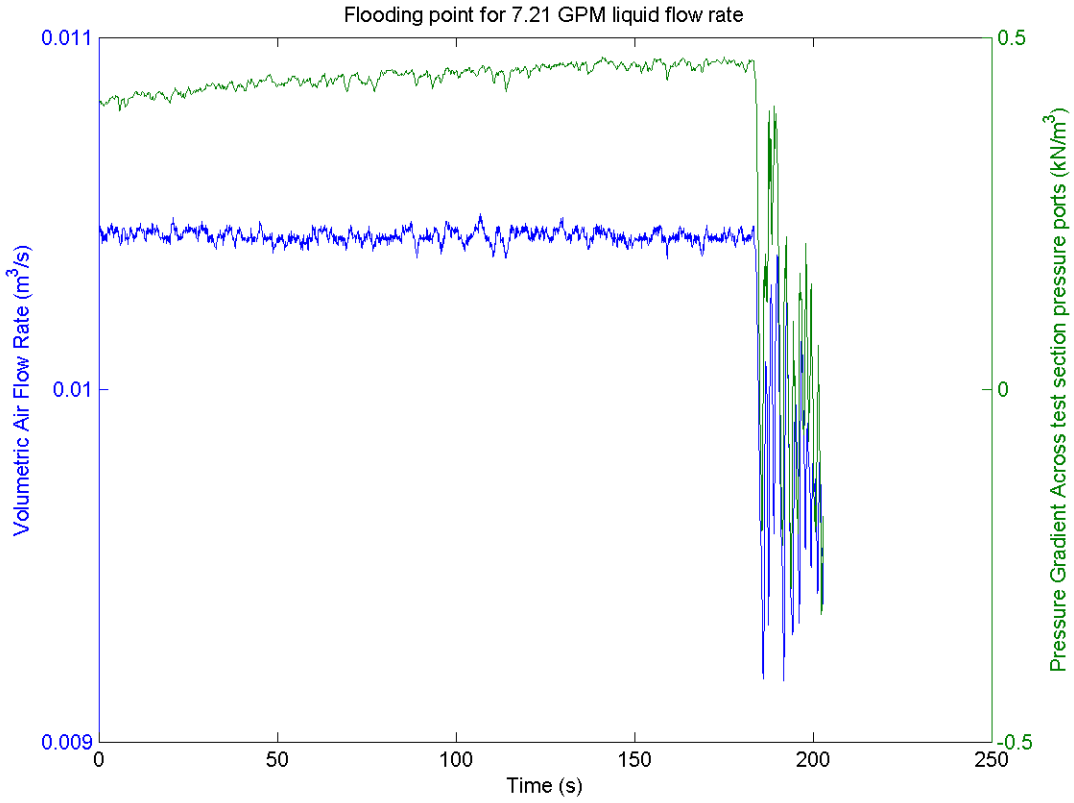
Flooding point for 7.21 GPM liquid flow rate
0.011
0.01
0.009
0.5
0
-0.5
0
50
100
150
200
250
Time (s)
Volumetric Air Flow Rate (m3/s)
Pressure Gradient Across test section pressure ports (kN/m3)

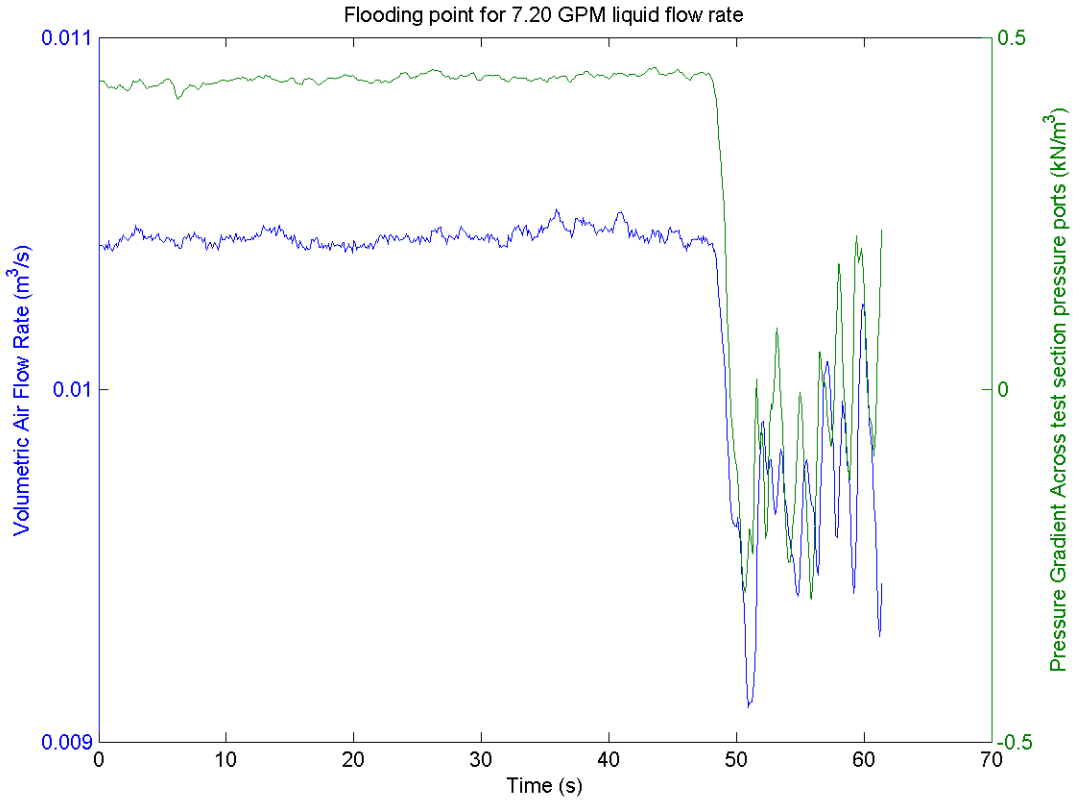
Flooding point for 7.20 GPM liquid flow rate
0.011
0.01
0.009
0.5
0
-0.5
0
10
20
30
40
50
60
70
Time (s)
Volumetric Air Flow Rate (m3/s)
Pressure Gradient Across test section pressure ports (kN/m3)

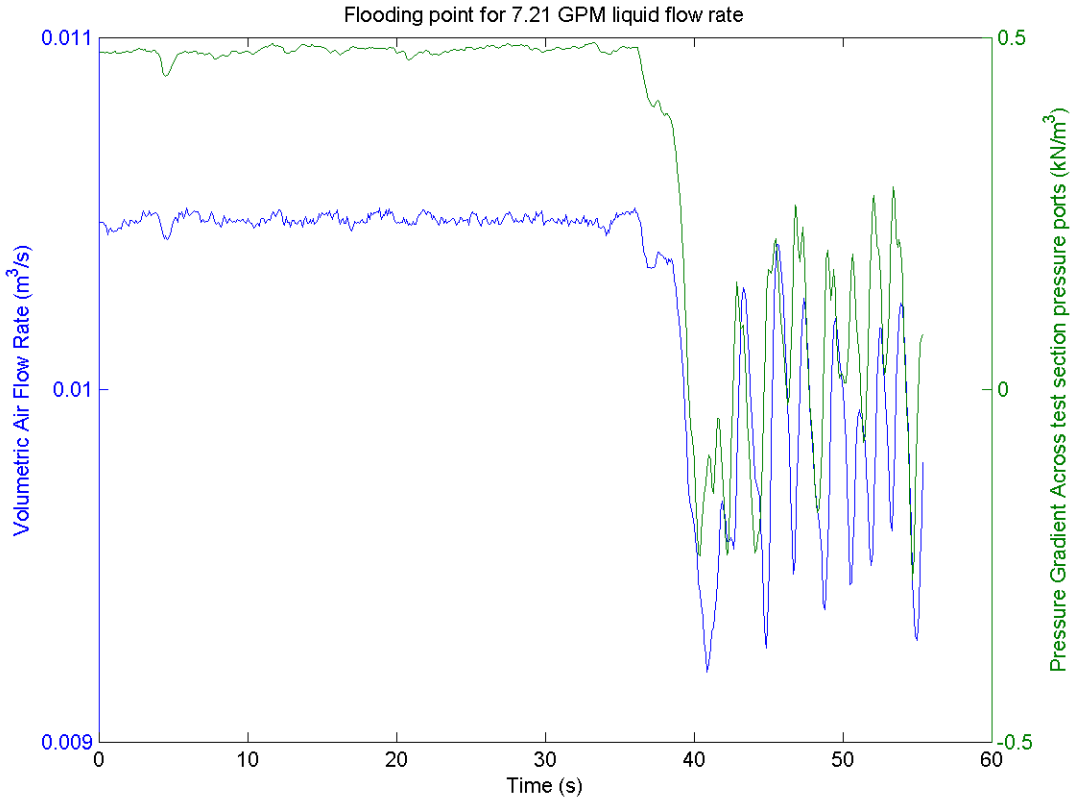
Flooding point for 7.21 GPM liquid flow rate
0.011
0.01
0.009
0.5
0
-0.5
0
10
20
30
40
50
60
Time (s)
Volumetric Air Flow Rate (m3/s)
Pressure Gradient Across test section pressure ports (kN/m3)

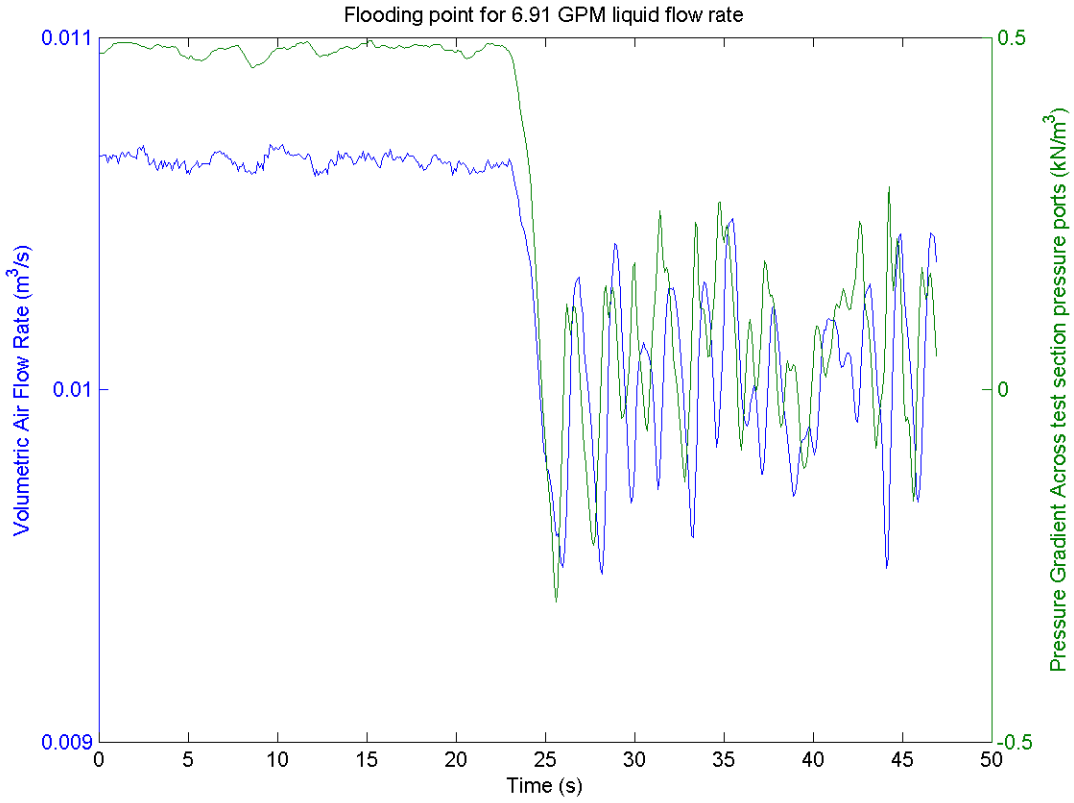
Flooding point for 6.91 GPM liquid flow rate
0.011
0.01
0.009
0.5
0
-0.5
0
5
10
15
20
25
30
35
40
45
50
Time (s)
Volumetric Air Flow Rate (m3/s)
Pressure Gradient Across test section pressure ports (kN/m3)

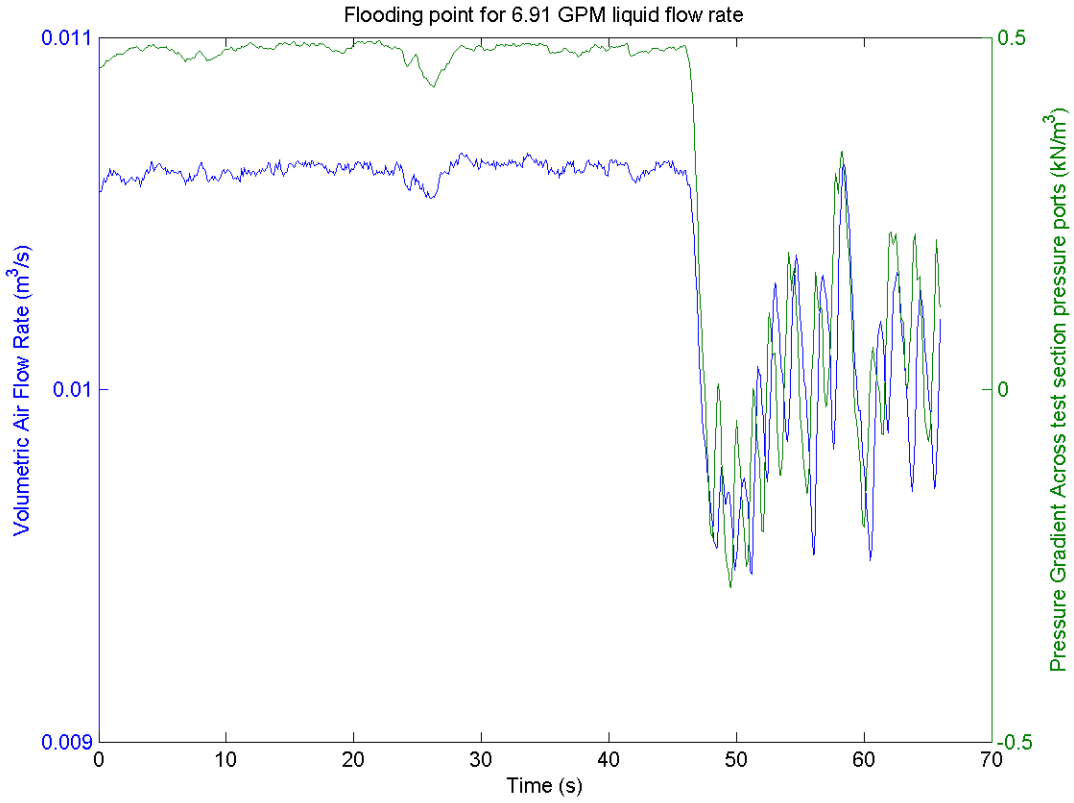
Flooding point for 6.91 GPM liquid flow rate
0.011
0.01
0.009
0.5
0
-0.5
0
10
20
30
40
50
60
70
Time (s)
Volumetric Air Flow Rate (m3/s)
Pressure Gradient Across test section pressure ports (kN/m3)

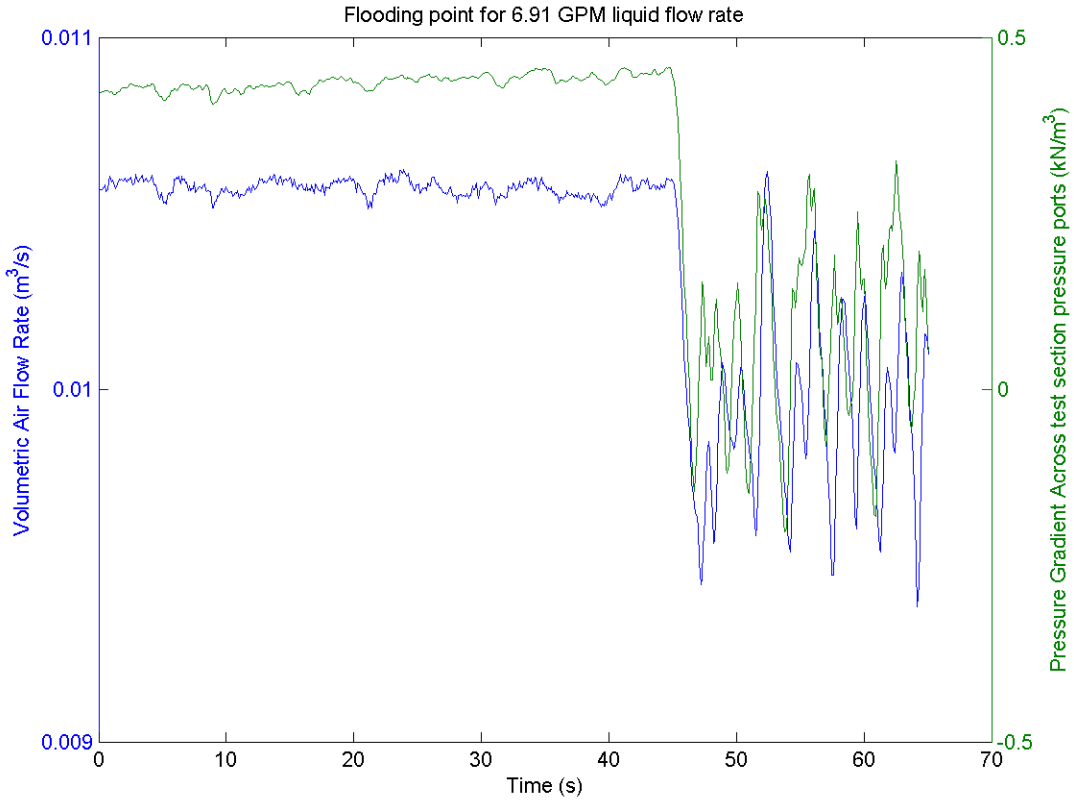
Flooding point for 6.91 GPM liquid flow rate
0.011
0.01
0.009
0.5
0
-0.5
0
10
20
30
40
50
60
70
Time (s)
Volumetric Air Flow Rate (m3/s)
Pressure Gradient Across test section pressure ports (kN/m3)

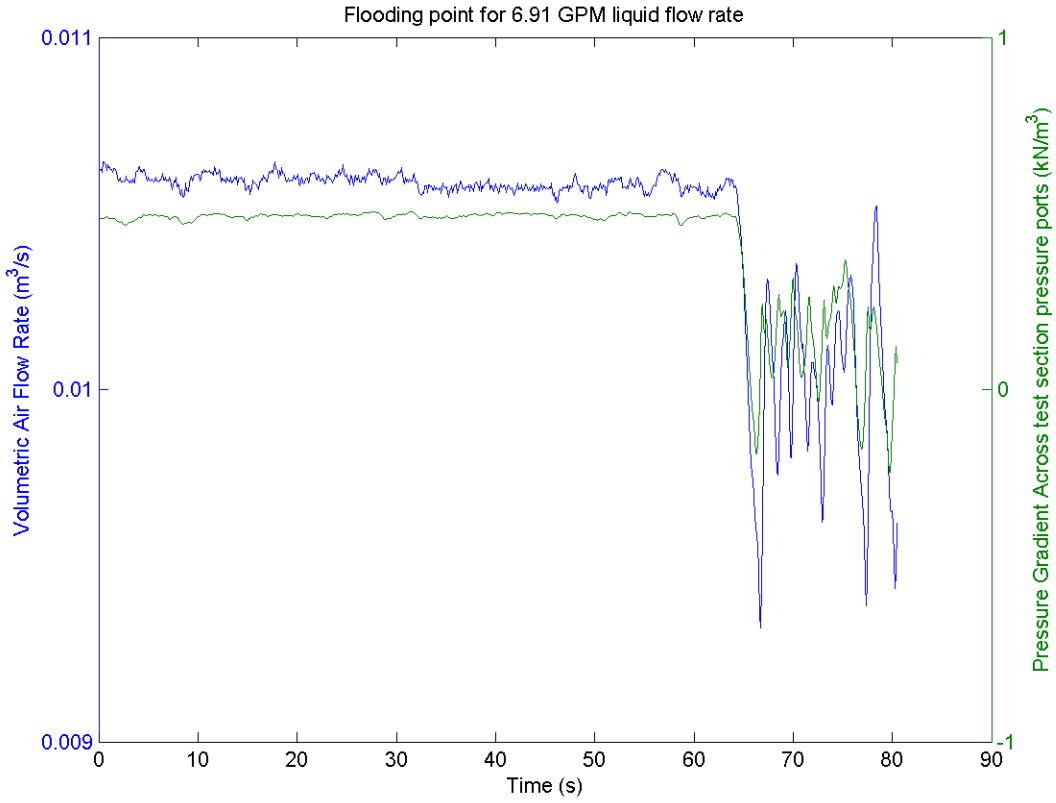
Flooding point for 6.91 GPM liquid flow rate
Volumetric Air Flow Rate (m3/s)
Pressure Gradient Across test section pressure ports (kN/m3)
Time (s)
0.011
0.01
0.009
1
0
-1
0
10
20
30
40
50
60
70
80
90

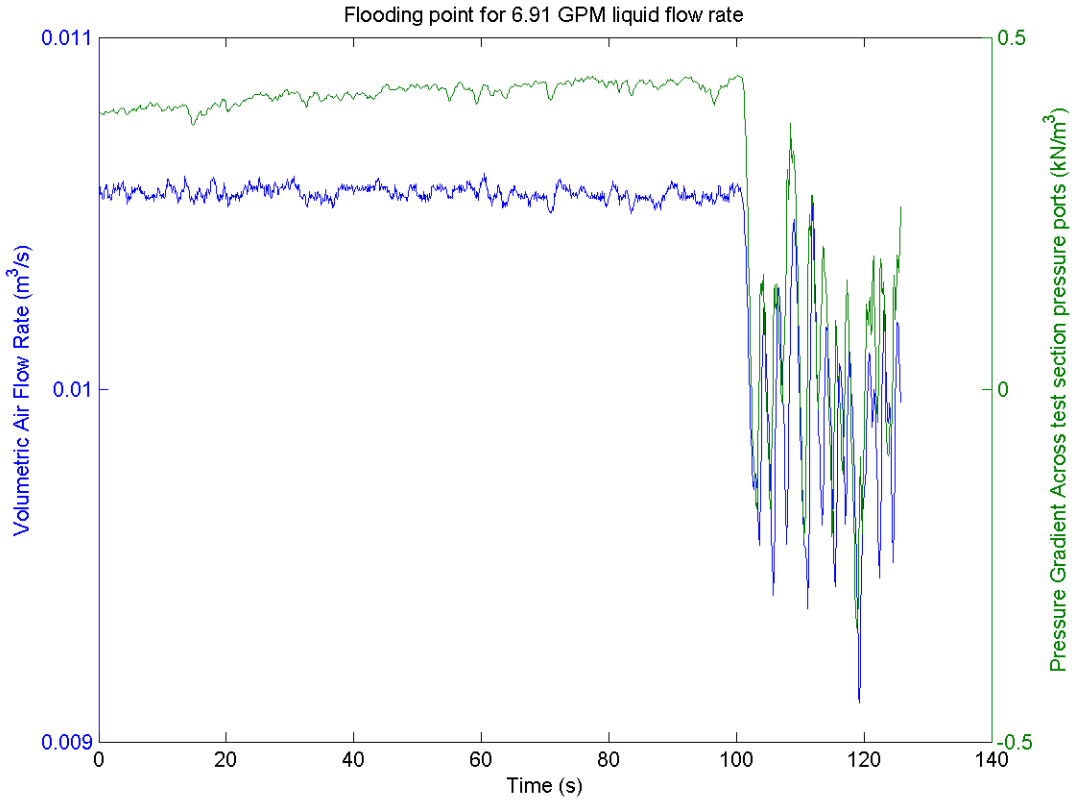
Flooding point for 6.91 GPM liquid flow rate
0.011
0.01
0.009
0.5
0
-0.5
0
20
40
60
80
100
120
140
Time (s)
Volumetric Air Flow Rate (m3/s)
Pressure Gradient Across test section pressure ports (kN/m3)

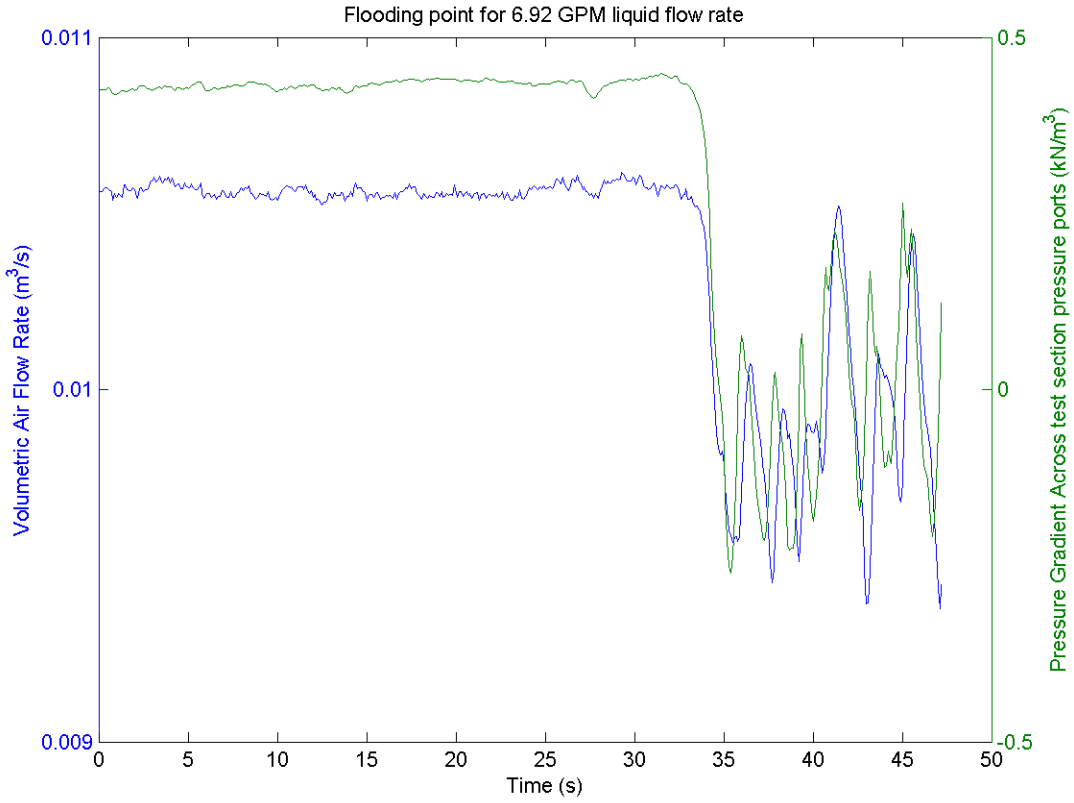
Flooding point for 6.92 GPM liquid flow rate
0.011
0.01
0.009
0.5
0
-0.5
0
5
10
15
20
25
30
35
40
45
50
Time (s)
Volumetric Air Flow Rate (m3/s)
Pressure Gradient Across test section pressure ports (kN/m3)

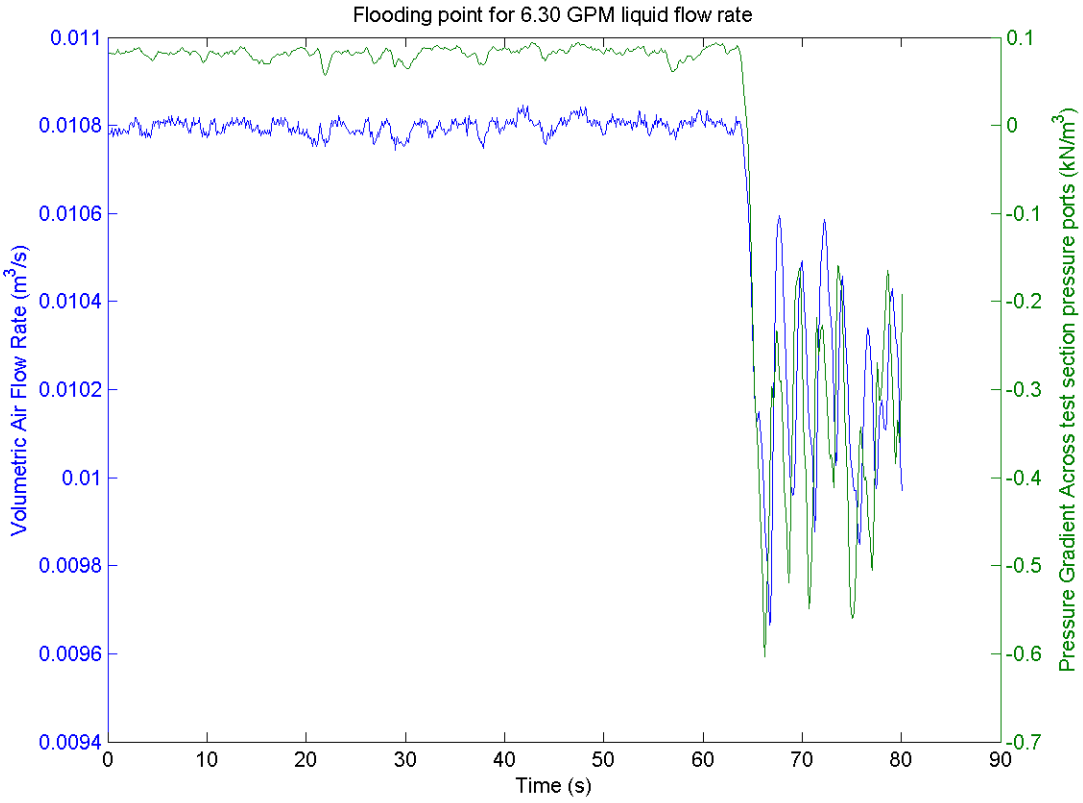
Flooding point for 6.30 GPM liquid flow rate
Volumetric Air Flow Rate (m3/s)
Pressure Gradient Across test section pressure ports (kN/m3)
Time (s)
0.011
0.0108
0.0106
0.0104
0.0102
0.01
0.0098
0.0096
0.0094
0.1
0
-0.1
-0.2
-0.3
-0.4
-0.5
-0.6
-0.7
0
10
20
30
40
50
60
70
80
90

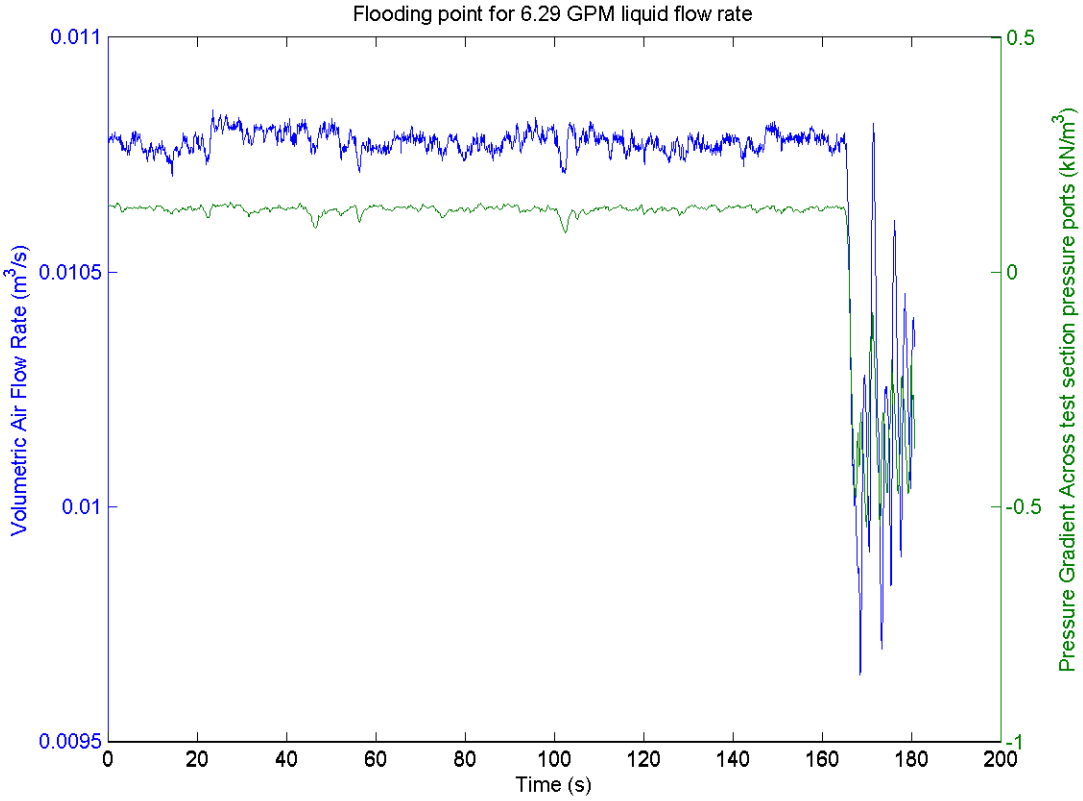
Flooding point for 6.29 GPM liquid flow rate
Volumetric Air Flow Rate (m3/s)
Pressure Gradient Across test section pressure ports (kN/m3)
Time (s)
0.011
0.0105
0.01
0.0095
0.5
0
-0.5
-1
0
20
40
60
80
100
120
140
160
180
200

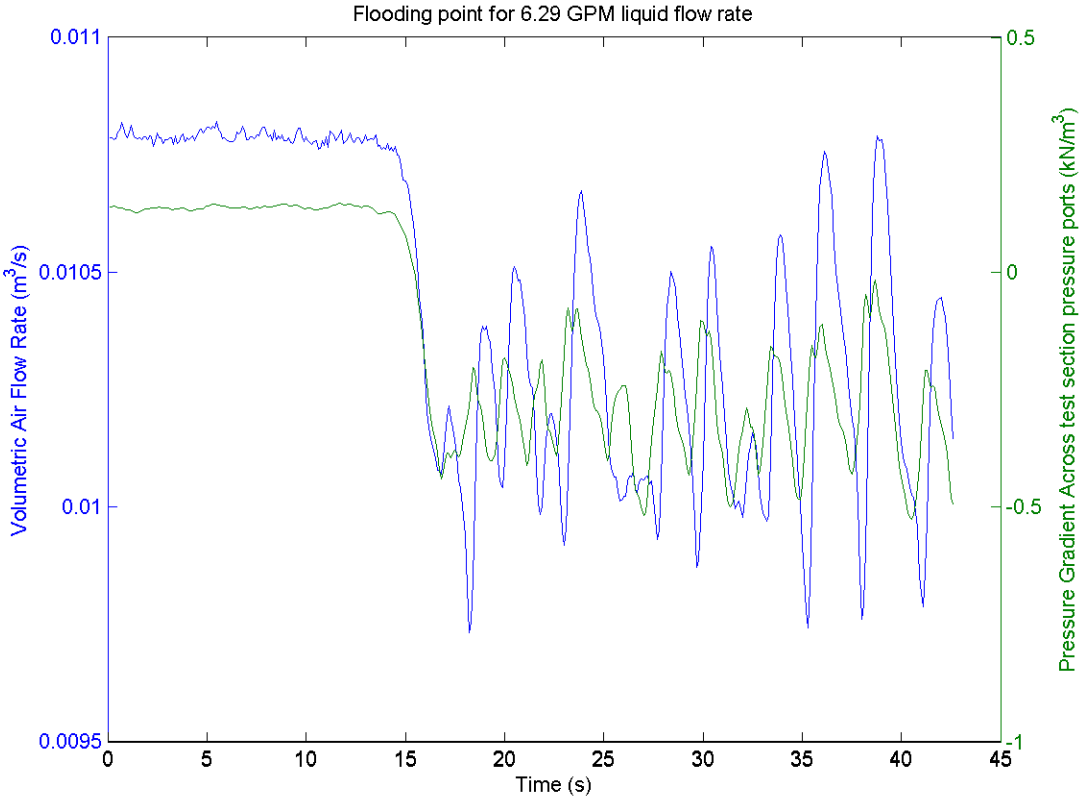
Flooding point for 6.29 GPM liquid flow rate
Volumetric Air Flow Rate (m3/s)
Pressure Gradient Across test section pressure ports (kN/m3)
Time (s)
0.011
0.0105
0.01
0.0095
0.5
0
-0.5
-1
0
5
10
15
20
25
30
35
40
45

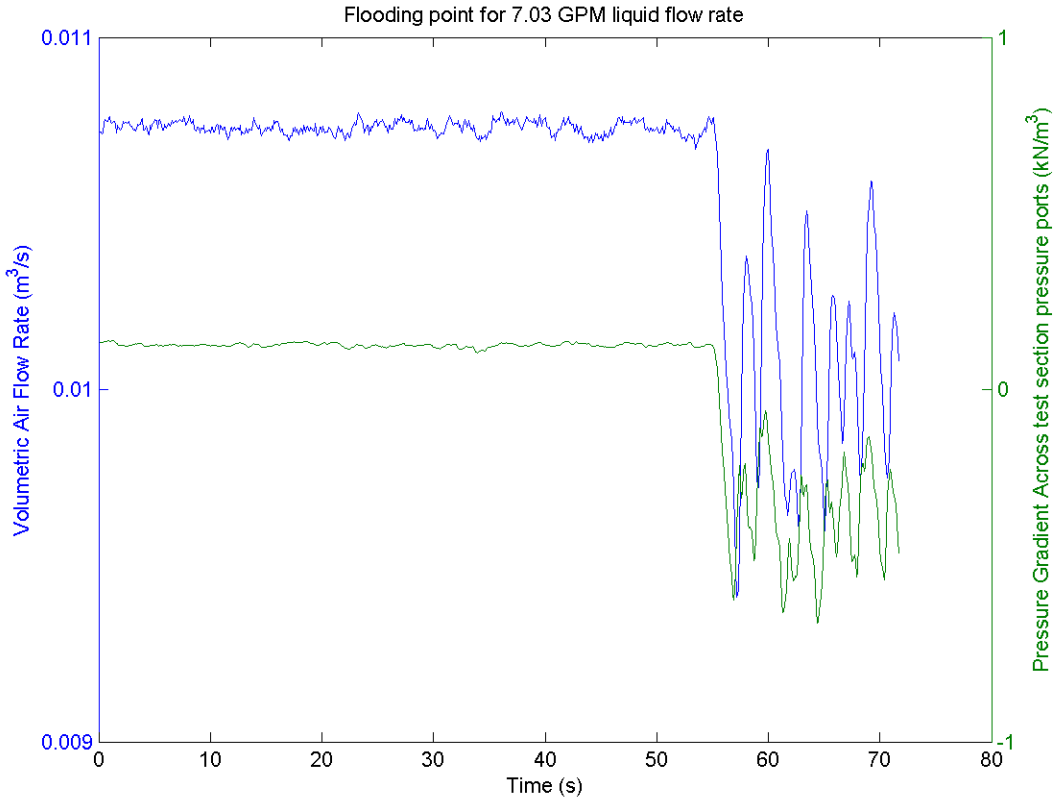
Flooding point for 7.03 GPM liquid flow rate
Volumetric Air Flow Rate (m3/s)
Pressure Gradient Across test section pressure ports (kN/m3)
Time (s)
0.011
0.01
0.009
1
0
-1
0
10
20
30
40
50
60
70
80

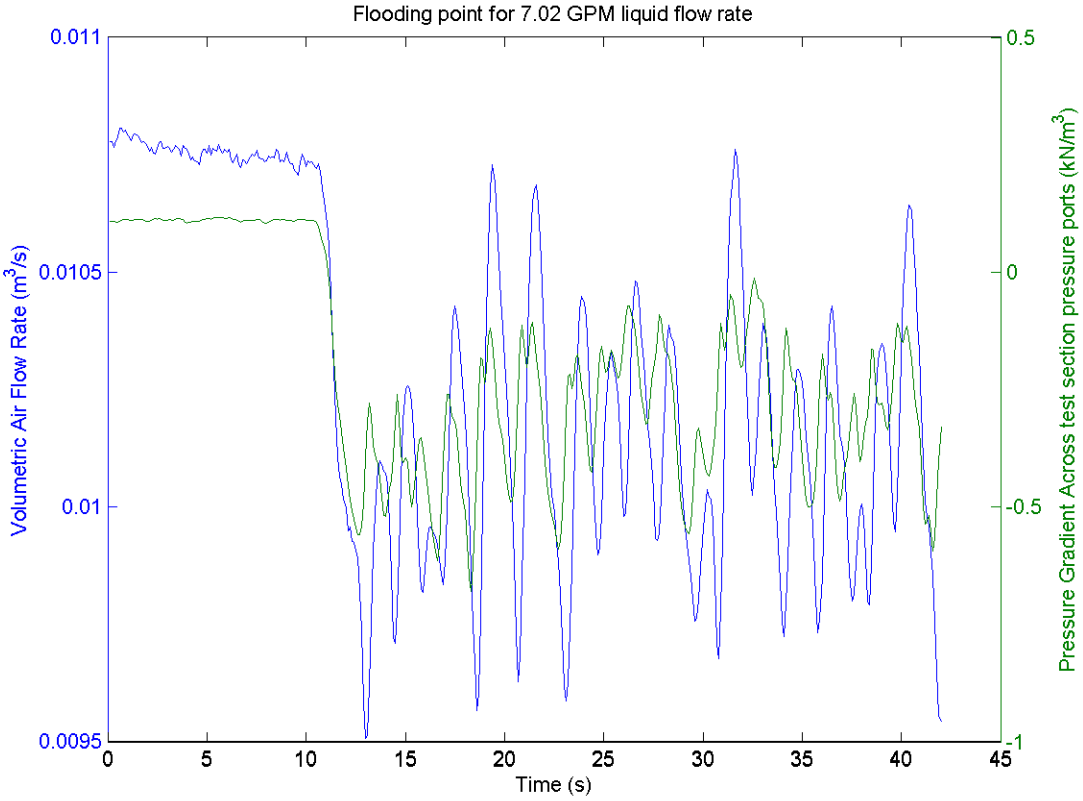
Flooding point for 7.02 GPM liquid flow rate
Volumetric Air Flow Rate (m3/s)
Pressure Gradient Across test section pressure ports (kN/m3)
Time (s)
0.011
0.0105
0.01
0.0095
0.5
0
-0.5
-1
0
5
10
15
20
25
30
35
40
45

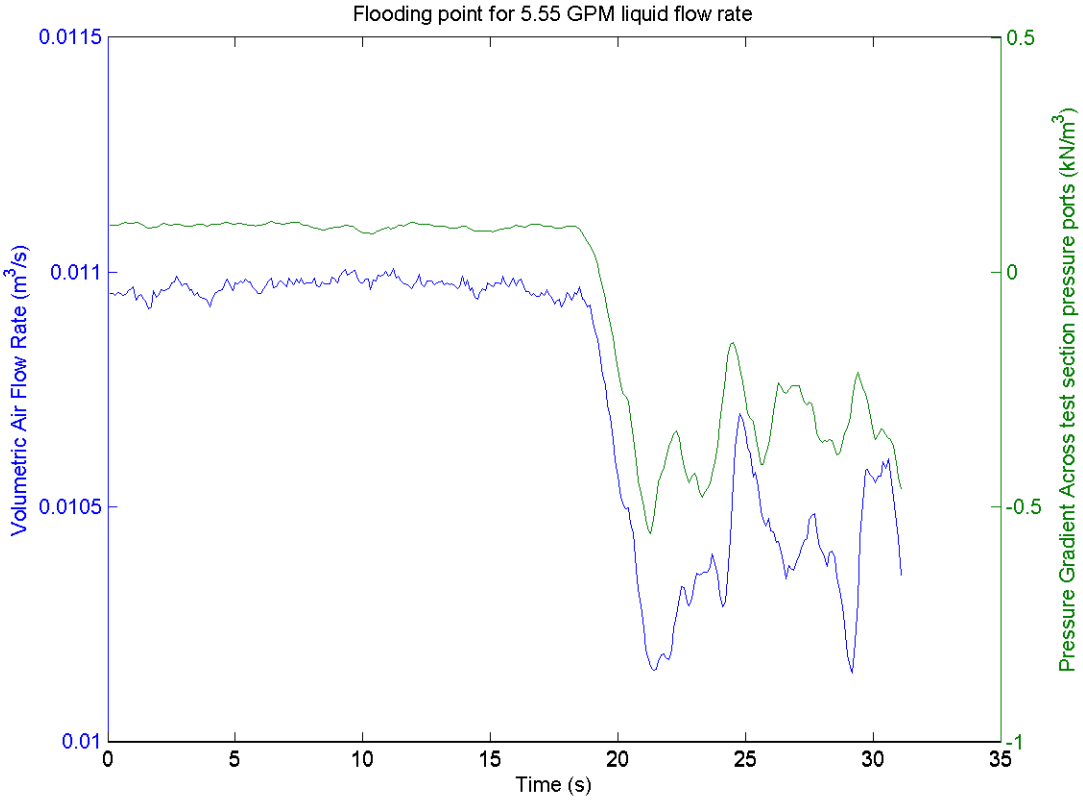
Flooding point for 5.55 GPM liquid flow rate
Volumetric Air Flow Rate (m3/s)
Pressure Gradient Across test section pressure ports (kN/m3)
Time (s)
0.0115
0.011
0.0105
0.01
0.5
0
-0.5
-1
0
5
10
15
20
25
30
35

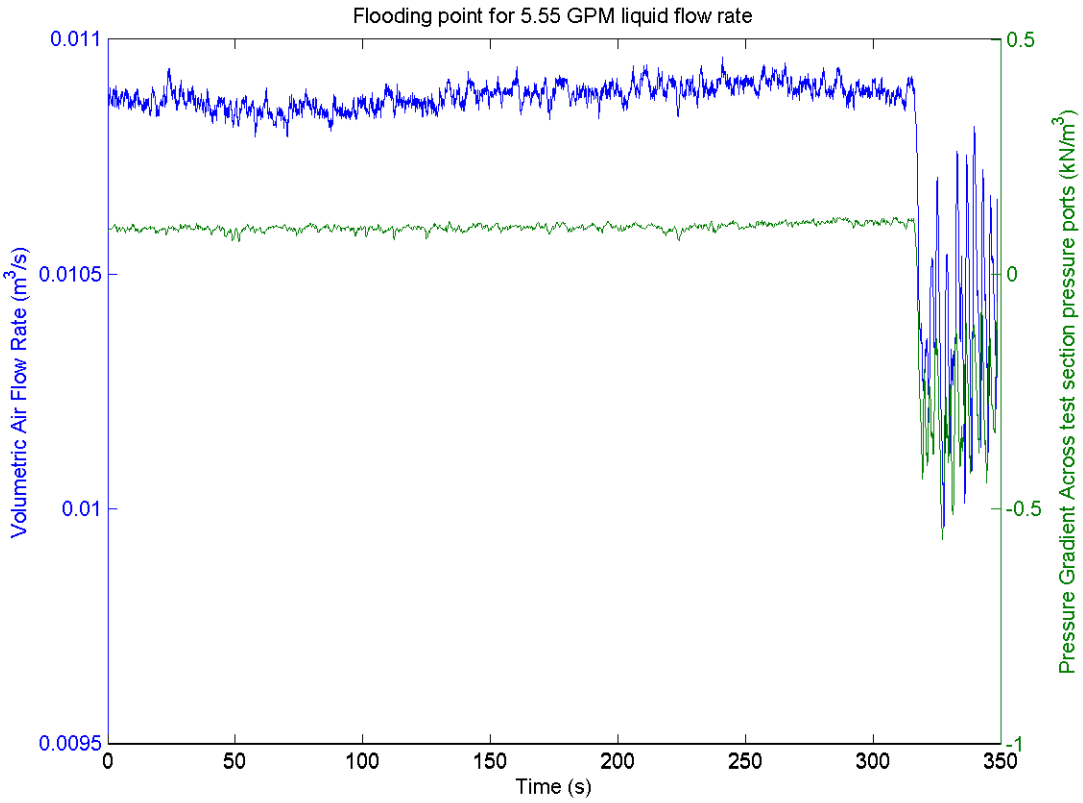
Flooding point for 5.55 GPM liquid flow rate
Volumetric Air Flow Rate (m3/s)
Pressure Gradient Across test section pressure ports (kN/m3)
Time (s)
0.011
0.0105
0.01
0.0095
0.5
0
-0.5
-1
0
50
100
150
200
250
300
350

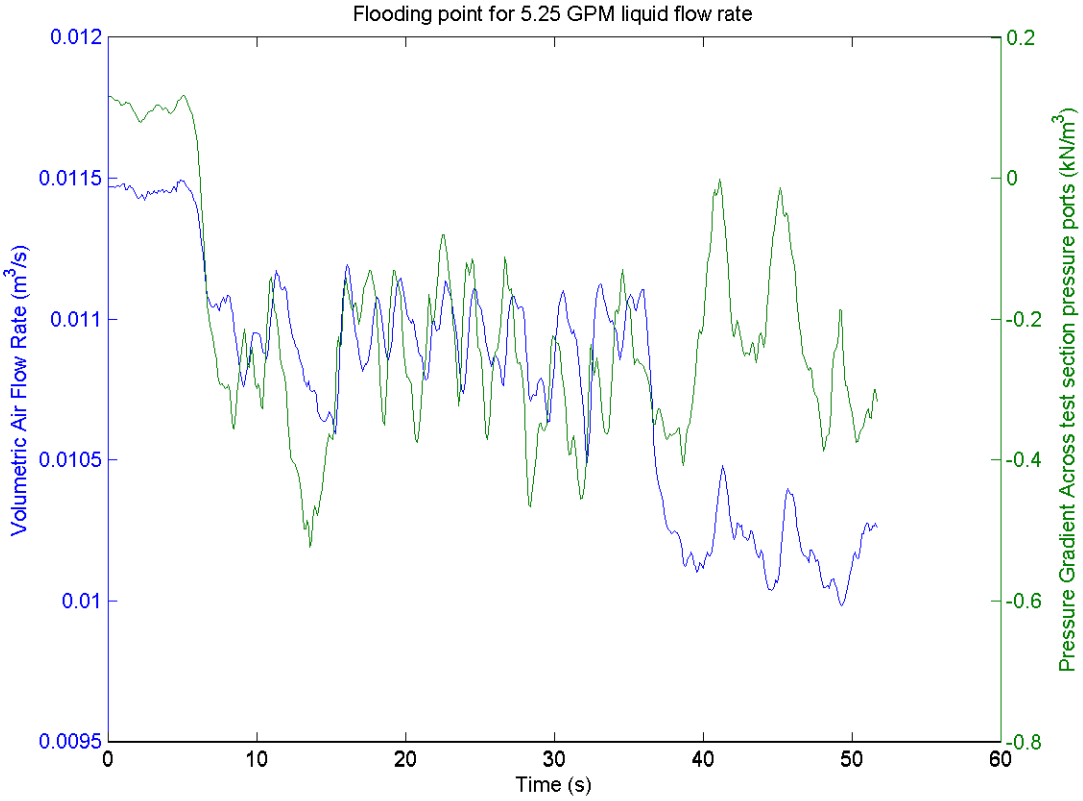
Flooding point for 5.25 GPM liquid flow rate
Volumetric Air Flow Rate (m3/s)
Pressure Gradient Across test section pressure ports (kN/m3)
Time (s)
0.012
0.0115
0.011
0.0105
0.01
0.0095
0.2
0
-0.2
-0.4
-0.6
-0.8
0
10
20
30
40
50
60

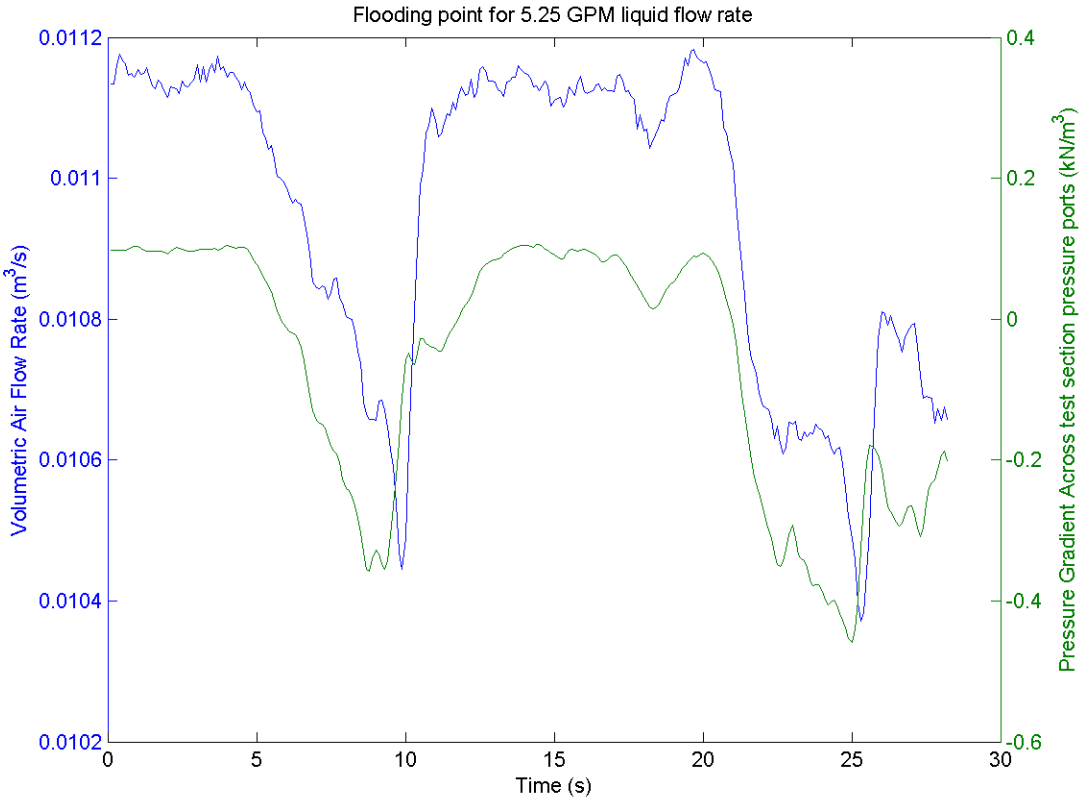
Flooding point for 5.25 GPM liquid flow rate
Volumetric Air Flow Rate (m3/s)
Pressure Gradient Across test section pressure ports (kN/m3)
Time (s)
0.0112
0.011
0.0108
0.0106
0.0104
0.0102
0.4
0.2
0
-0.2
-0.4
-0.6
0
5
10
15
20
25
30

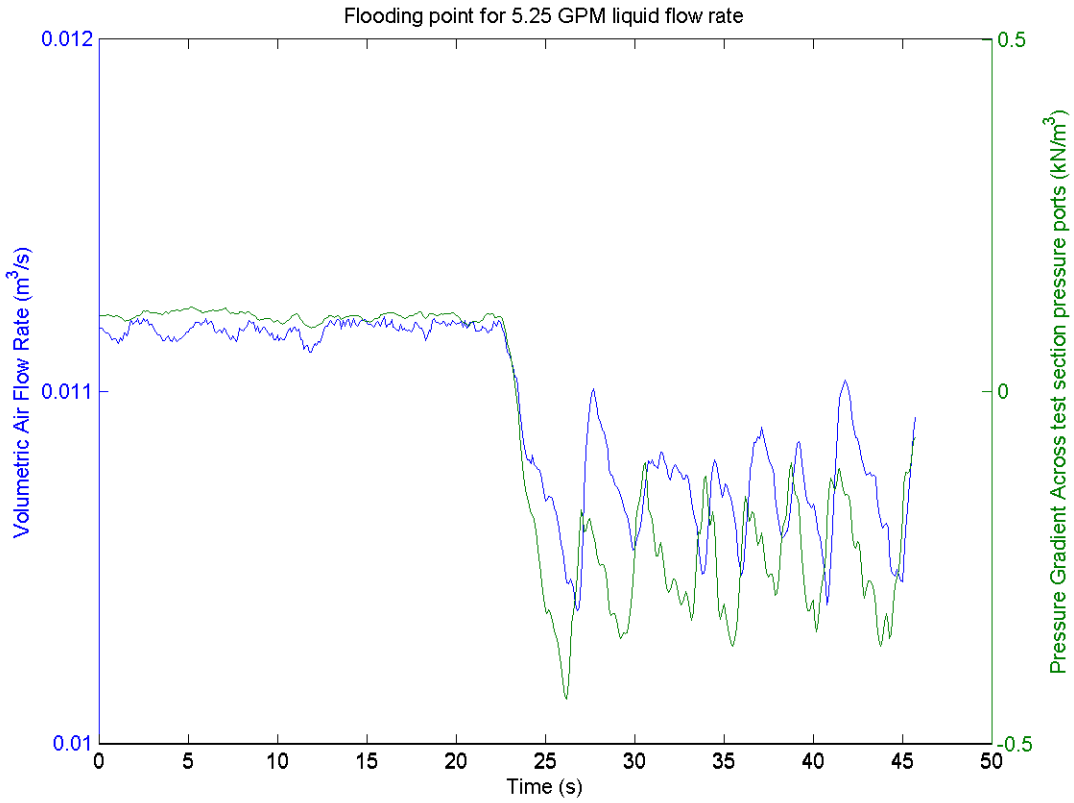
Flooding point for 5.25 GPM liquid flow rate
Volumetric Air Flow Rate (m3/s)
Pressure Gradient Across test section pressure ports (kN/m3)
Time (s)
0.012
0.011
0.01
0.5
0
-0.5
0
5
10
15
20
25
30
35
40
45
50

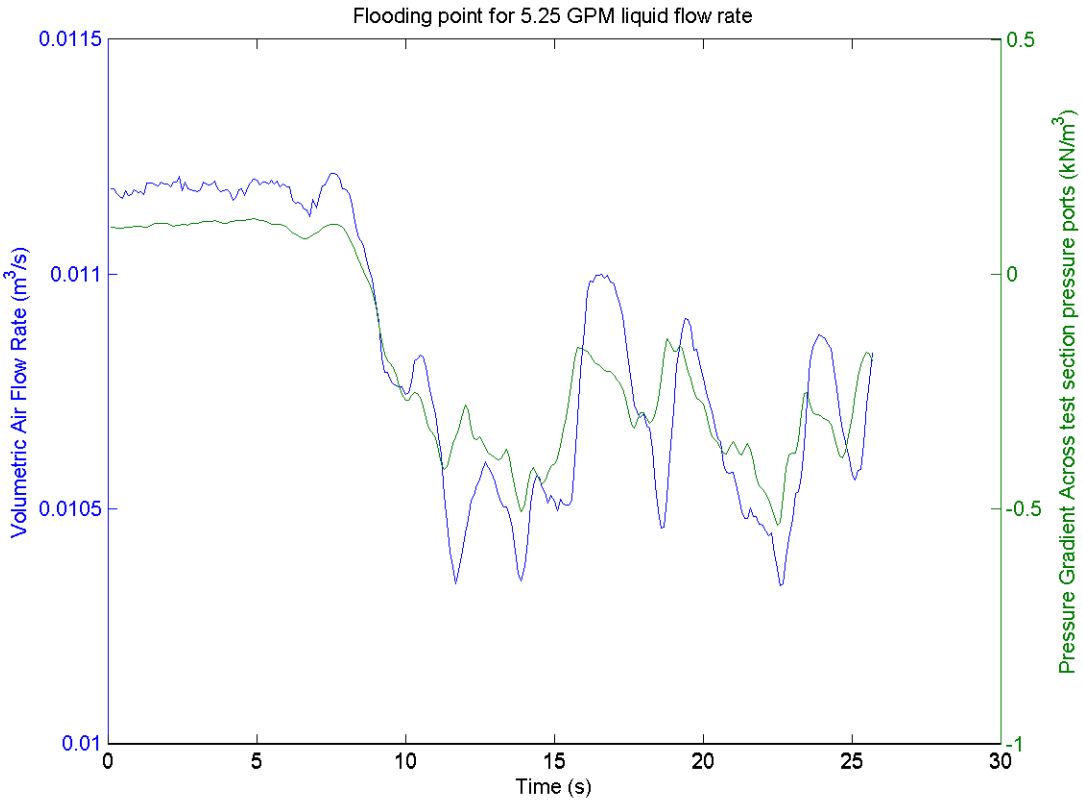
Flooding point for 5.25 GPM liquid flow rate
Volumetric Air Flow Rate (m3/s)
Pressure Gradient Across test section pressure ports (kN/m3)
Time (s)
0.0115
0.011
0.0105
0.01
0.5
0
-0.5
-1
0
5
10
15
20
25
30

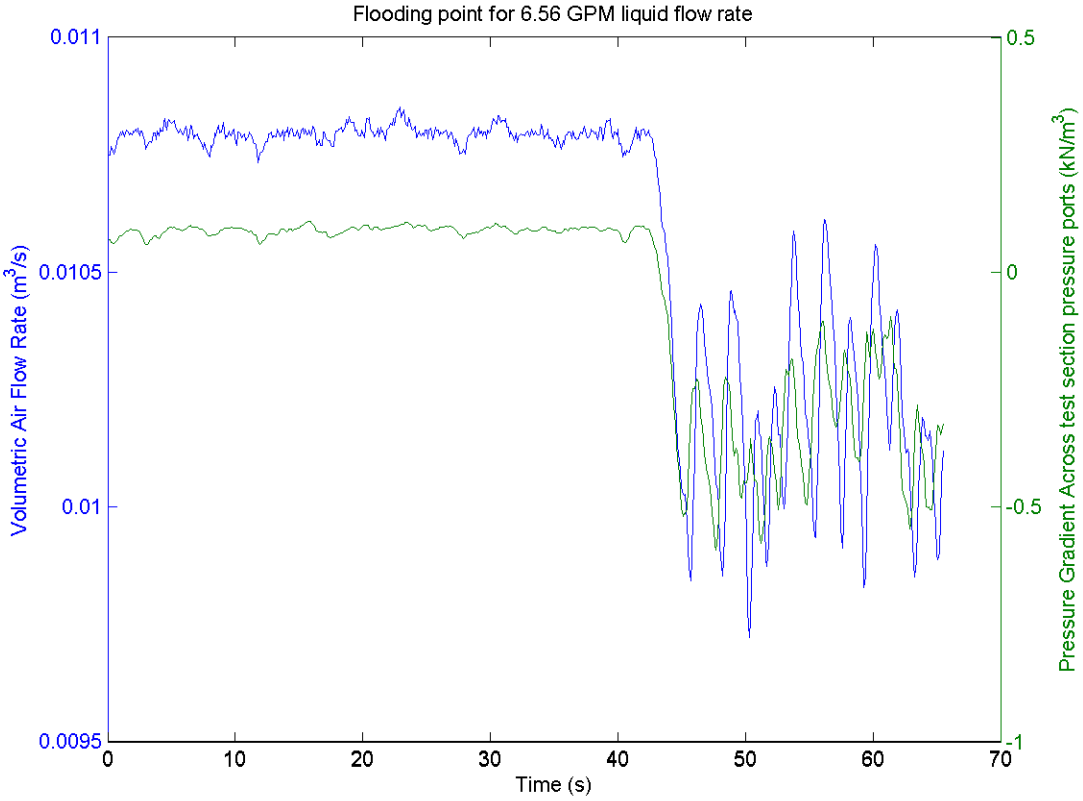
Flooding point for 6.56 GPM liquid flow rate
Volumetric Air Flow Rate (m3/s)
Pressure Gradient Across test section pressure ports (kN/m3)
Time (s)
0.011
0.0105
0.01
0.0095
0.5
0
-0.5
-1
0
10
20
30
40
50
60
70

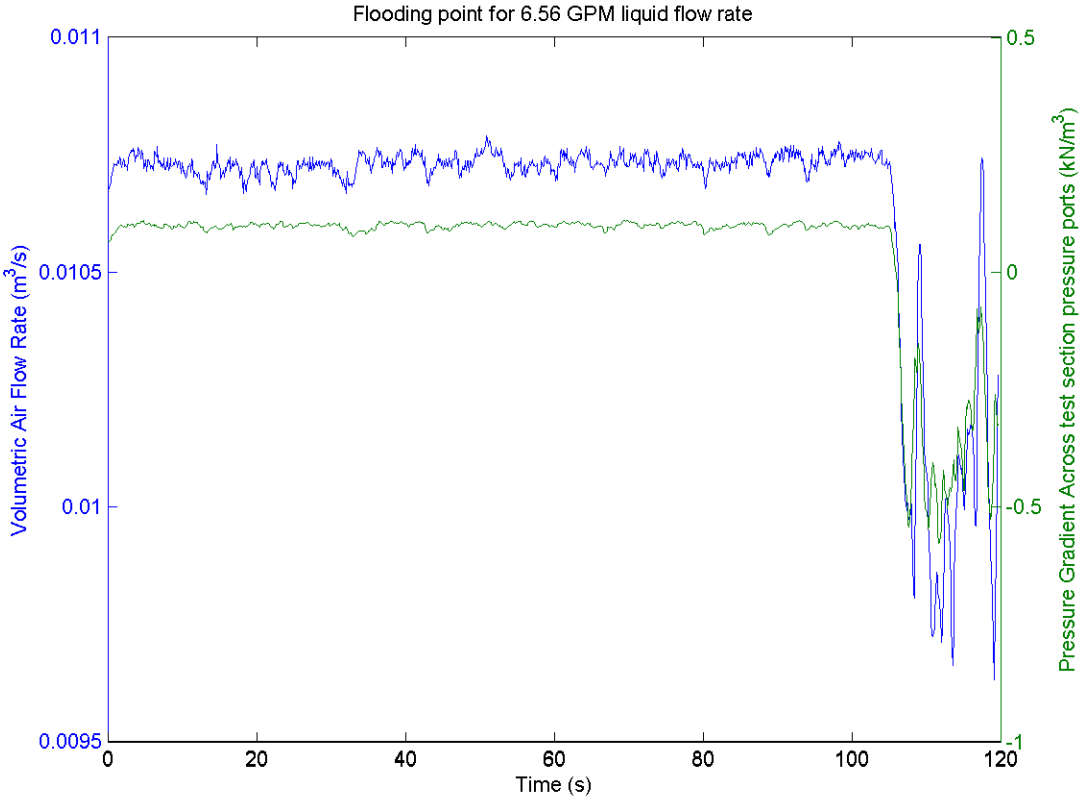
Flooding point for 6.56 GPM liquid flow rate
Volumetric Air Flow Rate (m3/s)
Pressure Gradient Across test section pressure ports (kN/m3)
Time (s)
0.011
0.0105
0.01
0.0095
0.5
0
-0.5
-1
0
20
40
60
80
100
120

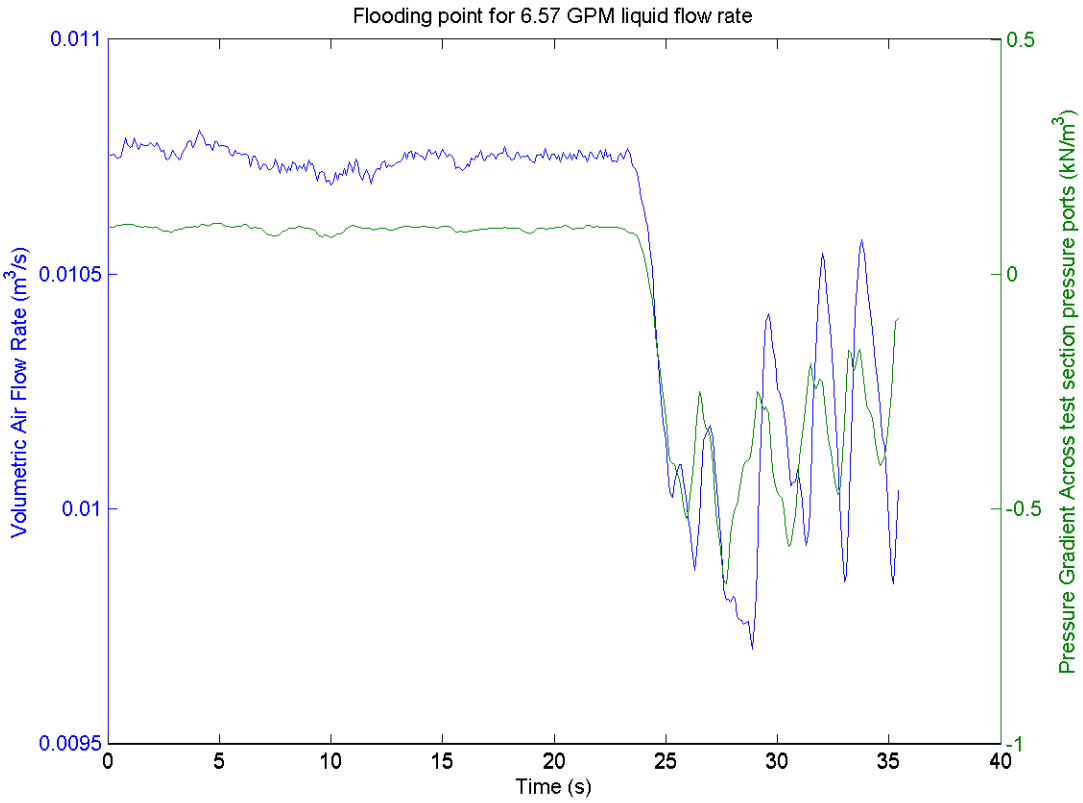
Flooding point for 6.57 GPM liquid flow rate
Volumetric Air Flow Rate (m3/s)
Pressure Gradient Across test section pressure ports (kN/m3)
Time (s)
0.011
0.0105
0.01
0.0095
0.5
0
-0.5
-1
0
5
10
15
20
25
30
35
40

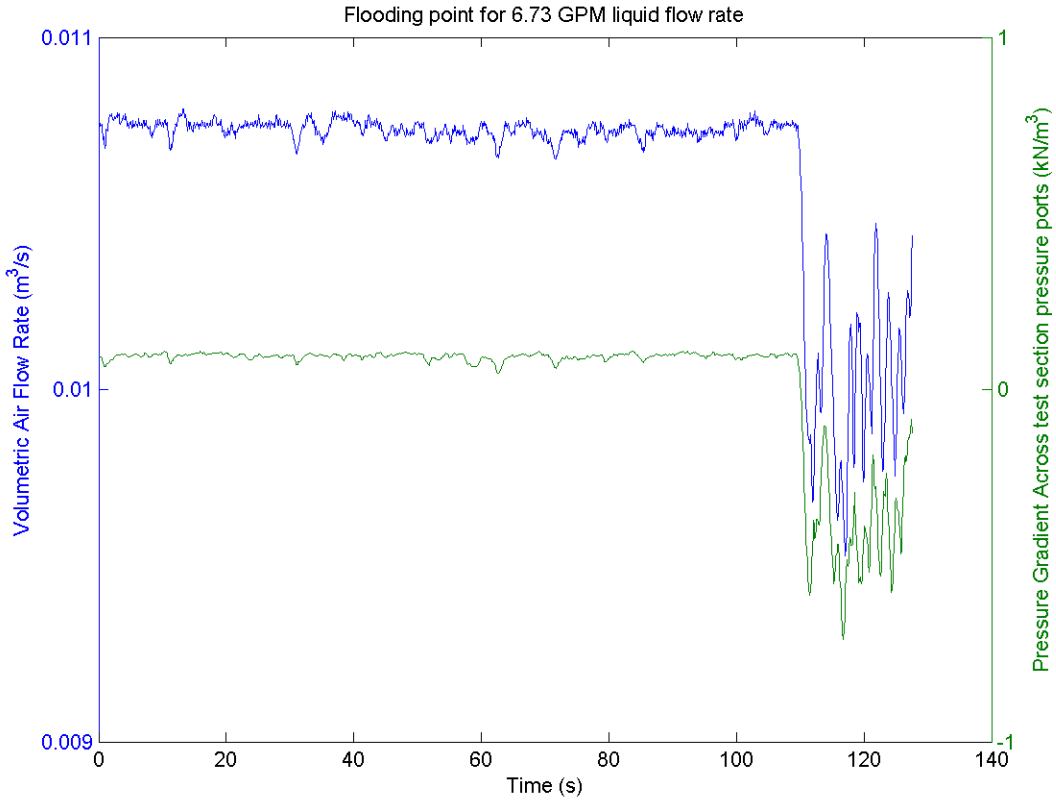
Flooding point for 6.73 GPM liquid flow rate
Volumetric Air Flow Rate (m3/s)
Pressure Gradient Across test section pressure ports (kN/m3)
Time (s)
0.011
0.01
0.009
1
0
-1
0
20
40
60
80
100
120
140

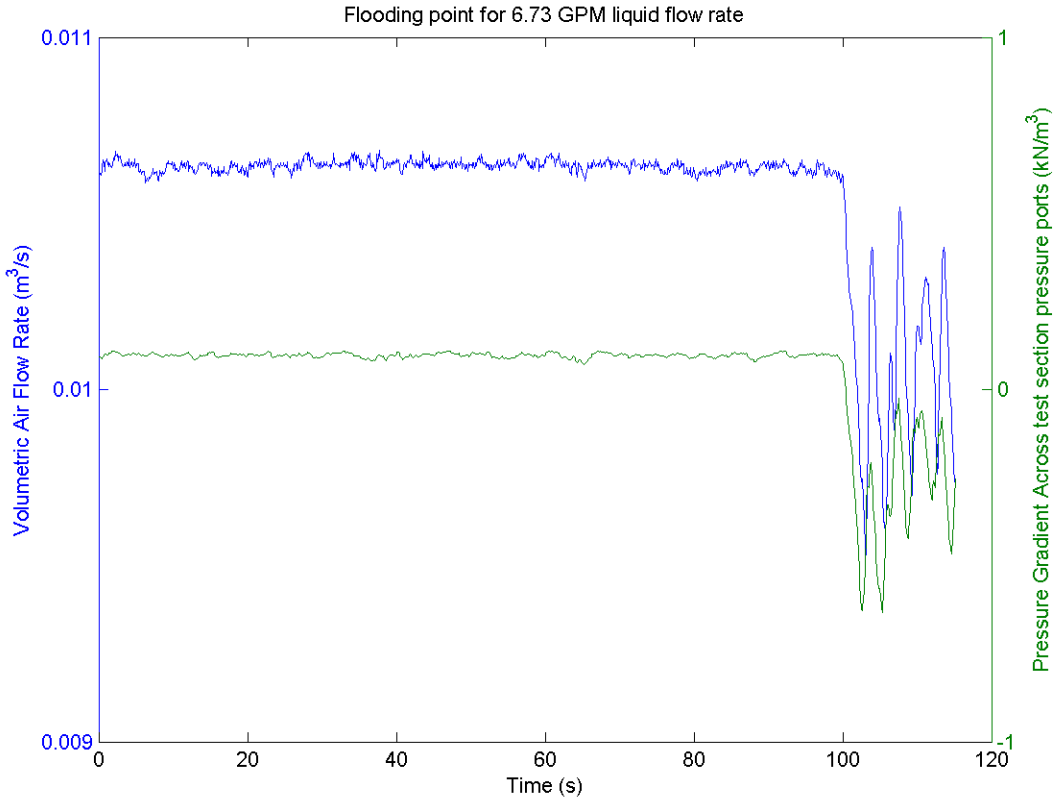
Flooding point for 6.73 GPM liquid flow rate
0.011
0.01
0.009
Volumetric Air Flow Rate (m3/s)
1
0
-1
Pressure Gradient Across test section pressure ports (kN/m3)
0
20
40
60
80
100
120
Time (s)

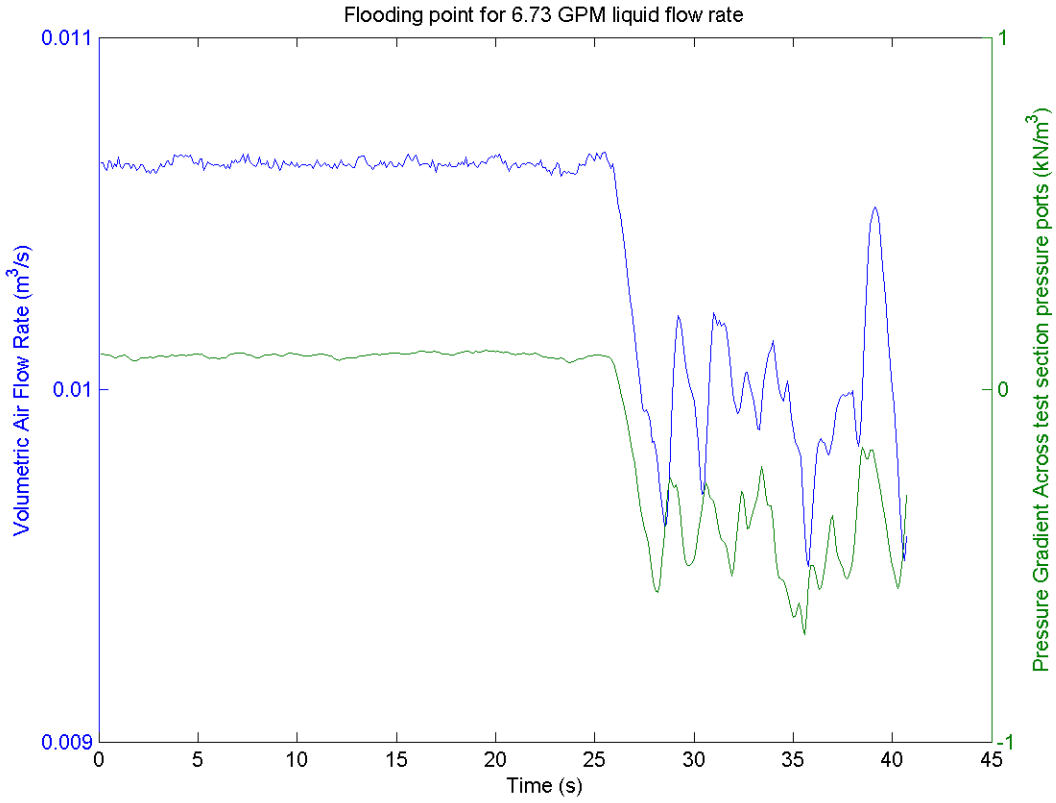
Flooding point for 6.73 GPM liquid flow rate
Volumetric Air Flow Rate (m3/s)
Pressure Gradient Across test section pressure ports (kN/m3)
Time (s)
0.011
0.01
0.009
1
0
-1
0
5
10
15
20
25
30
35
40
45

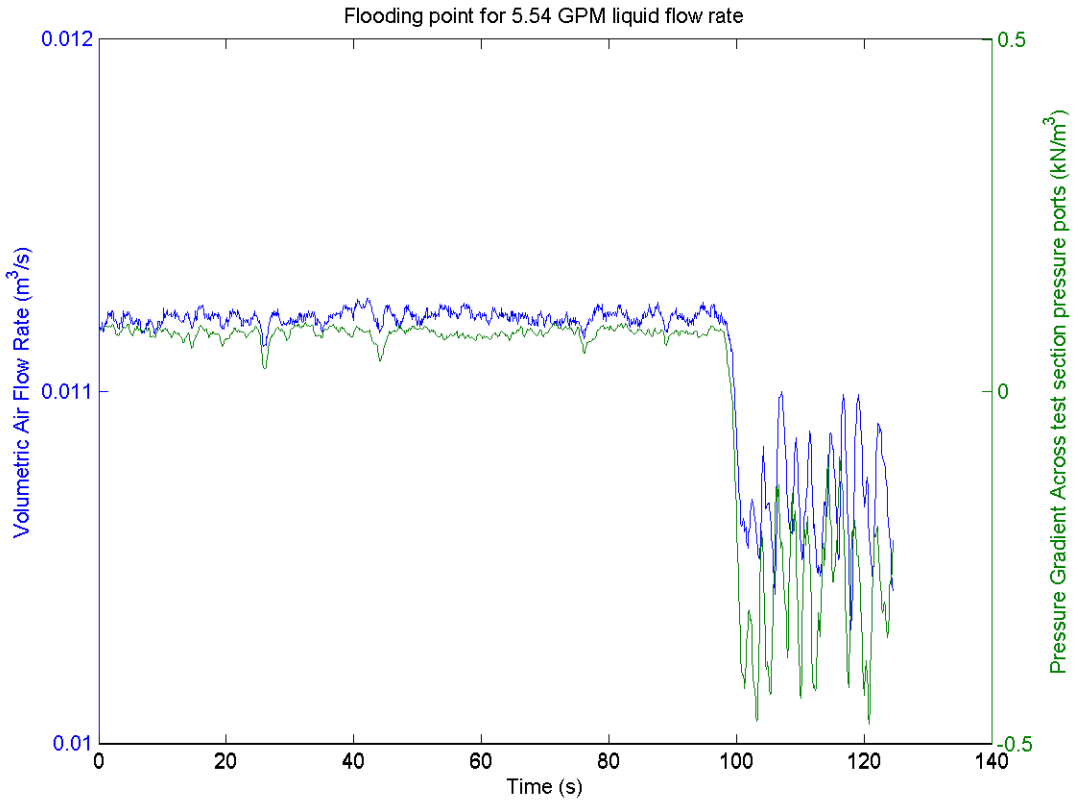
Flooding point for 5.54 GPM liquid flow rate
0.012
0.011
0.01
0.5
0
-0.5
0
20
40
60
80
100
120
140
Time (s)
Volumetric Air Flow Rate (m3/s)
Pressure Gradient Across test section pressure ports (kN/m3)

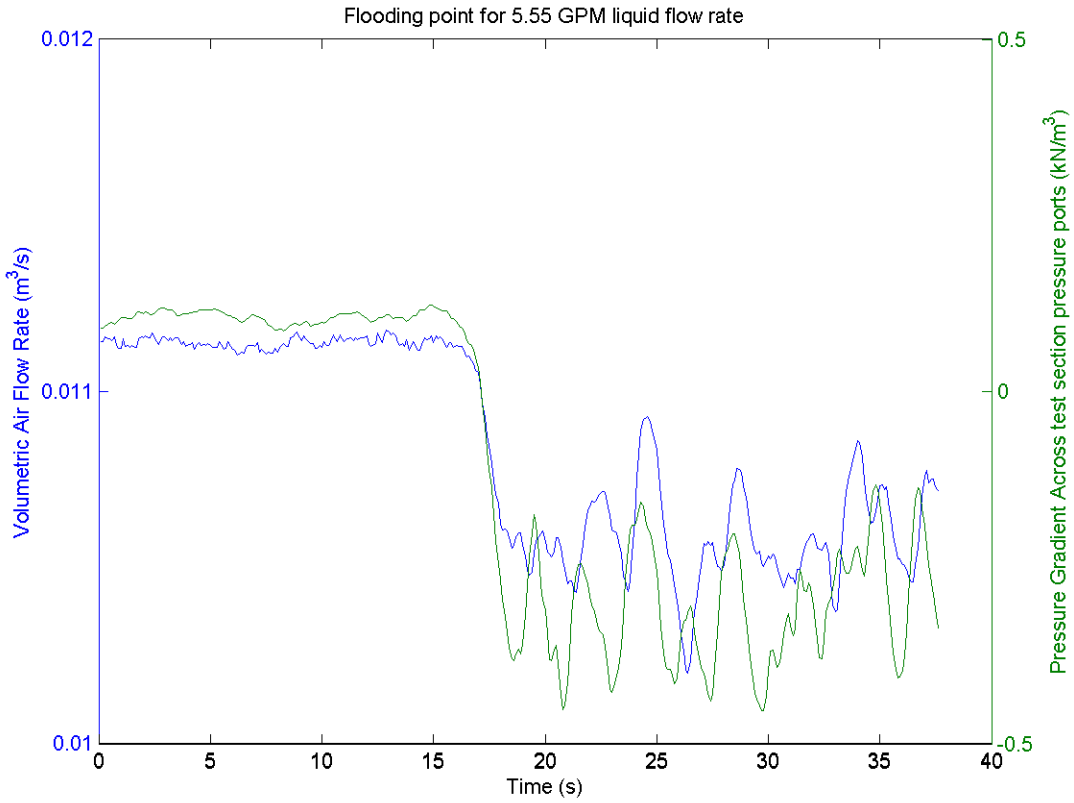
Flooding point for 5.55 GPM liquid flow rate
Volumetric Air Flow Rate (m3/s)
Pressure Gradient Across test section pressure ports (kN/m3)
Time (s)
0.012
0.011
0.01
0.5
0
-0.5
0
5
10
15
20
25
30
35
40

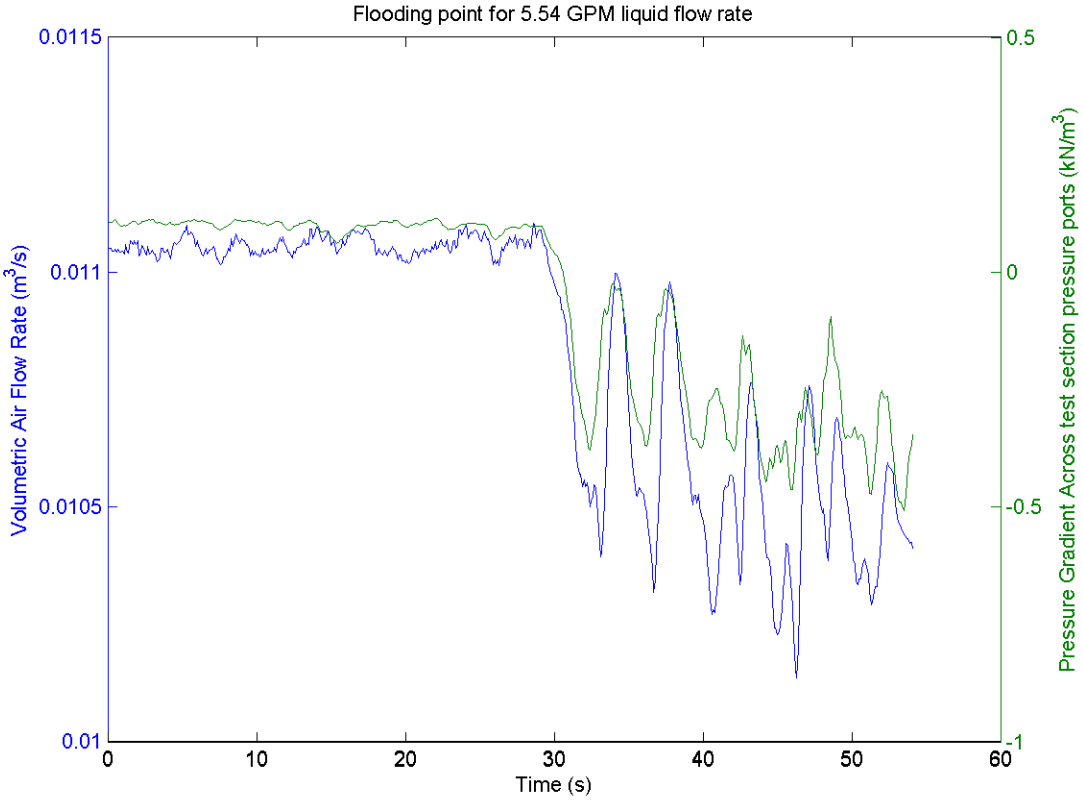
Flooding point for 5.54 GPM liquid flow rate
0.0115
0.011
0.0105
0.01
0.5
0
-0.5
-1
0
10
20
30
40
50
60
Time (s)
Volumetric Air Flow Rate (m3/s)
Pressure Gradient Across test section pressure ports (kN/m3)

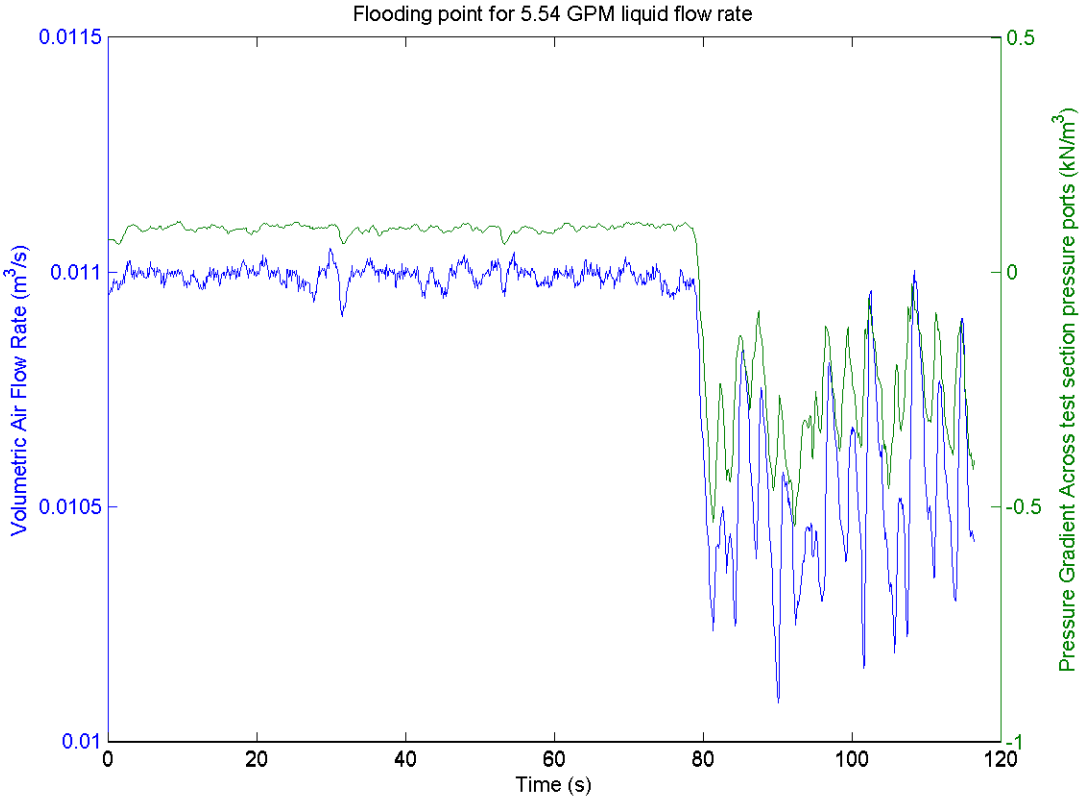
Flooding point for 5.54 GPM liquid flow rate
Volumetric Air Flow Rate (m3/s)
Pressure Gradient Across test section pressure ports (kN/m3)
Time (s)
0.0115
0.011
0.0105
0.01
0.5
0
-0.5
-1
0
20
40
60
80
100
120

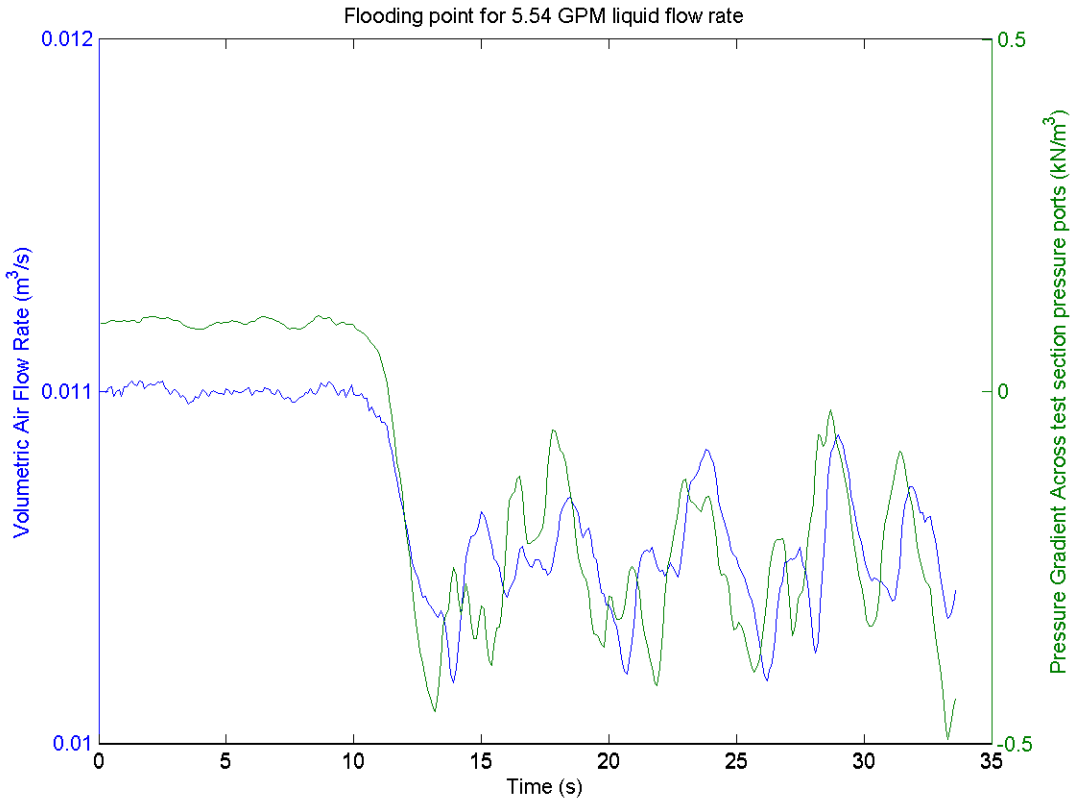
Flooding point for 5.54 GPM liquid flow rate
0.012
0.011
0.01
0.5
0
-0.5
0
5
10
15
20
25
30
35
Time (s)
Volumetric Air Flow Rate (m3/s)
Pressure Gradient Across test section pressure ports (kN/m3)

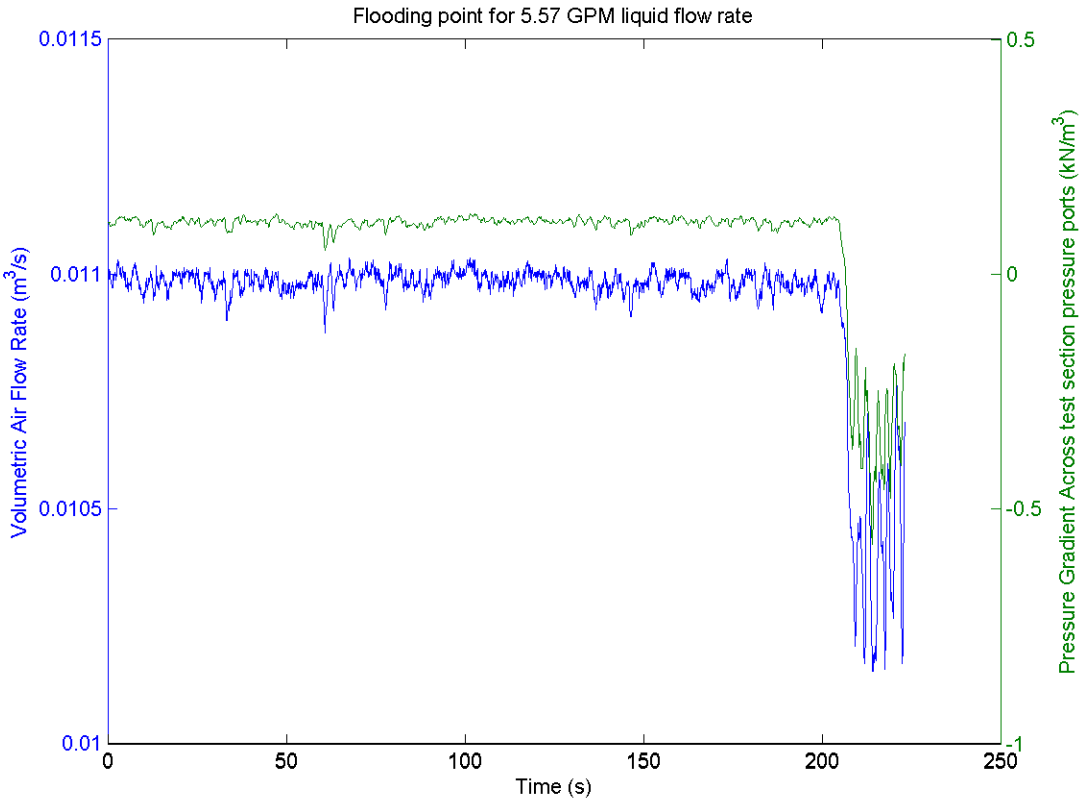
Flooding point for 5.57 GPM liquid flow rate
0.0115
0.011
0.0105
0.01
0.5
0
-0.5
-1
0
50
100
150
200
250
Time (s)
Volumetric Air Flow Rate (m3/s)
Pressure Gradient Across test section pressure ports (kN/m3)

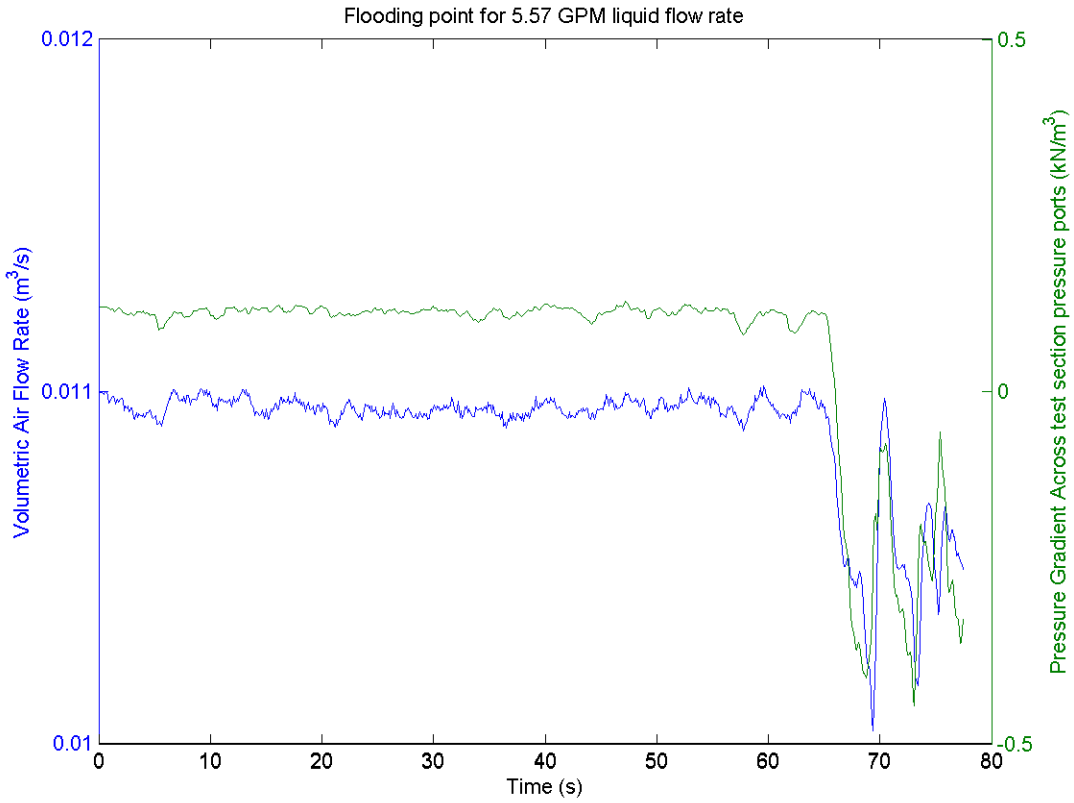
Flooding point for 5.57 GPM liquid flow rate
0.012
0.011
0.01
0.5
0
-0.5
0
10
20
30
40
50
60
70
80
Time (s)
Volumetric Air Flow Rate (m3/s)
Pressure Gradient Across test section pressure ports (kN/m3)

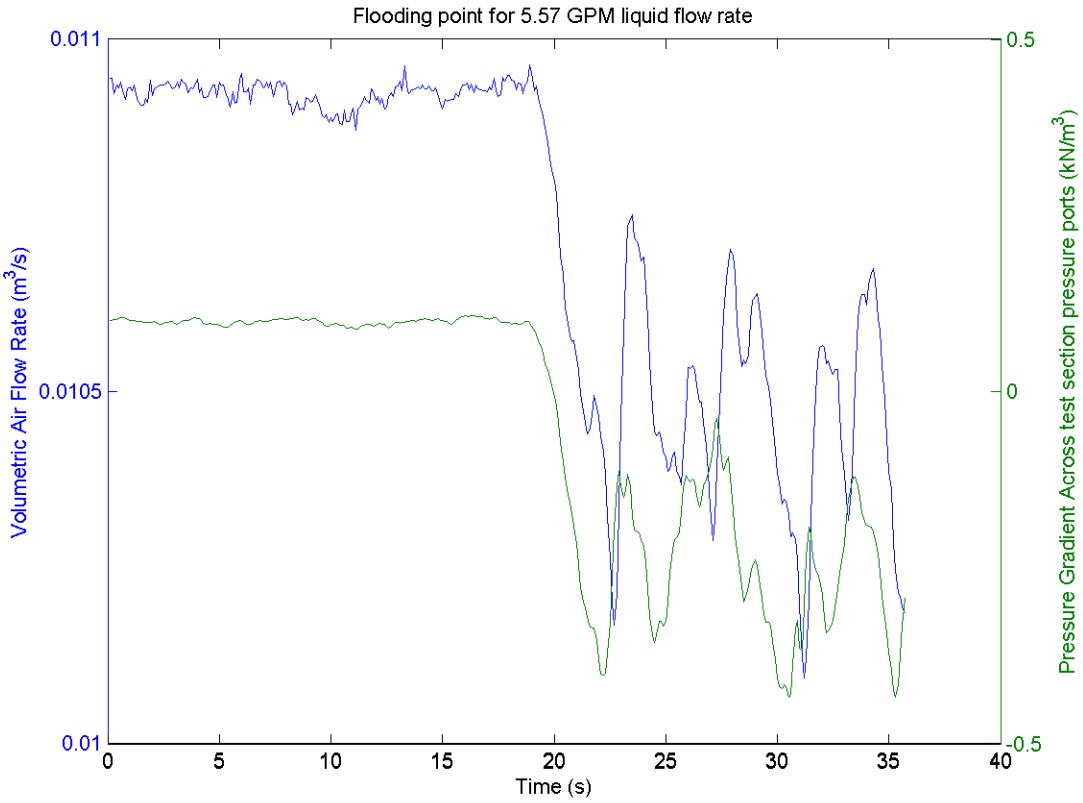
Flooding point for 5.57 GPM liquid flow rate
0.011
0.0105
0.01
0.5
0
-0.5
0
5
10
15
20
25
30
35
40
Time (s)
Volumetric Air Flow Rate (m3/s)
Pressure Gradient Across test section pressure ports (kN/m3)

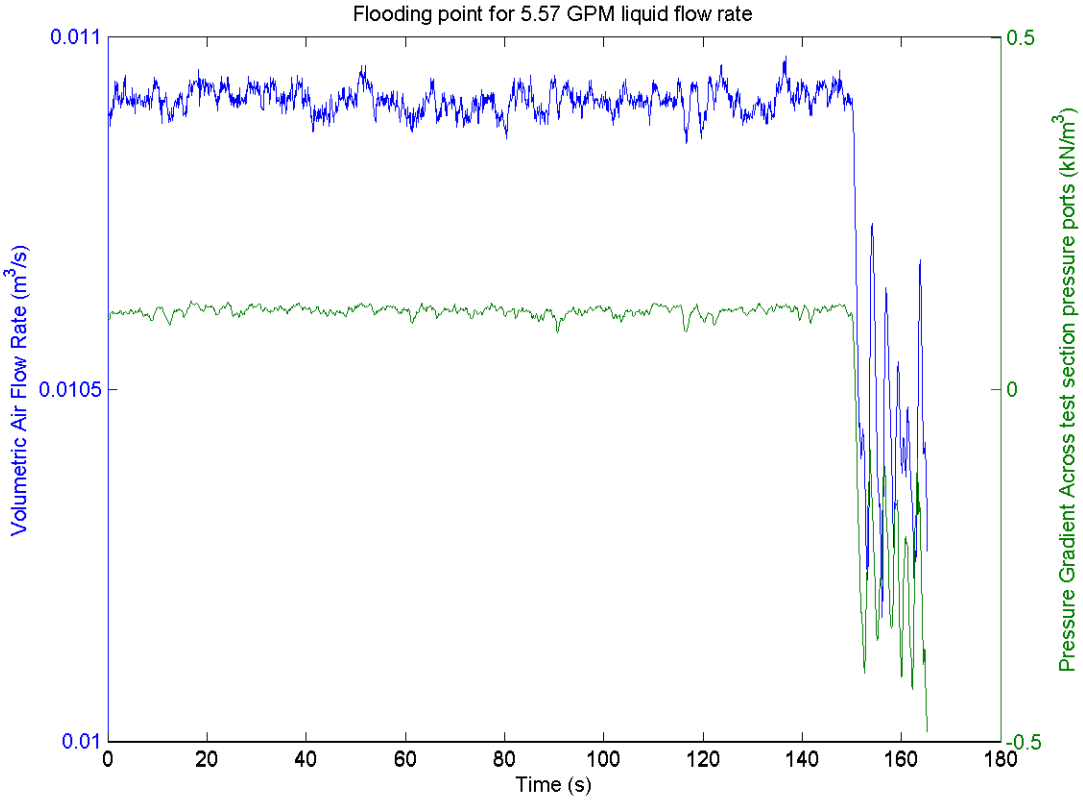
Flooding point for 5.57 GPM liquid flow rate
Volumetric Air Flow Rate (m3/s)
Pressure Gradient Across test section pressure ports (kN/m3)
Time (s)
0.011
0.0105
0.01
0.5
0
-0.5
0
20
40
60
80
100
120
140
160
180

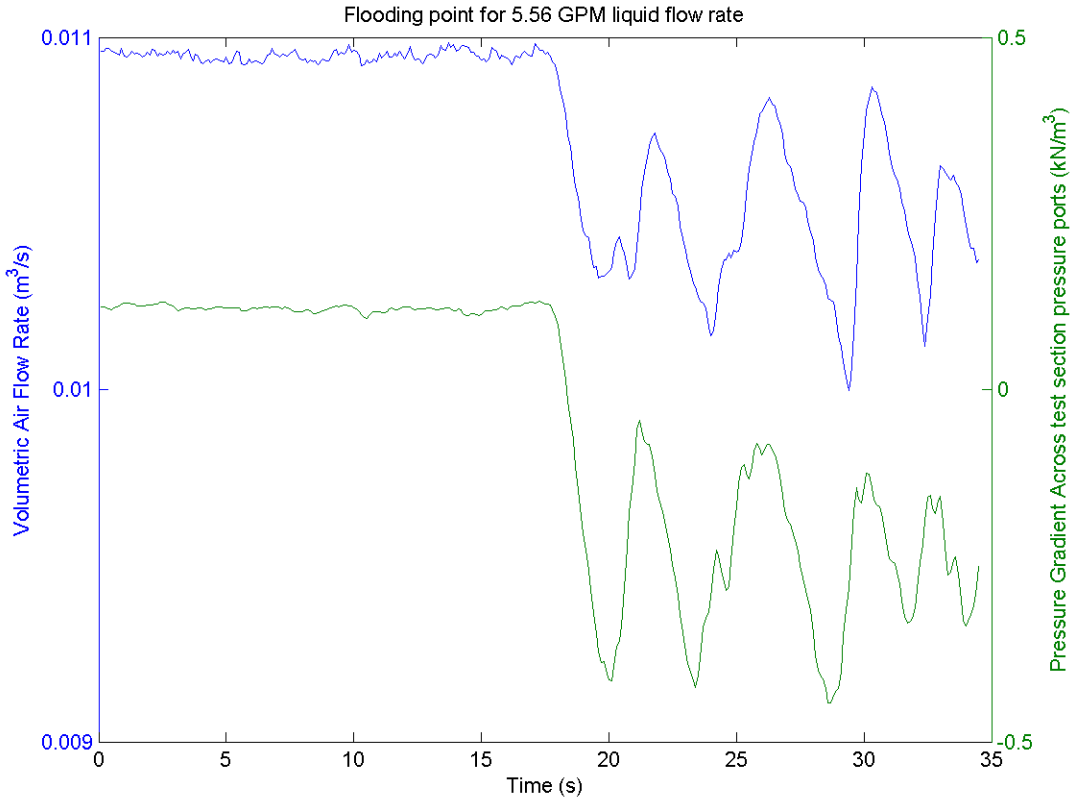
Flooding point for 5.56 GPM liquid flow rate
Volumetric Air Flow Rate (m3/s)
Pressure Gradient Across test section pressure ports (kN/m3)
Time (s)
0.011
0.01
0.009
0.5
0
-0.5
0
5
10
15
20
25
30
35

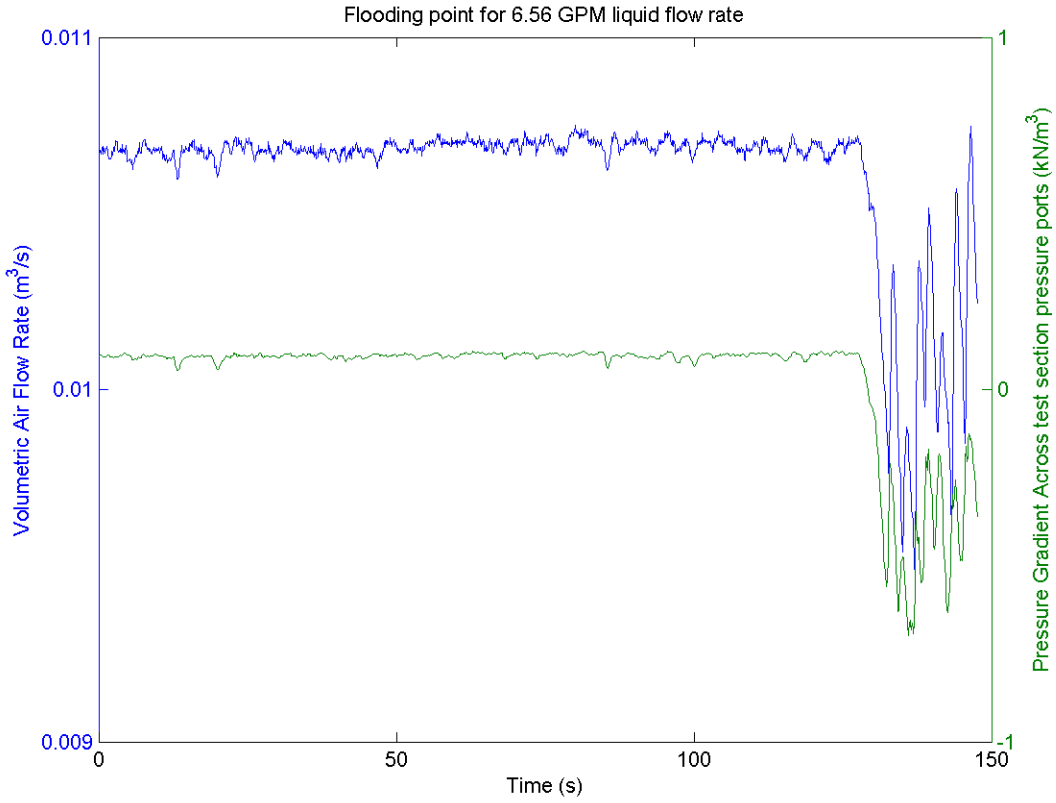
Flooding point for 6.56 GPM liquid flow rate
0.011
0.01
0.009
Volumetric Air Flow Rate (m3/s)
1
0
-1
Pressure Gradient Across test section pressure ports (kN/m3)
0
50
100
150
Time (s)

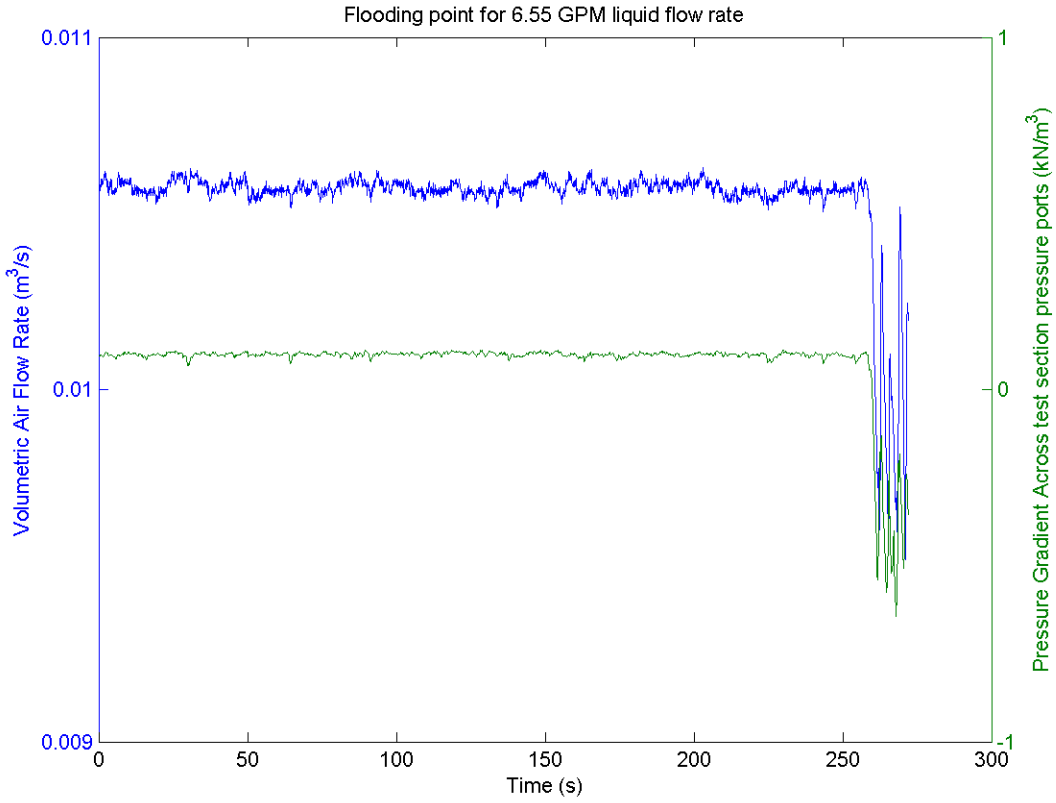
Flooding point for 6.55 GPM liquid flow rate
0.011
0.01
0.009
Volumetric Air Flow Rate (m3/s)
1
0
-1
Pressure Gradient Across test section pressure ports (kN/m3)
0
50
100
150
200
250
300
Time (s)

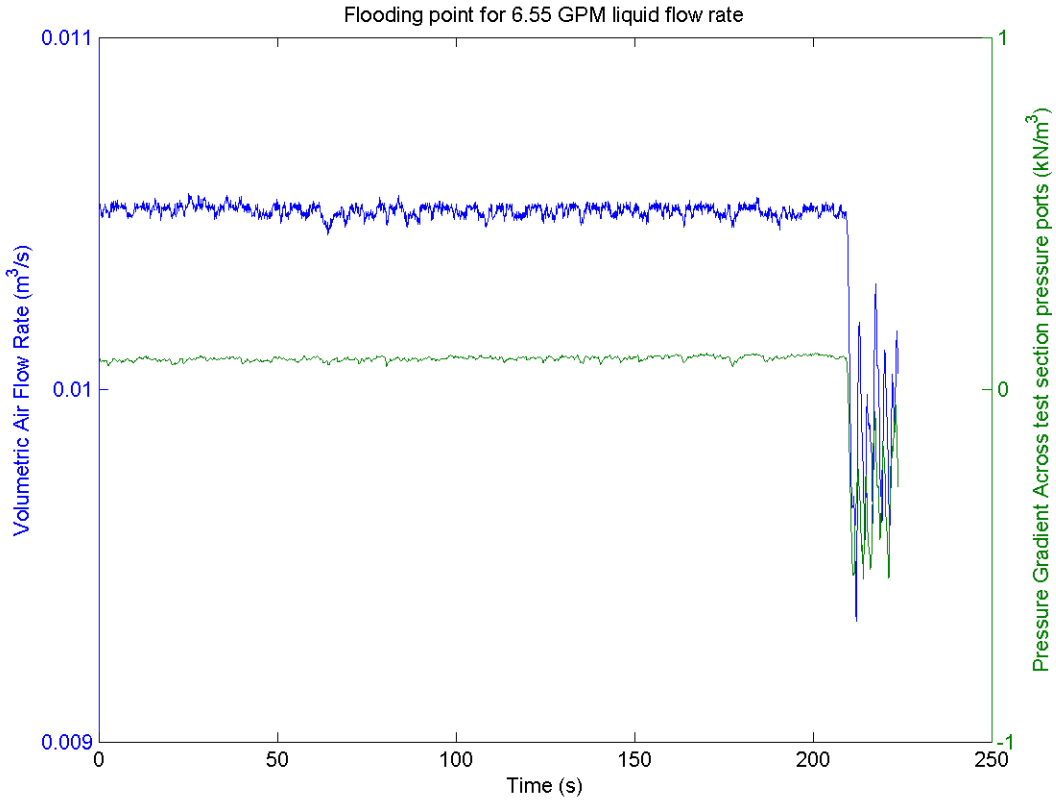
Flooding point for 6.55 GPM liquid flow rate
0.011
0.01
0.009
Volumetric Air Flow Rate (m3/s)
1
0
-1
Pressure Gradient Across test section pressure ports (kN/m3)
0
50
100
150
200
250
Time (s)

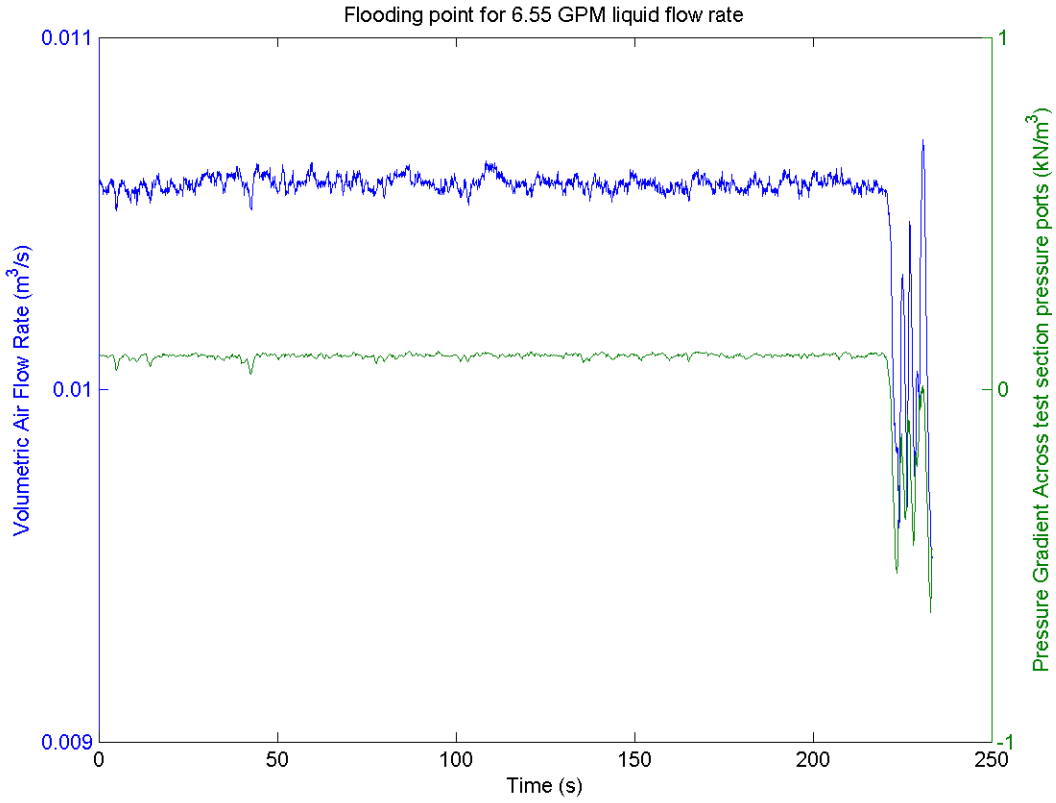
Flooding point for 6.55 GPM liquid flow rate
0.011
0.01
0.009
Volumetric Air Flow Rate (m3/s)
1
0
-1
Pressure Gradient Across test section pressure ports (kN/m3)
0
50
100
150
200
250
Time (s)

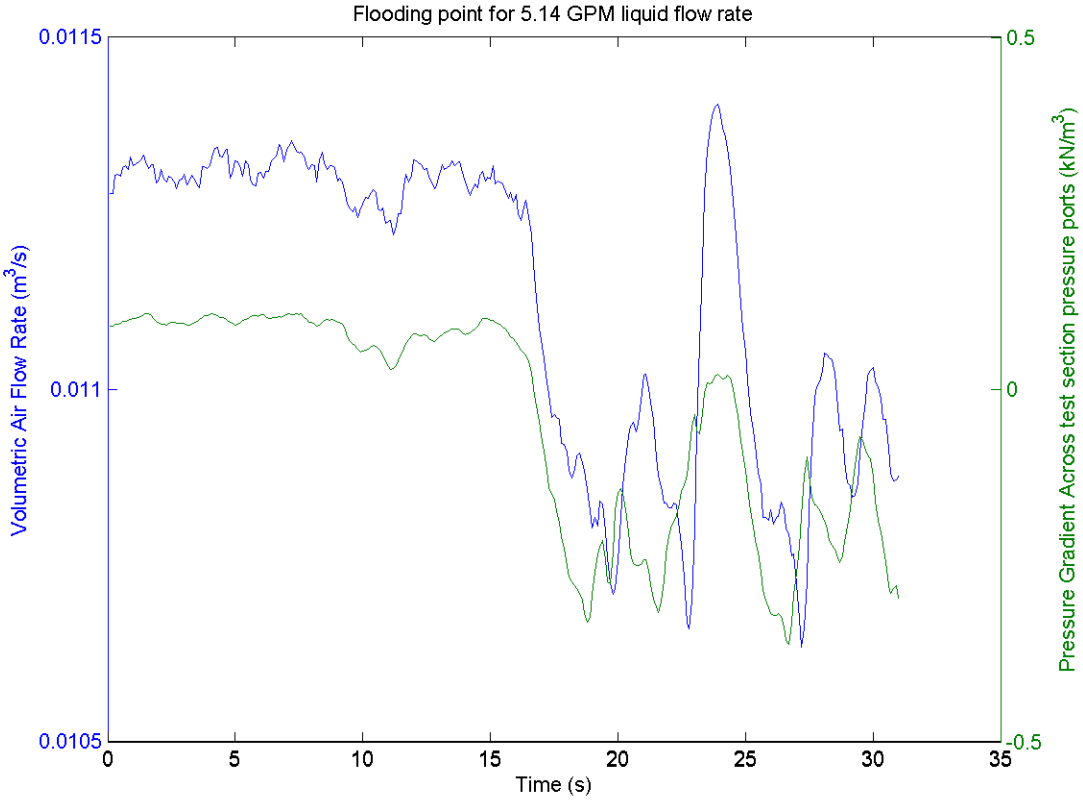
Flooding point for 5.14 GPM liquid flow rate
0.0115
0.011
0.0105
0.5
0
-0.5
0
5
10
15
20
25
30
35
Time (s)
Volumetric Air Flow Rate (m3/s)
Pressure Gradient Across test section pressure ports (kN/m3)

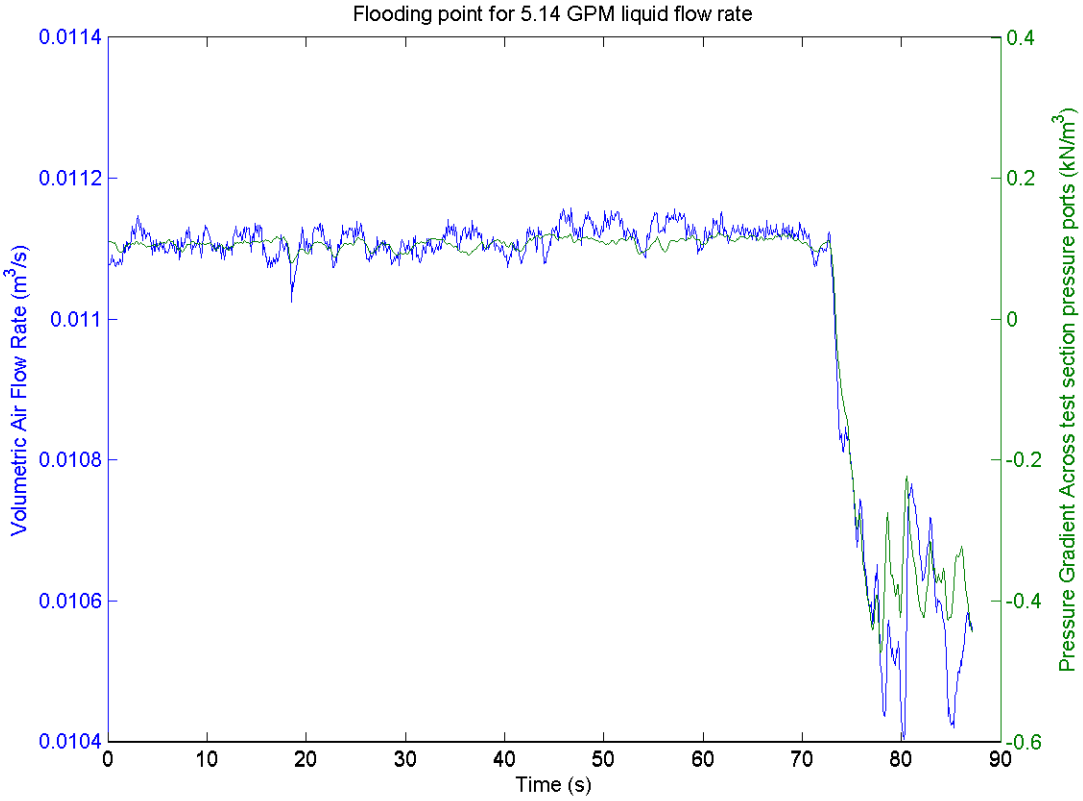
Flooding point for 5.14 GPM liquid flow rate
Volumetric Air Flow Rate (m3/s)
Pressure Gradient Across test section pressure ports (kN/m3)
Time (s)
0.0114
0.0112
0.011
0.0108
0.0106
0.0104
0.4
0.2
0
-0.2
-0.4
-0.6
0
10
20
30
40
50
60
70
80
90

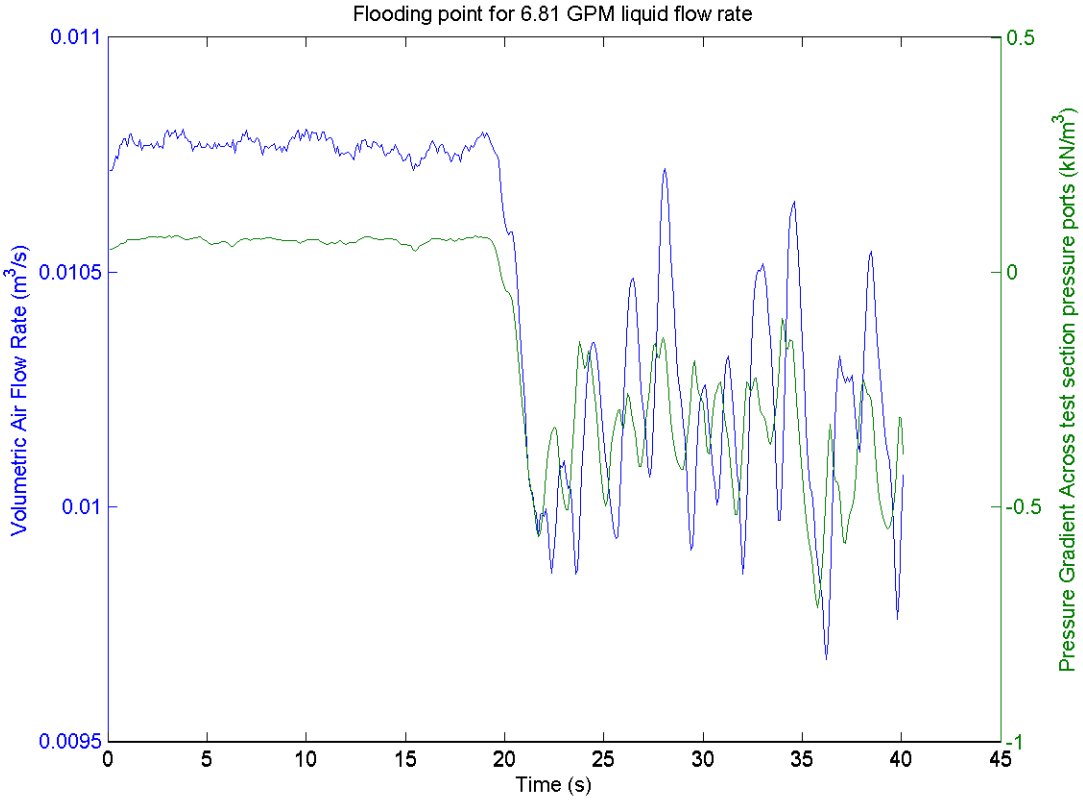
Flooding point for 6.81 GPM liquid flow rate
Volumetric Air Flow Rate (m3/s)
Pressure Gradient Across test section pressure ports (kN/m3)
Time (s)
0.011
0.0105
0.01
0.0095
0.5
0
-0.5
-1
0
5
10
15
20
25
30
35
40
45

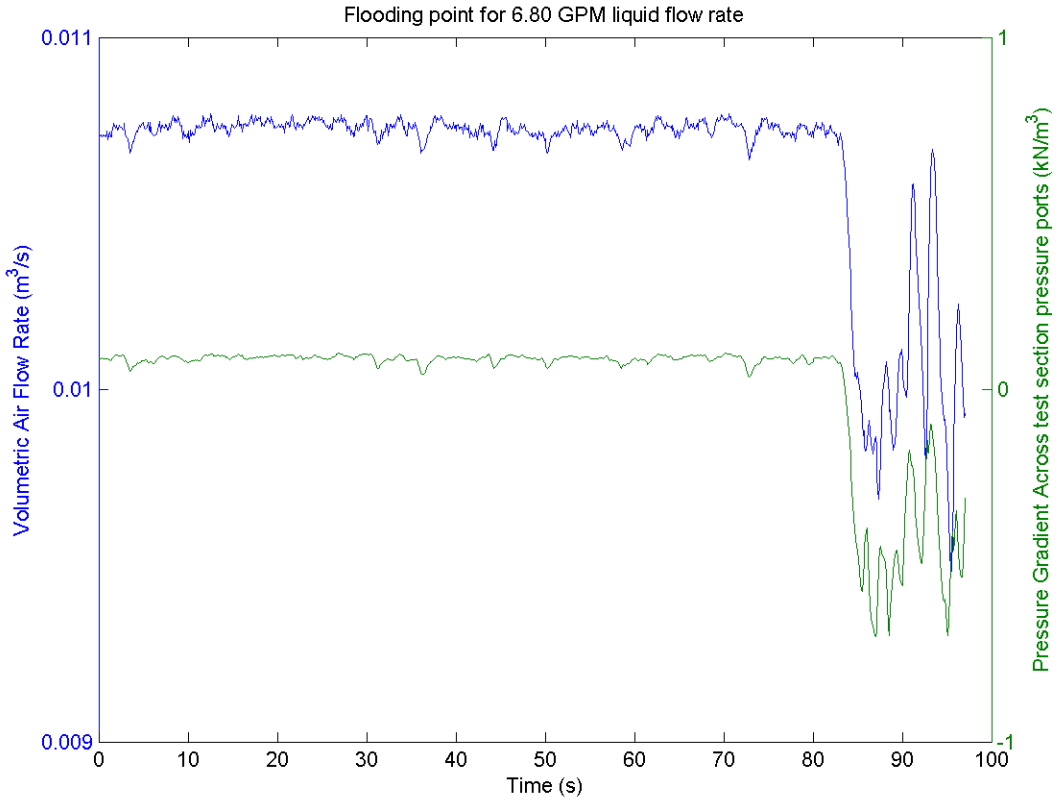
Flooding point for 6.80 GPM liquid flow rate
0.011
0.01
0.009
Volumetric Air Flow Rate (m3/s)
1
0
-1
Pressure Gradient Across test section pressure ports (kN/m3)
0
10
20
30
40
50
60
70
80
90
100
Time (s)

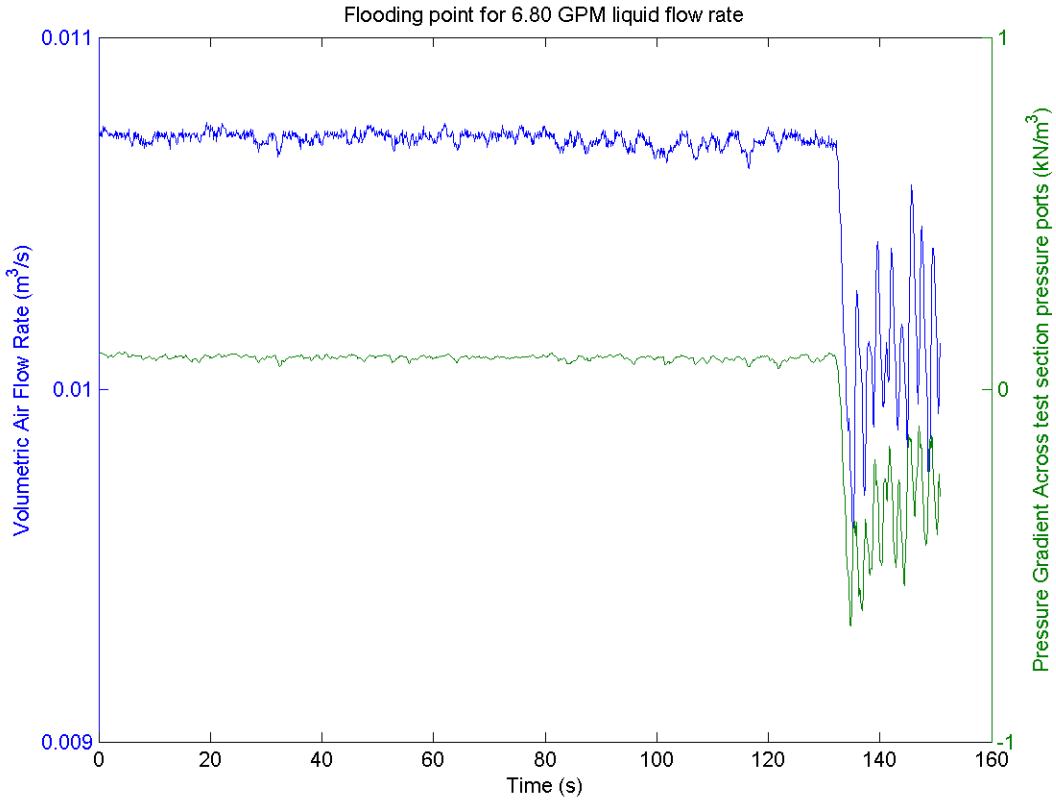
Flooding point for 6.80 GPM liquid flow rate
0.011
0.01
0.009
Volumetric Air Flow Rate (m3/s)
1
0
-1
Pressure Gradient Across test section pressure ports (kN/m3)
0
20
40
60
80
100
120
140
160
Time (s)

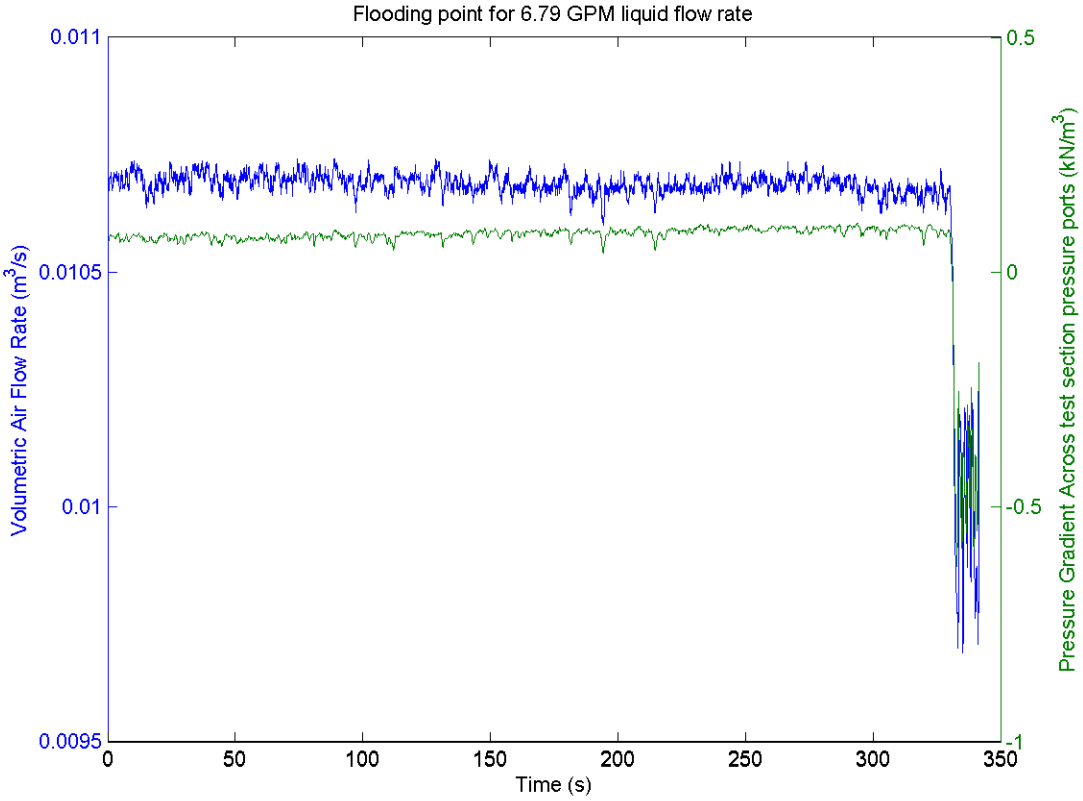
Flooding point for 6.79 GPM liquid flow rate
Volumetric Air Flow Rate (m3/s)
Pressure Gradient Across test section pressure ports (kN/m3)
Time (s)
0.011
0.0105
0.01
0.0095
0.5
0
-0.5
-1
0
50
100
150
200
250
300
350

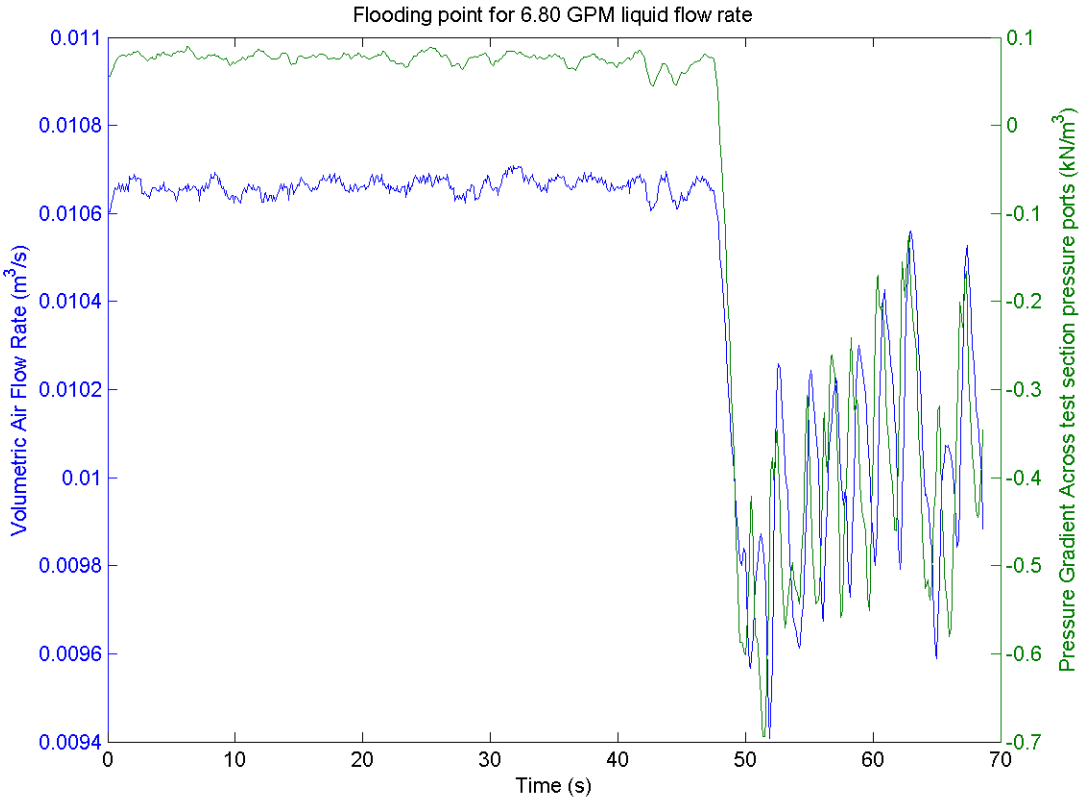
Flooding point for 6.80 GPM liquid flow rate
Volumetric Air Flow Rate (m3/s)
Pressure Gradient Across test section pressure ports (kN/m3)
Time (s)
0.011
0.0108
0.0106
0.0104
0.0102
0.01
0.0098
0.0096
0.0094
0.1
0
-0.1
-0.2
-0.3
-0.4
-0.5
-0.6
-0.7
0
10
20
30
40
50
60
70

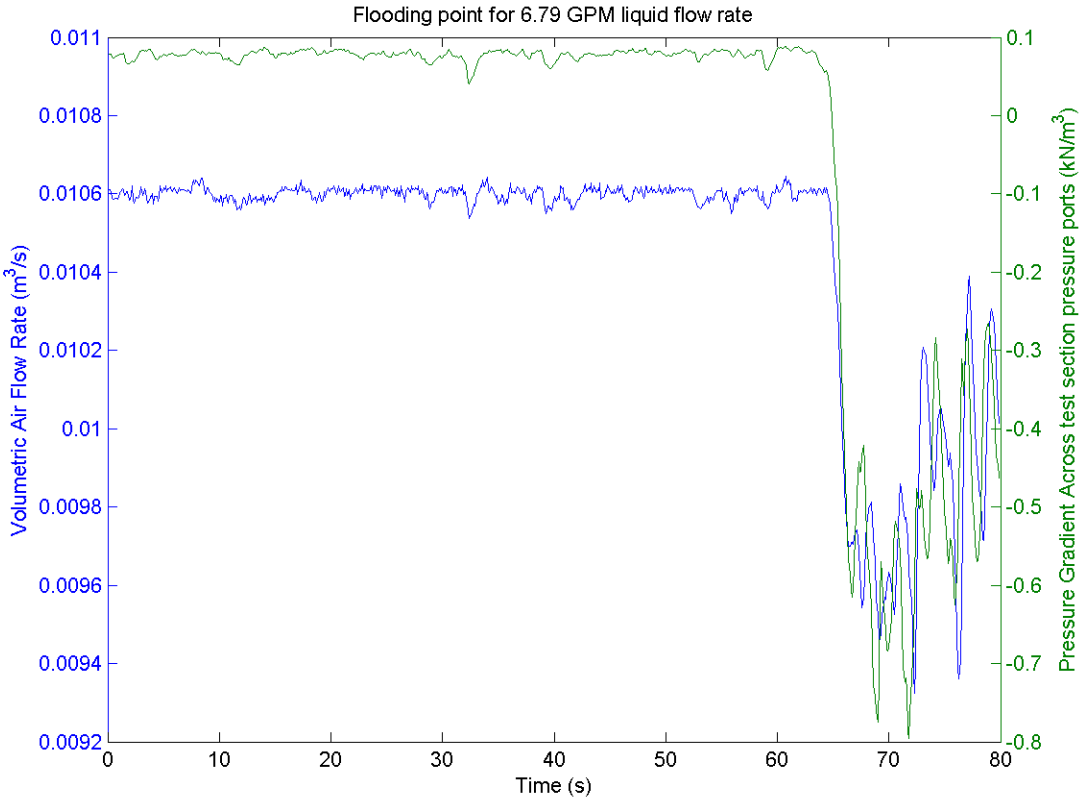
Flooding point for 6.79 GPM liquid flow rate
Volumetric Air Flow Rate (m3/s)
Pressure Gradient Across test section pressure ports (kN/m3)
Time (s)
0.011
0.0108
0.0106
0.0104
0.0102
0.01
0.0098
0.0096
0.0094
0.0092
0.1
0
-0.1
-0.2
-0.3
-0.4
-0.5
-0.6
-0.7
-0.8
0
10
20
30
40
50
60
70
80

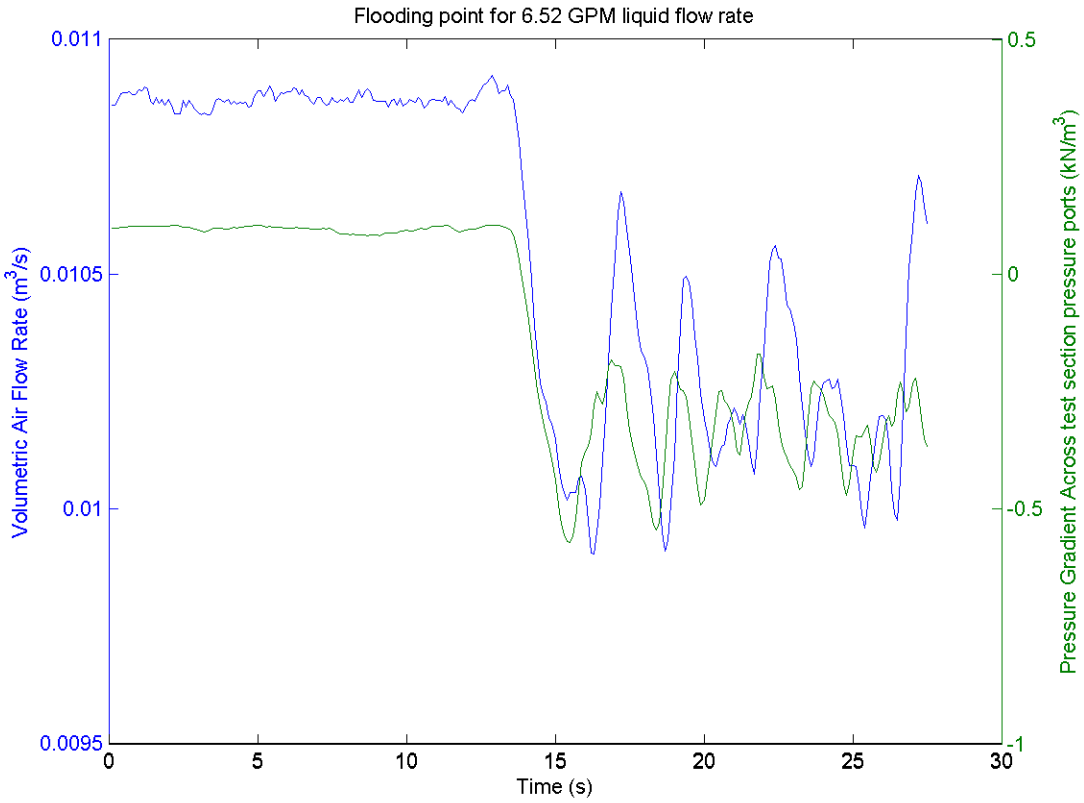
Flooding point for 6.52 GPM liquid flow rate
Volumetric Air Flow Rate (m3/s)
Pressure Gradient Across test section pressure ports (kN/m3)
Time (s)
0.011
0.0105
0.01
0.0095
0.5
0
-0.5
-1
0
5
10
15
20
25
30

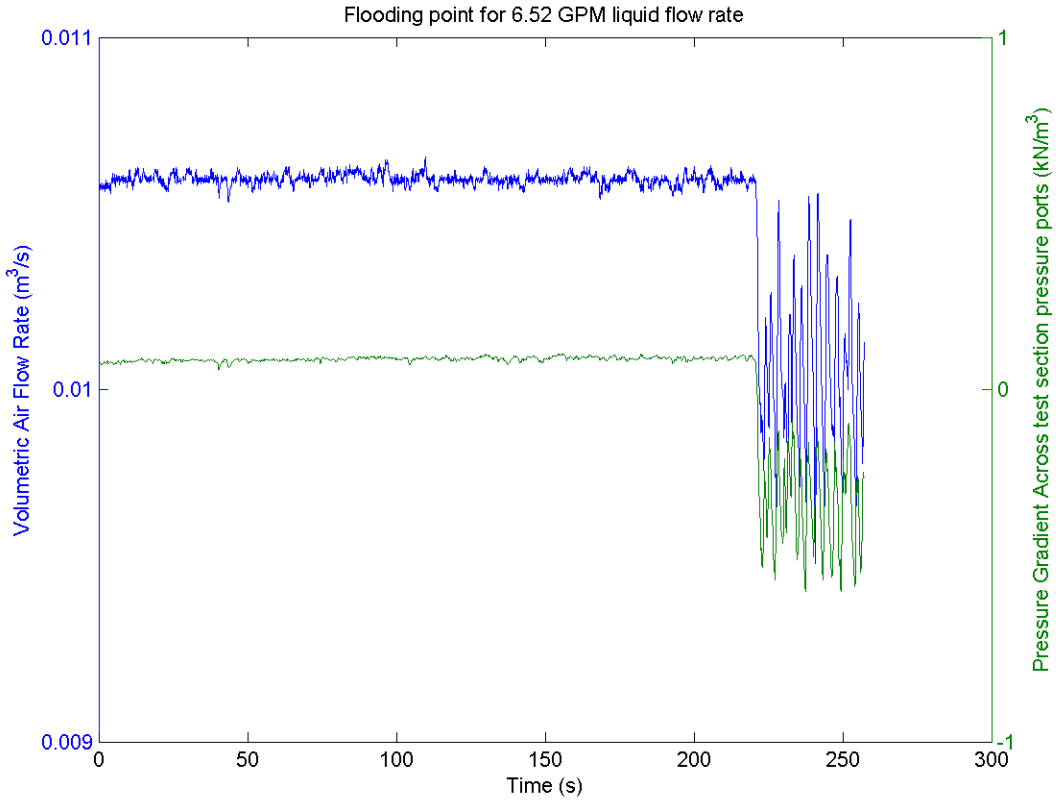
Flooding point for 6.52 GPM liquid flow rate
0.011
0.01
0.009
Volumetric Air Flow Rate (m3/s)
1
0
-1
Pressure Gradient Across test section pressure ports (kN/m3)
0
50
100
150
200
250
300
Time (s)

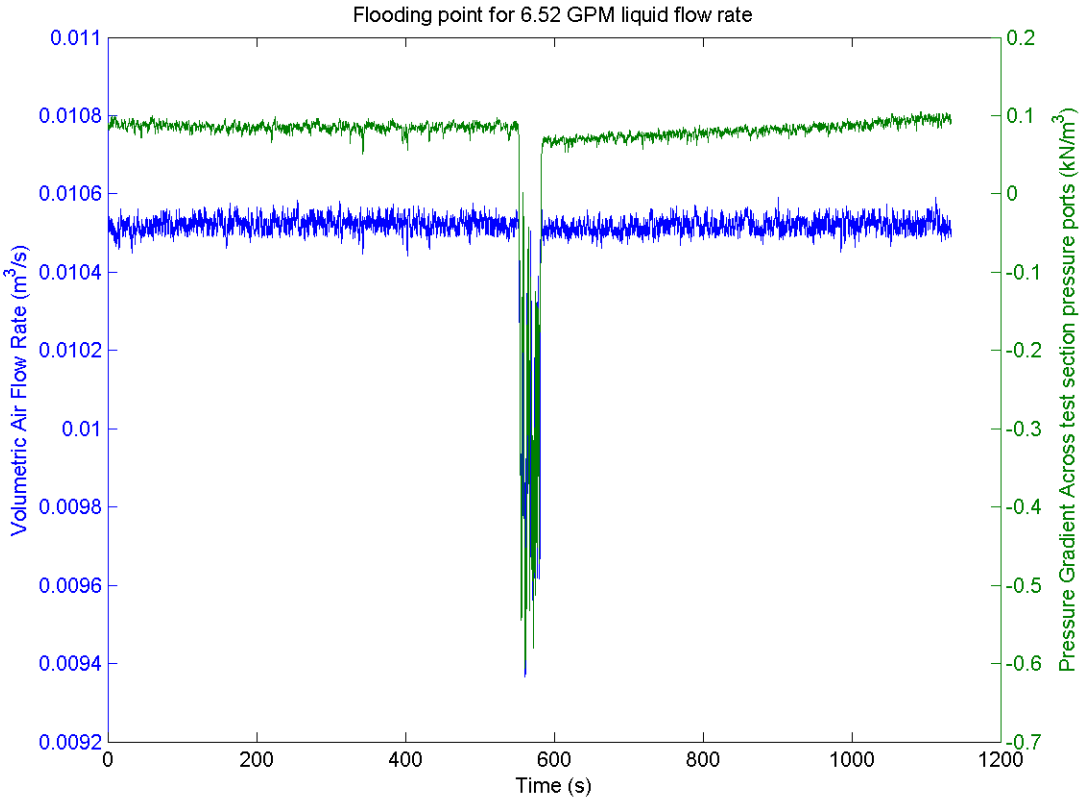
Flooding point for 6.52 GPM liquid flow rate
Volumetric Air Flow Rate (m3/s)
Pressure Gradient Across test section pressure ports (kN/m3)
Time (s)
0.011
0.0108
0.0106
0.0104
0.0102
0.01
0.0098
0.0096
0.0094
0.0092
0.2
0.1
0
-0.1
-0.2
-0.3
-0.4
-0.5
-0.6
-0.7
0
200
400
600
800
1000
1200

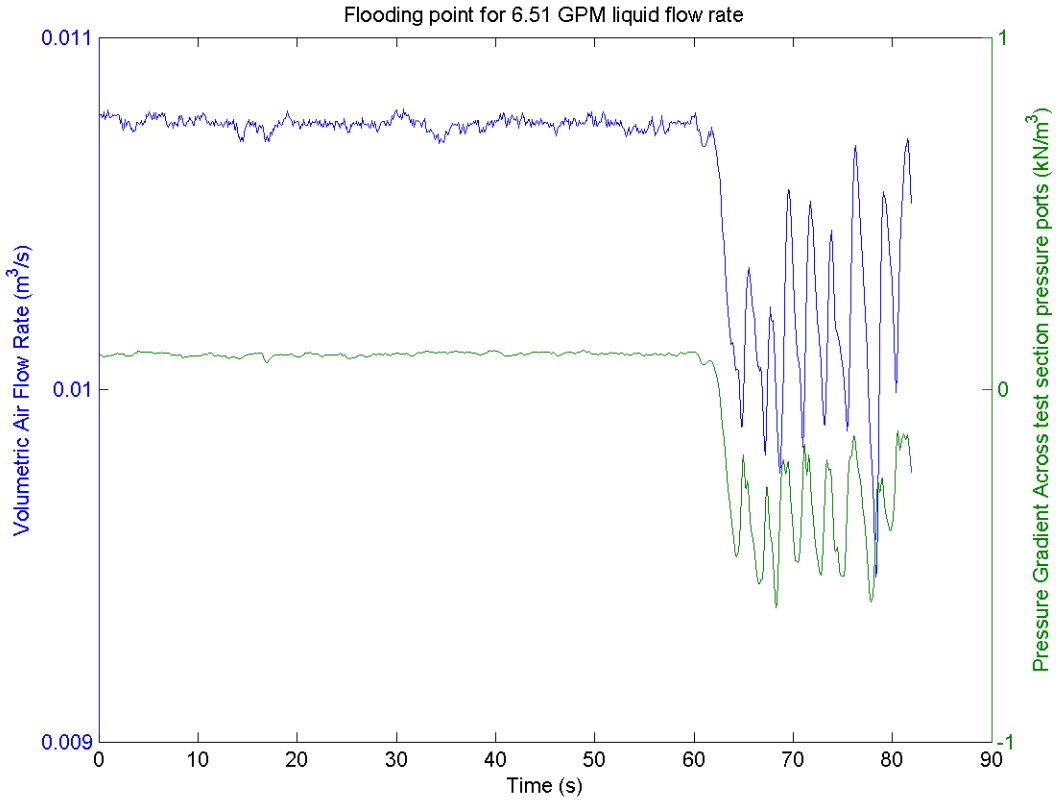
Flooding point for 6.51 GPM liquid flow rate
Volumetric Air Flow Rate (m3/s)
Pressure Gradient Across test section pressure ports (kN/m3)
Time (s)
0.011
0.01
0.009
1
0
-1
0
10
20
30
40
50
60
70
80
90

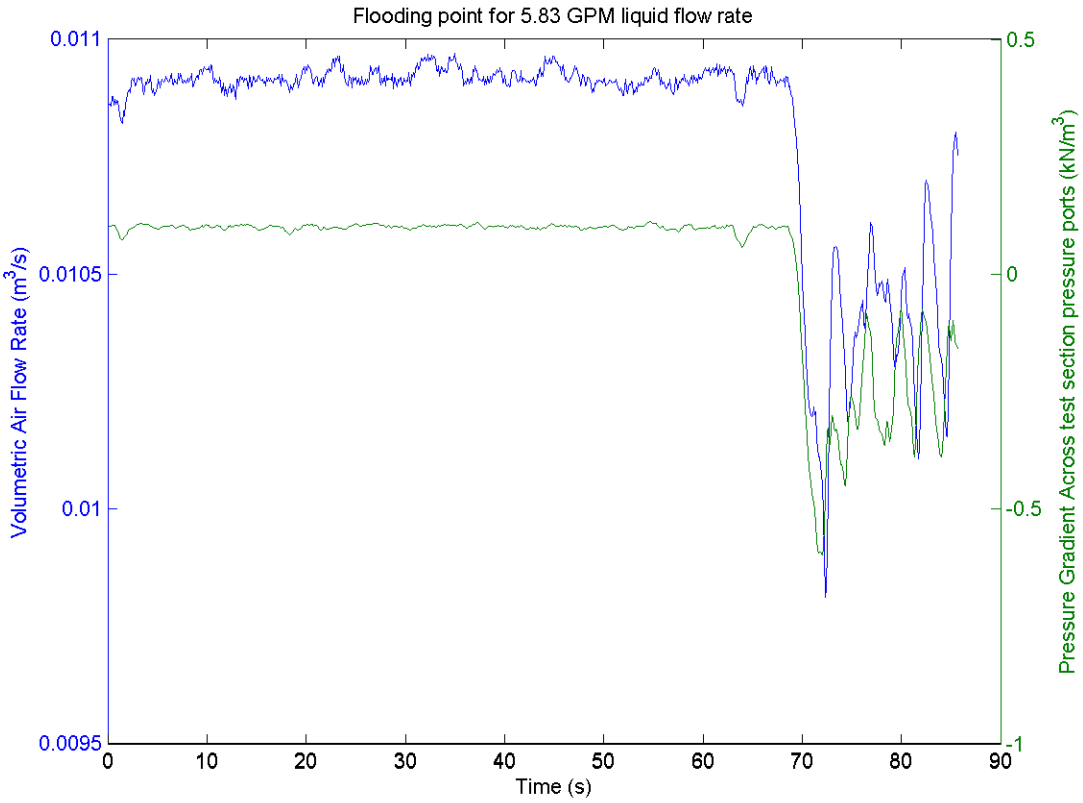
Flooding point for 5.83 GPM liquid flow rate
Volumetric Air Flow Rate (m3/s)
Pressure Gradient Across test section pressure ports (kN/m3)
Time (s)
0.011
0.0105
0.01
0.0095
0.5
0
-0.5
-1
0
10
20
30
40
50
60
70
80
90

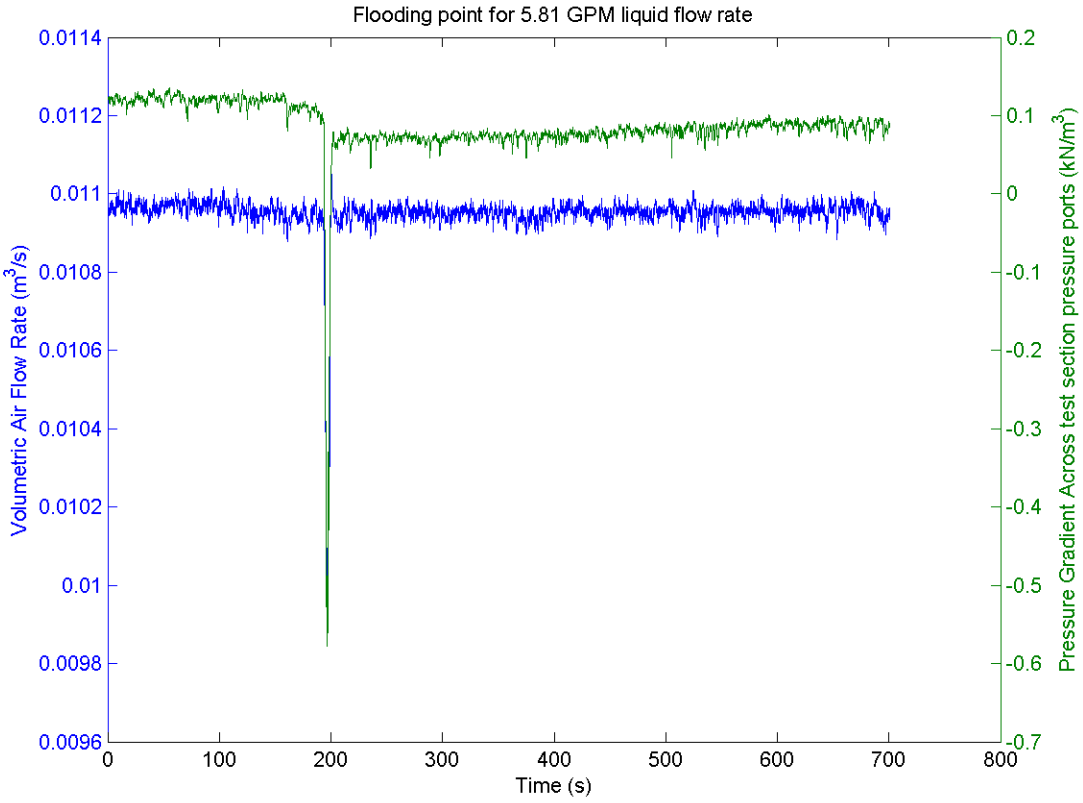
Flooding point for 5.81 GPM liquid flow rate
Volumetric Air Flow Rate (m3/s)
Pressure Gradient Across test section pressure ports (kN/m3)
Time (s)
0.0114
0.0112
0.011
0.0108
0.0106
0.0104
0.0102
0.01
0.0098
0.0096
0.2
0.1
0
-0.1
-0.2
-0.3
-0.4
-0.5
-0.6
-0.7
0
100
200
300
400
500
600
700
800

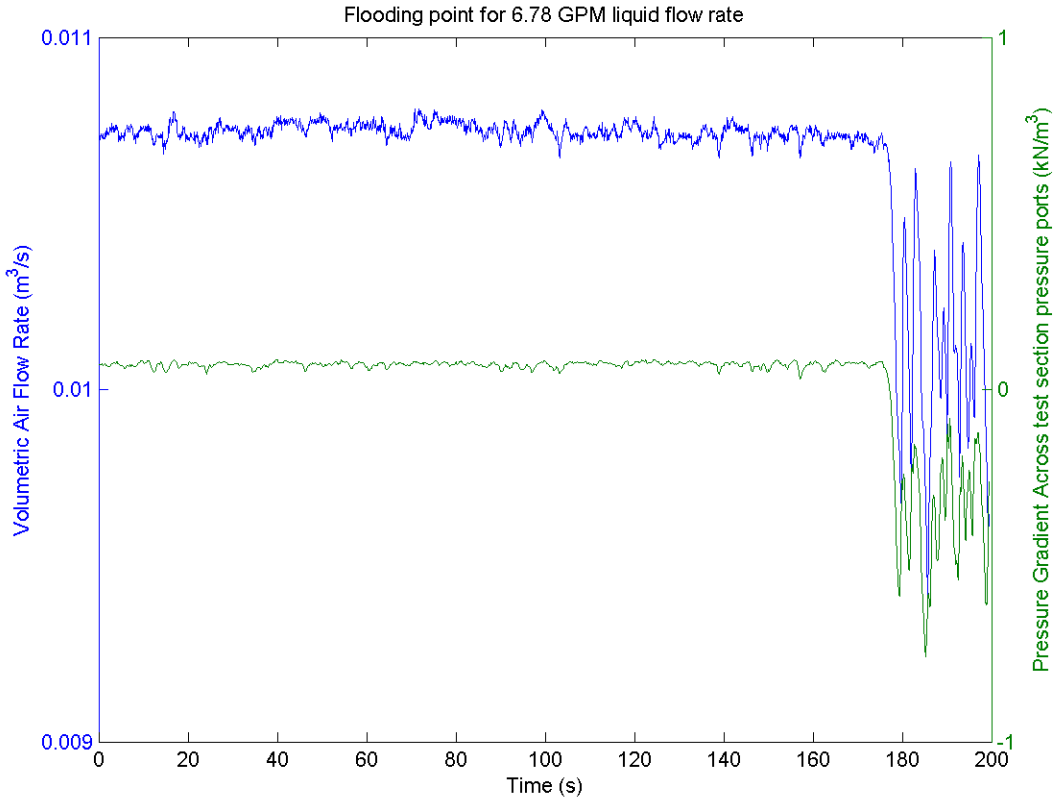
Flooding point for 6.78 GPM liquid flow rate
0.011
0.01
0.009
Volumetric Air Flow Rate (m3/s)
1
0
-1
Pressure Gradient Across test section pressure ports (kN/m3)
0
20
40
60
80
100
120
140
160
180
200
Time (s)

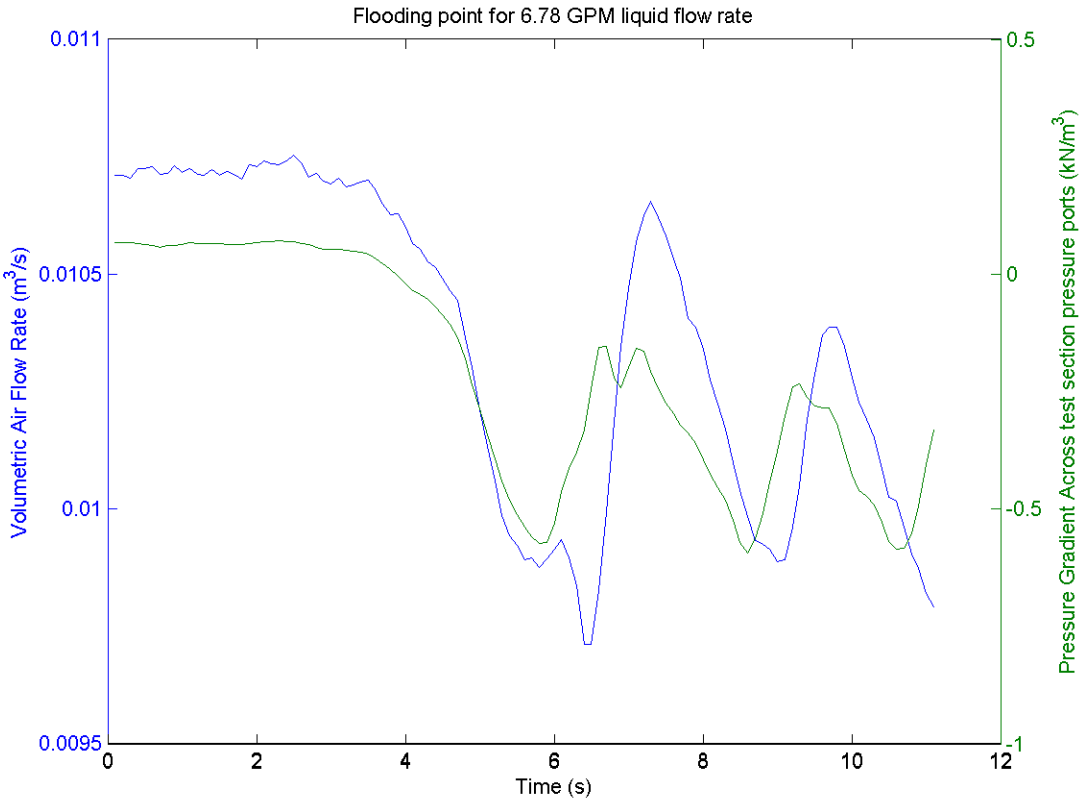
Flooding point for 6.78 GPM liquid flow rate
Volumetric Air Flow Rate (m3/s)
Pressure Gradient Across test section pressure ports (kN/m3)
Time (s)
0.011
0.0105
0.01
0.0095
0.5
0
-0.5
-1
0
2
4
6
8
10
12

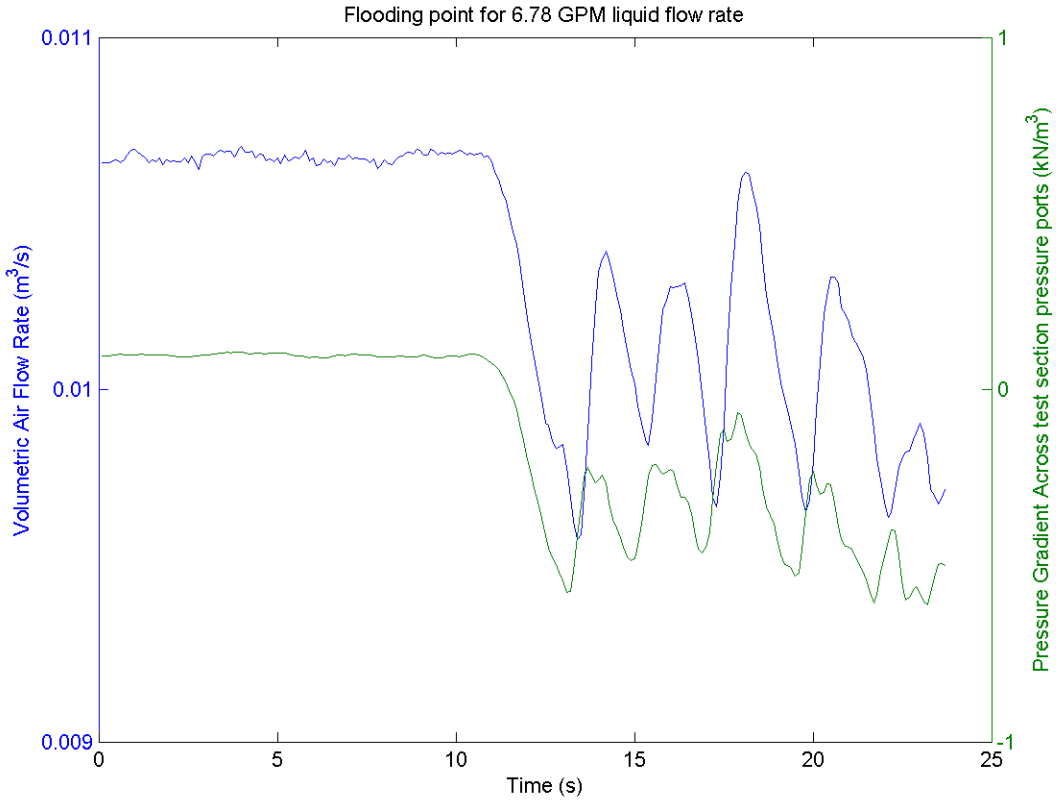
Flooding point for 6.78 GPM liquid flow rate
0.011
0.01
0.009
Volumetric Air Flow Rate (m3/s)
1
0
-1
Pressure Gradient Across test section pressure ports (kN/m3)
0
5
10
15
20
25
Time (s)

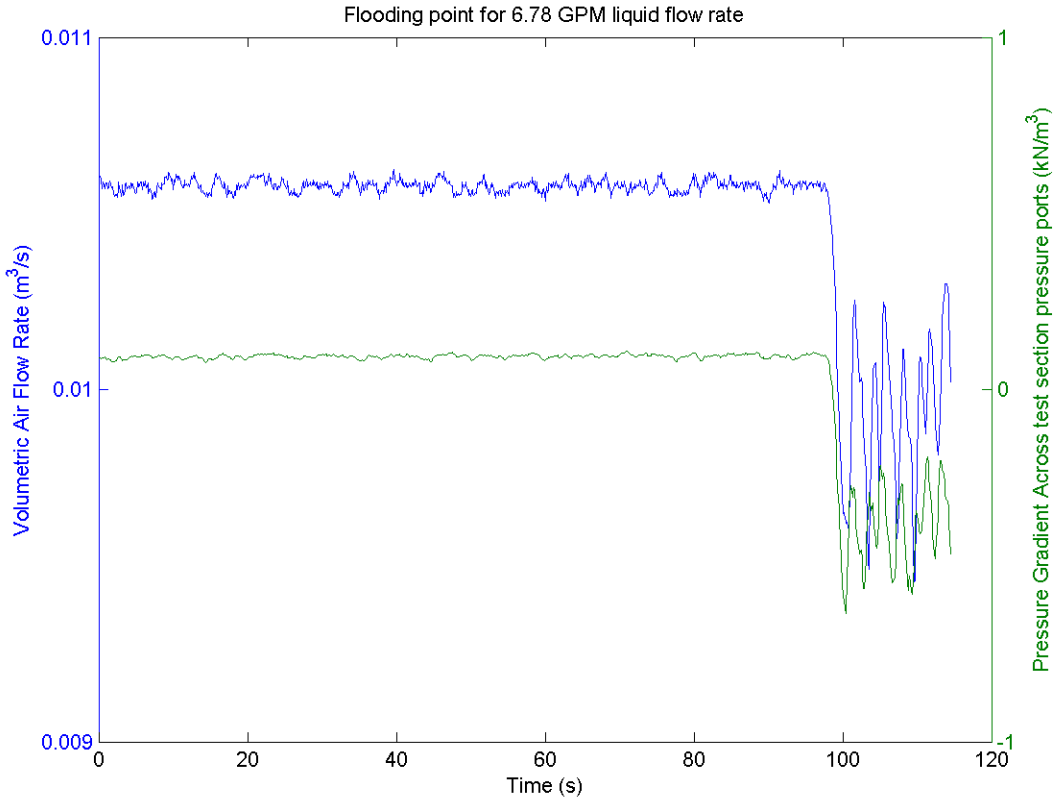
Flooding point for 6.78 GPM liquid flow rate
0.011
0.01
0.009
Volumetric Air Flow Rate (m3/s)
1
0
-1
Pressure Gradient Across test section pressure ports (kN/m3)
0
20
40
60
80
100
120
Time (s)

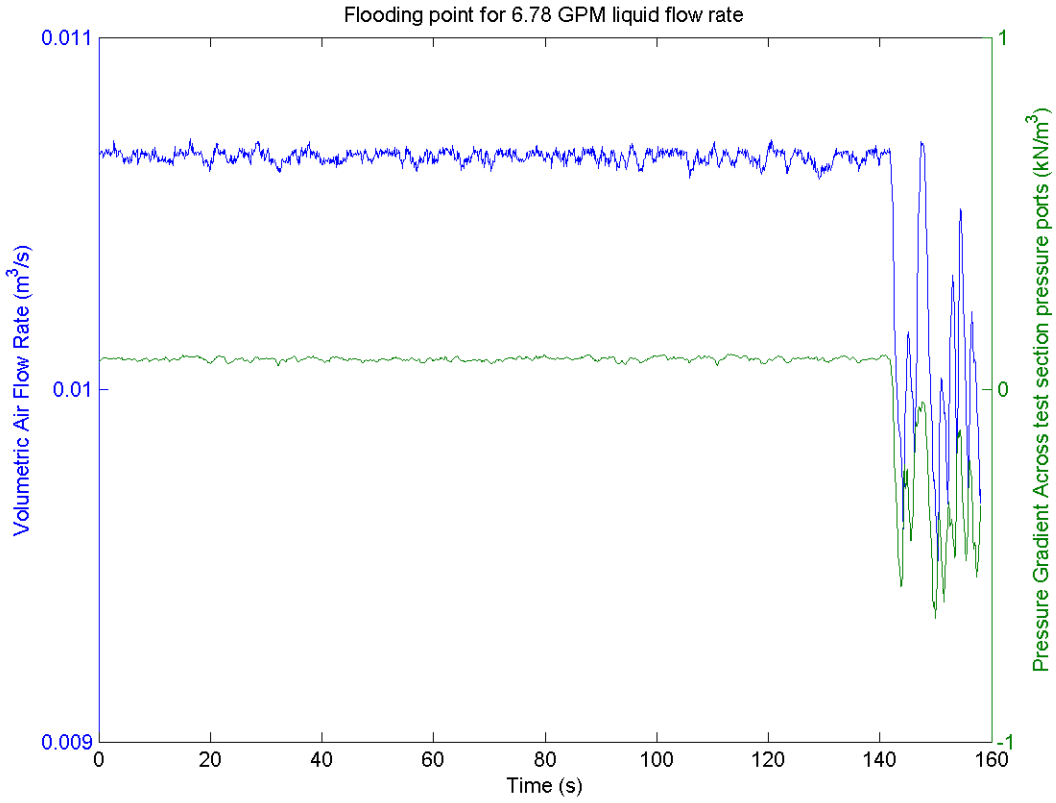
Flooding point for 6.78 GPM liquid flow rate
0.011
0.01
0.009
Volumetric Air Flow Rate (m3/s)
1
0
-1
Pressure Gradient Across test section pressure ports (kN/m3)
0
20
40
60
80
100
120
140
160
Time (s)

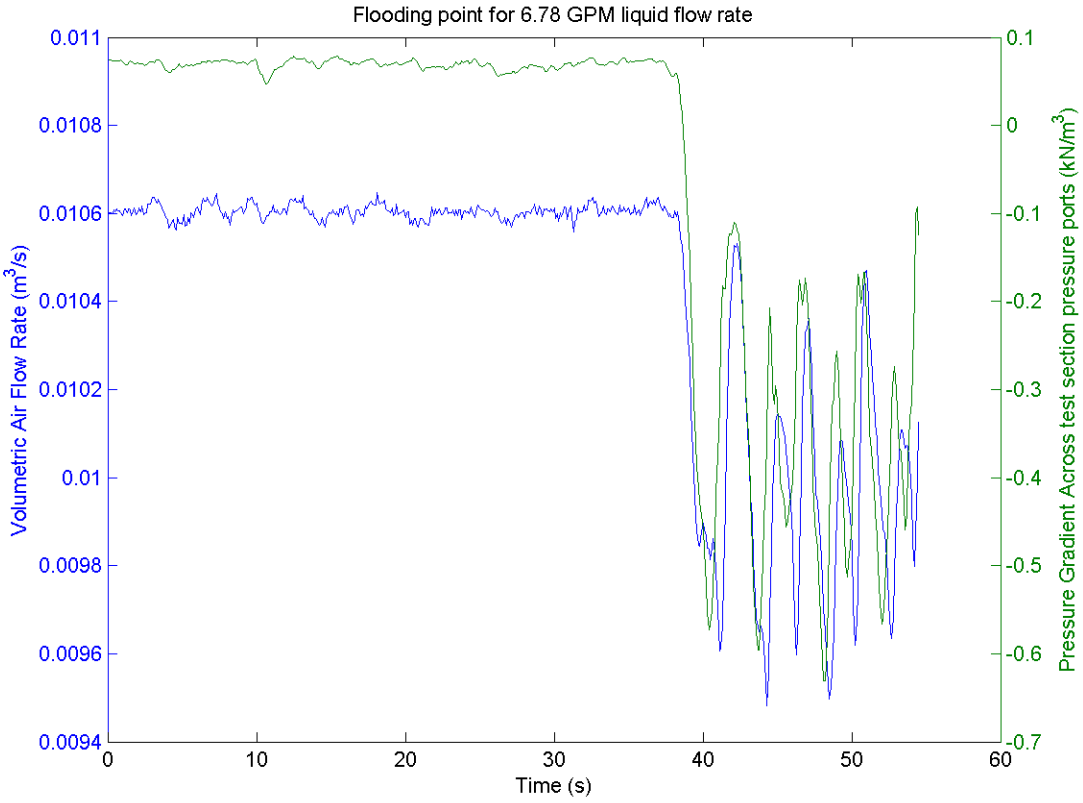
Flooding point for 6.78 GPM liquid flow rate
Volumetric Air Flow Rate (m3/s)
Pressure Gradient Across test section pressure ports (kN/m3)
Time (s)
0.011
0.0108
0.0106
0.0104
0.0102
0.01
0.0098
0.0096
0.0094
0.1
0
-0.1
-0.2
-0.3
-0.4
-0.5
-0.6
-0.7
0
10
20
30
40
50
60

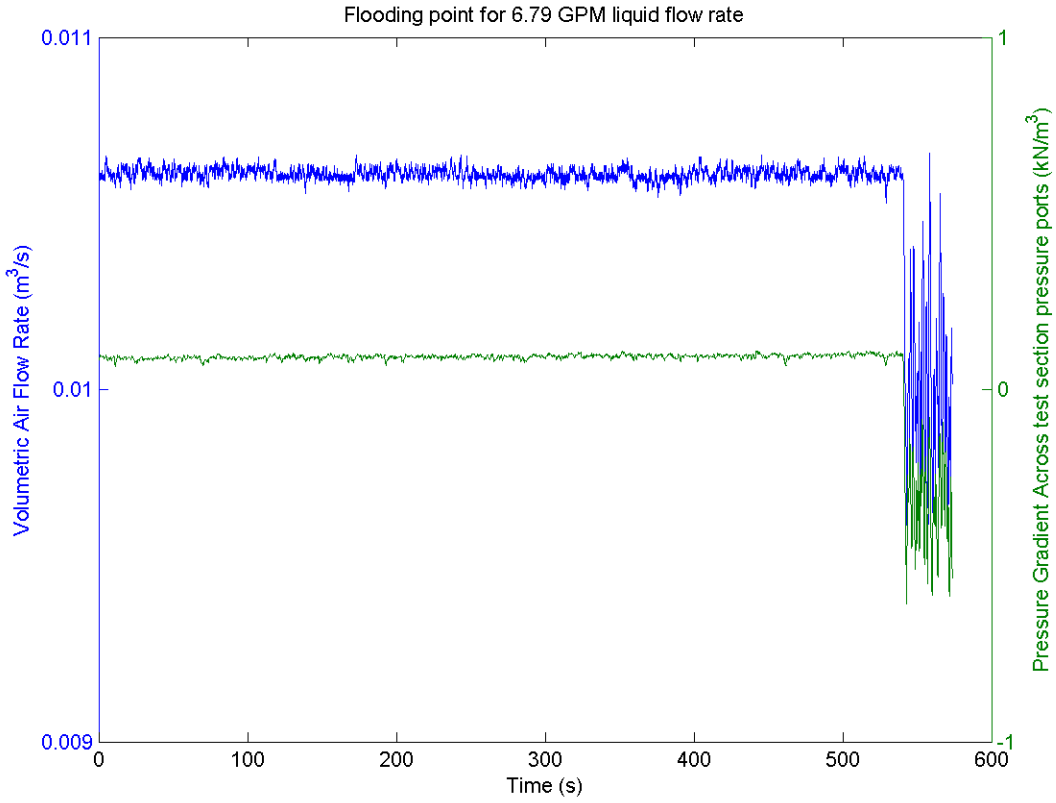
Flooding point for 6.79 GPM liquid flow rate
0.011
0.01
0.009
Volumetric Air Flow Rate (m3/s)
1
0
-1
Pressure Gradient Across test section pressure ports (kN/m3)
0
100
200
300
400
500
600
Time (s)

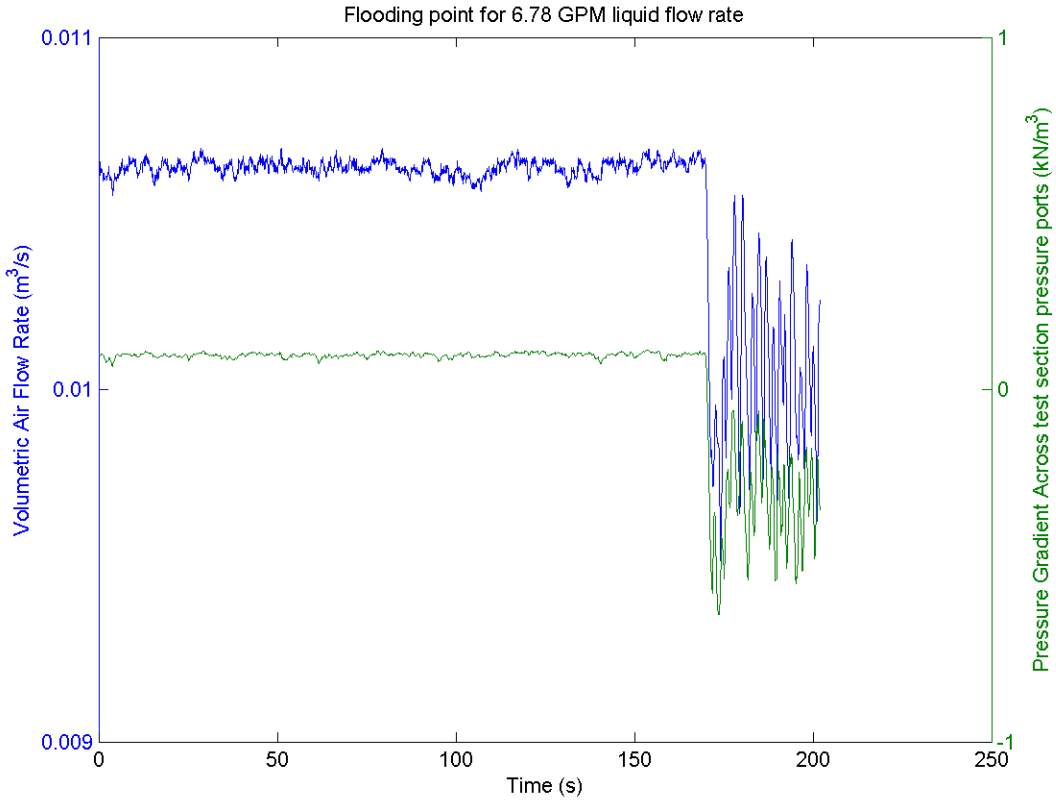
Flooding point for 6.78 GPM liquid flow rate
0.011
0.01
0.009
Volumetric Air Flow Rate (m3/s)
1
0
-1
Pressure Gradient Across test section pressure ports (kN/m3)
0
50
100
150
200
250
Time (s)

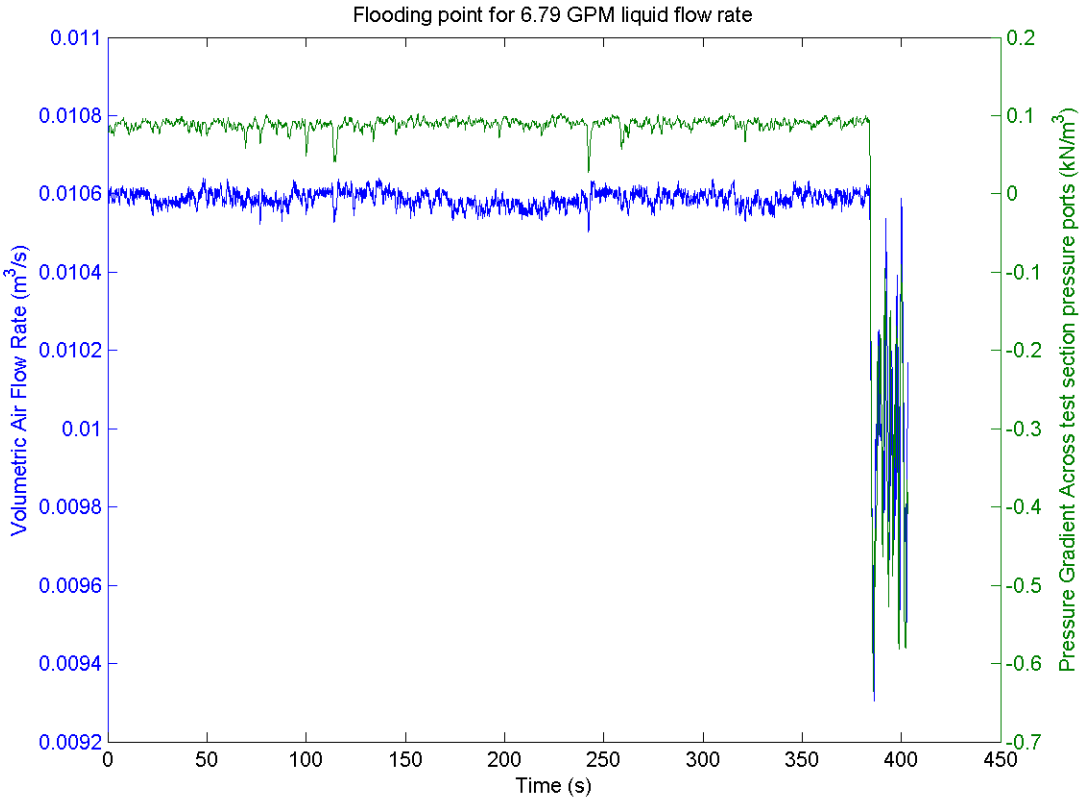
Flooding point for 6.79 GPM liquid flow rate
Volumetric Air Flow Rate (m3/s)
Pressure Gradient Across test section pressure ports (kN/m3)
Time (s)
0.011
0.0108
0.0106
0.0104
0.0102
0.01
0.0098
0.0096
0.0094
0.0092
0.2
0.1
0
-0.1
-0.2
-0.3
-0.4
-0.5
-0.6
-0.7
0
50
100
150
200
250
300
350
400
450

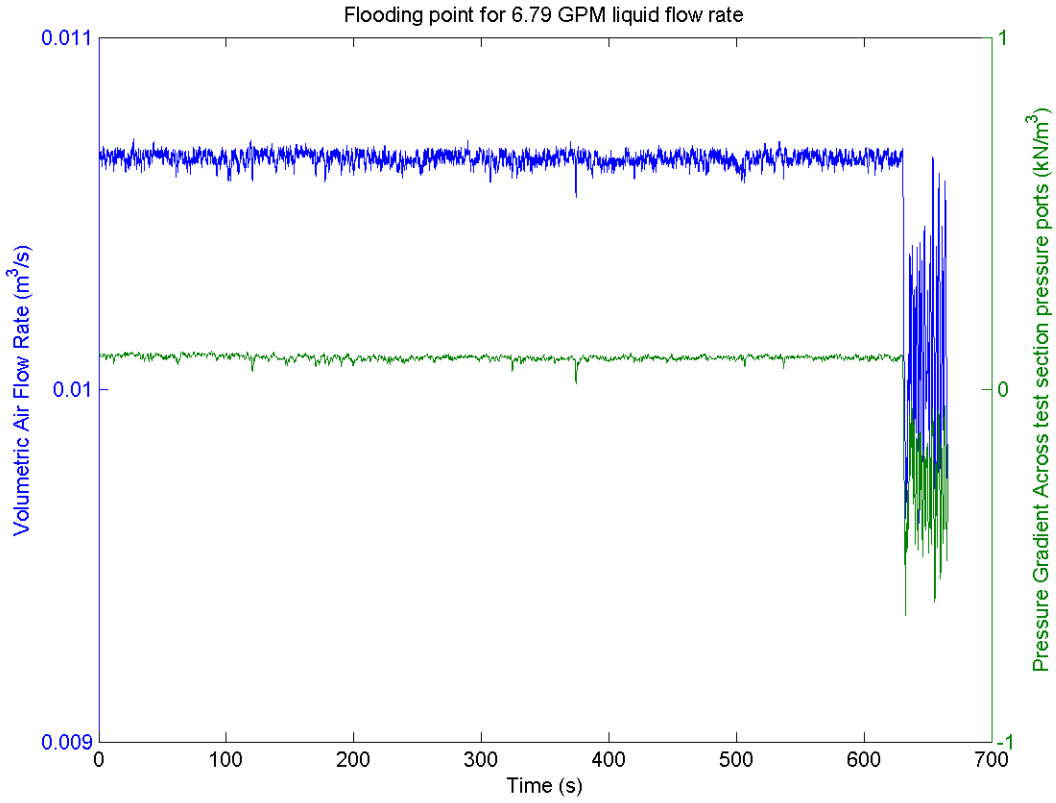
Flooding point for 6.79 GPM liquid flow rate
0.011
0.01
0.009
Volumetric Air Flow Rate (m3/s)
1
0
-1
Pressure Gradient Across test section pressure ports (kN/m3)
0
100
200
300
400
500
600
700
Time (s)

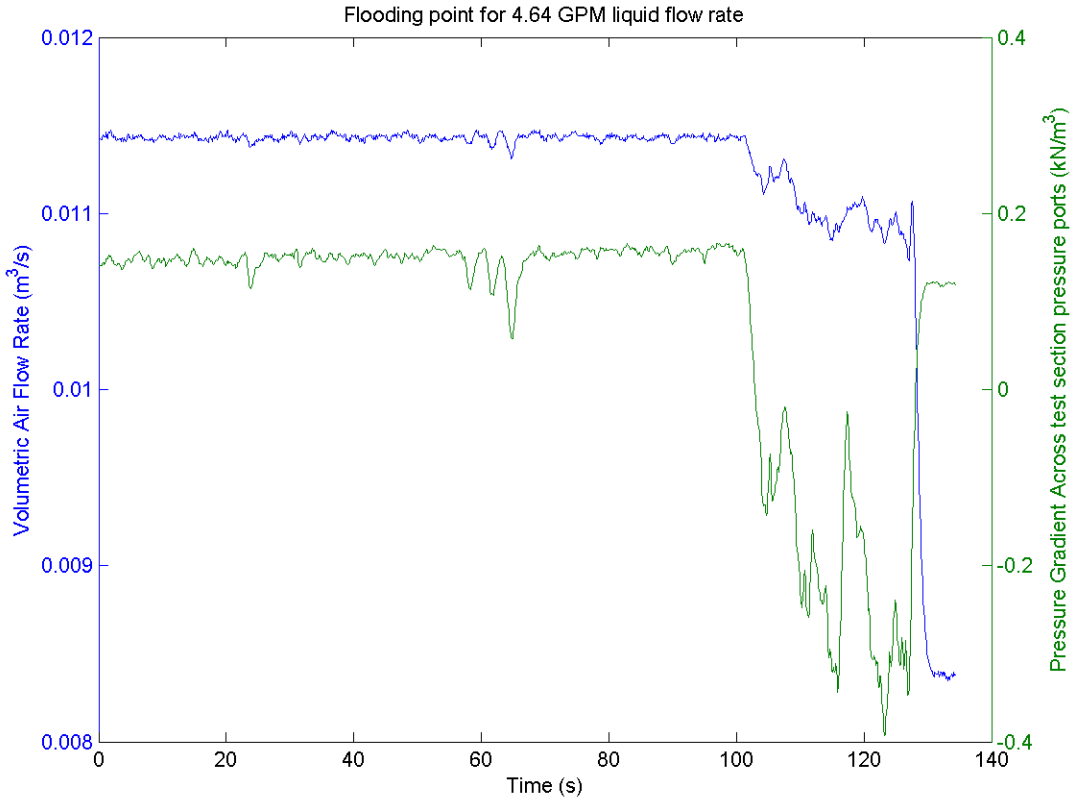
Flooding point for 4.64 GPM liquid flow rate
Volumetric Air Flow Rate (m3/s)
Pressure Gradient Across test section pressure ports (kN/m3)
Time (s)
0.012
0.011
0.01
0.009
0.008
0.4
0.2
0
-0.2
-0.4
0
20
40
60
80
100
120
140

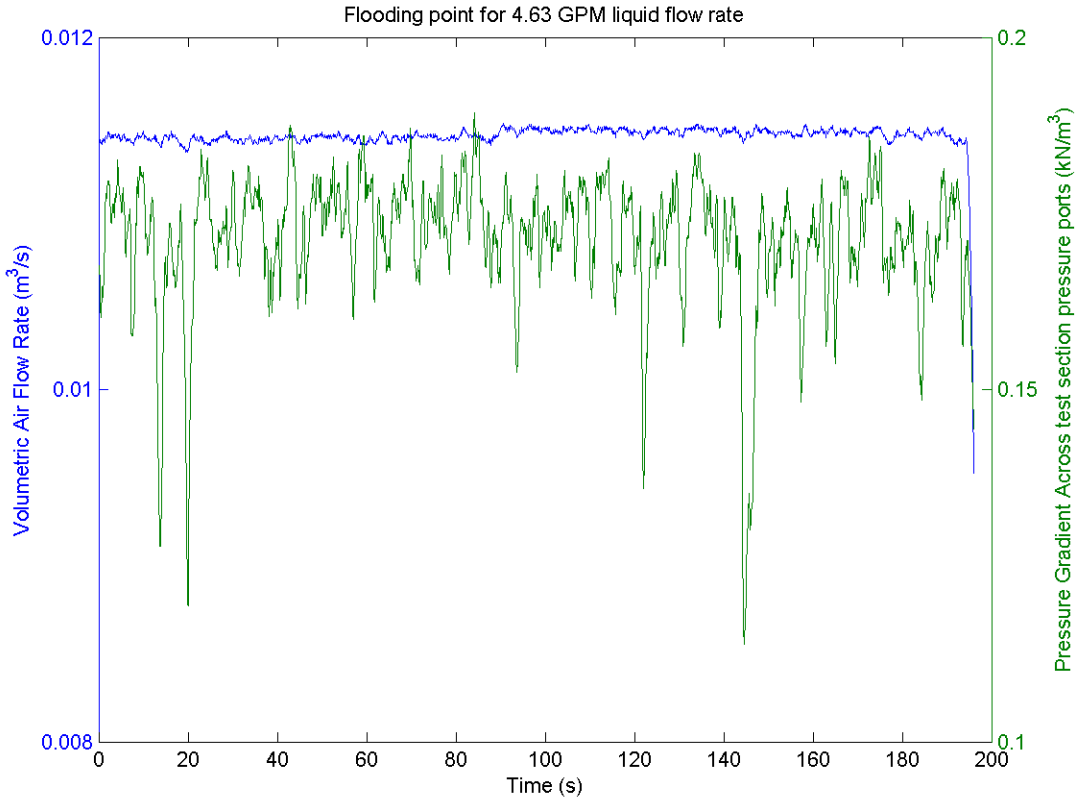
Flooding point for 4.63 GPM liquid flow rate
Volumetric Air Flow Rate (m3/s)
Pressure Gradient Across test section pressure ports (kN/m3)
Time (s)
0.012
0.01
0.008
0.2
0.15
0.1
0
20
40
60
80
100
120
140
160
180
200

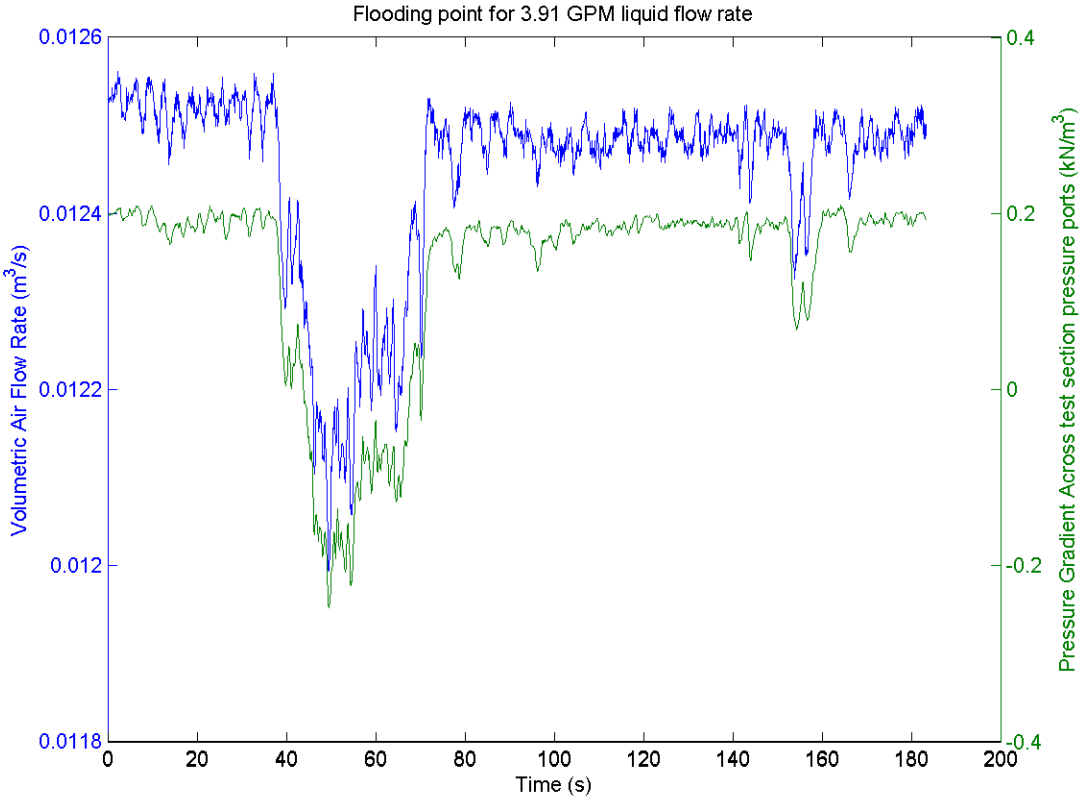
Flooding point for 3.91 GPM liquid flow rate
Volumetric Air Flow Rate (m3/s)
Pressure Gradient Across test section pressure ports (kN/m3)
Time (s)
0.0126
0.0124
0.0122
0.012
0.0118
0.4
0.2
0
-0.2
-0.4
0
20
40
60
80
100
120
140
160
180
200

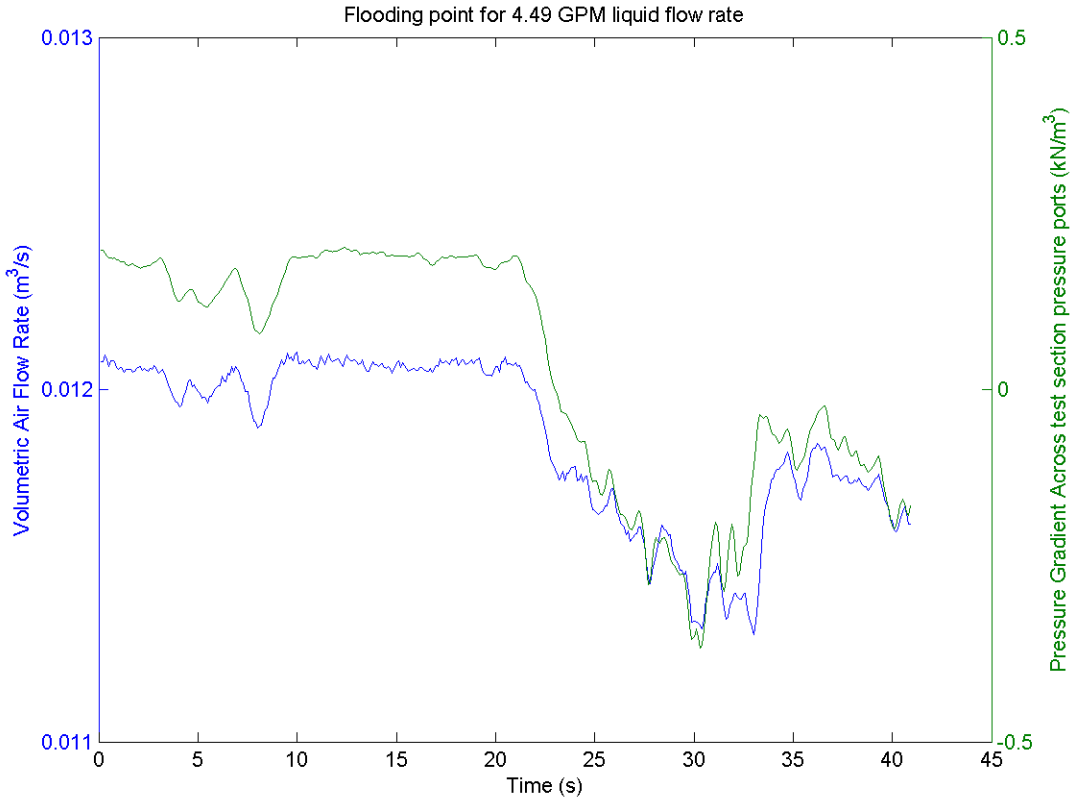
Flooding point for 4.49 GPM liquid flow rate
0.013
0.012
0.011
Volumetric Air Flow Rate (m3/s)
0.5
0
-0.5
Pressure Gradient Across test section pressure ports (kN/m3)
0
5
10
15
20
25
30
35
40
45
Time (s)

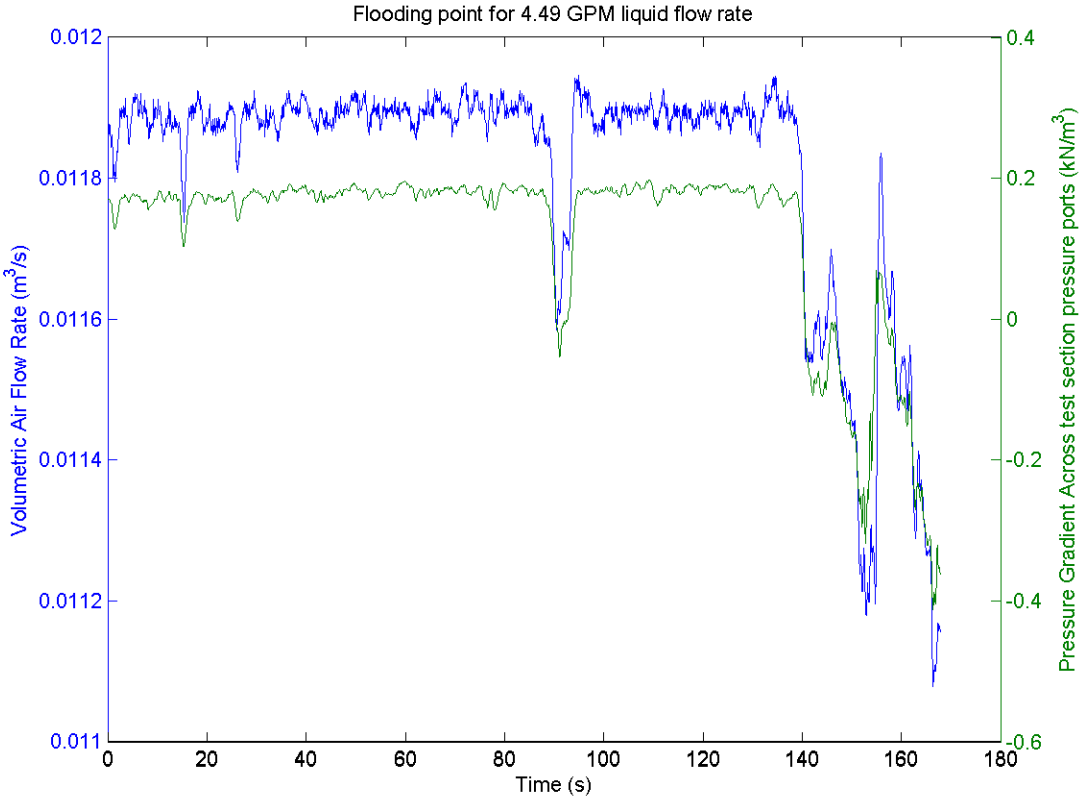
Flooding point for 4.49 GPM liquid flow rate
Volumetric Air Flow Rate (m3/s)
Pressure Gradient Across test section pressure ports (kN/m3)
Time (s)
0.012
0.0118
0.0116
0.0114
0.0112
0.011
0.4
0.2
0
-0.2
-0.4
-0.6
0
20
40
60
80
100
120
140
160
180

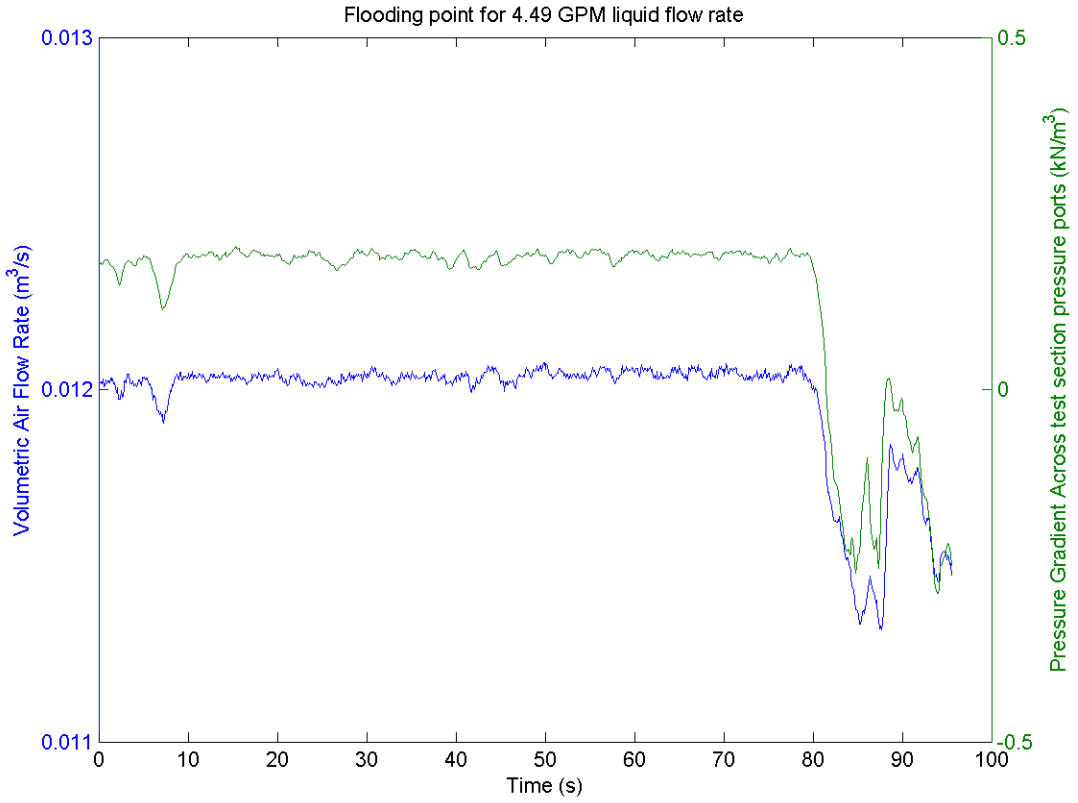
Flooding point for 4.49 GPM liquid flow rate
0.013
0.012
0.011
0.5
0
-0.5
0
10
20
30
40
50
60
70
80
90
100
Time (s)
Volumetric Air Flow Rate (m3/s)
Pressure Gradient Across test section pressure ports (kN/m3)

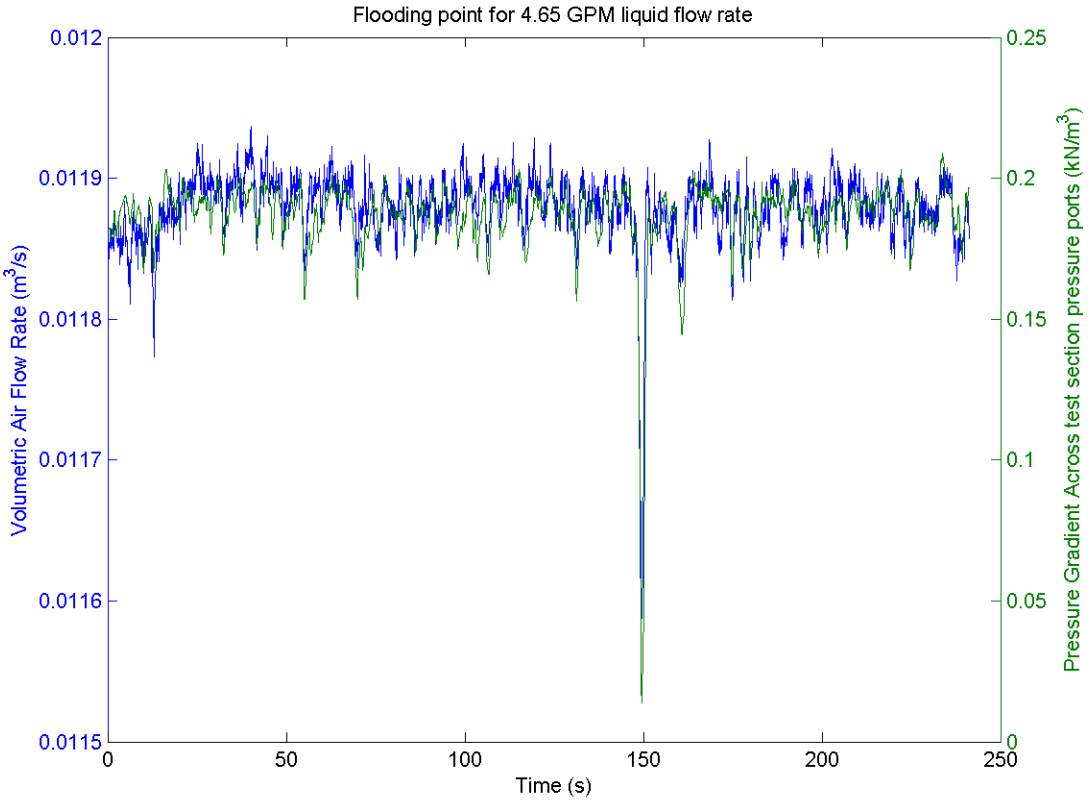
Flooding point for 4.65 GPM liquid flow rate
Volumetric Air Flow Rate (m3/s)
Pressure Gradient Across test section pressure ports (kN/m3)
Time (s)
0.012
0.0119
0.0118
0.0117
0.0116
0.0115
0.25
0.2
0.15
0.1
0.05
0
0
50
100
150
200
250

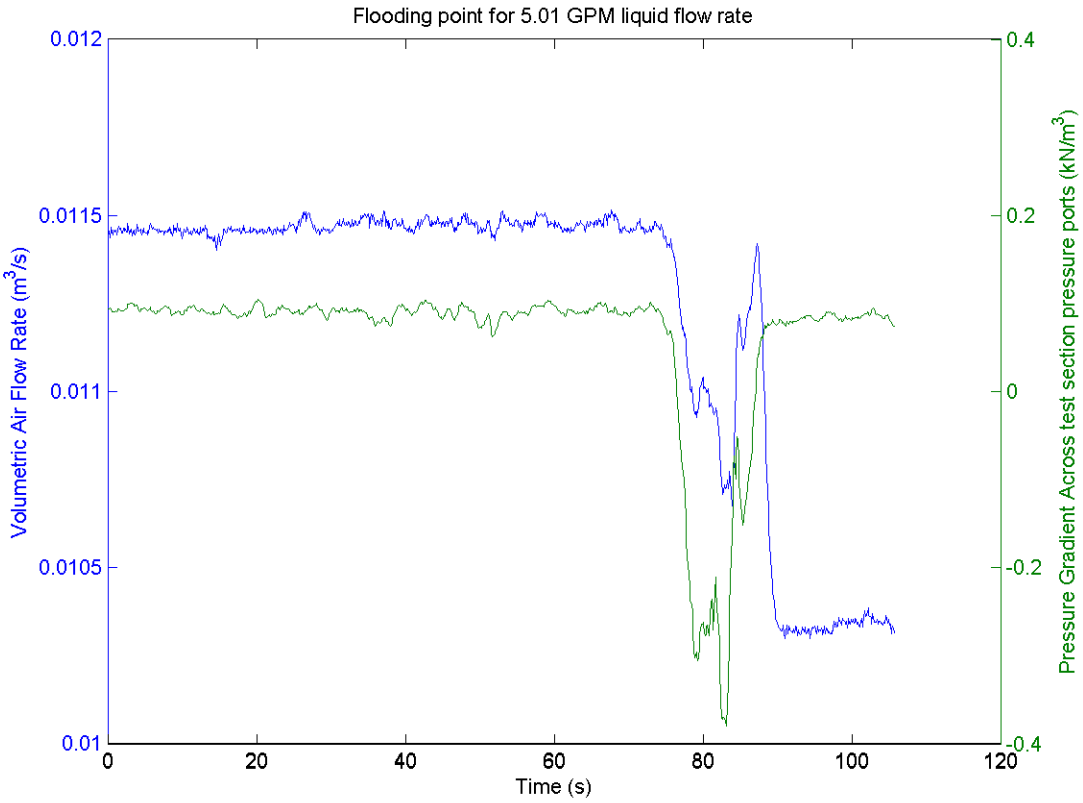
Flooding point for 5.01 GPM liquid flow rate
Volumetric Air Flow Rate (m3/s)
Pressure Gradient Across test section pressure ports (kN/m3)
Time (s)
0.012
0.0115
0.011
0.0105
0.01
0.4
0.2
0
-0.2
-0.4
0
20
40
60
80
100
120

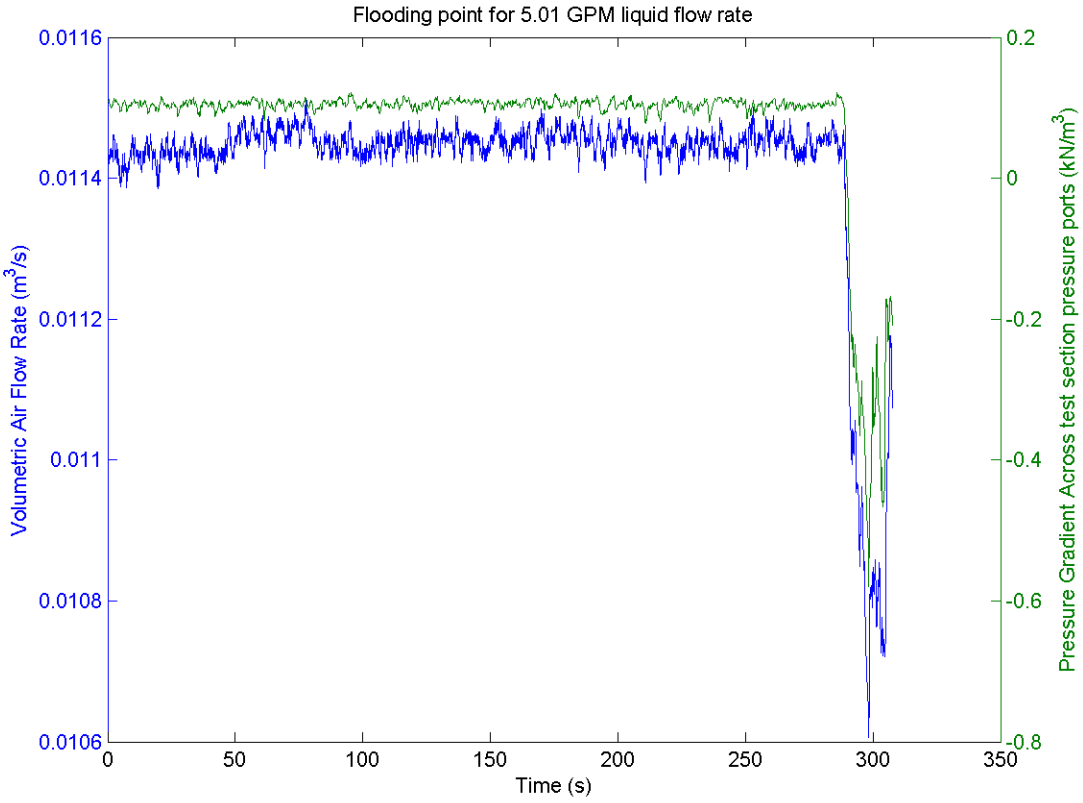
Flooding point for 5.01 GPM liquid flow rate
Volumetric Air Flow Rate (m3/s)
Pressure Gradient Across test section pressure ports (kN/m3)
Time (s)
0.0116
0.0114
0.0112
0.011
0.0108
0.0106
0.2
0
-0.2
-0.4
-0.6
-0.8
0
50
100
150
200
250
300
350

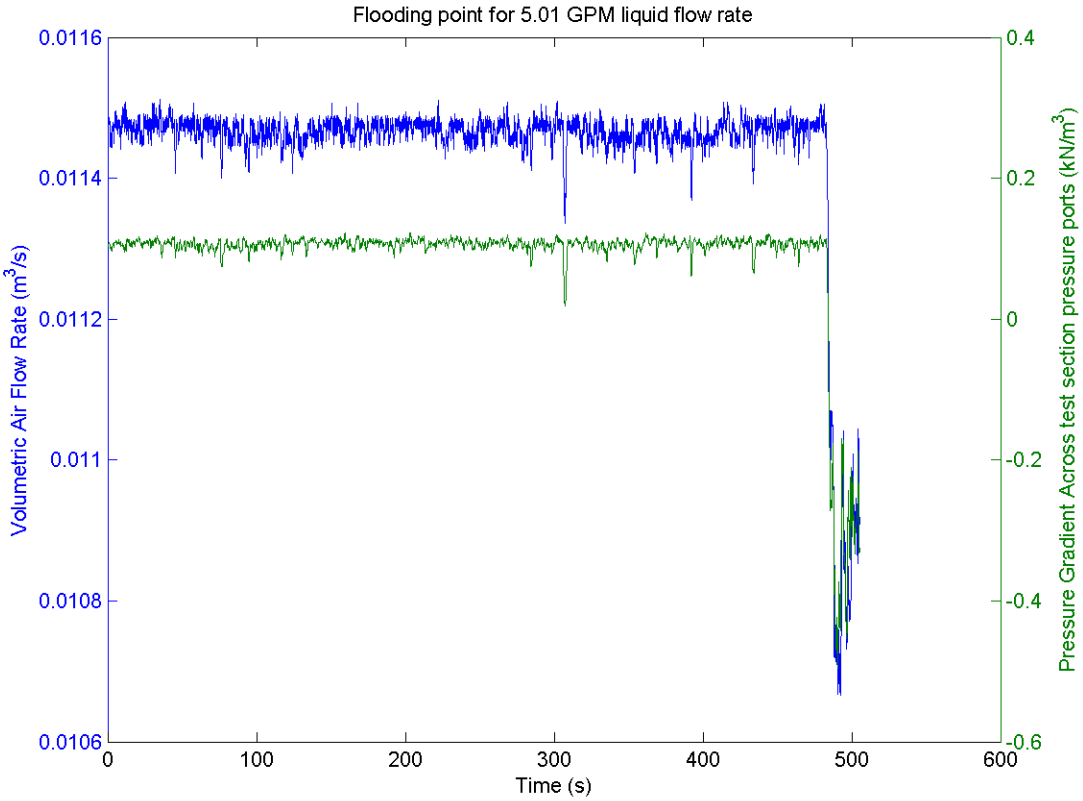
Flooding point for 5.01 GPM liquid flow rate
Volumetric Air Flow Rate (m3/s)
Pressure Gradient Across test section pressure ports (kN/m3)
Time (s)
0.0116
0.0114
0.0112
0.011
0.0108
0.0106
0.4
0.2
0
-0.2
-0.4
-0.6
0
100
200
300
400
500
600

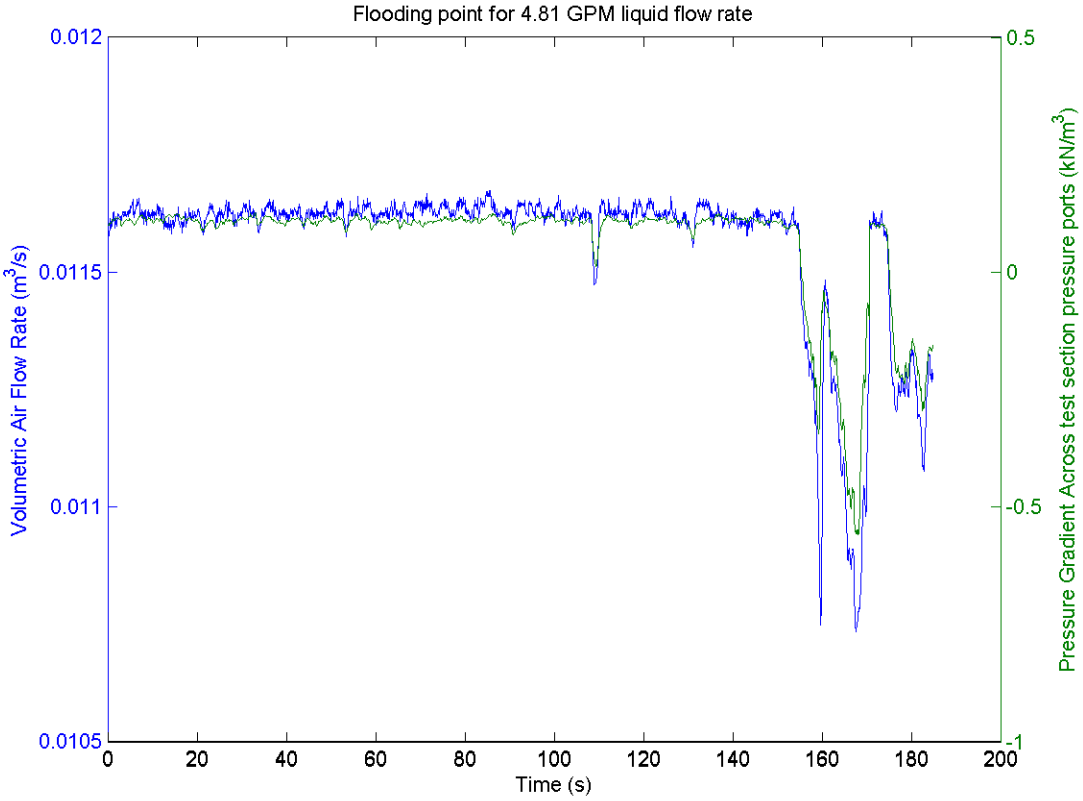
Flooding point for 4.81 GPM liquid flow rate
Volumetric Air Flow Rate (m3/s)
Pressure Gradient Across test section pressure ports (kN/m3)
Time (s)
0.012
0.0115
0.011
0.0105
0.5
0
-0.5
-1
0
20
40
60
80
100
120
140
160
180
200

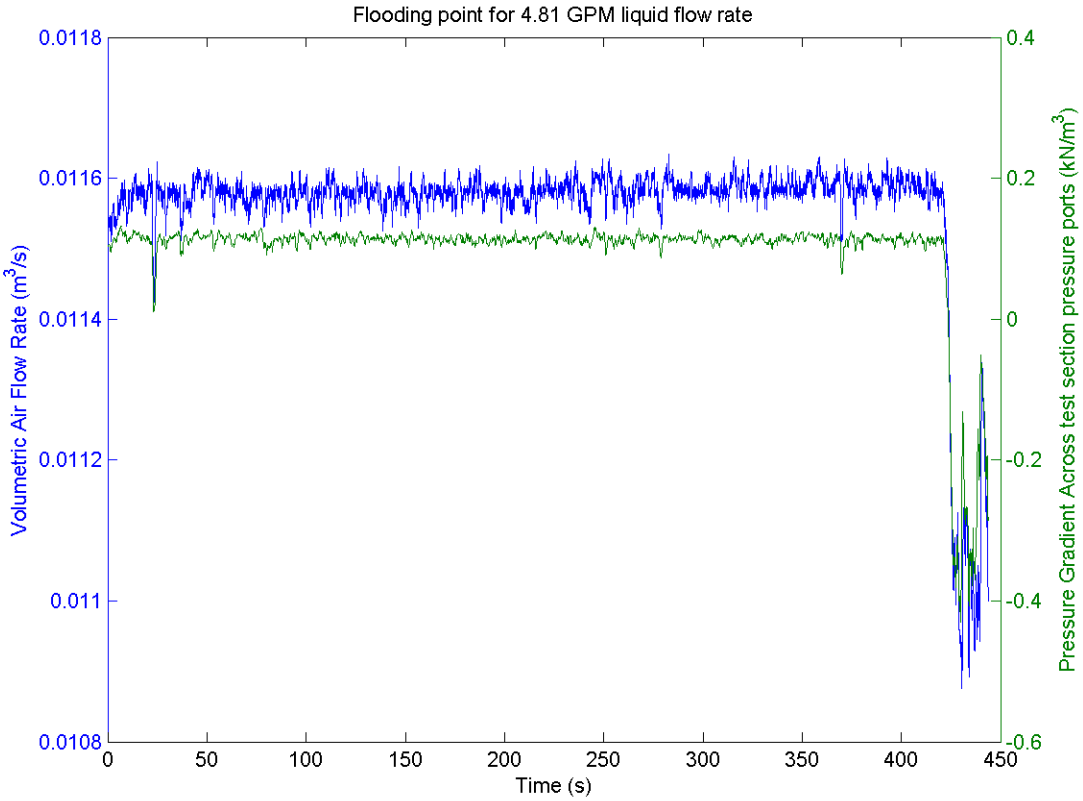
Flooding point for 4.81 GPM liquid flow rate
Volumetric Air Flow Rate (m3/s)
Pressure Gradient Across test section pressure ports (kN/m3)
Time (s)
0.0118
0.0116
0.0114
0.0112
0.011
0.0108
0.4
0.2
0
-0.2
-0.4
-0.6
0
50
100
150
200
250
300
350
400
450

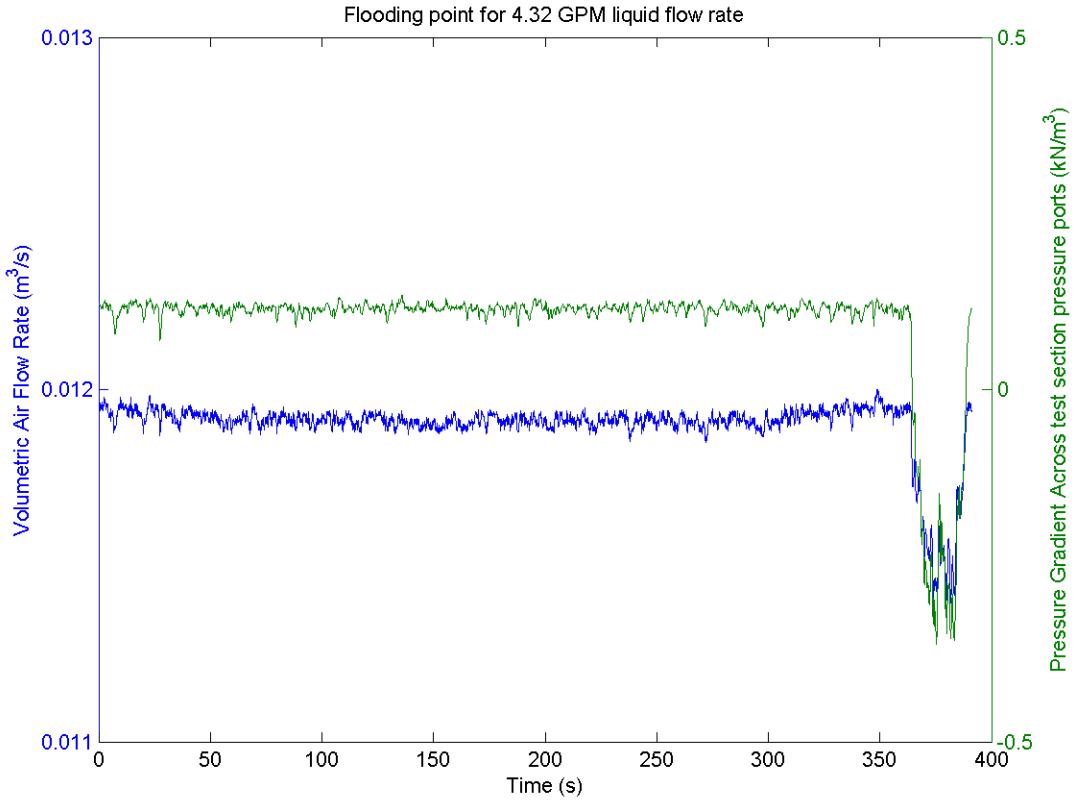
Flooding point for 4.32 GPM liquid flow rate
0.013
0.012
0.011
Volumetric Air Flow Rate (m3/s)
0.5
0
-0.5
Pressure Gradient Across test section pressure ports (kN/m3)
0
50
100
150
200
250
300
350
400
Time (s)

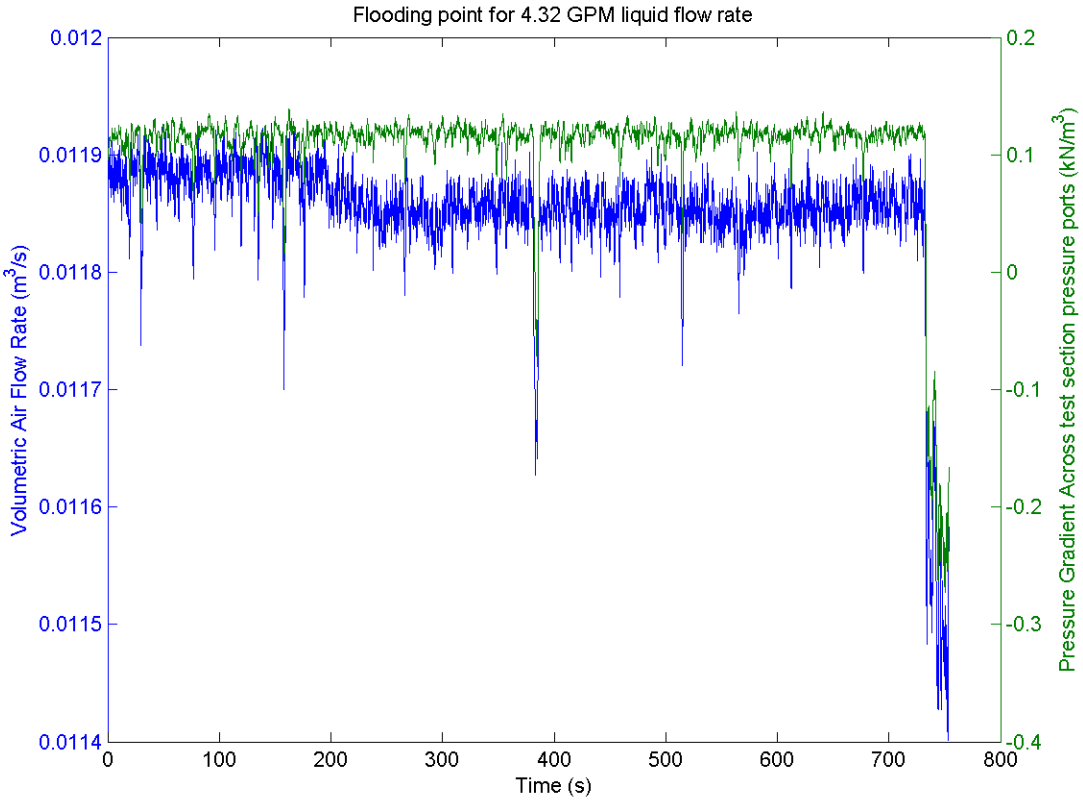
Flooding point for 4.32 GPM liquid flow rate
Volumetric Air Flow Rate (m3/s)
Pressure Gradient Across test section pressure ports (kN/m3)
Time (s)
0.012
0.0119
0.0118
0.0117
0.0116
0.0115
0.0114
0.2
0.1
0
-0.1
-0.2
-0.3
-0.4
0
100
200
300
400
500
600
700
800

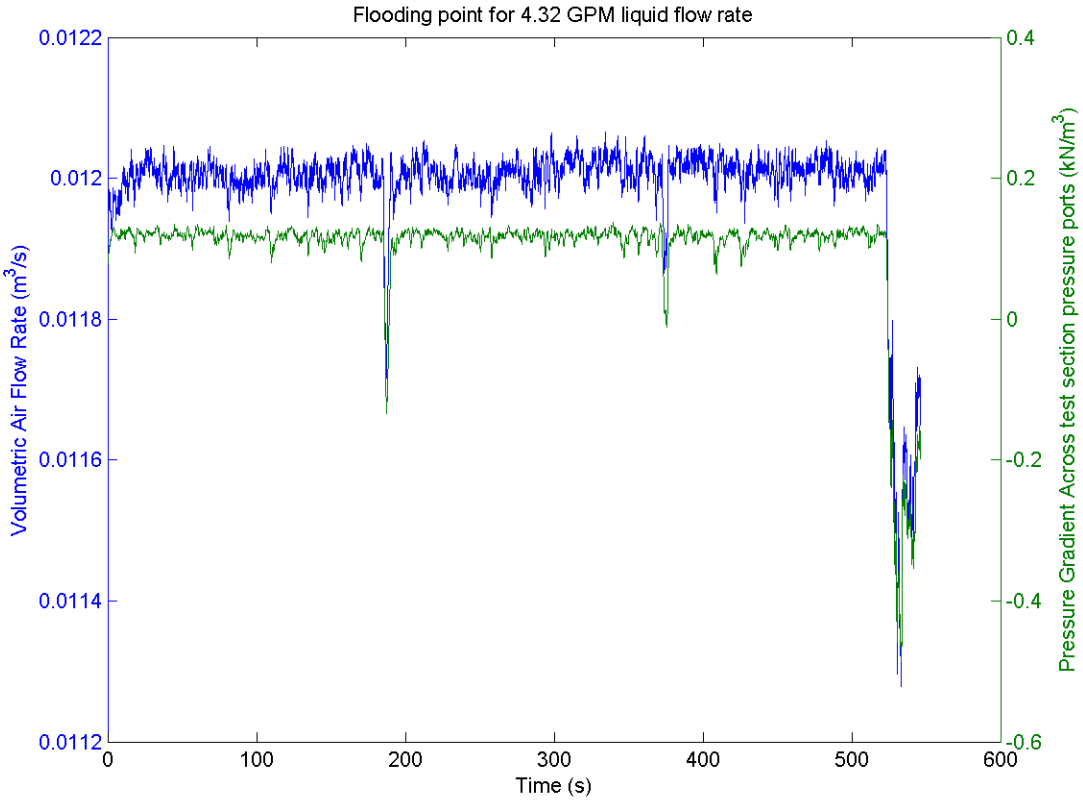
Flooding point for 4.32 GPM liquid flow rate
Volumetric Air Flow Rate (m3/s)
Pressure Gradient Across test section pressure ports (kN/m3)
Time (s)
0.0122
0.012
0.0118
0.0116
0.0114
0.0112
0.4
0.2
0
-0.2
-0.4
-0.6
0
100
200
300
400
500
600

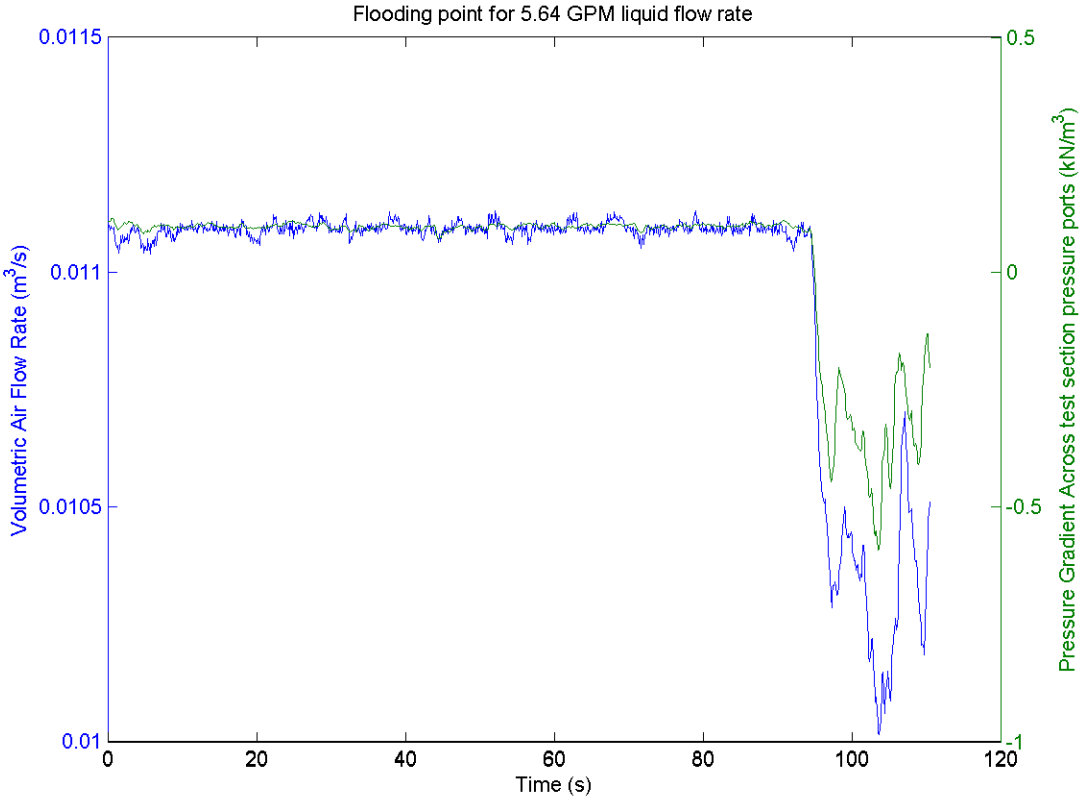
Flooding point for 5.64 GPM liquid flow rate
Volumetric Air Flow Rate (m3/s)
Pressure Gradient Across test section pressure ports (kN/m3)
Time (s)
0.0115
0.011
0.0105
0.01
0.5
0
-0.5
-1
0
20
40
60
80
100
120

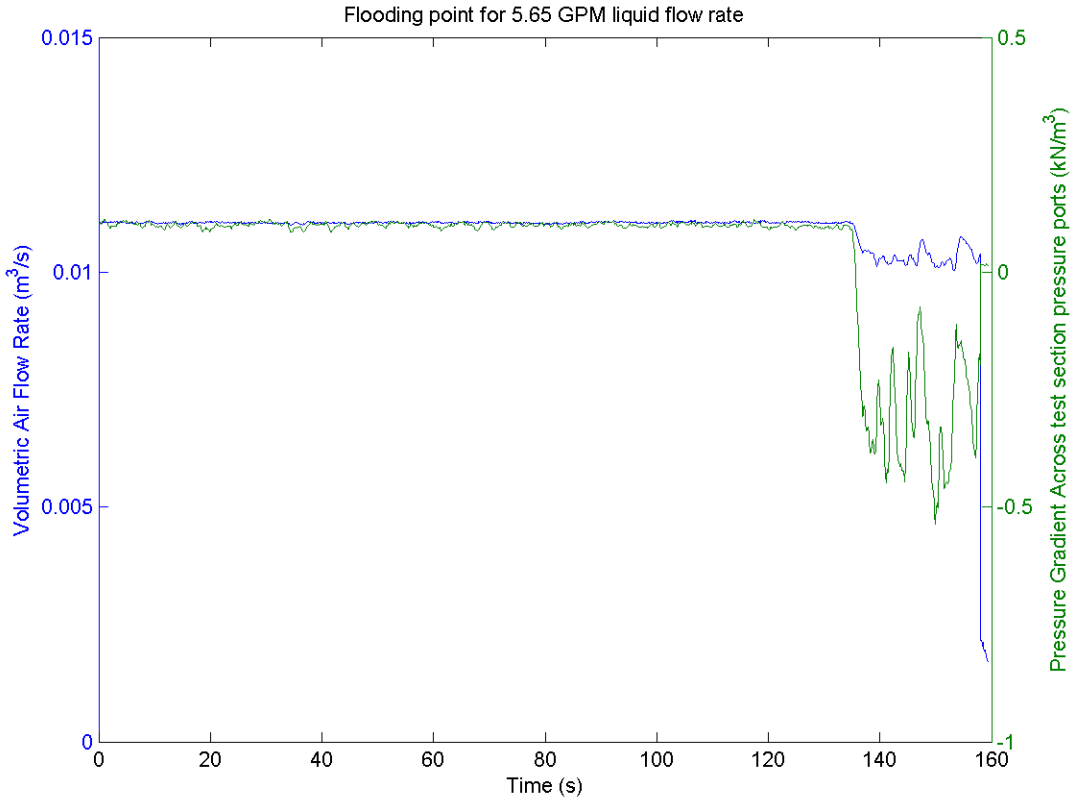
Flooding point for 5.65 GPM liquid flow rate
Volumetric Air Flow Rate (m3/s)
Pressure Gradient Across test section pressure ports (kN/m3)
Time (s)
0.015
0.01
0.005
0
0.5
0
-0.5
-1
0
20
40
60
80
100
120
140
160

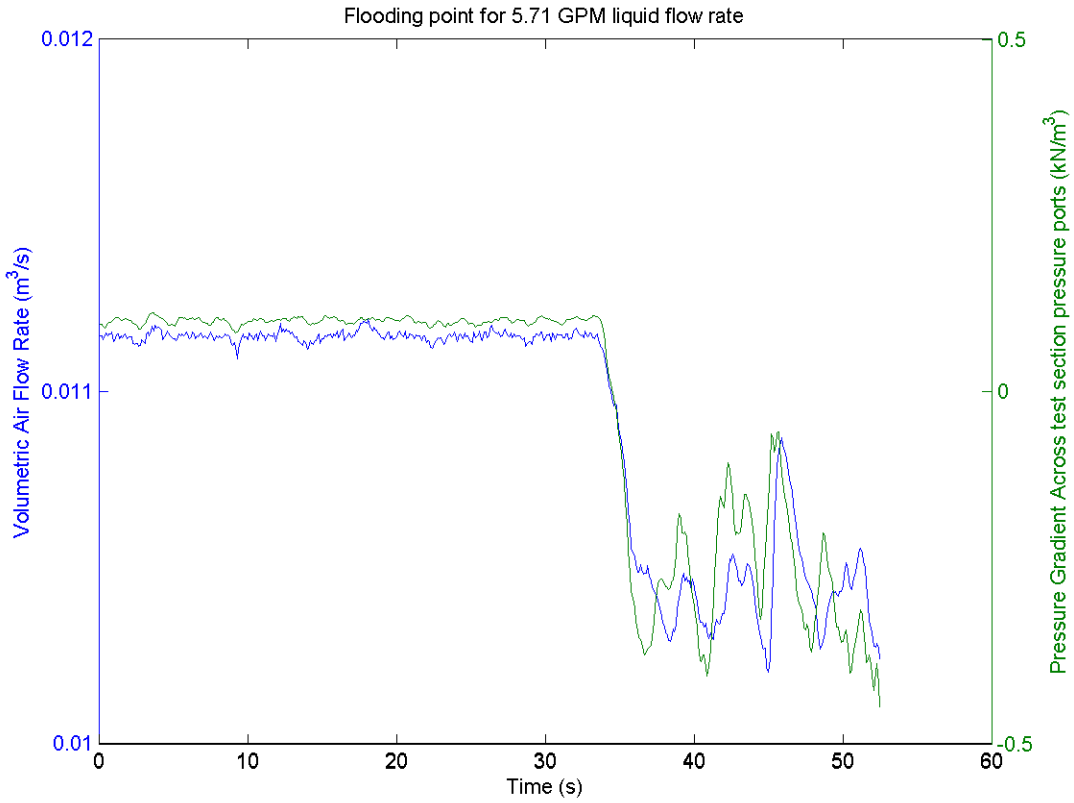
Flooding point for 5.71 GPM liquid flow rate
Volumetric Air Flow Rate (m3/s)
Pressure Gradient Across test section pressure ports (kN/m3)
Time (s)
0.012
0.011
0.01
0.5
0
-0.5
0
10
20
30
40
50
60

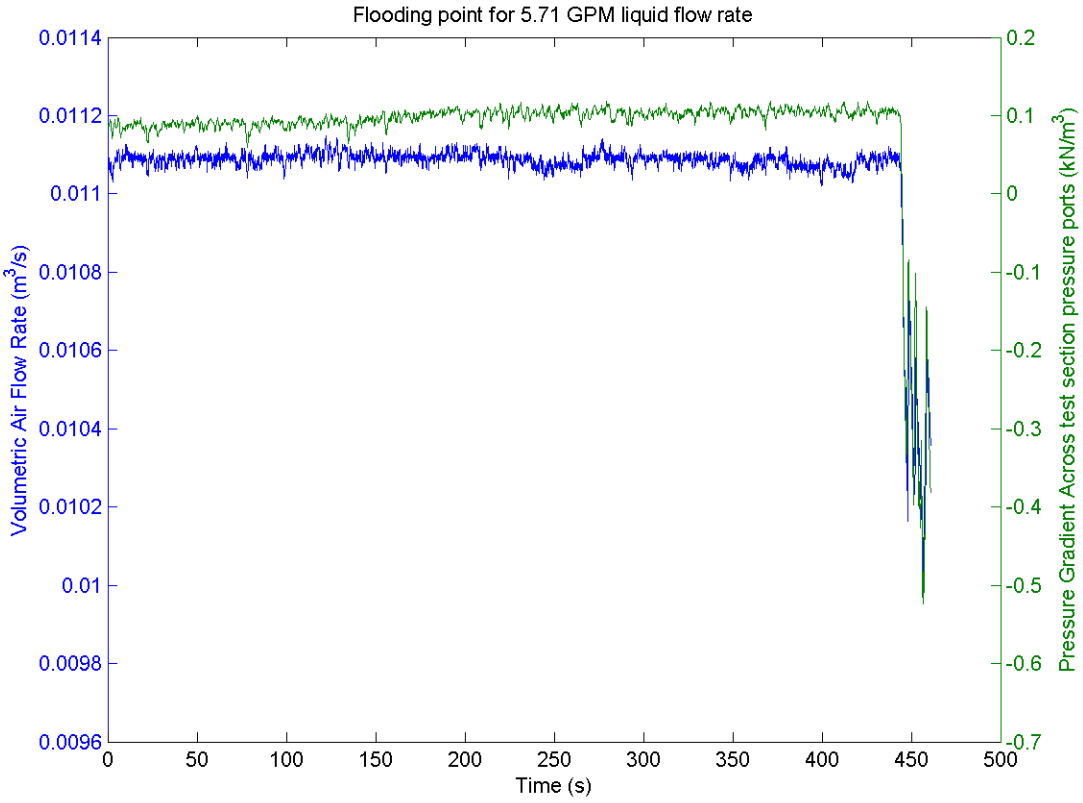
Flooding point for 5.71 GPM liquid flow rate
Volumetric Air Flow Rate (m3/s)
Pressure Gradient Across test section pressure ports (kN/m3)
Time (s)
0.0114
0.0112
0.011
0.0108
0.0106
0.0104
0.0102
0.01
0.0098
0.0096
0.2
0.1
0
-0.1
-0.2
-0.3
-0.4
-0.5
-0.6
-0.7
0
50
100
150
200
250
300
350
400
450
500

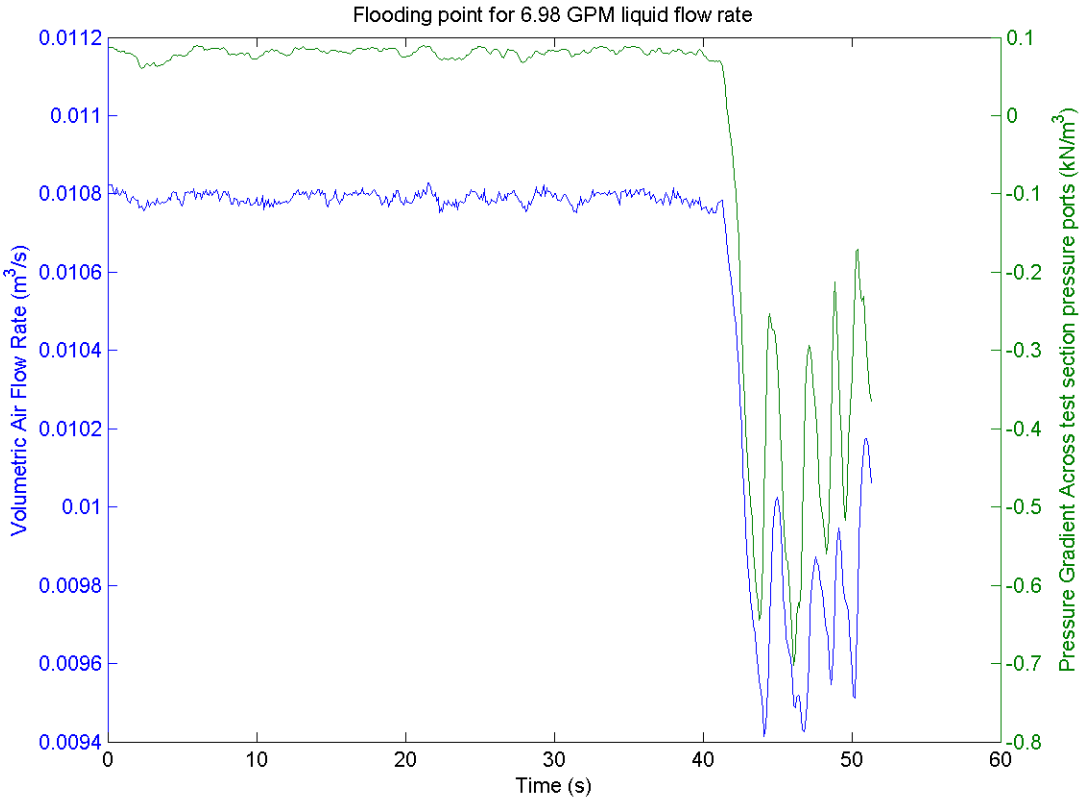
Flooding point for 6.98 GPM liquid flow rate
Volumetric Air Flow Rate (m3/s)
Pressure Gradient Across test section pressure ports (kN/m3)
Time (s)
0.0112
0.011
0.0108
0.0106
0.0104
0.0102
0.01
0.0098
0.0096
0.0094
0.1
0
-0.1
-0.2
-0.3
-0.4
-0.5
-0.6
-0.7
-0.8
0
10
20
30
40
50
60

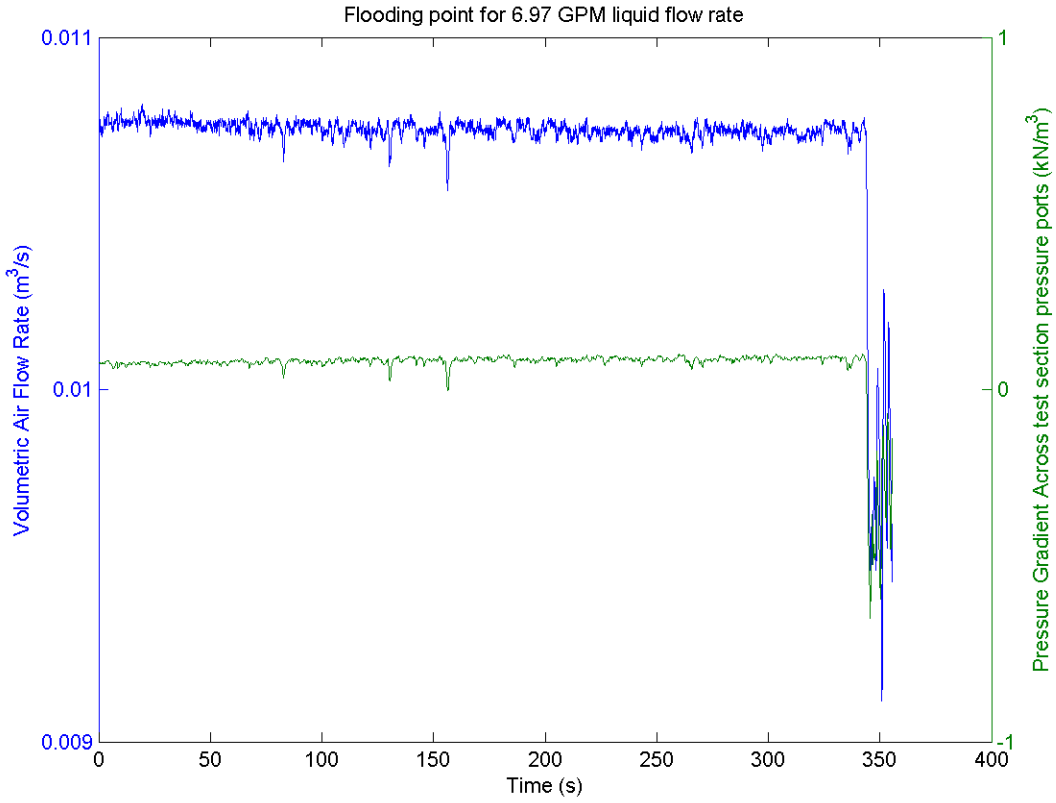
Flooding point for 6.97 GPM liquid flow rate
0.011
0.01
0.009
1
0
-1
0
50
100
150
200
250
300
350
400
Time (s)
Volumetric Air Flow Rate (m3/s)
Pressure Gradient Across test section pressure ports (kN/m3)

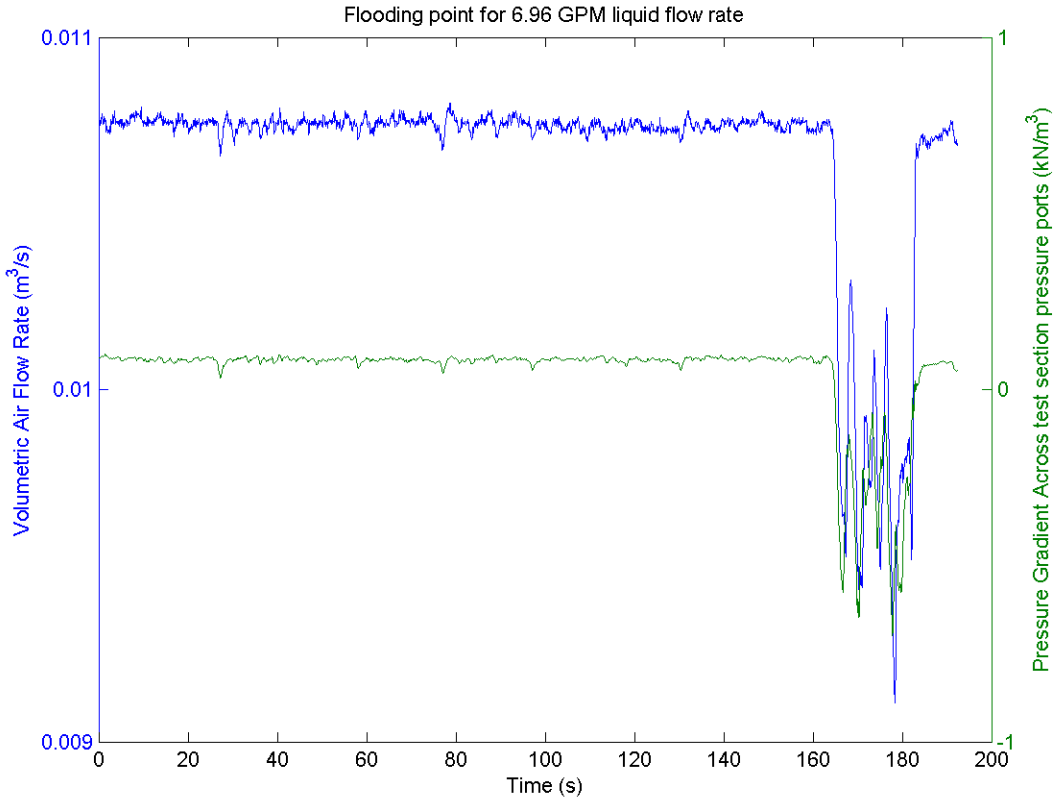
Flooding point for 6.96 GPM liquid flow rate
0.011
0.01
0.009
Volumetric Air Flow Rate (m3/s)
1
0
-1
Pressure Gradient Across test section pressure ports (kN/m3)
0
20
40
60
80
100
120
140
160
180
200
Time (s)

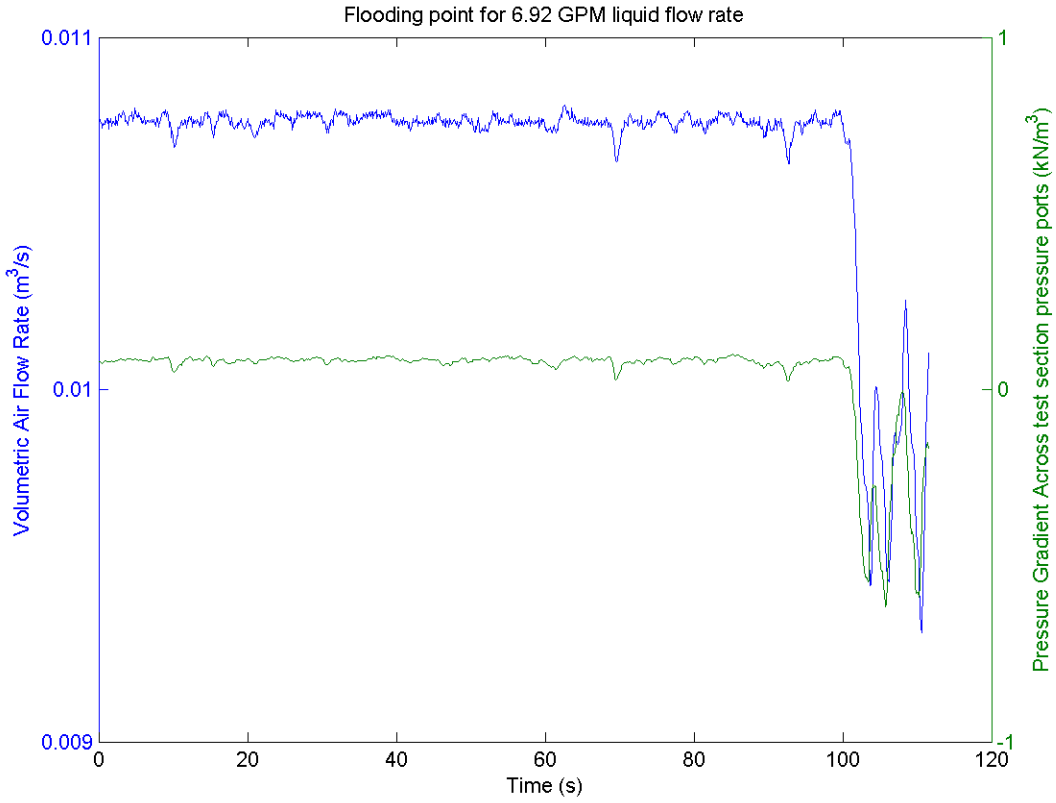
Flooding point for 6.92 GPM liquid flow rate
0.011
0.01
0.009
Volumetric Air Flow Rate (m3/s)
1
0
-1
Pressure Gradient Across test section pressure ports (kN/m3)
0
20
40
60
80
100
120
Time (s)

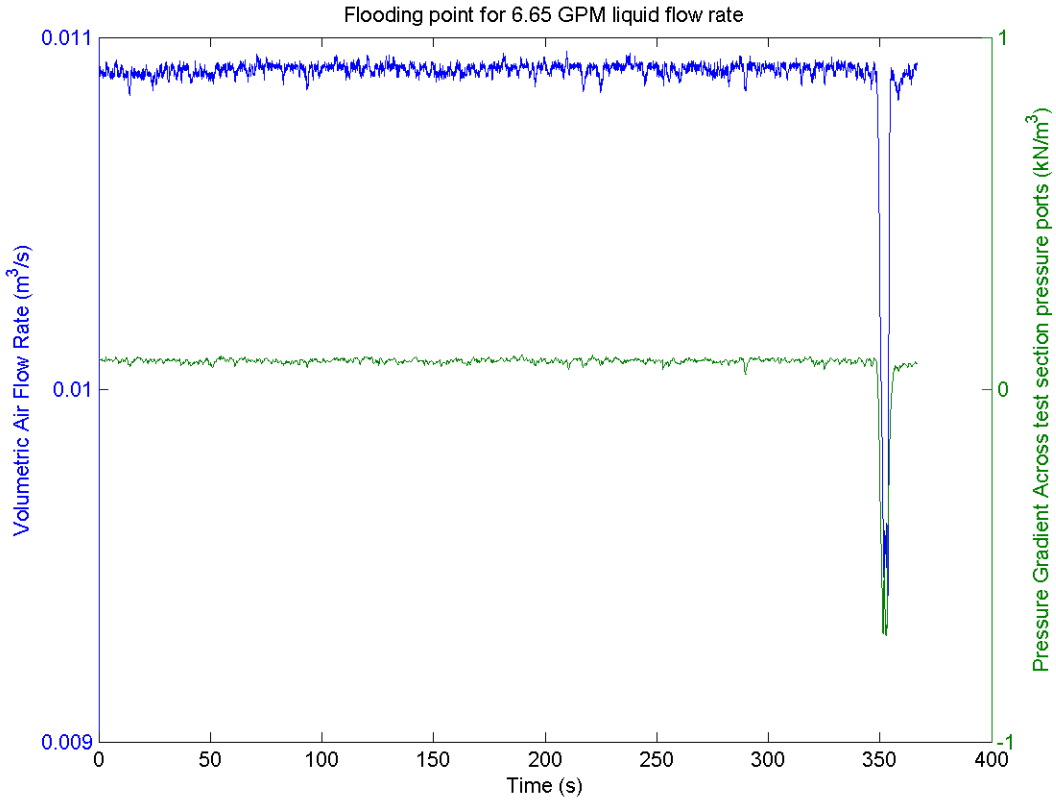
Flooding point for 6.65 GPM liquid flow rate
0.011
0.01
0.009
Volumetric Air Flow Rate (m3/s)
1
0
-1
Pressure Gradient Across test section pressure ports (kN/m3)
0
50
100
150
200
250
300
350
400
Time (s)

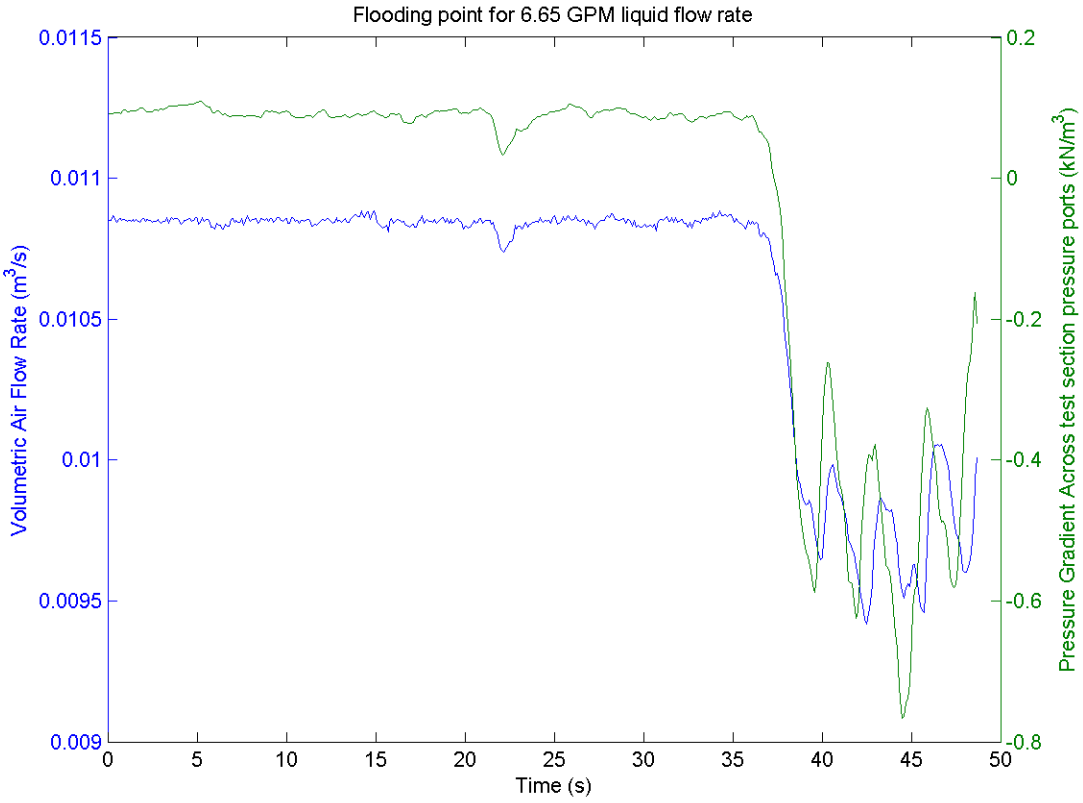
Flooding point for 6.65 GPM liquid flow rate
Volumetric Air Flow Rate (m3/s)
Pressure Gradient Across test section pressure ports (kN/m3)
Time (s)
0.0115
0.011
0.0105
0.01
0.0095
0.009
0.2
0
-0.2
-0.4
-0.6
-0.8
0
5
10
15
20
25
30
35
40
45
50

VITA

Matthew A. Solmos

Education

May 2008 Master of Science in Nuclear Engineering Department of Nuclear Engineering, Texas AM University

May 2006 Bachelor of Science in Nuclear Engineering School of Nuclear Engineering, Purdue University

Experience

Mar. 2008 to Present Safety and Performance Analysis Engineer GE Hitachi Nuclear Energy

Aug. 2006 to May 2008 Graduate Research Assistant. Laboratory for Nuclear Heat Transfer Systems Department of Nuclear Engineering, Texas AM University

Aug. 2005 to Aug. 2006 Undergraduate Research Assistant Laboratory Research Assistant. Laboratory for Nuclear Heat Transfer Systems School of Nuclear Engineering, Purdue University

Contact

3901 Castle Hayne Road, M/C A51
ATC1 3233
Wilmington, NC 28402